UNIVERSIDAD DE BUENOS AIRES

Facultad de Ciencias Exactas y Naturales

Departamento de Ciencias Geológicas

Caracterización tectosedimentaria 3D y evaluación del potencial de hidrocarburos de la transición entre las cuencas intracratónicas Chacoparanenses, el rift de Salta y las secuencias neógenas del antepaís Andino (Noroeste Argentino)

Tesis presentada para optar al título de Doctora de la

Universidad de Buenos Aires, área Ciencias Geológicas

Geol. Valentina Cortassa

Director de Tesis: Dr. Eduardo A. Rossello

Co-Director de Tesis: Dr. Manfred R. Strecker

Consejero de Estudios: Dr. Oscar Limarino

Lugar de trabajo: FCEN-UBA y Universidad de Potsdam

Fecha de defensa: Buenos Aires, 21/10/2025

3D Tectonosedimentary characterisation and hydrocarbon potential evaluation of the transition between the intracratonic Chacoparanaense Basin, the Salta Group Rift and the Neogene Andean foreland, Argentina

---

Geol. Valentina Cortassa

Dissertation

zur Erlangung des akademischen Grades

"Doctor rerum naturalium" (Dr. rer. nat.)
in der Wissenschaftsdisziplin "Geologie"

eingereicht an der
Mathematisch-Naturwissenschaftlichen Fakultät
Institut für Geowissenschaften
der Universität Potsdam

Ort und Datum der Dissertation: Buenos Aires, 21. Oktober 2025

Unless otherwise indicated, this work is licensed under a Creative Commons License Attribution-NonCommercial 4.0 International.

This does not apply to quoted content and works based on other permissions. To view a copy of this license, visit:

https://creativecommons.org/licenses/by-nc/4.0

BetreuerInnen: Prof. Dr. Eduardo A. Rossello

Prof. Manfred R. Strecker

MentorInnen: Dr. Robert Ondrak

GutachterInnen: Prof. Dr. Uwe Altenberger

Dr. Alejandro Bande

Prof. Dr. Luis Pedro Stinco

Declaration of Authorship

I hereby declare that this dissertation was prepared independently by the author, Valentina Cortassa, without the use of any other means than the specified. All ideas derived from other sources are indicated as such. This work has been submitted only to the University of Potsdam and the University of Buenos Aires, in compliance with an individual cotutelle agreement.

A mi abuelo Antonio,
quien inculcó en mí la curiosidad científica.

Acknowledgments

This thesis was primarily funded by CONICET (Consejo Nacional de Investigaciones Científicas y Técnicas, Argentina) and by the international cooperation program Germany–Argentina StRATEGy (Surface Processes, Tectonics and Georesources: The Andean Foreland Basin of Argentina). Research stays at the University of Potsdam, the GFZ German Research Centre for Geosciences, and RWTH Aachen University were supported by the DAAD (German Academic Exchange Service) and the GFZ Section 3.2. I thank YPF (Yacimientos Petrolíferos Fiscales, Argentina) for providing valuable data for this thesis.

I would like to express my sincere gratitude to my advisers, Prof. Eduardo Rossello and Prof. Manfred Strecker, for their guidance, support, generosity in sharing their knowledge, and human approach throughout this process. I am especially grateful to my mentor, Dr. Robert Ondrak, for his constant presence, for teaching me with patience, for helping solve countless problems, and for always being there to support me.

I also thank the institutions that provided the facilities and academic environment that made this thesis possible. To the University of Buenos Aires and the University of Potsdam, for welcoming me as a doctoral student and allowing me to carry out my research. To GFZ Potsdam, RWTH Aachen, and CICTERRA Córdoba, for opening their doors and for the support and friendship extended to me by their staff.

I am grateful to Dr. Stefan Back, who introduced me to the world of seismic interpretation—without his encouragement, I would not have discovered this passion or arrived where I am today. I also thank Dr. Cecilia del Papa for sharing with me her knowledge, both scientific and human. I am deeply thankful to Dr. Horacio Canelo, who taught me so much about geology and always approached me with patience and generosity.

To all the wonderful friends I made along the way — from the Strategy team, from UBA, Aachen, and Trieste — thank you. The list would be too long to name each of you, but please know that every one of you who helped me proofread a chapter, track a citation, navigate bureaucracy, host me during my travels, or simply stood by me emotionally, has played an invaluable role. A heartfelt thank you especially to Melanie, Sara, Paula, and Johanna — you've caught me when I fell and celebrated every small and big victory by my side.

To my family, thank you for always believing in me and reminding me I could achieve anything. I miss you dearly during the times I am away, but you have always been just one message away. Mum, you are and always have been the best — I will always strive to be as much like you as I can. Dad, thank you for your unwavering support and trust in me, no matter what.

To Ana and my “family away from home,” thank you for opening your doors and your hearts to me. To my friends in Córdoba, thank you for always being there, even with the distance. Pía, Santi, Nacho, and the whole Salado’s crew — thank you for always welcoming me back with open arms.

Finally, I want to deeply thank my entire support network — each and every one of you who believed in me, who is happy for me today, who stood by me during hard times, who patiently listened to endless thesis talk, who offered a word of encouragement, a “you can do it,” or simply stood next to me, in good times and bad — thank you, from the bottom of my heart.

Abstract

Although being an integral part of the Cenozoic Andean orogen, the Chacopampean plain of northern Argentina is an extensive, low-relief fluvial lowland in the Andean foreland, a vast region which is apparently devoid of current tectonic activity. Yet, this region hides a complex and little-known geological history beneath its recent sediments that reflects multiple deformation, erosion, and depositional episodes in the geological past. This thesis aims to reconstruct this history, in particular the evolution of the buried high-relief Alto del Quirquincho and associated domed areas of the Earth's crust, whose existence, geological evolution, and impact on sedimentary systems are debated.

The Alto del Quirchincho separates two major sedimentary basin systems in the subsurface: the ancient Chacoparanaense Basin, of Paleozoic and Mesozoic origin, and the Salta Rift, a late Mesozoic extensional basin. Both are now covered by the sediments of the Andean foreland basin, a generally wedge-shaped sedimentary basin formed by the uplift of the Andes, accompanying thrusting, sedimentary loading, and subsidence.

Foreland basins, formed beyond the flanks of high mountain ranges, are natural archives whose sediments reflect the interaction between deep-seated tectonic (orogenic) and climate-driven surface processes. Understanding these relationships helps to reconstruct the evolution of mountain belts, coeval exogenic processes, and the formation of sedimentary basins in the geological past. To investigate the subsurface characteristics of the sediment-covered Chacoparanaense plain, I analysed data from deep boreholes and seismic reflection

lines acquired during oil exploration efforts in the 20th century. Different seismic lines crossing an area of interest provide an 'X-ray' of the subsurface to a depth of about 10 km that is created by the reflection of artificially generated seismic waves at stratal boundaries and fault zones. Combined with the information on the physical characteristics of rocks retrieved from boreholes, the imaged horizons can be correlated with rock units and thus provide a direct look at rock units at depth. The imaged strata can therefore be used to develop scenarios of past deposition and deformation events, as well as the formation of oil and gas resources.

By combining information from the seismic lines with borehole data, I constructed a 3D structural model of the subsurface. This reconstruction allowed the identification and characterisation of two structural highs: the Quirquincho and the Pampeano-Chaqueño Highs, the latter of smaller size and located within the Chacoparanaense Basin. The analysis of the shape of the strata showed that these high-relief areas of the geological past were uplifted and eroded during the late Palaeozoic and early Mesozoic; subsequently, these vestiges of former processes have been progressively buried by sediments since the Cretaceous.

Importantly, both structural highs influenced the shape and distribution of the basins, acting as separators and modulators of sediment deposition at a regional scale. The most likely hypothesis for their origin is that they were formed by flexural deformation of the crust during the Paleozoic Gondwanan orogeny, an episode of mountain building similar to the processes that have been forming the Cenozoic Andes and their depositional systems until today.

In contrast to the flexural deformation during the Paleozoic, the present-day tectonic realm of the Andean orogen at these latitudes is characterized by disparate, active faults and range uplifts in the southern and southwestern sectors of the basin (Santa Bárbara System), whereas the regions to the north and east are gently inclined depositional plains. Most of the active structures in the Santa Bárbara System are compressionaly reactivated extensional faults of the buried Cretaceous Salta Rift.

The robust assessment of the tectonic and sedimentary evolution of this region enabled me to focus on evaluating the hydrocarbon potential of the Chacoparanaense Basin, which historically has not revealed economically viable reservoirs. However, technological advances and results from basin modelling carried out in this study now allow to consider unconventional hydrocarbon resources. Modelling of the thermal evolution of the basin, validated with well data, suggests that Silurian rocks may have generated unconventional reservoirs of oil and gas.

In conclusion, this thesis presents an unprecedented and detailed reconstruction of the subsurface geological evolution of the Chacoparanaense Basin, with both scientific and economic implications. The integrative analysis of seismic reflection lines and well data has allowed me to decipher the complex history of the different stages in sedimentary basin evolution and to assess the hydrocarbon potential of a region that is still little explored.

Zusammenfassung

Obwohl die Chaco-Pampa-Ebene im Norden Argentiniens ein integraler Bestandteil des känozoischen Anden-Orogens ist, handelt es sich um ein ausgedehntes, tiefliegendes fluviales Sedimentationsgebiet im Vorland, das außer der Santa-Bárbara-Region im Süden und Südwesten offenbar keine rezente tektonische Aktivität aufweist. Dennoch verbirgt diese Region unter ihren jüngsten Sedimenten eine komplexe und wenig bekannte geologische Geschichte von Deformation, Erosion und Ablagerung. Ziel dieser Arbeit ist es, diese Geschichte zu rekonstruieren, insbesondere die Entwicklung des von Sedimenten bedeckten Reliefs eines ehemaligen Hochgebiets. Hierbei handelt es sich um den Alto del Quirquincho und der damit verbundenen deformierten Bereiche der Erdkruste im Untergrund, deren Existenz, geologische Entwicklung und Auswirkungen auf spätere Sedimentationssysteme nicht genau bekannt sind.

Der Alto del Quirchincho trennt zwei große sedimentäre Beckensysteme im Untergrund: das alte Chacoparanaense-Becken, das paläozoischen und mesozoischen Ursprungs ist, und das Salta-Rift, ein spät-mesozoisches Extensionsbecken. Beide Paläobecken sind heute von den känozoischen Sedimenten des Andenvorlands bedeckt, einem im Allgemeinen keilförmigen Sedimentbecken, das durch die Hebung der Anden und der damit einhergehenden Überschiebungstätigkeit, Absenkung und Sedimentation entstanden ist.

Orogene Vorlandbecken, die sich an den Rändern großer Gebirgszüge bilden, sind natürliche Archive der Wechselwirkung zwischen tiefen tektonischen (orogenen) und klimatisch

gesteuerten Oberflächenprozessen. Ein besseres Verständnis dieser Prozesse hilft dabei, die Entwicklung von Gebirgsgürteln und Sedimentbecken in der geologischen Vergangenheit sowie die mögliche Verbreitung von Lagerstätten zu rekonstruieren. Zur Untersuchung des Charakters des tiefen Untergrundes des sedimentbedeckten Chacoparanaense-Beckens habe ich Daten aus Tiefbohrungen und seismischen Reflexionslinien ausgewertet, die bei der Ölexploration im 20. Jahrhundert generiert wurden. Verschiedene seismische Linien, die ein Gebiet von Interesse durchqueren, liefern gewissermaßen ein „Röntgenbild“ des Untergrunds bis zu einer Tiefe von etwa 10 km, das durch die Reflexion künstlich erzeugter seismischer Wellen an Schichtgrenzen und Störungszonen entsteht. In Kombination mit den Informationen über die physikalischen Eigenschaften der Gesteine, die aus Bohrungen gewonnen werden, können die abgebildeten Horizonte mit Gesteinseinheiten aus Bohrungen korreliert werden und ermöglichen somit einen direkten Blick auf die Verbreitung von Gesteinen in der Tiefe, die daraufhin zur Entwicklung von Szenarien für Kohlenwasserstoffvorkommen genutzt werden können.

Durch die Kombination von Informationen aus den seismischen Linien mit Bohrlochdaten konnte ich ein 3D-Strukturmodell des Untergrunds erstellen. Diese Rekonstruktion ermöglichte die Identifizierung und Charakterisierung zweier ehemaliger, strukturell bedingter Hochregionen. Hierbei handelt es sich um den Alto del Quirquincho und den Alto del Pampeano-Chaqueño, wobei letzterer von geringerer Größe ist. Die Analyse von Sedimenteinheiten zeigte dabei deutlich, dass diese ehemaligen Hochgebiete während des späten Paläozoikums und frühen Mesozoikums angehoben und erodiert wurden sowie anschließend seit der Kreidezeit allmählich von Sedimenten bedeckt wurden.

Die neuen Analysen zeigen weiterhin, dass beide strukturellen Hochgebiete die Form und Verteilung der Becken beeinflussten, indem sie Bereiche voneinander abtrennten und die Sedimentablagerung auf regionaler Ebene steuerten. Die wahrscheinlichste Hypothese für die Entstehung dieser Hochregionen ist, dass sie durch eine flexurbedingte Verformung der Erdkruste während der paläozoischen Gondwana-Orogenese gebildet wurden, einer tektonischen Episode, die hinsichtlich der Prozesse ähnelt, die bis heute das Anden-Orogen in seiner Gesamtheit beeinflussen.

Die rigorose Bewertung der tektonischen und sedimentären Entwicklung dieser Region ermöglichte es mir, mich in einem nächsten Schritt auf die Bewertung des Kohlenwasserstoffpotenzials des Chacoparanaense-Beckens zu konzentrieren, da hier in der Vergangenheit keine wirtschaftlich nutzbaren Lagerstätten gefunden wurden. Dank des technologischen Fortschritts und meiner Modellierungen können wir jetzt jedoch auch unkonventionelle Kohlenwasserstoff-Ressourcen für diese Region in Betracht ziehen. Die Modellierung der thermischen Entwicklung des Beckens, die anhand von Bohrlochdaten validiert wurde, deuteteindeutig darauf hin, dass die Sedimentgesteine des Silurs unkonventionelles Öl und Gas hervorgebracht haben könnten.

Zusammenfassend lässt sich sagen, dass diese Arbeit eine innovative und detaillierte Rekonstruktion der geologischen Entwicklung des Chacoparanaense-Beckens darstellt, die sowohl wissenschaftliche als auch wirtschaftliche Bedeutung hat. Die integrative Analyse von seismischen Reflexionslinien und Bohrlochdaten hat es mir dabei ermöglicht, die komplexe Geschichte der verschiedenen Schritte der Entwicklung des Sedimentbeckens zu

entschlüsseln und das Kohlenwasserstoffpotenzial einer bisher noch wenig erforschten Region zu bewerten.

Resumen

La llanura Chacopampeana, en apariencia una extensa planicie sin actividad tectónica actual, esconde bajo sus sedimentos recientes una compleja y poco conocida historia geológica. Esta tesis se centra en reconstruir esa historia, en particular la evolución de un relieve oculto del subsuelo: el Alto del Quirquincho, una zona abombada de la corteza terrestre cuya existencia y rol geológico apenas han sido explorados.

Este alto estructural separa dos grandes sistemas de cuencas sedimentarias: la antigua cuenca Chacoparanaense, de origen Paleozoico y Mesozoico, y el Rift de Salta, una cuenca extensional de edad mesozoica tardía. Ambas se encuentran cubiertas hoy por los sedimentos de la cuenca de antepaís andina, una cuenca formada por el levantamiento de los Andes.

Las cuencas de antepaís, formadas en el borde de grandes cordilleras, son archivos naturales de la interacción entre tectónica, orogénesis y clima. Comprenderlas nos ayuda a reconstruir cómo evolucionaron estas fuerzas en el pasado geológico. Para investigar lo que hay bajo esta planicie cubierta de sedimentos cuaternarios, analicé datos de pozos profundos y líneas sísmicas obtenidas durante exploraciones petroleras del siglo XX. Las líneas sísmicas permiten ver una "radiografía" del subsuelo hasta unos 10 km de profundidad, mediante la medición de vibraciones en el terreno. Mientras tanto, los pozos proporcionan muestras directas de las rocas en profundidad.

Combinando la información indirecta de las líneas sísmicas con los datos directos de los pozos, elaboré un modelo estructural en 3D del subsuelo. Esta reconstrucción permitió identificar y caracterizar dos altos estructurales: el Alto del Quirquincho y el Alto Pampeano-Chaqueño, este último de menor tamaño y dentro de la cuenca Chacoparanaense. El análisis de la forma de los estratos reveló que estos relieves estuvieron elevados durante el Paleozoico tardío y el Mesozoico temprano, y que fueron progresivamente enterrados por nuevos sedimentos desde el Cretácico.

Estos altos estructurales influyeron en la forma y distribución de las cuencas, actuando como divisores y moduladores del depósito de sedimentos. La hipótesis más probable sobre su origen es que se formaron por una deformación flexural de la corteza durante la orogenia Gondwánica, una orogenia similar a la que hoy forma los Andes.

A diferencia de la deformación flexural de entonces, la tectónica actual en los Andes, en estas latitudes, presenta fallas activas que escalonan la corteza, como se observa en las Sierras de Santa Bárbara. Esto podría explicarse por un evento de extensión tectónica posterior a la orogenia Gondwánica, que formó el Rift de Salta. Las fallas extensionales generadas en esa etapa habrían sido reutilizadas como fallas compresivas durante la posterior orogenia Andina.

Con la evolución tectónica y sedimentaria bien definida, me enfoqué en evaluar el potencial de hidrocarburos de la cuenca Chacoparanaense, que históricamente no ha producido yacimientos económicamente rentables. Sin embargo, los avances tecnológicos permiten hoy considerar recursos no convencionales. El modelado de la evolución térmica de la cuenca,

validado con datos de pozos, indica que las rocas silúricas podrían haber generado gas y petróleo almacenados en reservorios no convencionales.

En resumen, esta tesis presenta una reconstrucción inédita y detallada de la evolución geológica del subsuelo de la llanura Chacoparanaense, con implicancias tanto científicas como económicas. El análisis integrador de datos sísmicos y de pozos permitió entender la historia de las cuencas sedimentarias y resaltar el potencial de hidrocarburos de una región aún poco explorada.

Table of Contents

List of Figures

Figure 3.3: NW-SE-oriented North transect. A- Seismic profiles with interpreted color-coded horizons. B- Geological profile across the seismic units.

Figure 3.4: NW-SE-oriented South Transect. A- Seismic profiles with interpreted color-coded horizons. B- Geological profile across the seismic units.

Figure 3.5: Flattening of the horizons in the North Transect. A- Flattening of H2-Top Paleozoic. B- Flattening of H3-Top Cretaceous. C- Flattening of H4-Top Paleogene. D- Flattening of H5-Top Neogene.

Figure 3.6: Location of additional seismic surveys in the study area.

Figure 3.7: Legend for figures 3.8-3.11.

Figure 3.8: Survey pw_89_40. A- uninterpreted seismic line. B- Interpreted color-coded horizons. C- Geological profile across the interpreted units.

Figure 3.9: Survey 45054. A- uninterpreted seismic line. B- Interpreted color-coded horizons C- Geological profile across the interpreted units.

Figure 3.10: Survey TX_90_209. A- uninterpreted seismic line. B- Interpreted color-coded horizons. C- Geological profile across the interpreted units.

Figure 3.11: Survey 33049. A- uninterpreted seismic line. B- Interpreted color-coded horizons. C- Geological profile across the interpreted units.

Cretaceous, H11: Top Paleogene. C: model of the interpreted units: U1: Basement, U0: Precambrian metasediments, U3: Ordovician, U4: Silurian, U5: Devonian, U6: Carboniferous, U7: Permian, U9: Jurassic, U10: Cretaceous, U11: Paleogene. U12: Undifferentiated Neogene and Quaternary. Wells: LB-1: Las Breñas 1, LB-2: Las Breñas 2, LB-O: Las Breñas Oriental.

Figure 4.5: Seismic survey pw_89_40. A: uninterpreted seismic line. B: interpreted unit tops: H1: Top Basement, H0: Top Precambrian metasediments, H2: Top Cambrian, H3: Top Ordovician, H5: Top Devonian, H6: Top Carboniferous, H7: Top Permian, H8: Top Triassic, H9: Top Jurassic, H10: Top Cretaceous, H11: Top Paleogene.: C: model of interpreted units: U1: Basement, U0: Precambrian metasediments, U2: Cambrian, U3: Ordovician, U5: Devonian, U6: Carboniferous, U7: Permian, U8: Triassic, U9: Jurassic, U10: Cretaceous, U11: Paleogene. U12: Undifferentiated Neogene and Quaternary. Well: PB: Pampa Bandera.

Figure 4.6: Seismic survey 4141. A: uninterpreted seismic line. B: interpreted unit tops: H1: Top Basement, H2: Top Cambrian, H3: Top Ordovician, H4: Top Silurian, H5: Top Devonian, H7: Top Permian, H8: Top Triassic, H9: Top Jurassic, H10: Top Cretaceous, H11: Top Paleogene. C: model of interpreted units: U1: Basement, U2: Cambrian, U3: Ordovician, U4: Silurian, U5: Devonian, U7: Permian, U8: Triassic, U9: Jurassic, U10: Cretaceous, U11: Paleogene, U12: Undifferentiated Neogene and Quaternary. Well: AL: Alhuampa.

Figure 4.7: Seismic survey 4139. A: uninterpreted seismic line. B: interpreted unit tops: H1: Top Basement, H3: Top Ordovician H4: Top Silurian, H5: Top Devonian, H6: Top Carboniferous, H7: Top Permian, H10: Top Cretaceous, H11: Top Paleogene. C: model of interpreted units:

U1: Basement, U3: Ordovician, U4: Silurian, U5: Devonian, U6: Carboniferous, U7: Permian, U10: Cretaceous, U11: Paleogene. U12: Undifferentiated Neogene and Quaternary. Wells: EL: El Caburé, CR: Coronel Rico.

Figure 4.8: Seismic survey 44018. A: uninterpreted seismic line. B: interpreted unit tops: H1: Top Basement, H3: Top Ordovician, H4: Top Silurian, H5: Top Devonian, H6: Top Carboniferous, H7: Top Permian, H10: Top Cretaceous, H11: Top Paleogene, U12: Undifferentiated Neogene and Quaternary. C: model of interpreted units: U1: Basement, U3: Ordovician, U4: Silurian, U5: Devonian, U6: Carboniferous, U7: Permian, U10: Cretaceous, U11: Paleogene, U12: Undifferentiated Neogene and Quaternary. Wells: CR: Coronel Rico, ED: El Desierto.

Figure 4.9: Seismic survey 45026. A: uninterpreted seismic line. B: interpreted unit tops: H1: Top Basement, H2: Top Cambrian, H3: Top Ordovician, H4: Top Silurian, H5: Top Devonian, H6: Top Carboniferous, H7: Top Permian, H8: Top Triassic, H9: Top Jurassic, H10: Top Cretaceous, H11: Top Paleogene. C: model of the interpreted units: U1: Basement, U2: Cambrian, U3: Ordovician, U4: Silurian, U5: Devonian, U6: Carboniferous, U7: Permian, U8: Triassic, U9: Jurassic, U10: Cretaceous, U11: Paleogene, U12: Undifferentiated Neogene and Quaternary. Well: AL: Alhuampa.

Figure 4.10: Seismic survey 45054. A: uninterpreted seismic line. B: interpreted unit tops: H1: Top Basement, H2: Top Cambrian, H3: Top Ordovician, H4: Top Silurian, H5: Top Devonian, H6: Top Carboniferous, H10: Top Cretaceous, H11: Top Paleogene. C: model of the interpreted

units: U1: Basement, U2: Cambrian, U3: Ordovician, U4: Silurian, U5: Devonian, U6: Carboniferous, U10: Cretaceous, U11: Paleogene, U12: Undifferentiated Neogene and Quaternary.

Figure 4.11: Depth map showing the present-day subsurface position and morphology of the top of each stratigraphic unit of horizons 1 - 6: A) H1- Precambrian Top, B) H2- Cambrian Top, C) H3- Ordovician Top, D) H4- Silurian Top, E) H5- Devonian Top, F) H6- Carboniferous Top. Depth maps were constructed based on seismic interpretations, through interpolations in Petrel 2015 E&P Software (®Schlumberger).

Figure 4.12: Depth map showing the present-day subsurface position and morphology of the top of each stratigraphic unit of horizons 7 - 12: A) H7- Permian Top, B) H8- Triassic Top, C) H9- Jurassic Top, D) H10- Cretaceous Top, E) H11- Paleogene Top, F) H12- Neogene and Quaternary Top (Topography). Depth maps were constructed based on seismic interpretations, through interpolations in Petrel 2015 E&P Software (®Schlumberger).

Figure 4.13: Isopach maps showing the thickness distribution of units 1 to 6: A) U1- Cambrian, B) U2- Ordovician, C) U3- Silurian, D) U4- Devonian, E) U5- Carboniferous, F) U6- Permian. Isopach maps were constructed based on the difference between unit bounding depth maps in Petrel 2015 E&P Software (®Schlumberger).

Figure 4.14: Isopach maps showing the thickness distribution of units 7 to 11: A) U7- Triassic, B) U8- Jurassic, C) U9- Cretaceous, D) U10- Paleogene, E) U11- Neogene and Quaternary.

Thickness maps were constructed by calculating the difference between unit bounding depth maps in Petrel 2015 E&P Software (®Schlumberger).

Fig. 4.15: Erosion Map showing the amount of Permo–Triassic erosion from 250-220 Ma. Calculated based on the maximum thickness of the Permian and Triassic units (Figs. 4.13F & 4.14A) and considering uniform deposition.

Figure 4.16: Facies maps showing lithology distribution of units 1 to 6: A) U1- Cambrian, B) U2- Ordovician, C) U3- Silurian, D) U4- Devonian, E) U5- Carboniferous, F) U6- Lower Permian (preserved). Facies maps were constructed using the drilled lithologies in each well and unit (see Table 1).

Figure 4.17: Facies maps showing lithology distribution of units 7 to 11: A) U7- Triassic, B) U8- Jurassic, C) U9- Cretaceous, D) U10- Paleogene, E) U11- Neogene and Quaternary. Facies maps were constructed using the drilled lithologies in each well and unit (see Table 1).

Fig. 4.18: The black line shows the evolution of the mean temperature at 24° South from the Carboniferous until the present using the integrated PetroMod database (Wygrala, 1989).

Figure 4.19: Heat flow and temperature history for Model 1: constant heat flow (black line), temperature evolution through time (blue line), rapid burial and no erosion.

Figure 4.20: Maturity at El Caburé and Arbol Blanco boreholes for Model 1: constant heat flow and no erosion.

Figure 4.38: Transformation ratio (TR%) calculated for the Devonian unit using kerogen Tegelaar Type II Oklahoma (Woodford shale) (Tegelaar & Noble, 1994).

Figure 4.39: Transformation ratio (TR%) calculated for the Silurian unit using kerogen Abu-Ali Type II Quasiba (Silurian shale) (Tegelaar & Noble, 1994).

Figure 4.40: Transformation ratio (TR%) vs. time for A) Arbol Blanco, B) Campo Gallo, and C) El Caburé boreholes. The brown line shows TR for Devonian potential source rock using "Devonian Oklahoma" type II kinetics. The green line shows TR for Silurian potential source rock using "Silurian Qusaiba" type II kinetics (Tegelaar & Noble, 1994).

Figure 4.41: Vitrinite reflectance map of the Devonian unit.

Figure 4.42: Vitrinite reflectance map on the Silurian unit.

Resumen de tesis (español)

Capítulo 1: Introducción

La presente tesis se desarrolló en el marco del Grupo de Trabajo 3 (Modelado de Cuencas) del proyecto binacional StRATEGy (*Superficial Processes, Tectonics and Georesources: The Andean Foreland Basin of Argentina*), financiado por CONICET y DFG (Deutsche Forschungsgemeinschaft) y se localiza específicamente en la llanura Chacoparanaense en las provincias de Chaco, Formosa, Salta. El objetivo principal fue comprender la interacción espaciotemporal entre tres cuencas sedimentarias superpuestas de distinta edad y ambiente depositacional: a) la Cuenca neógena del Antepaís Andino, b) la Cuenca cretácica del *Rift* de Salta y c) la cuenca paleo-mesozoicos de la Cuenca Chacoparanaense. Mediante el análisis de datos de subsuelo, se buscó elucidar la estructura de los volúmenes sedimentarios subyacentes de la Llanura Chacopampeana y su impacto en la definición de recursos geológicos con potencial económico, poniendo especial foco en el Alto Quirquincho, una estructura basamental enterrada clave.

Las cuencas de antepaís constituyen archivos geológicos fundamentales, ya que sus secuencias sedimentarias registran la compleja interacción entre los procesos orogénicos (subsidencia tecto-sedimentaria y carga flexural), climáticos (variabilidad, patrones de erosión) y depositacionales. Además, pueden ser cruciales por su potencial en la formación y almacenamiento de recursos hidrocarburíferos. El antepaís andino, como un sistema de retroarco vinculado con la subducción de la Placa de Nazca, exhibe dos estilos estructurales principales: a) el continuo o ininterrumpido, caracterizado por la clásica secuencia de

depozonas, desde el orógeno hacia el antepaís: el *wedge top* que incluye las cuencas ubicadas sobre el frente de deformación; el *foredeep* o zona de subsidencia principal; el *forebulge* o zona de abombamiento periférico; y el *backbulge* o depocentro más distal extenso y somero, todas las zonas asociadas a la migración de la onda flexural; y b) el discontinuo o compartimentalizado, disectado por alzamientos de basamento constituidos por núcleos cristalinos por la acomodación del acortamiento de intraplaca a través de la reactivación de estructuras de basamento heredadas (e.g., el Sistema Santa Bárbara en el noroeste argentino). Si bien el antepaís compartimentalizado a menudo se ha asociado con la subducción de placa de bajo ángulo (e.g., Sierras Pampeanas), se considera que en la región de estudio la compartimentalización se explica de forma más viable por la inversión de estructuras extensionales heredadas del *Rift* de Salta.

Con la finalidad de analizar e interpretar estos objetivos, la tesis concentra los esfuerzos en el estudio del subsuelo de la Llanura Chacopampeana, una región con mínima actividad tectónica superficial, mediante un conjunto de datos de 120 perfiles sísmicos 2D (~3655 km) y 18 pozos de exploración que fueron reorganizados, adecuadamente digitalizados desde su formato original y articulados en una plataforma georreferenciada. El interés central es el análisis tectónico del Alto Quirquincho (QH), una elevación de basamento estratégicamente ubicada en la intersección de las cuencas de Salta *Rift*, Chacoparanaense y Andina. La correcta caracterización del funcionamiento de los altos de basamento contribuye con la exploración petrolera y de otros recursos económicos, ya que las estructuras, límites y evolución de los volúmenes sedimentarios asociados influyen directamente en la migración de depocentros y en el control de los sistemas hidrocarburiferos.

La investigación se guió por los siguientes dos conjuntos principales de preguntas. El primer conjunto (abordado en el Capítulo 3) se enfoca en la caracterización tectónica y geológica de los altos: determinar la morfología y el momento de alzamiento del Alto Quirquincho, identificar los mecanismos geológicos que causaron el movimiento vertical, evaluar su efecto en la distribución sedimentaria en las cuencas adyacentes y establecer el vínculo espaciotemporal con el Alto Pampeano-Chaqueño dispuesto subparalelamente en una posición más oriental.

El segundo conjunto (abordado en el Capítulo 4) se centra en el potencial de hidrocarburos de la Cuenca Chacoparanaense, una región menos estudiada considerada de "frontera exploratoria". Para ello, se buscó a) establecer su historia térmica vinculada con su soterramiento a través del modelado de cuencas (*basin modelling*), b) evaluar la madurez y el potencial de generación de hidrocarburos, y c) determinar si algunas secuencias pueden ser consideradas como un objetivo de recursos y reservorios no convencionales.

Finalmente, esta tesis proporciona una contribución significativa al entendimiento tectosedimentario del antepaís andino, al dilucidar la estructura enterrada y los aspectos depositacionales heredados del subsuelo del noroeste argentino, a través de una rigurosa interpretación sísmica y la integración de datos de pozo. Esto permite establecer una visión de la evolución geológica de las cuencas Chacopampeanas desde el Paleozoico temprano hasta el presente, y evaluar su potencial económico históricamente subestimado, en línea con las perspectivas tecnológicas de explotación no convencional.

Capítulo 2: Marco Geológico

Este capítulo establece el contexto geográfico y geológico regional de las características superficiales y de subsuelo de la Llanura Chacopampeana y las historias geológicas de las cuencas involucradas.

La Llanura Chacopampeana y su Subsuelo

La Llanura Chacopampeana es una extensa planicie de baja altitud. Está drenada en el área estudiada por el Río Bermejo, uno de los sistemas fluviales más grandes del sector andino argentino, caracterizado por un tramo entrelazado cerca del frente montañoso y un tramo meandriforme más distal en la llanura. Superficialmente, la región está cubierta por una capa delgada y continua de depósitos loessicos y fluviales cuaternarios (Formación Pampa). Este sector ha recibido sedimentos andinos desde el Eoceno medio, aunque en la actualidad se caracteriza por un almacenamiento o transferencia transitoria de sedimentos, con subsidencia y tasas de sedimentación limitadas, controladas por el nivel de base Atlántico.

Bajo esta cubierta cuaternaria se encuentran sedimentos más antiguos asociados a múltiples depocentros de distintas edades y separados por altos estructurales del basamento. Aunque la información superficial sugiere que la llanura ha sido poco afectada por el acortamiento neógeno-reciente, el subsuelo guarda una vasta historia tectónico-sedimentaria. Para su estudio es imprescindible el uso de datos geofísicos y de pozo para evaluar la deformación en el subsuelo.

Cuenca Chacoparanaense: Evolución Intracratónica y Registro Sedimentario

La Cuenca Chacoparanaense es una extensa cuenca intracratónica con orientación NNE que se extiende hacia Brasil y Paraguay. Su origen se remonta a un *rift* proterozoico, y su desarrollo continuó a lo largo del Paleozoico y Mesozoico, compartimentalizada por altos o dorsales, es el resultado de múltiples eventos geológicos, incluyendo la Orogenia Pampeana (Paleozoico), subsidencia y alzamiento de hombros de *rift* (Mesozoico) y la inversión cenozoica impulsada por la compresión andina. La cuenca se generó principalmente por procesos termales intracratónicos asociados al margen suroeste de Gondwana. La exploración petrolera, que comenzó en la década de 1950, ayudó a establecer su marco estratigráfico, aunque el nivel de información sigue siendo muy bajo.

El basamento cristalino subyacente representa una amalgama de terrenos cratónicos acrecionados durante la consolidación del Gondwana, donde se destaca el lineamiento Transbrasiliano, que posiblemente delimita la frontera entre el terreno Pampia y el cratón Río de la Plata, y que estaría asociado a zonas de debilidad mecánica que guiaron la deformación. Además, estudios geofísicos sugieren la posición de un Moho poco profundo y una composición dominantemente félsica de la corteza.

El registro sedimentario de la región estudiada se distribuye en tres grandes eventos tectosedimentarios: Paleozoico, Mesozoico y Cenozoico.

El evento Paleozoico (Precámbrico Tardío-Pérmico) comienza de forma discordante sobre el basamento y refleja una larga historia tectosedimentaria. Al respecto, se distinguen tres ciclos sedimentarios separados por discordancias angulares:

a) El primer ciclo lo constituyen los depósitos más antiguos del hemigraben de Las Breñas (metasedimentos del Precámbrico tardío-Paleozoico temprano). Incluye sedimentos marinos (Cámbrico-Ordovícico) de plataforma (ej., Formaciones Árbol Blanco, Pirané, Las Breñas).

b) El segundo ciclo (Silúrico-Devónico) se inicia con diamictitas (Formación Zapla) que pasan a sedimentitas marinas profundas (Formación Copo).

c) El tercer ciclo (Carbonífero-Pérmico) es predominantemente continental, con depósitos glaciolacustres que incluyen sedimentitas negras ricas en materia orgánica (Formaciones Sachayoj, Charata, Chacabuco).

El evento Mesozoico (Cretácico-Paleoceno): representado por secuencias enteramente continental y clástica, dominada por sedimentos cretácicos con areniscas rojas fluviales (Formación Buena Vista y Tacuarembó). La Formación Mariano Boedo (Cretácico tardío-Paleoceno) marca una transición hacia un ambiente de plataforma somera y lagunar.

El evento Cenozoico (Eoceno-Cuaternario): contituido por la Formación Chaco (Eoceno-Mioceno temprano) dispuesta sobre una posible discordancia erosiva, consistente en areniscas de planicie aluvial. El Mioceno medio registra una transgresión marina mayor

(Formación Paraná) seguida por una regresión (Formación Entre Ríos). Finalmente, los sedimentos cuaternarios (Formación Pampa) son depósitos eólicos y fluviales.

Cuenca de *Rift* de Salta: *Rift*, Subsidencia y Compresión Andina

La Cuenca de *Rift* de Salta (Cretácico-Paleógeno) está ubicada en el noroeste argentino y se desarrolló como una zona de extensión asociada al desmembramiento Gondwanico vinculado con la apertura del Océano Atlántico. Posee una forma de "Y" y se divide en las subcuencas Tres Cruces, Lomas de Olmedo y Metán-Alemanía, siendo las dos últimas relevantes para el presente estudio. El Grupo Salta representa el registro sedimentario clave, dividido en tres subgrupos que documentan su evolución tecto-sedimentario que cesó con el incremento del acortamiento andino.

a) Subgrupo Pirgua (Sin-*Rift*, Cretácico temprano): Consiste en capas rojas, areniscas y basaltos confinados a los grabens y hemigrabens, con una fuerte influencia del relieve controlado por fallas.

b) Subgrupo Balbuena (Post-*Rift*, Maastrichtiano-Paleógeno temprano) constituido por secuencias tabulares como resultado de la subsidencia térmica temprana, que solapan los flancos de falla. Incluye areniscas (Formación Lecho), carbonatos (Formación Yacoraite) y pelitas oscuras (Formación Olmedo/Tunal). La Formación Yacoraite es de alto interés económico por sus características de roca madre/reservorio.

c) Subgrupo Santa Bárbara (Post-*Rift* final, Paleógeno tardío): Representa la etapa final con baja tasa de subsidencia termal, compuesto por areniscas finas y pelitas verdes (Formaciones Mealla, Maíz Gordo y Lumbrera).

La deformación cenozoica en el Sistema Santa Bárbara refleja una progresión diacrónica hacia el este que invirtió preferencialmente las estructuras extensionales cretácicas. Existe cierta controversia sobre el momento exacto de la transición del régimen extensional al compresivo: a) por un lado se sugiere un inicio temprano del acortamiento (Paleógeno) que explica la sedimentación del Subgrupo Santa Bárbara como subsidencia flexural; mientras b) por otro lado se postula que el mecanismo dominante durante el Paleógeno fue la subsidencia térmica por enfriamiento cortical, ubicando la primera secuencia relacionada con la orogenia andina alrededor del Eoceno medio (después de 49 Ma.). La conservación de la geometría original en gran parte de la subcuenca de Lomas de Olmedo apoya esta última hipótesis, destacándose la influencia de las heterogeneidades corticales heredadas que se reactivaron durante la compresión.

Capítulo 3: Interpretación Sísmica – Evolución de los Altos de Basamento

Este capítulo presenta la metodología y los resultados de la interpretación sísmica, cruciales para desentrañar la evolución morfoestructural del Alto Quirquincho (QH) y el Alto Pampeano-Chaqueño (PCH), estructuras enterradas bajo la Llanura Chacopampeana que separan las Cuencas de *Rift* de Salta y Chacoparanaense. La falta de afloramientos

superficiales obligó a basar la investigación en una extensa base de datos de 120 perfiles sísmicos 2D (~3.655 km) y datos de 18 pozos de exploración. La metodología incluyó: a) la construcción de dos transectas principales (Norte, ~750 km; y Sur, ~500 km) (Figuras 3.2, 3.3, y 3.4), b) la elaboración de un modelo de velocidad general para la conversión tiempo-profundidad (Figura 3.12), y c) el uso de técnicas de aplanamiento de horizonte (*horizon flattening*) para la restauración palinspástica (Figura 3.5). La interpretación permitió definir cinco horizontes marcadores (H1 a H5) y cinco unidades sísmicas (U1 a U5), desde el Basamento Precámbrico (H1) hasta el Cuaternario (U5).

Interpretación Sísmica y Rasgos Estructurales

Los resultados sísmicos revelaron que los Altos Quirquincho y Pampeano-Chaqueño son elementos basamentales topográficos elevados de gran extensión, orientados NE-SO. El Alto Quirquincho, más extenso y con una pendiente de ~ 0.9 % en sus flancos oriental y occidental, muestra que las unidades Paleozoicas (U1) están truncadas en su tope (H2), lo que indica una discordancia. Las unidades Cretácicas (U2) y Paleógenas (U3) exhiben terminaciones de solapamiento (*onlap*) contra los flancos del alto, adelgazándose hasta desaparecer sobre su cresta (Figuras 3.3, 3.5B, 3.9 y 3.15). Este patrón depositacional y la ausencia de depósito o la baja sedimentación sobre el alto, visibles en los mapas isopáquicos (Figura 3.14B y 3.14C), sugieren que el QH se mantuvo como un rasgo topográfico positivo durante el Cretácico y el Paleógeno. La distribución del espesor de la unidad Paleozoica (U1) sugiere incluso que el QH fue una zona de depositación durante el Paleozoico, lo que cambió drásticamente en el Mesozoico debido al alzamiento.

De manera similar, el Alto Pampeano-Chaqueño muestra un adelgazamiento de las unidades Paleozoicas y Cretácicas. En este alto, los reflectores Cretácicos (U2) están plegados y truncados por una discordancia (Figura 3.3), lo que indica un control tectónico activo durante su depositación y posterior denudación antes de la acumulación del Paleógeno.

Ambos altos fueron completamente cubiertos por los sedimentos Neógenos (U4) y Cuaternarios (U5), que muestran una geometría tabular, lo que marca el cese de la actividad tectónica de los altos.

En cuanto a la cuenca de *rift* de Salta adyacente, las transectas revelan claras estructuras extensionales. El depocentro Metán-Alemanía (Transecta Sur) está delimitado por fallas normales N-S que cortan todas las unidades y que posteriormente fueron invertidas durante el Cuaternario por la compresión andina (Figura 3.4). El depocentro Lomas de Olmedo (Transecta Norte), limitado por fallas E-O, no muestra una inversión tectónica significativa en el Cenozoico. Finalmente, el aplanamiento del horizonte Neógeno (H5) documenta una cuña sedimentaria de engrosamiento hacia el oeste (Figura 3.5D), la geometría típica de la Cuenca de Antepaís Andino, que es el sistema depositacional final.

Modelos Conceptuales y Tectónica Heredada

La integración de las terminaciones de los estratos y las variaciones de espesor permiten descartar una generación cenozoica de los altos como abultamientos (*forebulges*) de la Orogenia Andina, ya que los sedimentos Neógenos y Cuaternarios no presentan deformación en su posición subhorizontal original. La evidencia apunta a un origen paleo-tectónico en el

Paleozoico tardío, probablemente causado por la Orogenia Gondwánica (Figura 3.16). Bajo este escenario, el QH y el PCH representarían paleo-abultamientos formados por la carga flexural durante la migración del frente de deformación Gondwánico. El QH sería el abultamiento principal, y el PCH un segundo menos pronunciado, coherente con la morfología, el tiempo de alzamiento (truncamiento de U1) y las relaciones transgresivas de las unidades posteriores (U2 y U3).

Esta interpretación pone de manifiesto la importancia de la herencia cortical. Mientras que el antepaís Gondwánico (Paleozoico) tuvo un estilo continuo y flexural, el Andino (Cenozoico) en esta latitud desarrolló un estilo roto o compartimentalizado (deformación de piel gruesa). Este cambio se debe a que la fase extensional Mesozoica (*Rift* de Salta) introdujo fallas y heterogeneidades que actuaron como zonas de debilidad, las cuales fueron posteriormente reactivadas e invertidas por la compresión andina cenozoica, determinantes de la geometría y estilo de la deformación final del antepaís.

En conclusión, la morfología y las relaciones estratales de los Altos Quirquincho y Pampeano-Chaqueño son rasgos heredados del Paleozoico tardío que persistieron como elementos topográficos positivos durante los ciclos extensionales del Mesozoico y fueron finalmente sepultados por la cuña sedimentaria Neógena-Cuaternaria. La identificación de estas estructuras es de interés para la exploración, ya que las terminaciones de *onlap* del Cretácico (U2) contra el QH tienen potencial para la formación de trampas de hidrocarburos.

Capítulo 4: Modelado de Cuencas de la Cuenca Chacoparanaense

El Capítulo 4 tiene como objetivo principal la reconstrucción temporal de la evolución geológica de la Cuenca Chacoparanaense mediante el modelado dinámico progresivo (*forward modelling*) de cuencas utilizando programas específicos (PetroMod), para evaluar su potencial de recursos hidrocarburíferos.

El modelo estructural 3D, construido a partir de 12 horizontes interpretados en un área de 56.150 km^2, reveló una historia de subsidencia compleja. La interpretación sísmica detallada confirmó la existencia del hemigraben de Las Breñas (Precámbrico tardío, invertido en el Devónico) y claramente, una discordancia angular mayor entre el Pérmico y el Cretácico, marcada por la ausencia de sedimentos Triásicos y Jurásicos, lo que coincide espacialmente con el Alto Quirquincho (Capítulo 3). Esta discordancia se interpretó como resultado de un significativo episodio de alzamiento y erosión Permo-Triásico (Figura 4.15).

La historia térmica del subsuelo se simuló bajo seis escenarios geológicos, calibrados con mediciones de reflectancia de vitrinita (% Ro) de pozos. Los modelos iniciales, sin incluir una unidad sedimentaria extra, Permo-Triásico erosionada (Modelos 1 y 2) o sin un pico de flujo de calor (Modelos 1 y 3), subestimaron la madurez observada. Esto sugirió que tanto un enterramiento más profundo como un aporte térmico extra fueron necesarios para alcanzar la madurez actual. Los Modelos 4, 5 y 6, que combinaron la presencia de los sedimentos erosionados con un pico de flujo de calor elevado, lograron una buena correlación con los datos medidos. El Modelo 4 (pico de flujo de calor de 88 mW/m^2 en el Permo-Triásico y

erosión en el Triásico temprano) se seleccionó como el escenario más consistente. Esto permite vincularlo con el máximo enterramiento asociado con el pico térmico del evento termal Permo-Triásico regional propuesto por otros autores y con el alzamiento del Alto Quirquincho. El análisis del Rango de Transformación (*Transformation Ratio*, TR) *vs.* tiempo corroboró que la generación de hidrocarburos debió ocurrir principalmente durante el máximo enterramiento, coincidente con el evento termal Permo-Triásico, sin generación posterior o actual significativa.

La evaluación del potencial de hidrocarburos se enfocó en las unidades Paleozoicas con potencial de roca madre: Carbonífero, Devónico y Silúrico. El análisis integrado de la Madurez, el TR y el Carbono Orgánico Total (TOC) arrojó resultados consistentes. La unidad Carbonífera resultó ser térmicamente inmadura y con TR insignificante, careciendo de capacidad generadora. La unidad Devónica mostró madurez de ventana de petróleo a gas húmedo temprano (0.6 - 1.2% Ro) y valores de TOC moderados (0.4 - 0.6 % *wt*), lo que apoya un potencial convencional modesto y potencial para sistemas híbridos a partir de fuente-reservorio no convencionales. La unidad Silúrica se presentó como el objetivo más prometedor para la exploración no convencional: alcanzó la etapa de sobremadurez (2.0 % Ro) y valores de TR cercanos al 100% en gran parte de la cuenca, lo que indica que generó extensamente gas seco. A pesar de su sobremadurez, la presencia de TOC residual (0.5 % *wt*) y espesores significativos (hasta 1.500 m) en las zonas NO y E del área estudiada sugiere que la unidad tiene potencial como reservorio no convencional de *shale gas* o *tight gas* debido al gas adsorbido, especialmente en el contexto de la alta madurez que pudo generar microfracturas naturales. Si bien el potencial convencional es limitado, la cuenca

Chacoparanaense retiene un significativo potencial no convencional subexplorado, concentrado principalmente en el intervalo Silúrico.

Capítulo 5: Conclusiones

Esta tesis confirmó que bajo la aparentemente monótona Llanura Chacopampeana subyace una rica historia geológica que se remonta al Precámbrico tardío. Esta evolución compleja incluye procesos extensionales localizados seguidos por subsidencia regional, sedimentación marina y continental, erosión, y deformación de longitud de onda larga. La evolución tectosedimentaria de la región estudiada involucró tres cuencas sedimentarias distintas y dos altos de basamento heredados, con el Alto Quirquincho el más relevante. Sus características Paleozoicas y Mesozoicas han influido en el desarrollo subsiguiente del antepaís andino Cenozoico, destacándose la influencia duradera de las estructuras geológicas heredadas.

Mediante la reinterpretación de una extensa base de datos de líneas sísmicas que fue vectorizada y articulada en plataformas georreferenciadas, informes de pozos y registros, se pudo reconstruir la historia geológica del subsuelo, con especial énfasis en la formación del Alto Quirquincho. Morfológicamente, el Alto Quirquincho se extiende con una longitud parcial NE-SO de ~470 km entre ~115 km y ~190 km de ancho, y una inclinación de su cresta de ~0.9 % en su flanco noroeste. El Alto Pampeano-Chaqueño, más pequeño (~60 km de ancho y ~160 km de largo parcial), presenta pendientes similares (~1%).

Las interpretaciones sísmicas confirman que el Alto Quirquincho ya estaba elevado en el Mesozoico temprano y persistió como un rasgo topográfico positivo hasta el Paleógeno, a

partir del cual los estratos comenzaron a solaparse en su tope. Se concluye que el levantamiento del Alto Quirquincho, junto con el Alto Pampeano-Chaqueño influenciado por debilidades corticales heredadas de la sutura Pampia-Río de la Plata, fue causado principalmente por la flexura por abultamiento de la corteza en el antepaís de los Andes Ancestrales durante la Orogenia Gondwánica (Paleozoico tardío al Mesozoico temprano).

El modelado de cuencas permitió refinar la evolución temporal. Se determinó que la sedimentación en la cuenca Chacoparanaense fue continua desde el Precámbrico tardío hasta el Triásico temprano cuando parte de ella emergió, experimentando erosión en el Triásico. Este episodio erosivo, seguido por un período de quiescencia tectónica y un hiato, marcó la transición de un ambiente depositacional marino a uno continental para el Cretácico.

Durante el Cretácico, la Cuenca de *Rift* de Salta se formó en el lado opuesto del Alto Quirquincho como parte del régimen extensional asociado a la apertura del Atlántico Sur. Esta fase de *rift* se caracterizó por fallamiento normal seguido de subsidencia térmica *post-rift* hasta el Paleógeno. El acortamiento andino Neógeno subsiguiente provocó la inversión estructural de las fallas normales del graben en los depocentros Metán-Alemanía y Tres Cruces. Sin embargo, la ausencia de una inversión significativa en el depocentro Lomas de Olmedo, más distal, y en los Altos Quirquincho y Pampeano-Chaqueño, se atribuye a la localización de la deformación andina en las fallas del *Rift* de Salta, lo que facilitó el desarrollo de un estilo tectónico de piel gruesa (*thick-skinned*) y la formación del sistema de antepaís compatimentalizado (*broken foreland*) de Santa Bárbara. En consecuencia, el estilo de antepaís continuo y flexural de la orogenia Gondwánica fue reemplazado por un antepaís roto

Cenozoico, debido a la superposición de condiciones geodinámicas cambiantes y la reactivación compresional de provincias extensionales previas.

La presencia de los altos de basamento heredados influyó en la distribución de sedimentos a largo plazo: el Alto Quirquincho interrumpió la continuidad de la cuenca Paleozoica, separando la Cuenca Tarija de la Chacoparanaense. La erosión de los altos en el Mesozoico temprano proporcionó material, y el Alto Pampeano-Chaqueño segmentó aún más los depocentros cretácicos dentro de la Cuenca Chacoparanaense. El modelado de cuencas confirmó la importancia de la discordancia erosiva Permo-Cretácica, que eliminó una parte significativa de las unidades Permo-Triásicas hacia el Alto Quirquincho. El período de máximo enterramiento coincidió con un pico de flujo de calor asociado a la anomalía térmica Permo-Triásica a lo largo del margen occidental de Gondwana, incrementando la madurez en la cuenca.

La evaluación integrada de madurez térmica, Rango de Transformación (TR) y TOC demostró que las unidades Carboníferas y superiores son inmaduras y no son rocas madre viables. La unidad Devónica exhibe madurez moderada y limitado potencial orgánico, siendo de interés económico solo en intervalos específicos. En contraste, la unidad Silúrica muestra las características más prometedoras: alta madurez (2% Ro), TOC residual significativo (0.5% *wt*) y gran espesor (hasta 1.500 m) en los sectores NO y E. Esta unidad representa un objetivo viable para la exploración de gas de pizarra (*shale gas*) no convencional, siempre que la mineralogía (zonas frágiles ricas en cuarzo) y las condiciones estructurales para la estimulación sean favorables.

A pesar que se considera que la Cuenca Chacoparanaense no es un prospecto convencional prometedor, los estratos Silúricos merecen una exploración detallada por su potencial no convencional. Los resultados de este estudio brindan nuevos conocimientos sobre las estructuras enterradas y la influencia de la herencia estructural, como el Alto Quirquincho, en el desarrollo tanto de los estilos de antepaís continuo como de antepaís compartimentalizado.

Chapter 1. Introduction

This thesis was developed within Work Package 3 of the bi-national and co-funded project StRATEGy, under the auspices of CONICET Argentina and the German Science Foundation (DFG). StRATEGy is the acronym for Surface Processes, Tectonics and Georesources: The Andean Foreland Basin of Argentina. Work Package 3 of the StRATEGY project concentrates on Basin Modelling and focuses on the northern Argentine section of the Andean foreland basin.

In this section, I introduce the relevance and the main objective of the thesis. I discuss the state of knowledge concerning geological investigations that have been carried out in the study area, the reasons for its selection, and the scientific questions that arose and were addressed in the following chapters. This introductory note is followed by a brief description of the general approach and organisational structure of the dissertation.

1.1. Andean foreland basin: state of the art

A profound understanding of active foreland basins is crucial because these regions that straddle the border between the flanks of major mountain belts and the adjacent foreland are important archives that provide rich stratigraphic and lithologic information on the interplay between orogenic and climatic processes, as they receive sediments from these regions of high topography and relief. Over time, foreland basins subside due to tectono-sedimentary loading along the developing mountain ranges, creating large accommodation space for sediments and ensuing protracted subsidence (De Celles, 2011).

Major thrust belts, such as the Andes and the Himalayas, exert a major influence on atmospheric circulation, rainfall distribution and the evolution of fluvial networks, and ultimately, Earth's climate (Molnar *et al.*, 1993; Grujic *et al.*, 2006; Strecker *et al.*, 2007; Bookhagen & Strecker, 2008). The sedimentary sequences of foreland basins thus constitute important archives that store unique data on climate variability, erosion patterns, process-rate changes, and exposure history (e.g., De Celles, 2011). In addition, foreland unconformities in non-collisional, Andean-type orogens can provide insights into hiatus duration and extent (Horton et. al, 2022) and the lateral extent of foreland deformation. Importantly, these basins not only contain archives that reflect orogenic and climatic evolution, but they are also sites for the formation, migration and storage of hydrocarbons as well as other resources (e.g., Llanos basin, Campos & Mann, 2015, Garcia Bautista *et al.*, 2015; Maracaibo basin, Stauffer, *et al.*, 1995, Escalona & Mann, 2006, Mann, 2006; Magdalena Valley basin, Sarmiento & Rangel, 2004, Spickert, 2014; Neuquén basin, Howell *et al.*, 2005, Barredo & Stinco, 2014). These basins are even recorders of lateral, foreland-directed fluid flow from the orogen and the emplacement of metalliferous resources, as documented in the Paleozoic Appalachian foreland basin (e.g., Oliver, 1986).

Taken together, foreland basins, a term coined by Dickinson (1974), constitute sedimentary accumulations of substantial thickness in generally undeformed regions (forelands) adjacent to deforming orogens as a result of compressional tectonism and crustal stacking (García-Castellanos & Cloetingh, 2011). As a result, the formation of foreland basins additionally involves flexural isostatic subsidence in response to increasing orogenic loading (Price, 1973).

Foreland-basin systems include depositional areas on continental crust located behind major fold-and-thrust belts (De Celles, 2011); these can be located in a retroarc realm, in collisional geodynamic settings, or they may be associated with non-collisional subduction zones, such as the retroarc of the Andes. Retroarc thrust belts (Fig. 1.1) typically evolve in truly convergent plate-tectonic settings, where fixed points on each plate converge relatively rapidly (e.g., Heuret and Lallemand, 2005; Schellart, 2008). Foreland basins in retroarc settings may span continental spatial scales, extending thousands of kilometres parallel and hundreds of kilometres perpendicular to adjacent orogenic belts. Such a setting is exemplified by the Cenozoic Andean foreland basin system (De Celles, 2011).

The Andean-type margin of South America underscores the close genetic association between thrust belts and convergent margins (Price, 1973; Dickinson, 1974; De Celles, 2011). These basins can be broadly classified as continuous/unbroken or realms of broken, formerly contiguous sectors, where spatially limited uplifts have subdivided and modified the fluvial network and modified sediment-transport and depositional patterns (Fig. 1.2). Foreland basins therefore differ in morphology and the characteristics of major sediment-routing systems, but both foreland-basin types ultimately result from a protracted compressional stress field and associated shortening.

Continuous/unbroken foreland basins, as described by De Celles and Giles (1996), involve four depozones: wedge-top, foredeep, forebulge and backbulge, reflecting different local kinematic and subsidence conditions. The wedge-top depozone comprises sedimentation on the

active frontal part of the thrust belt, including piggy-back basins; these settings are characterised by textural immaturity and growth structures (De Celles & Giles, 1996; García-Castellanos & Cloetingh, 2011). The forebulge depozone consists of sediments deposited in the flexural 'moat' formed by thrust-belt loading and shows the greatest subsidence (Price, 1973; Jordan, 1981). Toward the foreland, the forebulge represents flexural uplift and is usually characterised by stratal condensation, disconformities or soil development (DeCelles and Giles, 1996). The backbulge depozone, which follows the forebulge, is characterised by shallow environments related to secondary flexural subsidence. Forebulge and backbulge sediments and morphological features associated with them are not always preserved. This series of depozones creates a flexural waveform in the foreland that decreases by up to three orders of magnitude from the forebulge to the backbulge (DeCelles, 2011).

Continental-scale thrust belts and foreland systems, such as the Andes, exhibit flexural profile wavelengths in the range of 500 km to 1000 km, with the foreland basin potentially migrating a distance greater than half its wavelength over (e.g., Flemings and Jordan, 1989; Sinclair *et al.*, 1991; Waschbusch & Royden, 1992; Blisniuk *et al.*, 1998; Cardozo & Jordan, 2001; DeCelles & DeCelles, 2001; Cloetingh *et al.*, 2004; Chase *et al.*, 2009). This migration can be gradual or episodic and results in the vertical stacking of depozones in the stratigraphic record, which aids in the interpretation of thrust-belt propagation and shortening rates (Flemings & Jordan, 1989; Coakley & Watts, 1991; Sinclair *et al.*, 1991; Verges *et al.*, 1998; Burkhard & Sommaruga, 1998). The duration of the forebulge disconformity/condensation zone can be used to infer the rate and nature of flexural wave migration and its time span involving several to tens

of millions of years (DeCelles, 1994; Ford *et al.*, 1997; Williams *et al.*, 1998; Lawton *et al.*, 1999; Chiang *et al.*, 2004; Demko *et al.*, 2004; del Papa *et al.*, 2010; De Celles, 2011).

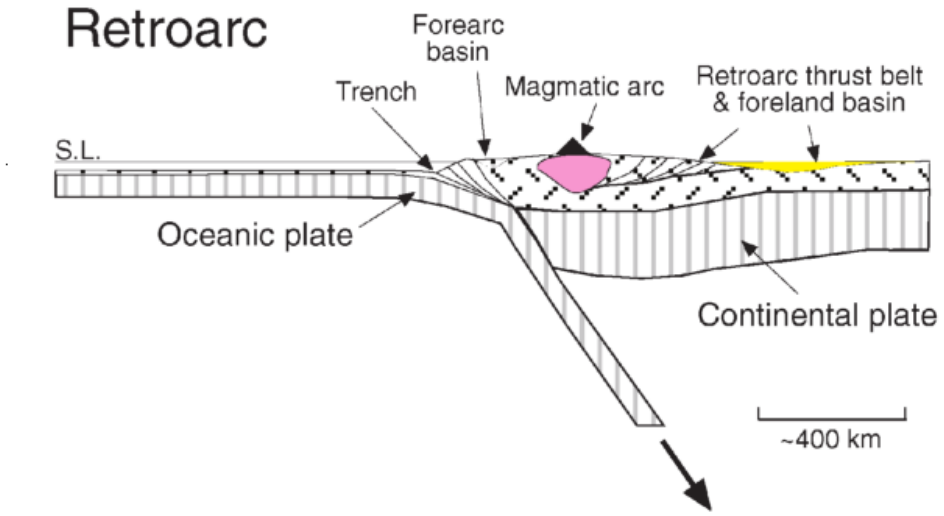

Figure 1.1: Simplified Andean retroarc thrust belt setting and foreland basin system. Modified from De Celles (2011).

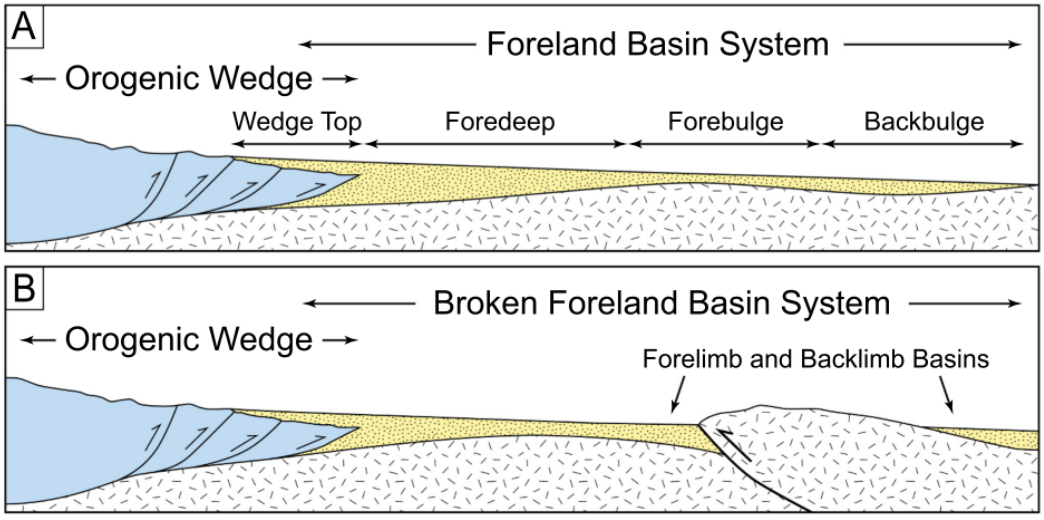

Figure 1.2: Schematic cross-sections comparing (A) a contiguous (unbroken) foreland basin (after DeCelles and Giles, 1996) with (B) a broken foreland basin. Taken from Horton *et al.* (2022).

Broken foreland basins, which are compartmentalised by positive topographic features, generally associated with basement-cored range uplifts, differ significantly from contiguous foreland basins (Horton *et al.*, 2022). Broken-foreland basins form where retroarc convergence is primarily accommodated along reactivated high-angle basement structures, resulting in temporally and spatially uneven rock uplift and isolated areas of limited longitudinal extent (Jordan & Allmendinger, 1986; Hilley *et al.*, 2005; Strecker *et al.*, 2011).

Unlike continuous foreland basins, broken foreland basins lack well-developed foredeep, forebulge and backbulge systems (Strecker *et al.*, 2011). Instead, they are controlled by isolated topographic loading and structural tilting associated with widely spaced crustal-scale reverse faults that accommodate intraplate basement shortening, often associated with reactivated inherited crustal heterogeneities (e.g., Marshak *et al.*, 2000; Hain *et al.*, 2011; Lacombe & Bellahsen, 2016; Arnous *et al.*, 2024).

In retroarc systems, basin compartmentalisation has often been associated with flat-slab subduction zones (e.g., Bird, 1984; Gutscher *et al.*, 2000; Liu *et al.*, 2008; Martinod *et al.*, 2010; Eakin *et al.*, 2014; Wagner *et al.*, 2017; Axen *et al.*, 2018; Bishop *et al.*, 2018; Horton, 2018). Flat subduction has been inferred to influence the architecture of the modern Andes of South America and the US Rocky Mountains during the late Cretaceous–Paleogene Laramide orogeny (Coney & Reynolds, 1977; Dickinson & Snyder, 1978; Constenius, 1996; Bird, 1998; Ramos *et al.*,

2002; Dickinson, 2004; Ramos, 2009; Ramos & Folguera, 2009; Carlotto, 2013; Yonkee & Weil, 2015; Horton *et al.*, 2022). However, as pointed out by Kley *et al.* (1999; 2005), the formation of broken foreland basins is not solely dependent on flat-slab subduction. This has also been emphasized by Hongn *et al.*, (2010) and Ammirati *et al.* (2022), who invoked reactivated orogenic structures related to tectonic deformation in the geologic past to explain the isolated range uplifts of these regions.

Similarly, Horton *et al.* (2022) proposed two circumstances that favor the development of broken-foreland basins. First, inherited anisotropies and zones of weakness from preceding geological processes, including pre-existing structural, stratigraphic, rheological, and thermal properties. Second, specific orogenic driving mechanisms, such as elevated stress, long-distance stress transfer, and/or crustal strengthening or weakening within intraplate regions that may trigger distributed shortening in the foreland.

As pointed out above, in the Cenozoic Andes, morphotectonic provinces such as the Sierras Pampeanas (Fig. 1) have been considered as broken forelands that are associated with the flat-slab subduction of the Nazca Plate at this latitude (e.g., Cahill & Isacks, 1992; Portner *et al.*, 2020; Rodríguez *et al.*, 2021). These authors also propose a broken-foreland concept adjacent to the Santa Bárbara System morphotectonic province of NW Argentina, approximately between 24° and 27° South, but this foreland region is not underlain by a flat slab segment of the subducting Nazca Plate; instead, it appears more viable that compressional tectonic stresses are large enough in the foreland and the neighbouring Eastern Cordillera (Fig. 1) to the west

(Figueroa *et al.*, 2021) causing inherited zones of weakness to fail during focused reactivation along favorably oriented anisotropies (e.g., Iaffa *et al.*, 2011; Barcelona *et al.*, 2014; Arnous *et al.*, 2024).

These conclusions are also supported by DeCelles (2011), who stated that foreland-basin systems located on flexed continental lithosphere are sensitive to the reactivation of inherited basement structures. In this context, structural fabrics associated with ancient cratonic structures and pre-existing rift margins, for example, are particularly susceptible to reactivation (Schwartz & DeCelles, 1988; Bradley & Kidd, 1991; Meyers *et al.*, 1992; Crampton & Allen, 1995; Blisniuk *et al.*, 1998; Gupta & Allen, 2000; Zaleha *et al.*, 2001; Londoño & Lorenzo, 2004).

In the Central Andes, between 15° and 35° S, retroarc topography, deformation, and deposition are the result of the combined effects of convergence between the oceanic Nazca and the continental South American plates, influenced by the geometry of the subducting oceanic slab (Barazangi & Isacks, 1976; Bevis & Isacks, 1984; Ramos *et al.*, 2002; Pons *et al.*, 2023), but also by the effects of reactivated basement heterogeneities under the Cenozoic compressional stress field (e.g., Kley and Monaldi, 2005). North of 24° South, the subducting plate exhibits a relatively steep dip of about 30°, transitioning to a subhorizontal geometry between 26° and 27° South (Cahill & Isacks, 1992).

Between 15° and 27°S, the Andean Cordillera includes the wide and high-altitude Altiplano-Puna Plateau (Fig. 1), which is bordered to the east by the Eastern Cordillera; in northernmost Argentina and Bolivia, this morphotectonic province is followed by a thin-skinned

foreland fold-and-thrust belt (Fig. 1) and a continuous foreland farther east (e.g., Jordan *et al.*, 1983). Conversely, in NW Argentina, this deformation style disappears and gives way to thick-skinned deformation within the Santa Bárbara (24°-27°S) and the Sierras Pampeanas (27°-33°S) ranges (Allmendinger *et al.*, 1983; Jordan *et al.*, 1983; Mon & Salfity, 1995). In the Santa Bárbara region the uplifts are intimately associated with compressionally reactivated, primarily inherited structures from the Cretaceous Salta Rift Basin (Mon & Salfity, 1995; Del Papa *et al.*, 2013; Zapata *et al.*, 2020).

The sedimentary depositional system in the foreland of NW Argentina consists of variably connected, partially separated depocenters that are delineated by basement uplift along reactivated faults. In contrast to the continuous foreland basin system of the sub-Andean fold-and-thrust belt to the north, this region lacks a deep and extensive foredeep and has only subdued back and forebulge areas (Strecker *et al.*, 2011). Deformation at these latitudes is highly disparate, resulting in variable storage and accumulation of sediments (Bossi & Palma, 1982; Strecker *et al.*, 1989, 2009; Hilley *et al.*, 2005; Carrapa *et al.*, 2009). Here, flexural basins occur adjacent to individual ranges and are of limited spatial extent compared to foreland depocenters in continuous foreland basins (Hilley *et al.*, 2005).

Zapata *et al.* (2020) proposed a four-stage model of tectonic evolution for NW Argentina from the Cretaceous to the Pliocene. This model considers extensional tectonics during the Cretaceous (120–75 Ma), the subsequent formation of a broken foreland basin between 55 and 30 Ma due to compressional inversion of normal faults, and reheating during the Miocene (18–

13 Ma) caused by burial of basement blocks below more than 2 km of sediments. Finally, the tectono-sedimentary evolution was dominated by deformation, exhumation, and surface uplift during the late Miocene and Pliocene (13–3 Ma). Their model also challenges earlier correlations between broken foreland and flat-slab subduction, suggesting that the causative mechanism for uplift and compartmentalization rather stems from reactivated inherited extensional structures now inverted by Cenozoic shortening.

1.2. Research topic and principal research questions

To the east of the broken foreland involving the Santa Bárbara System, the Andean foreland basin constitutes an apparently monotonous plain (Fig. 1.3) characterised by Quaternary sedimentation with minimal recent tectonic activity visible at the surface (Ramos *et al.*, 2006). However, beneath this surficial layer of recent sediments lie the vestiges of a complex structural and sedimentological history revealed by subsurface data (Russo *et al.*, 1989; Chebli *et al.*, 1999). The integration of different methodologies, including the analysis of seismic reflection data and borehole information, plays a key role in unravelling both the current landscape and the complex past events of foreland-basin evolution in northern Argentina.

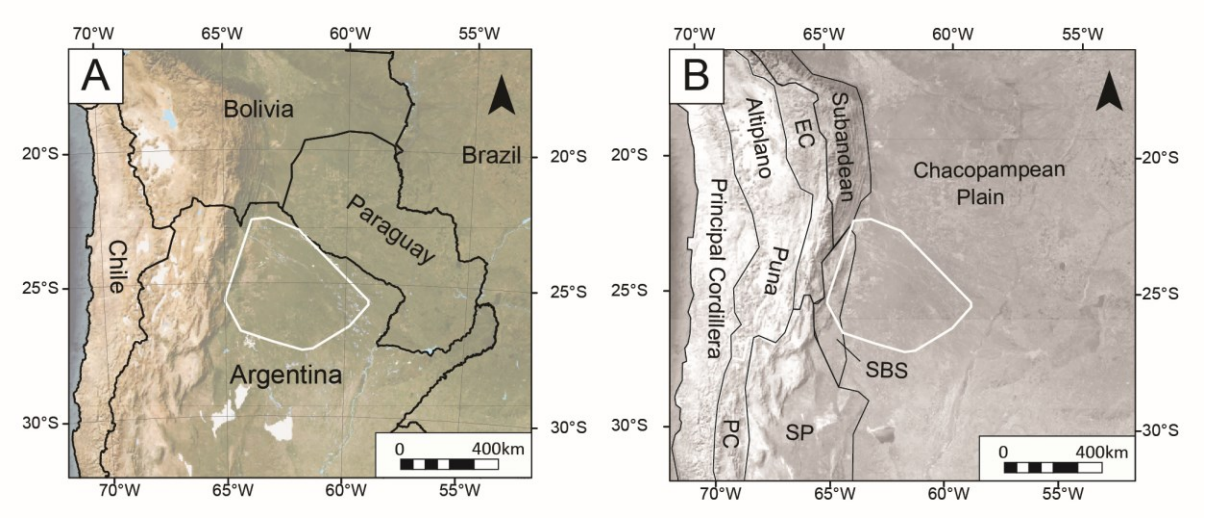

Figure 1.3: Location of the study area (white polygon). A) Relief map and political boundaries. B) Shaded relief map and principal morphotectonic provinces of the southern Central Andes (after Jordan *et al.*, 1983). Santa Barbara System, SBS; Sierras Pampeanas, S. Pampeanas; Frontal and Precordillera, Pre-Cord.

In this thesis, a comprehensive analysis was carried out using a unique data set comprising 120 2D seismic surveys (approximately 3655 km) and 18 exploration boreholes within the Chacopampean Plain, which is an integral part of the present-day Andean foreland morphotectonic province. The focus on this area emerged from an initial review of the available data, including the Quirquincho High, a higher elevation, yet buried sector within subsurface units located between the intracratonic Chacoparanaense Basin (Paleozoic to Cenozoic) to the east and the Salta Rift Basin (Cretaceous to Paleogene) to the west and northwest (Fig. 1.4). Although previously mentioned by various authors (e.g., Russo *et al.* 1979, Chebli *et al.* 1999), this subsurface structure has remained poorly researched and understood in terms of its age, effect on sedimentary basin evolution, and its influence on the formation of geological resources.

The main objective of this study is to comprehend the relationship and spatiotemporal interaction between three adjacent sedimentary basins of different age — namely, the Andean

foreland basin, the Salta Rift basins, and the Chacoparanaense Basin (Fig. 1.4). These basins, characterized by distinct genetic mechanisms and different ages, play a crucial role in understanding the evolution of the current contiguous foreland and the adjacent broken foreland of the Santa Bárbara System and associated sediment-routing systems. Furthermore, the study aims to elucidate the subsurface structure beneath the Chacopampean Plain and its impact on the distribution of valuable economic resources.

The key area in the study area is the Quirquincho High (Fig. 1.4), strategically positioned between the Chacoparanaense and Salta Rift basins and intersected by the Andean foreland deposits, thus serving as a nexus that links these geological entities.

A basement high is a general term for topographic, bathymetric, and/or geological features within a region where some or all of the rocks are higher than those of the same age in the surrounding areas (Blake *et al.*, 1978; Dickinson, 1979; Peacock & Banks, 2020). These phenomena are named basin highs when they are located in a sedimentary basin, but they are also considered basement highs if the basement rocks are higher than in the surrounding areas. The Quirquincho High constitutes both, a basin and a basement high.

Peacock & Banks (2020) highlight that basement highs have received much attention, mainly from the petroleum industry, due to recent reservoir discoveries in and around them, such as on the Utsira High, Norwegian Continental Shelf (e.g., Olsen *et al.* 2017; Riber *et al.* 2015); the Rona Ridge, UK Continental Shelf (e.g., Trice, 2014); Bach Ho “buried hill”, offshore SE

Vietnam (e.g., Cuong & Warren, 2009), and the Zeit Bay field fractured basement, Egypt (El Sharawy, 2015).

These studies also point out how important it is to properly characterise basement highs, to describe their structure, boundaries, flanks, and to determine the history of depositional environments of the surrounding sedimentary units and their onlap and offlap relationships. A close inspection of these characteristics is needed to elucidate the timing of tectonic and sedimentary processes and their rates, to determine whether the High developed before, during or after the adjacent strata, and to unravel the sequence of events that have modified the basement High through time. Combined, such an analysis may constrain uplift and sedimentary processes that were either triggered by local forces associated with diapirism (Ziegler & Dezes, 2007) or regional effects associated with plate-tectonic processes at distant plate boundaries (Miller & Mitra, 2011). The origin and tectonic setting of any basin high should be incorporated into the characterization of basin evolution because the process(es) that created the High may have influenced other geological processes in adjacent areas (Merewerher & Cobban, 1986; Bruhn *et al.*, 1986), including sedimentation, migration of depocenters, the initiation of erosion in source areas, and those that control petroleum systems (e.g., Peacock & Banks, 2020 and references therein).

After collecting seismic and borehole data from northern Argentina to develop a robust database for my analysis, I delineated the study area in detail (Fig. 1.3), strategically including information that adequately represented the Andean foreland, Salta Rift, and Chacoparanaense basins (Fig. 1.4), with the Quirquincho High as the center, while excluding tectonically inverted

areas in the Andean orogen *sensu stricto*. During the preparation for this study, the existence and importance of another significant basement High emerged. This High is the Pampeano-Chaqueño High located within the Chacoparanaense Basin (Fig. 1.4) and it has similarities, albeit on a smaller scale, compared to the Quirquincho High. In light of these considerations concerning the causes, consequences, and spatial patterns of uplift in basement-high regions, several specific research questions can be identified that guided my work and that helped to design a research strategy; this strategy included the analysis of topographic, geophysical and borehole data in the regions of the Quirquincho and Pampeano-Chaqueño highs, which are presented in Chapter 3 (cf. 1.3):

- What is the morphology of the Quirquincho High?
- When did the Quirquincho High region start to be uplifted?
- What geological mechanisms caused vertical tectonic movements in this region?
- How did the existence of this basement High affect the distribution of sediments and the formation of depocenters in the Chacoparanaense and Salta Rift sedimentary basins?
- What is the spatiotemporal link between the Quirchincho and Pampeanao-Chaqueño highs?

Once the overall research questions regarding the geological and tectonic characterisation of both highs were identified, their potential influence on hydrocarbon systems was evaluated and addressed in a follow-up study. Oil companies have explored and exploited the neighbouring Salta Rift Basin hydrocarbon systems for several decades. The original database has remained largely confidential, making correlations between that region and the basement highs in the foreland farther east difficult. In contrast to the well-studied Salta Rift, the

Chacoparanaense Basin, considered a frontier exploration basin (Fernandez Garrasino *et al.*,2015; Reinante *et al.*,2014), has not been extensively studied, and gaps in our understanding of the geological evolution and hydrocarbon potentials exist. Despite the confidential nature of the vitrinite reflectance calibration information, YPF S.A. expressed interest in a research project that addresses these issues and, therefore, kindly provided data to further study this basin and its evolution.

Combined, and particularly concerning the generation of hydrocarbons, the evolution of the Chacoparanaense Basin with its Quirchincho High lends itself to rigorous analysis and thus the formulation of several overarching critical research questions that form the basis for the second part of the study, which is presented in Chapter 4 (cf. section 1.3):

What was the thermal and burial history of the basin?

Are there levels mature enough, and with sufficient organic matter, to produce hydrocarbons?

Can the Chacoparanaense Basin be considered an unconventional reservoir?

To answer these questions, I performed basin modelling of a representative, smaller area (Fig. 1.4) with a maximum density of wells, which allowed a detailed structural model to be derived and calibrated in combination with available seismic surveys.

Basin modelling is a quantitative geological method used to simulate the evolution of sedimentary basins over geological time (e.g., Welte *et al.*, 1997; Allen and Allen, 2005; Hantschel

& Kauerauf, 2009). It involves the construction of mathematical models based on geological data to understand various processes such as sedimentation, burial, compaction, thermal history, hydrocarbon generation, and migration within sedimentary basins (Welte *et al.*, 1997; Hantschel & Kauerauf, 2009; Bjørlykke, 2010; Jing-Zhou Zhao *et al.*, 2019). This technique enables characterising the geohistory of a sedimentary basin over time and evaluating its economic resources, such as hydrocarbon potential. This information could allow a large basin such as the Chacoparanaense to be classified as a potential target, comparable to other sedimentary basins within the Cenozoic Andean foreland in other sectors of the orogen, such as the Llanos basin in Colombia and the Maracaibo basin in Venezuela (Macellari, 2025), and the Magdalena Valley basin in Peru (Mathalone & Montoya, 1995).

In summary, this thesis was designed to provide a significant contribution to our understanding of foreland basins by elucidating the structure and inherited aspects of the extensive Andean foreland basin in NW Argentina, focusing in particular on the Quirquincho and Pampeano-Chaqueño highs in the subsurface of the gently sloping present-day Chacopampean plain. The study provides unprecedented insights and results in the context of a detailed investigation of buried structures and paleo-geomorphic conditions as well as their influence on the evolution of sedimentary basins, spanning the early Paleozoic to the present-day. This expanded state of knowledge was achieved through extensive seismic interpretation using 3655 km of seismic reflection lines and the integration of borehole data from 18 wells. Moreover, this thesis evaluates the burial and thermal history of the Chacoparanaense Basin, an area that has historically received limited attention due to the lack of surface exposures and the scarcity of

economically viable hydrocarbon discoveries during the 20th century (Fernández Garrasino *et al.*, 2005; Reinante *et al.*, 2014). As such, this evaluation is in line with current technological perspectives regarding unconventional hydrocarbon exploitation.

1.3. Workflow and structure of the dissertation

The thesis is divided into 5 chapters. The core of the thesis comprises chapters 3 and 4, and the general conclusions presented in Chapter 5. Chapter 3 addresses the first set of scientific questions and was developed in an areally extensive study area; this part deals with the integration of data and the evolving relationships between the three basins and the influence of the Quirquincho and Pampeano-Chaqueño highs with respect to sedimentary evolution (Fig. 1.4). Chapter 4, focuses on the Chacoparanaense Basin; this part addresses the second set of scientific questions that motivated this research while addressing a smaller, yet representative area of the foreland, which is exemplary with regards to the open questions that exist in foreland-basin assessments outlined above (Pages 25–31); the subsurface database for this section is a dense network of seismic reflection and borehole data (Fig. 1.4).

Below, I provide a brief description of the workflow that guided me in answering the identified research questions. A more detailed account of the individual methods is provided in the method section in Chapters 3.2 and 4.1.2.

The backbone of this study is the interpretation of all available, good-quality seismic surveys and other geophysical databases in the area. Due to the lack of outcrops in the gently sloping surface area, the combination of a rigorous seismic interpretation and correlated borehole data was fundamental to the development of this thesis and to answering the research questions. I mainly performed interpretations on 2D seismic surveys, but with a 3D approach. I generated velocity models from sonic surveys in boreholes and shot points available on the seismic lines. Velocity models allowed the seismic interpretation to be translated from its original time domain to a depth conversion of the imaged units. Once the depth domain had been established, I produced depth and thickness maps of the units of interest for both parts of the thesis. Importantly, these maps allowed the present position and distribution of the ancient sedimentary units to be located in a 3D framework to create structural models.

Chapter 3 focuses on the analysis of the structural model, the relationships between basins and highs, constraining the timing, and elucidating the mechanisms of the formation of the highs. It was possible to construct two 2D transects that image the distribution of sediments in the three basins very well, which show relevant stratigraphic terminations and lateral pinch-outs. The available data illustrate the position and stratigraphic relationships of the highs, and which strata are imaged in the adjacent basins. Two transects and the construction of depth and thickness maps enabled constraining the timing of the tectonic activity associated with the evolution of the highs, thus providing important information regarding the tectonic mechanisms that account for these uplifted features.

In Chapter 4, I focused on the Chacoparanaense Basin; here, I was able to exploit the dense network of borehole information and seismic reflection lines. The resulting more detailed structural model of this smaller area confirms the observations and interpretations made in the context of the more general structural model. Calibration data were integrated, and the basin model was developed, discussing six main models and the hydrocarbon potential of the basin in the most probable scenario.

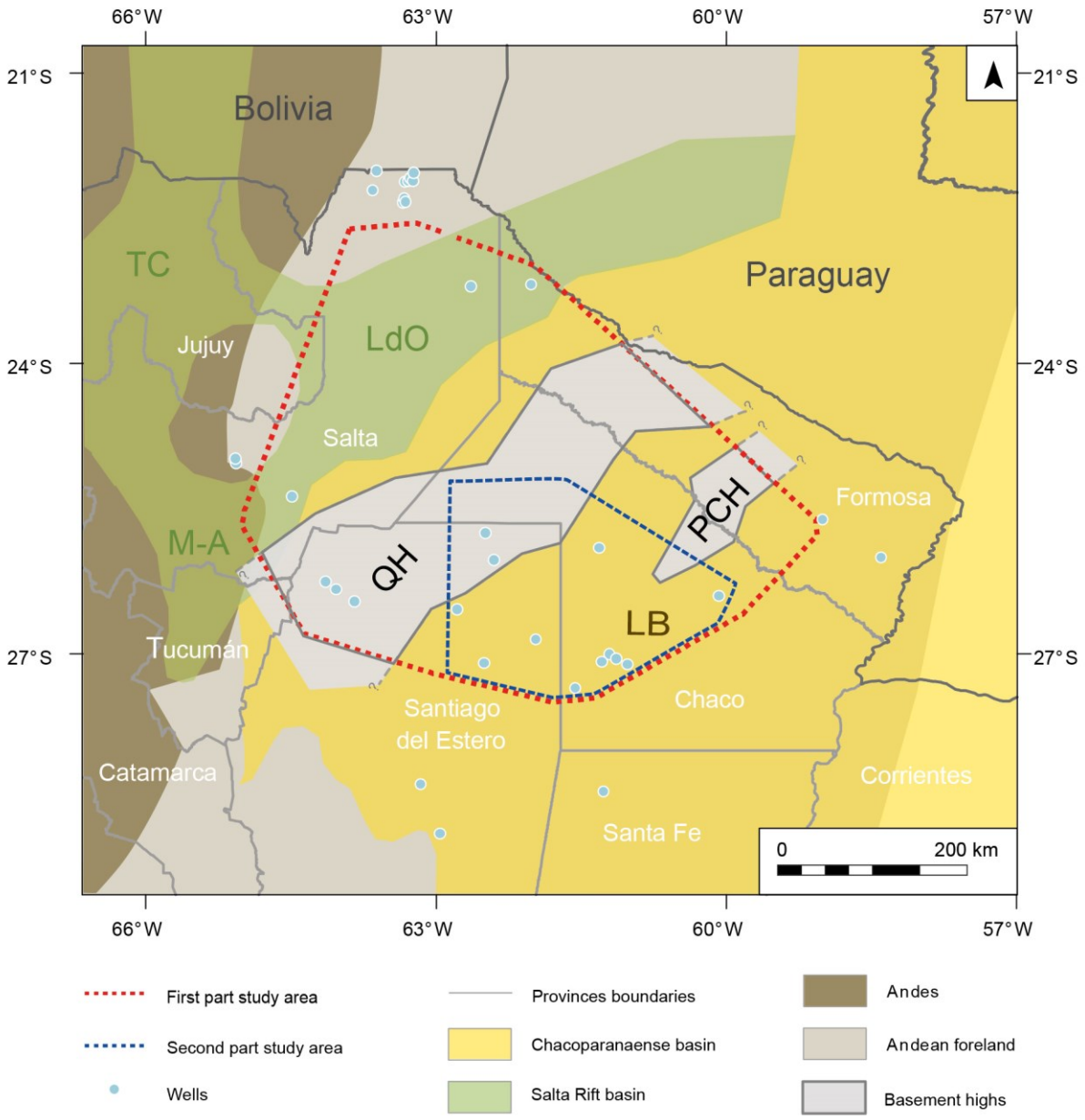

Figure 1.4: Province boundaries, location of the study area for Chapter 3 (red) and Chapter 4 (blue) in the Andean foreland and the outline of the buried Cretaceous sedimentary basins. TC Tres Cruces depocenter, LdO, Lomas de Olmedo depocenter, M-A, Metán-Alemanía depocenter; LB: Las Breñas depocenter; QH: Quinquincho High; PCH: Pampeano-Chaqueño High.

Chapter 2: Geological setting

2.1. Chacopampean Plain

The Chacopampean Plain is an areally extensive lowland located close to sea level in the east and at up to 500m elevation in the immediate vicinity of the Andean orogen to the west. The region is currently drained by the Rio Bermejo and its upstream tributaries, one of the largest drainage areas in the Andean realm of Argentina. In the lowland sector, the Rio Bermejo is more than 1300 km long and drains into the Rio Paraguay. In the upper 300 km, close to the Andean mountain front, the river is braided, the remainder is primarily characterized by a meandering geometry. The Chacopampean Plain is covered by a thin, but continuous layer of Quaternary loessoid and fluvial deposits that cover several sedimentary sub-basins of different ages and geological histories (Russo *et al.*, 1979). The Chacopampean Plain is an integral part of the present-day Andean foreland basin (Fig. 1.4) and has received sediments from the uplifting Andes since the middle Eocene (Carrapa *et al.,* 2012; del Papa *et al.,* 2013), but at present the main processes that characterize this region are either transient sediment storage or transfer of sediments from the Andean orogen to the Atlantic Ocean, with limited subsidence and a low sedimentation rate (Russo *et al.*, 1979; Chebli *et al.*, 1999; Repasch *et al.*, 2021).

Beneath the veneer of Quaternary foreland-basin deposits are older sediments that are associated with several depocenters of different geological ages and that are separated by structural highs (Russo *et al.*, 1979; Chebli *et al.* 1999). This is also the case in the study area,

where parts of the Chacoparanaense and Salta Rift basins are buried under the Quaternary cover sediments.

The available surface information of deformation associated with compressive Neogene to recent tectonics of the Andes and their foreland, suggests that this region has hardly been affected by shortening (Chebli *et al.*, 1999), although closer to the Andean mountain front there is evidence for neotectonic activity that appears to be linked with inverted Cretaceous extensional structures (e.g., Ramos *et al.*, 2006), but it is possible that other sectors of the foreland are also affected by deep-seated structures such as blind faults that have not reached the surface yet (Arnous *et al.*, 2024). Therefore, to assess the degree of tectonic deformation farther away from the Andean mountain front it is necessary to additionally employ geophysical and borehole data to probe the subsurface for an evaluation of potential deformation phenomena within the basin strata.

2.2. Chacoparanaense Basin

The Chacoparanaense Basin is a large oval, NNE-trending part of the Andean foreland basin that extends northward into Brazil and Paraguay. The basin originated from a Proterozoic rift and continued to develop throughout the Paleozoic and Mesozoic, mainly as a result of deep-seated intracratonic thermal processes associated with the active south-western margin of Gondwana, which ultimately resulted in a compartmentalised basin with distinct depocenters (Reinante *et al.*, 2014).

Petroleum exploration in the Chacoparanaense Basin began in the 1960s, which helped establish the basic stratigraphic and structural framework of this part of the Andean foreland. By 1979, most of the subsurface information had been acquired, including 36 wells and 37.000 kilometres of 2D seismic lines. Most of this information was summarised by Russo *et al.* (1979) in a paper describing the tectonic events and the main stratigraphic and tectonic features of the region. Later, Chelbi *et al.* (1999) summarised the newest stratigraphic findings in light of the previous investigations. These authors also reviewed structural aspects and concluded that the "stratigraphic lineaments" of Russo *et al.* (1979) – synthesized in this chapter– are still correct and were later incorporated in the regional maps of Pezzi and Mozetic (1989). Fernandez Garrasino *et al.* (2005) and Reinante *et al.* (2014) updated these syntheses and reviewed the potential petroleum systems of the basin; they concluded that knowledge about the petroleum systems in the Chacoparanaense Basin is still speculative and the level of exploration is very low.

The general feature of the Chacoparanaense Basin is the broken basement with several depocenters bordered by highs or dorsals, uplifted as a consequence of different geological events, including the Paleozoic Pampean orogeny (e.g., Fernandez Garrasino *et al.,* 2005), Mesozoic subsidence and potentially rift-shoulder uplift (e.g., Fernandez Garrasino *et al.*, 2005), and Cenozoic basin inversion driven by Andean compression (e.g., Chelbi *et al.,* 1999; Ramos *et al.*, 2006).

2. 2. 1. Basement

As a result of tectono-sedimentary processes, most of the crystalline basement of the basin is currently overlain by sedimentary strata. Although some boreholes have penetrated the basement rocks (e.g., Marengo, 2015), the understanding of the intracrustal structure and composition has remained limited. Decades of multidisciplinary research, including geochemistry, paleomagnetism, and geochronology applied to borehole samples as well as the study of rock outcrops in the Andes that were combined with geophysical investigations, have shed light on the general tectonic evolution of the region and the complex history of the basement rocks; this also involved the study of xenoliths retrieved from deep boreholes in eastern Argentina and Uruguay (e.g., Rapela *et al.*, 2007).

The South American continent consists of an amalgamation of Archean to Proterozoic terranes that were accreted at its western margin during the Paleozoic (de Almeida *et al.*, 2000; Charrier *et al.*, 2015; Ramos, 1988). About 620 million years ago, during the formation of western Gondwana, the amalgamation of these terranes gave rise to the Transbrasiliano-Kandi mega-shear zone, which extends over 6,000 km in a NE-SW direction (Cordani *et al.*, 2013). In northern Argentina and Paraguay, the Transbrasiliano lineament, which is inferred to represent the southern extension of this shear zone, has been proposed to delineate the boundary between the Pampia terrane and the Río de la Plata craton (Cordani & Sato, 1999). However, the exact nature of this boundary and its level of activity through time remains controversial and is subject to ongoing discussion (e.g., Chernicoff & Zappettini, 2004; Peri *et al.*, 2013, 2015; Ramos *et al.*,

2010, Meessen *et al.*, 2018). In one of the recent geophysical studies, Meessen *et al.* (2018) identified a zone of low crustal density that spatially coincides with the Transbrasiliano lineament and viewed this characteristic to reflect the presence of mechanically weaker rocks that could have guided deformation processes.

Further geophysical insight into the intracrustal structure was provided by the PANDA and CHARGE seismic experiments, which investigated the vertical velocity structure of the Cuyania, Pampia and Famatinia terranes (Alvarado *et al.*, 2007). The latter authors inferred a predominantly felsic, quartz-rich composition for the Pampia terrane and the Río de la Plata craton based on low Vp and Vp/Vs ratios. While these inferences are consistent with basement outcrops of granites and migmatites in the Sierras Pampeanas (Mon, 1979; Simpson *et al.*, 2003), they contrast with observations from drill cores of the southern Río de la Plata craton as noted by Meessen *et al.* (2018). In addition, mafic rocks (gabbro and granodiorite) were identified as part of the plutonic crystalline basement in drill holes that reached the basement (Rapela *et al.*, 2007; Winn & Steinmetz, 1998).

Early seismic tomographic studies in South America indicated an average Moho depth beneath the Chacoparanaense Basin of 32 km (Snoke & James, 1997), which was corroborated by Assumpção *et al.* (2013) and Rosa *et al.* (2016), who reported Moho depths of approximately 28 km beneath the basin. Snoke and James (1997) characterised the upper mantle beneath the Chacoparanaense Basin as rather asthenospheric, with S-wave velocities of about 4.2 km/s. Assumpção *et al.* (2013) reported velocities between 4.3 and 4.2 km/s in the upper mantle

beneath the northwestern part of the basin, with higher shear wave velocities of 4.5 to 4.6 km/s in the southern region

Based on lithological, geochemical and geophysical data, Ibarra (2021) developed a gravity-constrained density model for the Chacoparanaense Basin with several units, including the crust beneath the Chacoparanaense Basin. In this region, the model is divided vertically into sediments, upper crust and lower crust. According to the bibliographic review carried out by the author and the model results, the sediments consist mainly of sandstones and shales, with a bulk density of 2450 kg/m³ and Vp between 3.1 and 5.1 km/s. The upper crust consists mainly of felsic metamorphic and igneous rocks with a bulk density of 2880 kg/m³ and Vp between 6.1 and 6.4 km/s. The lower crust potentially contains both felsic and mafic metamorphic and igneous rocks, with a bulk density of 3020 kg/m^3 and Vp between 6.7 and 6.9 km/s. Assuming that these densities are representative on a regional scale, the model predicts a relatively thin lower crust thickening towards the west (~5-15 km), which is consistent with the felsic nature of the crust suggested by Alvarado *et al.* (2007).

2. 2. 2. Sedimentary record

The sedimentary sequence in the Chacoparanaense Basin (Fig. 2.1) lies unconformably on the crystalline basement rocks, which is covered by deposits of different ages due to its original, structurally controlled irregular shape and paleo-topography (Russo *et al.*, 1979; Chebli *et al.*, 1999, Fernandez Garrasino *et al.*, 2005).

Russo *et al.* (1979) distinguished three main sedimentary cycles and related deposits during the Paleozoic: a Cambrian–Ordovician, a Silurian–Devonian, and the third, a Carboniferous–Permian cycle, separated by very distinct angular unconformities.

The oldest deposits in the basin are located in the Las Breñas halfgraben (Fig. 1.4) (Chebli *et al.*, 1999, Fernandez Garrasino *et al.*, 2005). This structure is an elongated asymmetric NE-SW-trending depression controlled by a large east-dipping normal fault that accommodated deposition of about 5 km of late Precambrian and early Paleozoic metasediments. The normal fault bounding the halfgraben was probably inverted before the Silurian (Chebli *et al.*, 1999).

The Cambrian–Ordovician strata of the first sedimentary cycle contain sediments from marine shelf environments (Russo *et al.*, 1979; Chebli *et al.*, 1999; and Fernández Garrasino *et al.*, 2005). Sedimentary rocks associated with this episode are the Árbol Blanco (Mingramm, 1966b), Pirané (Mingramm, 1965) and Las Breñas (Russo *et al.*, 1979) formations that are mainly comprised of quarzitic sandstones. Their stratigraphic position is below the Zapla Fm. of lower Silurian age and above the crystalline basement rocks (Russo *et al.*, 1979); in addition, these rocks correlate with similar units that are exposed in the sub-Andean ranges and the Cordillera Oriental (Chebli *et al.*, 1999).

The second sedimentary cycle, according to Russo *et al.* (1979), spans the time between the Silurian and Devonian. During this cycle the Zapla (Schlagintweit, 1943 in Mingramm & Russo,

1972), Copo, Caburé and Rincón formations were deposited (Padula *et al.*, 1967). The oldest unit in the sequence is a layer of diamictites from the Zapla Fm.; these deposits gradually transition into dark-grey, pyritic, laminated shales from the Copo Fm. That was deposited in a calm, relatively deep marine environment (Russo *et al.*, 1979). The units are superseded by fine, whitish-grey quarzitic sandstones of the Caburé Fm. and black shales of the Rincón Fm.

The Carboniferous and Permian rocks of the third sedimentary cycle (Russo *et al.*, 1979) include marine and non-marine deposits, although the marine deposits do not reach the study area in northern Argentina; here, the sediments are only continental. The deposits of this sedimentary cycle lie unconformably on crystalline basement, as well as Cambrian–Ordovician and Silurian–Devonian sedimentary strata (Russo *et al.* 1979). These relationships highlight the importance of the deformation events that preceded the Carboniferous–Permian sedimentation and the generation of paleo-topography. The strata associated with the Carboniferous–Permian cycle includs the Sachayoj, Charata (Mingramm, 1966a) and Chacabuco (Padula, 1972) formations. The cycle starts with sandstones and gradually progresses to black shales with high organic content (Fernandez Garrasino *et al.*, 2005).

Mesozoic

All of the Mesozoic sedimentary rocks of the Chacoparanaense Basin are continental and mainly of clastic origin (Fernández Garrasino *et al.*, 2005). The Mesozoic sediments in the Argentine part of the basin are predominantly Cretaceous in age. However, there may be also Triassic or Jurassic sedimentary rocks (Chebli *et al.*, 1999), yet due to the continental nature of

the units and lithological similarities, it is difficult to unambiguously identify individual Triassic and Jurassic units as has been done in Brazil and Uruguay (e.g., Veroslavsky, 2004). Here, I describe the complete Mesozoic stratigraphic sequence, based on the geological criteria outlined in the industry drilling reports (e.g., Rolleri, 1965; Rolleri, 1966; Rolleri, 1967; Bottcher, 1965; Bottcher, 1974; Di Persia, 1969; Di Persia, 1970; Moreno, 1973; Pluspetrol, 1990; Pluspetrol, 1995).

The Mesozoic strata begin with the Buena Vista Fm. (Russo *et al.*, 1979), composed of red quarzitic sandstones deposited in a braided fluvial system. These strata are superseded by the Tacuarembó Fm. (Falconier, 1931); the name of this unit has been widely and variably used in subsurface stratigraphic correlations to refer to different clastic continental units (Fernández Garrasino *et al.*, 2005). Consequently, the use of this formation name in drill reports is not always reliable. The Tacuarembó Fm. is interbedded with the mafic lavas of the Serra Geral Fm. of late Jurassic to early Cretaceous age (Mira *et al.*, 2015); correlative units are absent in the study area.

The youngest Mesozoic unit is the Mariano Boedo Fm. (Padula y Mingramm, 1968) of late Cretaceous—Paleocene age, which is in paraconformity with respect to the previous units. The Mariano Boedo Fm. begins with a basal conglomerate with basaltic clasts, followed by sandstones intercalated with shales and limestones towards the top. This unit marks the transition from a continental environment to a shallow-water platform environment and littoral lagoonal bodies, with some degree of marine influence (Fernández Garrasino *et al.*, 2005).

Cenozoic

The Mariano Boedo Fm. described above has a Paleocene age at its top. It is covered by the Eocene—early Miocene Chaco Fm. via an inferred erosional unconformity, which may have been associated with erosional processes during a pronounced regression at the end of the Paleocene (Russo *et al.*, 1979).

The Chaco Fm. begins with coarse sandstones at the base, followed by predominantly fine-grained sandstones, with fine interbeds of conglomerates, siltstones, and shales; micro- and cryptocrystalline gypsum occasionally cements the sandstones. This unit is sourced from continental deposits that accumulated in an extensive alluvial plain in a low-energy environment (Russo *et al.*, 1979).

In the middle Miocene, there was a major transgression in the Chacoparanaense Basin, followed by a regression in the upper Pliocene (Russo *et al.*, 1979). This sedimentary cycle is represented by the Paraná Fm. (transgressive) and the Entre Ríos Fm. (regressive). The Paraná Sea was shallow, warm, and covered almost the entire extent of the basin and even reached the location of the present-day Andean Cordillera Oriental (Russo *et al.*, 1979; Quattrocchio *et al.*, 2003). The Paraná Fm. consists of green shales with an abundance of marine invertebrates and microfossils (Chebli *et al.*, 1999). These strata are conformably overlain by the calcareous green sandstones of the Entre Ríos Fm. (Russo *et al.* 1979). Both formations have not always been identified in the drill boreholes and may have been eroded, and in some cases, they were reported to be part of the Chaco Fm. (Fernández Garrasino *et al.*, 2005).

The ubiquitous Quaternary sediments constitute the Pampa Fm. (Russo *et al.* 1979); they are mainly composed of loess and re-transported loess interbedded with fine to very fine sandstones. Calcareous concretions, fillings and veins of gypsum are also found in this unit of aeolian and fluvial origin (Fernández Garrasino *et al.*, 2005).

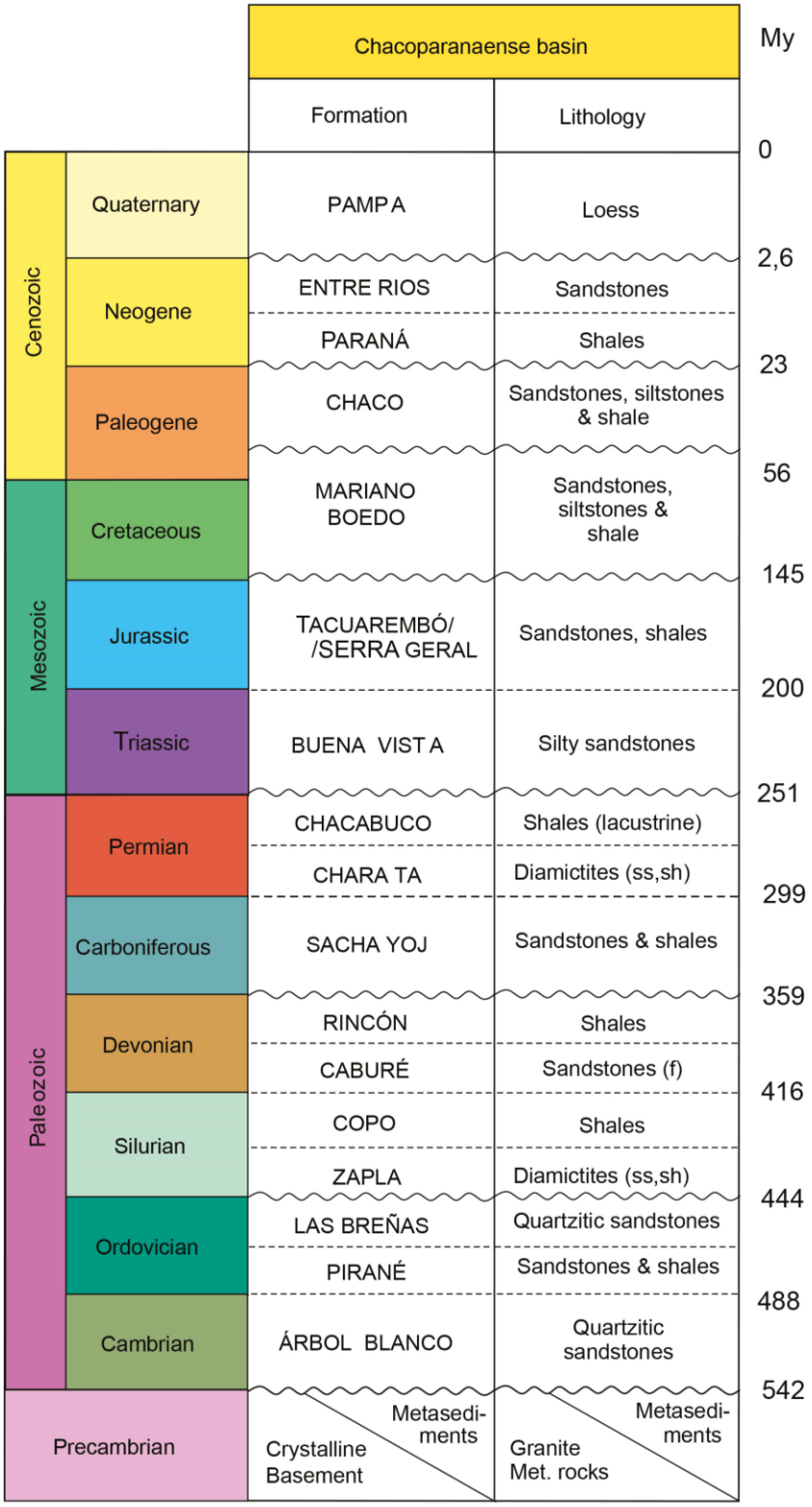
Chacoparanaense basin
My
Formation
Lithology
0
Cenozoic
Quaternary
PAMPA
Loess
2,6
Neogene
ENTRE RIOS
Sandstones
PARANÁ
Shales
23
Paleogene
CHACO
Sandstones, siltstones & shale
56
Mesozoic
Cretaceous
MARIANO BOEDO
Sandstones, siltstones & shale
145
Jurassic
TACUAREMBÓ/ /SERRA GERAL
Sandstones, shales
200
Triassic
BUENA VISTA
Silty sandstones
251
Paleozoic
Permian
CHACABUCO
Shales (lacustrine)
CHARATA
Diamictites (ss,sh)
299
Carboniferous
SACHA YOJ
Sandstones & shales
359
Devonian
RINCÓN
Shales
CABURÉ
Sandstones (f)
416
Silurian
COPO
Shales
ZAPLA
Diamictites (ss,sh)
444
Ordovician
LAS BREÑAS
Quartzitic sandstones
PIRANÉ
Sandstones & shales
488
Cambrian
ÁRBOL BLANCO
Quartzitic sandstones
542
Precambrian
Crystalline Basement
Metasedi-ments
Granite Met. rocks
Metasedi-ments

Figure 2.1: Lithostratigraphic column of the Chacoparanaense Basin. Formation named after Russo *et. al* (1979). Lithology after well reports from the study area (e.g., Rolleri, 1965; Rolleri, 1966; Rolleri, 1967; Bottcher, 1965; Bottcher, 1974; Di Persia, 1969; Di Persia, 1970; Moreno, 1973; Pluspetrol, 1990; Pluspetrol, 1995). Abbreviations: Ss: sandstones, Sh: Shales, f: fine.

2.3. Salta Rift Basin

The Cretaceous Salta Rift Basin is located in NW Argentina in the provinces of Salta and Jujuy and Formosa. The Salta Rift was a magmatically active zone of extension in the South American continental plate that was associated with the opening of the Atlantic Ocean (Starck, 2011).

The basin is "Y"-shaped and has three main depocenters or subbasins; these are the Tres Cruces sub-basin to the NW, the Metán-Alemanía sub-basin to the S, and the Lomas de Olmedo sub-basin to the E (Fig. 1.3). In this study, I address the Lomas de Olmedo and the eastern part of the Metán-Alemanía rift-basin infills of the Salta Group (Turner, 1959). The Salta Group is divided into 3 subgroups: The Pirgua subgroup (Reyes & Salfity, 1973), deposited during the syn-rift stage; the Balbuena subgroup (Moreno, 1970), and the Santa Bárbara subgroup (Moreno, 1970), both of the latter groups were deposited during the post-rift thermal subsidence stage (Fig. 2.2). The basin records sedimentation from the early Cretaceous to the Eocene.

The Salta Group is exposed in the Subandean ranges, the Eastern Cordillera, the northern Sierras Pampeanas and the Puna Plateau in the Andean interior (Fig. 1.1) (Salfity & Marquillas, 1994), whereas it is buried by foreland deposits in the Chacopampean Plain.

The basin evolved on heterogeneous basement rocks that span from the Precambrian to the Jurassic. The Precambrian units are metasediments of the marine Puncoviscana Fm. that was deposited at the western margin of Gondwana (Turner, 1960; Turner & Mon, 1979). The superseding Paleozoic sediments mainly correspond to fluvial, lacustrine, deltaic, and shallow marine facies and belong to strata that are associated with the Tarija Basin in Bolivia (e.g., Cediel *et al.*, 2003; Fuentes *et al.*, 2009).

During the early Cretaceous, several grabens and half-grabens opened in NW Argentina, initially isolated, and later connected (Starck, 2011). The syn-rift sediments of the Pirgua subgroup are confined to these basins and comprise conglomeratic red beds, sandstones, shales and interbedded rhyolites and basalts, dated at 82-75 Ma (Gallinsky & Viramonte, 1988). During the syn-rift phase, the distribution of sedimentary strata was strongly influenced by fault-controlled relief contrasts, causing narrow facies belts and pronounced lateral changes (Starck, 2011).

Between the Maastrichtian and the early Paleogene, the Balbuena subgroup was deposited, reflecting the early post-rift cooling and subsidence stage (Marquillas *et al.*, 2005). Thermal subsidence was the main mechanism, and the deposits show a tabular regional shape, onlapping the fault-bounded graben flanks. From bottom to top the Balbuena subgroup is composed of white sandstones (Lecho Fm.), yellow carbonates (Yacoraite Fm.) and dark pelites with evaporites (Olmedo/Tunal Fm.). The origin of the carbonates has been associated with marine settings, but a lacustrine origin has also been proposed (Mutti *et al.*, 2023, Vallati *et al.*, 2023). The Yacoraite

Fm. and its associated sandstones of the Lecho Fm. are of high economic interest because of mixed source rock/reservoir characteristics (e.g., Ruiz-Monroy, 2021).

During the late Paleogene, the sedimentary strata of the Santa Bárbara subgroup were deposited on the Yacoraite Fm., representing the final post-rift thermal subsidence stage; this episode was characterized by a low subsidence rate (Marquillas *et al.*, 2005). The sediments associated with this subgroup are fine red sandstones, siltstones and green shales of the Mealla, Maiz Gordo and Lumbrera formations.

The tectono-sedimentary cycle of the Salta Group ceased with the onset of Andean shortening (Cobbold *et al.*, 2007; Starck, 2011). The structural evolution during the Andean orogeny in the Santa Bárbara System and the adjacent foreland regions to the east reflects eastward-directed, diachronous deformation that inverted different parts of the structures that bound the Salta Rift (Jordan *et al.*, 1983; Coutand *et al.*, 2001; Kley & Monaldi, 2002; Oncken *et al.*, 2006; Carrera & Muñoz, 2008; Hain *et al.*, 2011; Arnous, 2021; 2024). The prograding stratigraphic relationships of the tectono-sedimentary cycles also vary in an eastward direction (Starck & Vergani, 1986). The interpretation of these tectono-sedimentary scenarios is furthermore supported by the presence of angular unconformities and an Eocene depositional hiatus (Reynolds *et al.*, 2000; Del Papa *et al.*, 2010).

The inherited tectonic structures, crustal heterogeneities and the strike of Cretaceous normal faults have strongly influenced the deformation style in the different sectors that correspond to the former rift. These crustal anisotropies dictated which extensional structures

of the Cretaceous–Paleogene sub-basins were preferentially reactivated during the compressional tectonic stress field of the Andean orogeny (Grier *et al.*, 1991; Allmendinger *et al.*, 1997; Kley & Monaldi, 2002; Carrapa *et al.*, 2005; Carrera *et al.*, 2006; Kley *et al.*, 2005; Iaffa *et al.*, 2011; Arnous *et al.*, 2024). For example, Cenozoic Andean deformation inverted the Tres Cruces sub-basin and most of the Metán-Alemanía sub-basin (e.g., Iaffa *et al.*, 2011; DeCelles *et al.*, 2011), leaving most of the Lomas de Olmedo sub-basin in its original geometry, although limited reactivation of structures has been reported from that area as well (Ramos *et al.*, 2006). In light of this, the end of the deposition of the Salta Group appears to have been diachronous, ending first in the west and later in the eastern foreland (Starck, 2011; Arnous *et al.*, 2024).

There is some controversy about the temporal characteristics of the transition between the activity of the Mesozoic extensional tectonic regime, with associated thermal subsidence, and the subsequent shortening and flexural subsidence that created the Cenozoic foreland basin. In this context, DeCelles *et al.* (2011) postulate an early onset of shortening that explains the sedimentation of the Santa Bárbara subgroup in terms of flexural subsidence, supported by the presence of a 'supersoil'/disconformity that these authors describe as having been associated with an early forebulge setting. The corresponding fold belt that was probably associated with this foreland basin system is thought to have been located in the Domeyko Range of Chile (Starck, 2011). This hypothesis would imply that a flexural foreland basin formed during the Paleocene and migrated at least 600 km eastward at an unsteady rate, forced by periods of abrupt eastward propagation of the orogenic deformation front (DeCelles *et al.*, 2011).

Starck (2011) estimated that sedimentation controlled by flexural subsidence was initiated during the deposition of the coarsening-upward cycle that formed the upper member of the Santa Bárbara subgroup. This would assign the first sequences related to orogeny to the middle Eocene, after 49 Ma. Before this event, however, the dominant subsidence mechanism during the Paleogene appears to have been essentially related to crustal cooling following the waning Cretaceous tectono-magmatic processes (e.g., Starck, 2011; Marquillas *et al.*, 2005). The latter hypothesis is supported by the spatial overlap between the formation of the Cretaceous graben system and the deposition of the Balbuena and Santa Barbara subgroups related to thermal subsidence centred on the locations of the extensional basins (e.g., Starck, 2011; Marquillas *et al.*, 2005). This situation is most evident in the Lomas de Olmedo sub-basin, but can also be seen in the rest of the Salta Rift Basin, such as at the western margin of the Metán-Alemanía sub-basin; here, post-rift units extend beyond the faults that bound the syn-rift strata, overlapping and pinching out westward over the normal-fault bounded basin flanks (Starck, 2011; Marquillas *et al.*, 2005).

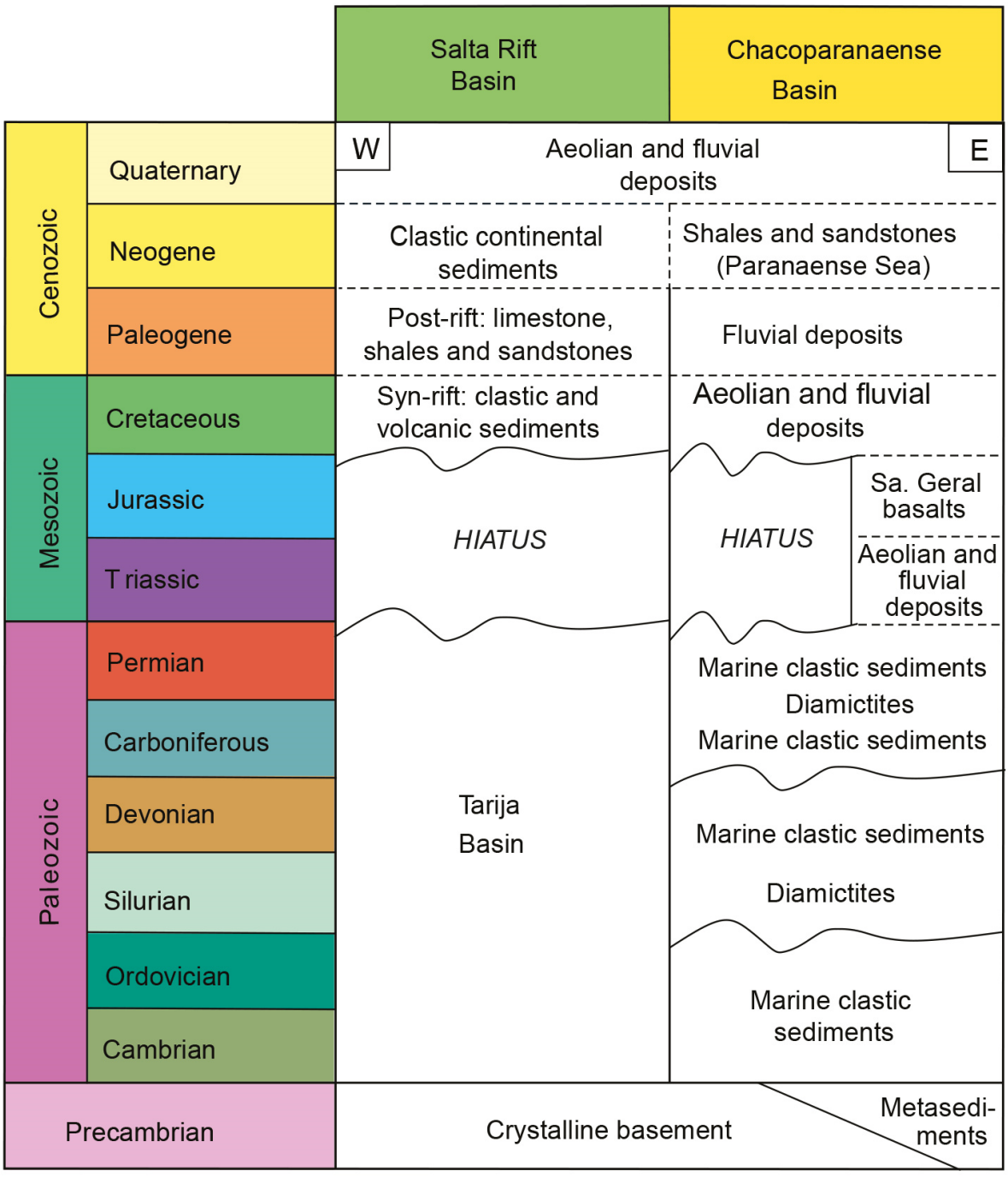

Figure 2.2: Generic stratigraphic column comparing the areas of Salta Rift and Chacoparanaense Basin based on Russo *et al.* (1979), well reports (e.g., Rolleri, 1965; Rolleri, 1966; Rolleri, 1967; Bottcher, 1965; Bottcher, 1974; Di Persia, 1969; Di Persia, 1970; Moreno, 1973; Pluspetrol, 1990; Pluspetrol, 1995), Starck, 2011, and Marquillas *et al.,* 2005.

Chapter 3: Seismic interpretation – Evolution of basin highs

3.2. Introduction

The Quirquincho High, also known as Rincón Caburé High (Russo *et al.*, 1989; Chebli *et al.*, 1999), is covered by the sedimentary cover of the Cenozoic Andean foreland basin. With respect to the paleo-surface characteristics of the Paleozoic basement rocks in that region, the Quirquincho High is an elevated, buried topographic feature, where older units are topographically higher than neighbouring younger units; the Quirquincho High separates the Salta Rift Basin to the west, and the Chacoparanaense Basin to the east. At the surface, these relationships are not exposed, and all of these features are in the subsurface, covered by the clastic sediments that constitute the gently eastward-sloping Quaternary plains of the Salta, Chaco, Formosa, and Santiago del Estero provinces (Fig. 1.2).

The lack of geological outcrop information (Fig. 3.1) and limited subsurface data in this region have made an unambiguous evaluation of the buried topographic High and its adjacent basement areas difficult. Consequently, the evolution of the basement High in the context of vertical movements of the Paleozoic basement and the Mesozoic to Cenozoic cover sequences has remained unclear. Due to the limited database, the morphology and the geological mechanism that ultimately controlled basin geometry and sedimentary-fill histories could not be studied properly in the past. With the recent availability of subsurface geological and geophysical data, however, this situation has changed fundamentally.

Aided by an extensive geophysical and well data set, I first describe the morphology of the Quirquincho High and the lateral characteristics of facies associated with this feature to provide an interpretation of its evolution, underlying tectonic mechanisms, and its relationship with the spatiotemporal evolution of depocenters. This approach has helped to unveil the genesis and history of this enigmatic structural high, its relationship with the architecture of the present-day Andean foreland basin, and the depositional history of the sediments deposited in the Cretaceous Salta Rift Basin, resulting in a better understanding of the distribution of hydrocarbons and other resources. Moreover, with the subsurface data, I also address the evolution of the Pampeano-Chaqueño High farther east, which is a similar basement high, although areally less extensive. As the more extensive Quirquincho High, the Pampeano-Chaqueño High also profoundly influences sedimentary basin geometry and separates strata in depocenters of the deeper levels of the Chacoparanaense sedimentary infill.

During the data analysis in the context of my dissertation work I reinterpreted the subsurface information comprised of seismic reflection profiles and well reports using a regional approach that considers the the Chacoparanaense and Salta Rift basins and the Andean foreland basin as complex spatiotemporal, transitional systems that record protracted transitions in sedimentation from earlier, individual and compartmentalized basin configurations to a late-stage setting with increased depositional connectivity.

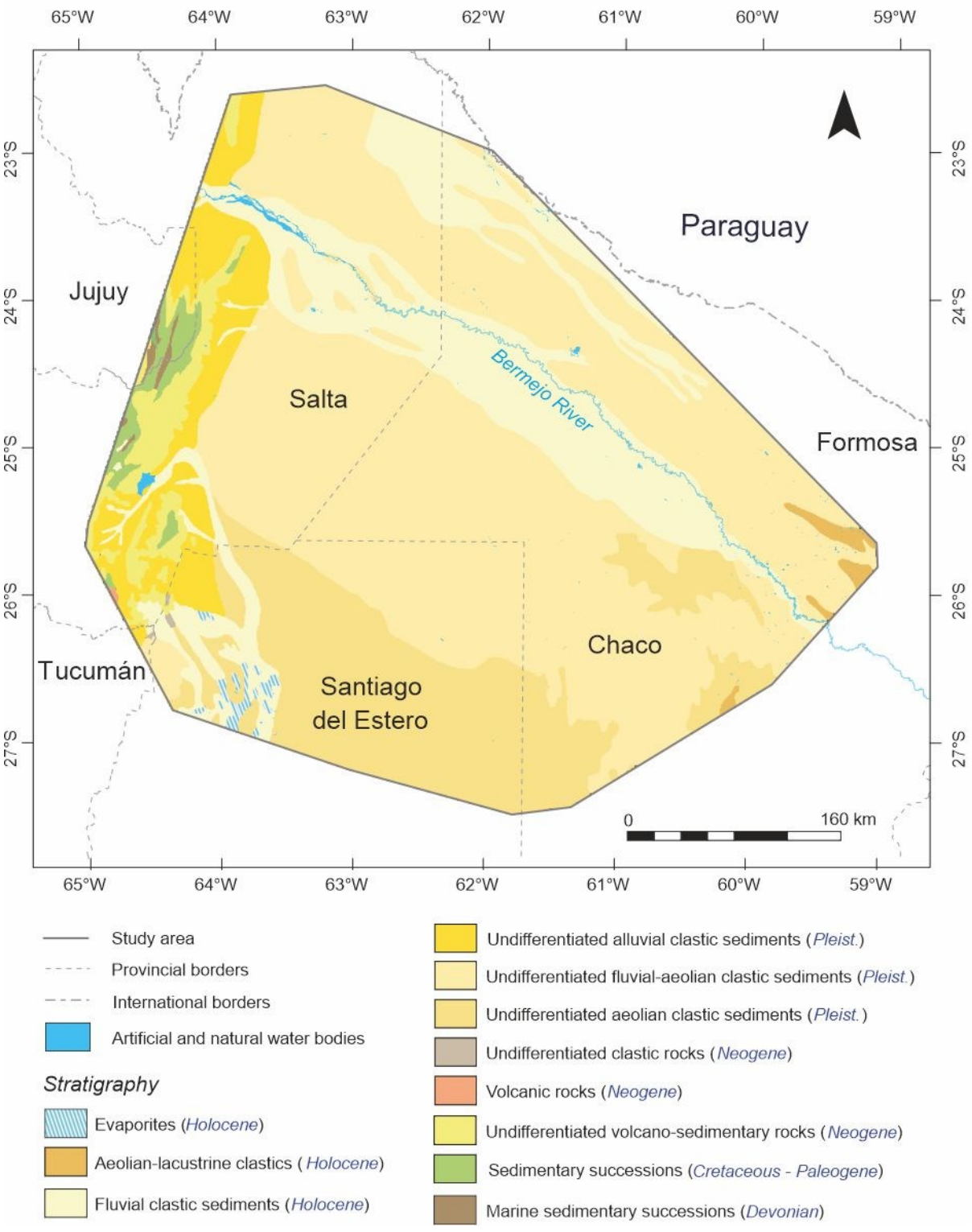

Figure 3.1: Geological map of the study area (Modified from IGN Argentina - www.ign.gob.ar).

3.2. Data and Methods

I used a total of 120 2D seismic profiles in paper or scan format and information from 18 petroleum exploration wells (Fig. 3.2). The seismic profiles in the studied area were acquired by different oil companies mainly before the 1990s and are of variable quality, ranging from poor to medium concerning the identifiable amplitudes and reflection patterns. I converted the 2D-reflection seismic profiles stored in paper format to a digitized SEG-Y format by scanning them with a poster scanner and using the free software Kogeo Seismic Toolkit to convert the file format. I georeferenced the seismic profiles based on digital maps and interpreted them using Kingdom Suite 2016 (®IHS) software. The information from the boreholes includes coordinates, well tops, lithology, electric and sonic surveys from the wells reports of Pirané (Rolleri, 1965) and Chirete (Pluspetrol, 1990), for the northern transect (Fig. 3.2 & 3.3); and Las Breñas 1 (Bottcher, 1974), Las Breñas 2 (Rolleri, 1967), Las Breñas Oriental (Rolleri, 1966), Coronel Rico (Di Persia, 1969), El Caburé (Bottcher, 1965), Los Horcones 1 (Di Persia, 1970), Los Horcones 2 (Moreno, 1973), and Cerro Colorado (Pluspetrol, 1995) for the south transect (Fig. 3.2 & 3.4).

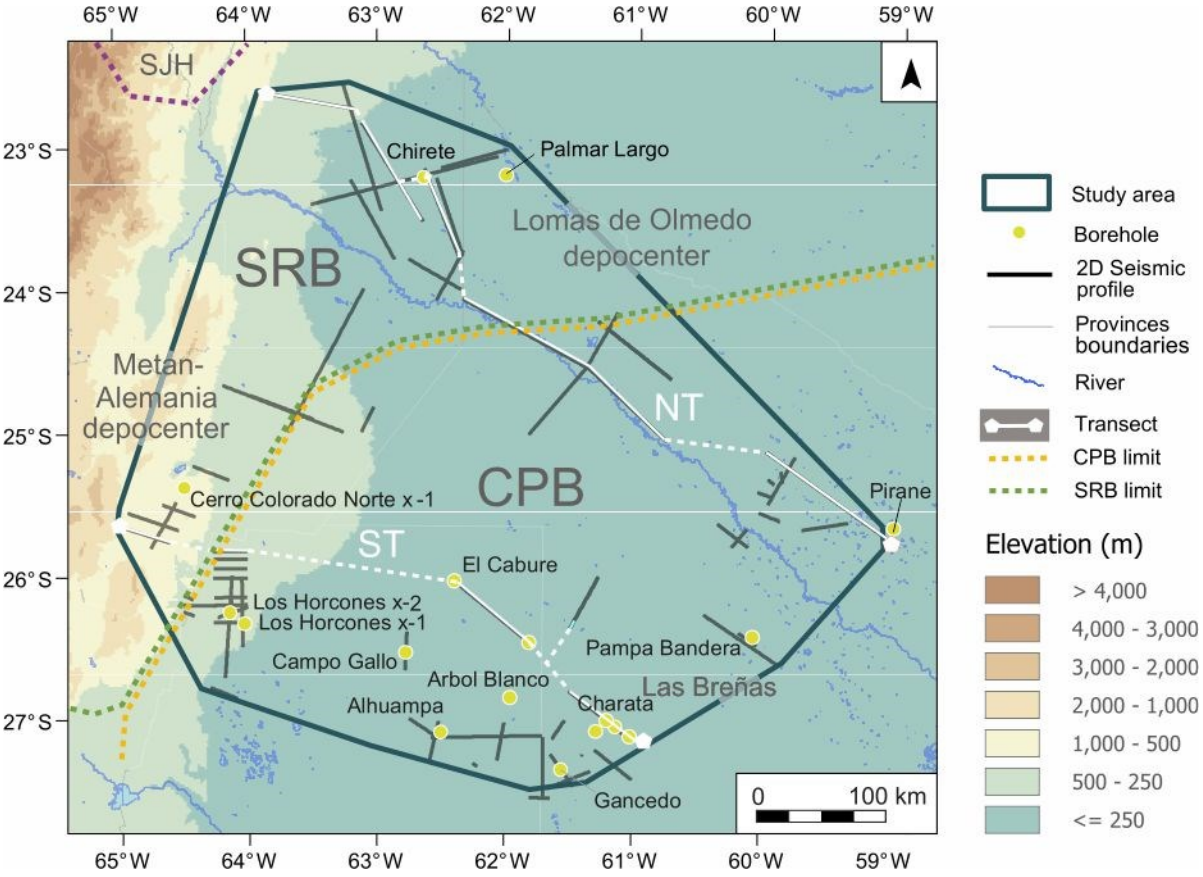

Figure 3.2: Distribution of the available data (see location in Fig. 1b): location of 2D seismic profiles, wells, North (NT) and South (ST) seismic transects. Location of the Salta Rift Basin (SRB) and Chacoparanaense Basin (CPB) with the main depocenters in the study area. Digital elevation model (data from the USGS Earth Explorer portal) and surface hydrographic distribution (data from the IGN-Argentina database - www.ign.gob.ar).

Seismic interpretation and horizon flattening

I used well data (in the Kingdom Suite 2016®IHS project) to tie the seismic interpretations to the units described in the wells and to identify the reflectors corresponding to unit tops. I tracked them across the study area and marked unconformities related to onlap and truncation of stratal terminations.

By combining several seismic profiles and their interpreted horizons, I constructed the North transect (NT) of 750 km length and the South transect (ST) of 500 km length (Figs. 3.3 & 3.4). Both transects are approximately NW-SE-oriented. The North transect (Fig. 3.3) has better lateral continuity and is composed of nine individual 2D seismic reflection surveys. The South transect (Fig. 3.4) comprises four 2D seismic surveys plus a portion of one N-S-oriented survey. The South transect has less lateral continuity, which I compensated by geological interpretation and extrapolation based on the interpreted lines (Figs. 3.4, 3.8, 3.9, 3.10 & 3.11), well information, and horizon interpolation. The location of both transects is marked in Fig. 3.2; the continuous white lines indicate the location of the analyzed seismic profiles and the dotted white lines denote the data gaps or interpolated areas.

To better understand the stratal terminations and the relation between horizons, I flattened the horizons in the North transect using the flatten tool in Kingdom Suite 2016®IHS. The purpose of horizon flattening (Fig. 3.5) was a fast-track palinspastic reconstruction of the original position of the underlying horizons at the time of deposition of the flattened horizon, assuming that the deposition of the selected level was regionally horizontal. For this purpose, I shifted each horizon of the North transect to ground level - 0ms TWT. (Fig. 3.5). This method enables one to observe the relationship between a horizon and reflections, horizons and structures above, below and/or adjacent in a view that portrays the depositional system during deposition of the individual layers.

I present the interpretation of horizons, seismic transects, and flattening in the original time domain in order to alter the data and interpretations as little as possible.

Velocity models for time-depth conversion

To correlate the formation well tops with the seismic horizons, I produced velocity models. I analyzed and compiled data from the headers of 19 seismic profiles of the Salta Rift Basin and 9 seismic profiles of the Chacoparanaense Basin. Two-way travel time (TWT) in milliseconds and depth (Z) in meters were plotted in XY charts with each point corresponding to a one-point value of the check shot. With this data cloud I calculated trend lines of time-depth conversion rates (Fig. 3.12).

The resulting XY graphs and the trend lines are expressed in three quadratic equations (Fig. 3.12), one characteristic for each basin, and one general for the entire study area. This allowed converting the seismic interpretation results from the time domain to a depth section. For correlations between the basins, I used the general trend equation of both basins for time-depth conversion. This approach is the best compromise to study, correlate, and compare a region as extensive as my study area. Nevertheless, using the general trend correlation leads to some variation in the depths of the horizons and the thickness of the units. For a detailed study of smaller areas in one of the basins studied, the trend for the respective basin should be used instead of the general trend for the entire study area.

Depth and thickness maps

I imported all of the interpreted lines and their depth-converted horizons into Petrel 2015 E&P Software (®Schlumberger), where I interpolated them to create depth maps for each geological unit of interest. Finally, I constructed thickness maps by calculating the difference between two adjacent interpreted geological horizons.

3.3. Results

3.3.1 Seismic Interpretation

I divided the sedimentary infill of the Cenozoic Andean, the Cretaceous Salta Rift, and the Chacoparanaense basins into five marker horizons and five principal seismic reflection units. From base to top (old to young), the marker horizons are H1 (Top Precambrian), H2 (Top Paleozoic), H3 (Top Cretaceous), H4 (Top Paleogene), and H5 (Top Neogene). The present-day topography is the upper boundary of the interpreted sedimentary succession. Above the acoustic basement, the horizons bound the seismic reflection units labelled U1 to U5 (from old to young). Formation tops determined in boreholes defined horizons and unit ages, while all horizons follow (relatively) continuous seismic reflectors.

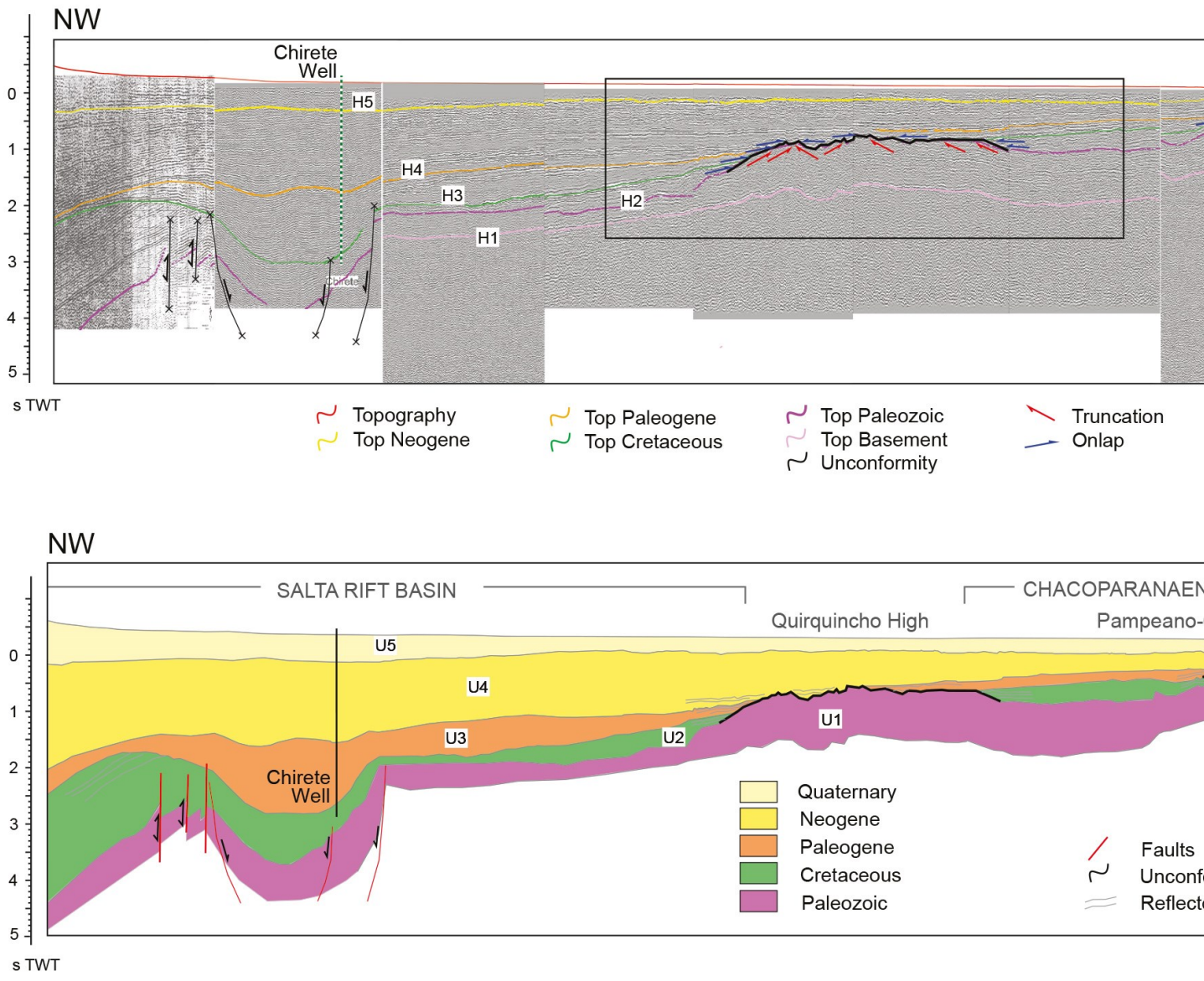

Figure 3.3: NW-SE-oriented North transect (NT) (see location in Fig. 3.2). A- Seismic profiles with interpreted color-coded horizons (H1: Top Precambrian basement, H2: Top Paleozoic, H3: Top Cretaceous, H4: Top Paleogene, H5: Top Neogene). B- Geological profile across the seismic units (U1: Paleozoic, U2: Cretaceous, U3: Paleogene, U4: Neogene, U5: Quaternary).

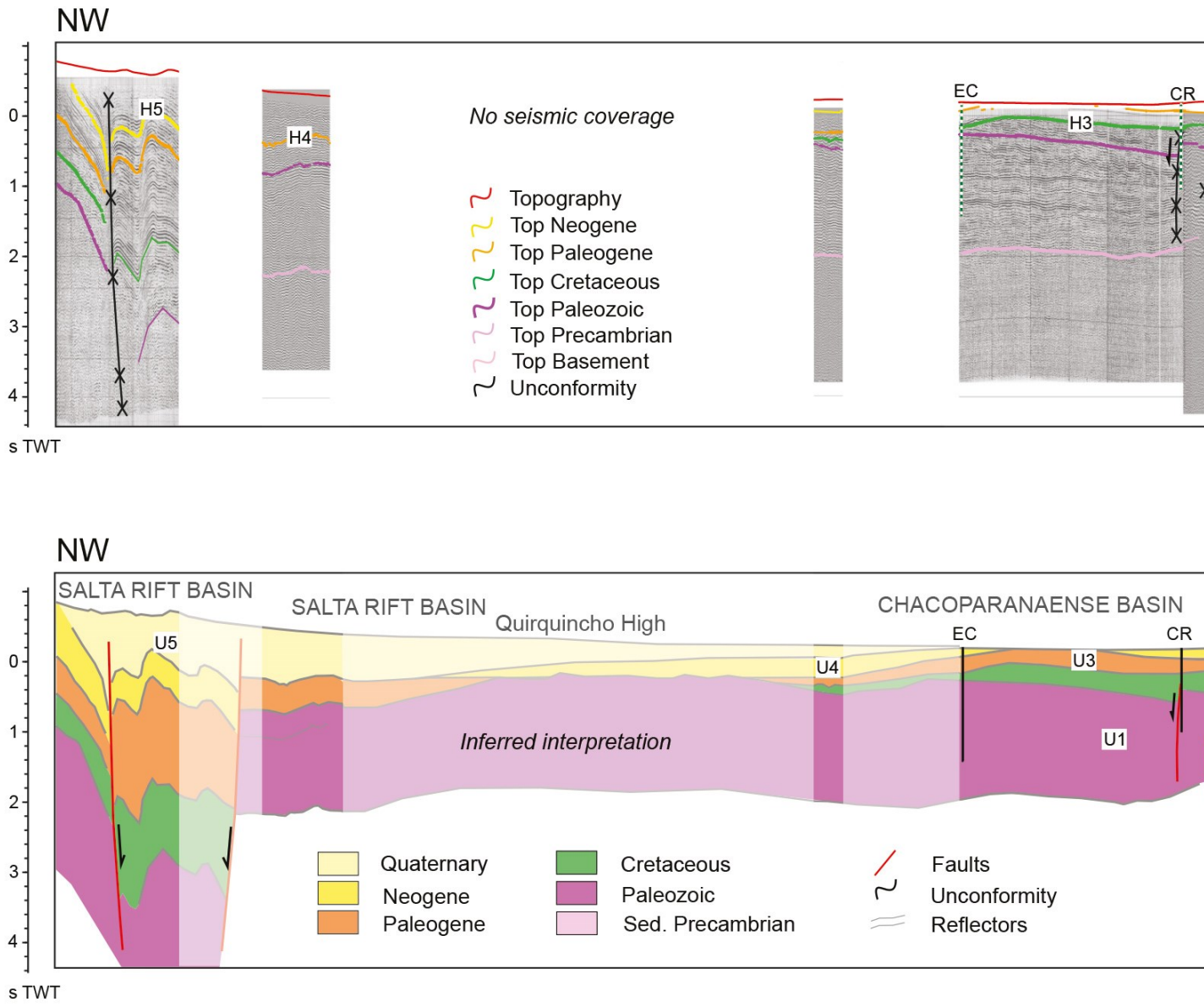

Figure 3.4: NW-SE-oriented South Transect (ST) (see location in Fig. 3.2). A- Seismic profiles with interpreted color-coded horizons (H0: Local top basement, H1: Top Precambrian, H2: Top Paleozoic, H3: Top Cretaceous, H4: Top Paleogene, H5: Top Neogene). B- Geological profile across the seismic units (U0: Precambrian metasediments, U1: Paleozoic, U2: Cretaceous, U3: Paleogene, U4: Neogene, U5: Quaternary). In strong colour observed data, interpreted areas are shown in transparent colors. Boreholes: EC-El Caburé, CR-Coronel Rico, LB1- Las Breñas 1, LB2- Las Breñas 2, LBO- Las Breñas Oriental.

Horizon Interpretation

Seismic horizon H1 is the deepest horizon marked, it can be recognized in many sectors of the study area. It defines the boundary between chaotic, disrupted low-to-medium amplitude reflections -interpreted as the acoustic basement-, and overlying semi-continuous to continuous reflections with subparallel, parallel, and in places divergent reflection patterns. H1 follows a high-amplitude positive reflection and it is recognized at different depths, being much deeper in the west. H1 is intersected by a normal fault in the area of the Pampeano-Chaqueño High in the North transect (Fig. 3.3) and by a normal fault bounding the Las Breñas halfgraben in the South transect (Fig. 3.4). In the South transect (Fig. 3.4), a local H0 horizon is included, separating acoustic basement units of the Las Breñas halfgraben of sedimentary Precambrian at the top, from the underlying metasedimentary units.

I mapped seismic horizon H2 on a high amplitude reflector of variable continuity. H2 is much deeper in the west than in the east. Its morphology is irregular with a wavy to distorted character in the east and the center of the South transect (Fig. 3.4), and generally west-dipping. Several faults displace/cut H2 in the western part of the study area, with the most prominent graben structures in both transects bounded by normal faults (Figs. 3.3 & 3.4). To the east, in the southern transect (Fig. 3.4), H2 is displaced by a west-dipping normal fault near the Coronel Rico (CR) well and by a series of normal faults at the eastern end of the transect near the Las Breñas 2 (LB2) well.

Seismic horizon H3 is a reflector with high amplitude flanked by two parallel low-amplitude reflections. In the west of the study area (Fig. 3.3), H3 dips to the west and is cut by two faults delimiting a graben structure about 100 km wide and 1000 ms (TWT) deep. A similar graben is observed in the South transect (Fig. 3.3), with dimensions of approximately 50 km width and 800 ms (TWT) depth. H3 onlaps onto H2 at the Quirquincho High (Fig. 3.3) and is missing in the central part of the High. I interpreted a similar onlap and distribution of the disappearance of H3 in the South transect (Fig. 3.4). East of the South transect, two paired normal faults cut H3 close to the Las Breñas 2 well.

The H4 seismic horizon is a laterally continuous reflector with high positive amplitude that varies greatly in depth, but less than the older horizons. H4 onlaps the Pampeano-Chaqueño High and in large sectors of the Quiquincho High (North transect and interpreted in South transect). In the South transect (Fig. 3.4) H4 is very shallow in the central-east area. Seismic horizon H5 is a laterally continuous reflector with high amplitude, and which varies much less in depth than older horizons. This reflector is absent in most of the South transect (Fig. 3.4).

Unit Interpretation

In the deepest parts of the profiles, the acoustic basement is characterized by chaotic, disrupted low-to-medium amplitude reflections.

Reflection unit U0 (Fig. 3.4) is located at the eastern end of the South transect between H0 at the base and H1 at the top. U0 has low-amplitude, low-frequency and low-continuity

reflections. This unit has a wedge shape and it is bounded by a normal fault in the thickest extreme (west), whereas it thins and pinches out to the east.

Reflection unit U1 (Figs. 3.3 & 3.4) is bounded by H1 (base) and H2 (top) and has reflections of variable amplitude, medium frequency, and medium to low continuity. U1 exhibits an irregular sheet shape with some thicker areas. An example is the area beneath the Quirquincho High (Fig. 3.3), with a thickness of about 1100 ms (TWT) in the North transect and 1600 ms (TWT) in South transect. Toward the west of Quirquincho High, U1 attains a minimum thickness of *ca*. 300 ms (TWT) (North transect, Fig. 3.3). U1 is laterally discontinuous due to two normal faults forming a graben, which is part of the Cretaceous Metán- Alemanía depocenter of the Salta Rift (Fig. 3.2) in the South transect (Fig. 3.4).

Reflection Unit U2 (Figs. 3.3 & 3.4) is bounded by H2 (base) and H3 (top). U2 has high-amplitude reflectors in the east and central parts of the study area that decrease in amplitude strength towards the Salta Rift Basin area to the west (Figs. 3.3 & 3.4). The reflections have medium frequency, and medium lateral continuity. U2 displays a lens shape in its lower part between the Quirquincho and Pampeano-Chaqueño highs and disappears in the central part of the Quirquincho High while attaining a subtle wedge geometry in the west of this high, thickening towards the west. In the region of the Province of Salta (North transect, Fig. 3.3) U2 fills the graben (thickness *ca*. 1000 ms TWT) bounded by a large normal fault (Lomas de Olmedo depocenter – Fig. 3.2). Within this graben, the internal reflections of U2 are subparallel and locally folded. In the South transect (Fig. 3.4), the unit disappears on the top and the west side of the

Quirquincho High, reappearing in the sedimentary infill of the extensional Metán-Alemanía depocenter.

Reflection unit U3 (Figs. 3.3 & 3.4) has medium to low amplitude reflectors with medium to low frequency and medium lateral continuity. Its reflections are parallel in the east, subparallel in the central-western area, and locally folded within the graben structure (Fig. 3.3). As in the underlying unit U2, the Quirquincho and Pampeano-Chaqueño highs intersect U3. In the western and central parts of the study area, the unit has the shape of a large westward thickening wedge with an irregular lower boundary due to the presence of faults. In the Metán-Alemanía graben, U3 reaches a maximum thickness of *ca*. 1700 ms (TWT). U3 significantly thins towards the Quirquincho and Pampeano-Chaqueño highs, and onlaps both structures (North transect, Fig. 3.3). To the east of the Pampeano-Chaqueño High, U3 maintains a constant thickness of *ca.* 100 ms. At the eastern end of ST (Fig. 3.4), normal faults cut U3 in its lower section at the location of the Las Breñas 2 (LB2) well. Between the El Caburé and Coronel Rico wells, U3 is located at the surface.

Reflection unit U4 (Figs. 3.3 & 3.4) has high-amplitude reflectors, showing some stronger amplitude reflectors in the medium and lower parts of the unit with medium frequency, and strong lateral continuity. U4 contains parallel reflectors that are slightly curved upwards on top of the Pampeano-Chaqueño High. U4 has a general wedge-shaped geometry in the North transect (Fig. 3.3), with much greater thickness in the west, (*ca*. 2000 ms TWT) than in the east (300 ms TWT). In the South transect (Fig. 3.4), U4 has an irregular and interrupted wedge shape,

with a maximum thickness of 400 ms (TWT), locally decreasing or absent, as between the Quirquincho High and the Metán-Alemanía graben. The unit onlaps and covers the Quirquincho and Pampeano-Chaqueño highs.

Reflection unit U5 (Figs. 3.3 & 3.4) has medium to high amplitude reflectors with high frequency and low continuity due to their near-surface location. Reflections within this unit are horizontal. The unit is generally tabular with a slight thickness increase to the west in the North transect (Fig. 3.3), and it has a gentle wedge shape in South transect (Fig. 3.4) with maximum thickness to the west; it is thinning toward the east, where it eventually disappears.

Chronolithostratigraphy

Based on biostratigraphic data recorded in the well reports (Pirané, Rolleri, 1965; Chirete, Pluspetrol, 1990; Las Breñas 1, Bottcher, 1974; Las Breñas 2 , Rolleri, 1967; Las Breñas Oriental, Rolleri, 1966; Coronel Rico, Di Persia, 1969; El Caburé, Bottcher, 1965; Los Horcones 1, Di Persia, 1970; Los Horcones 2, Moreno, 1973; Cerro Colorado ,Pluspetrol, 1995) seismic units U1 to U5 correspond to Paleozoic (U1), Mesozoic – mainly Cretaceous– (U2), Paleogene (U3), Neogene (U4) and Quaternary (U5) sedimentary units.

Horizon H1 at the top of the acoustic basement defines the top of a Precambrian crystalline basement, except in the eastern sectors of the South transect (Fig. 3.4) where Precambrian metasediments are represented by unit U0.

Horizon H2 corresponds to the top of various Paleozoic units (Figs. 2.1 y 2.2) of the Chacoparanaense Basin and the Paleozoic Tarija Basin of southern Bolivia in the vicinity of the Salta Rift Basin area. The top of the Paleozoic unit (U1) contains marine clastic sedimentary rocks intercalated with diamictite levels.

Horizon H3 was penetrated by all wells and corresponds to the top of the Mesozoic (U2). The Mesozoic strata are mainly of Cretaceous age, whereas Triassic and Jurassic strata are absent in most of the basins (U2). According to the well reports, U2 in the Chacoparanaense Basin includes conglomerates, sandstones, and shales with limestone components, while in the Salta Rift Basin U2 includes sandstones cemented by calcite and limestones.

Horizon H4 is the top of unit Paleogene (U3); it comprises continental sandstones in the Chacoparanaense Basin, as well as fluvial and lacustrine sandstones and shales in the Salta Rift Basin.

Horizon H5 top-bounds the Neogene units (U4); this unit contains shales and sandstones in the Chacoparanaense Basin; and sandstones, siltstones, and conglomerates in the Salta Rift Basin.

The Quaternary sediments (U5) at the top of the stratigraphic succession mostly consist of unconsolidated fluvial clastic rocks (conglomerates, sandstones, siltstones, claystone); the coarsest fractions are part of alluvial fans that cover the sediments of the Salta Rift Basin. Finer-grained sandstone-to-clay units mark the distal areas of the Chacoparanaense Basin.

3.3.2. Flattening of horizons

Individual flattening was performed for each horizon marked in the North transect, from H2 to H5 (Fig. 3.5). Flattening of H2 – Paleozoic Top– (Fig. 3.5A) shows how the horizon below (H1) is approximately horizontal, exhibiting a slight depression in the area of the metasediments of Quirquincho High. The horizons above H3 and H4 show onlap terminations towards the H2 in the region of the Pampeano-Chaqueño High and the Quirquincho High.

Flattening of H3 –Top Cretaceous – (Fig. 3.5B) emphasizes the onlap on H2 in the area of both highs and illustrates how H4 –Top Paleogene- terminates in onlap with respect to H2 and H3.

Flattening of H4 – Top Paleogene – (Fig. 3.5C) documents onlap terminations on H2 and H3 in the region of the Pampeano-Chaqueño and Quirquincho highs. To the west, H3 exhibits a depocenter with a graben, whose faults also affect the top of H2 by faults; this area corresponds to the Lomas de Olmedo depocenter of the Salta Rift Basin.

Flattening of H5 – Top Neogene – (Fig. 3.5D) resembles the original North transect (Fig. 3.3). The most notable feature is the westward-thickening wedge shape of the Neogene sediments.

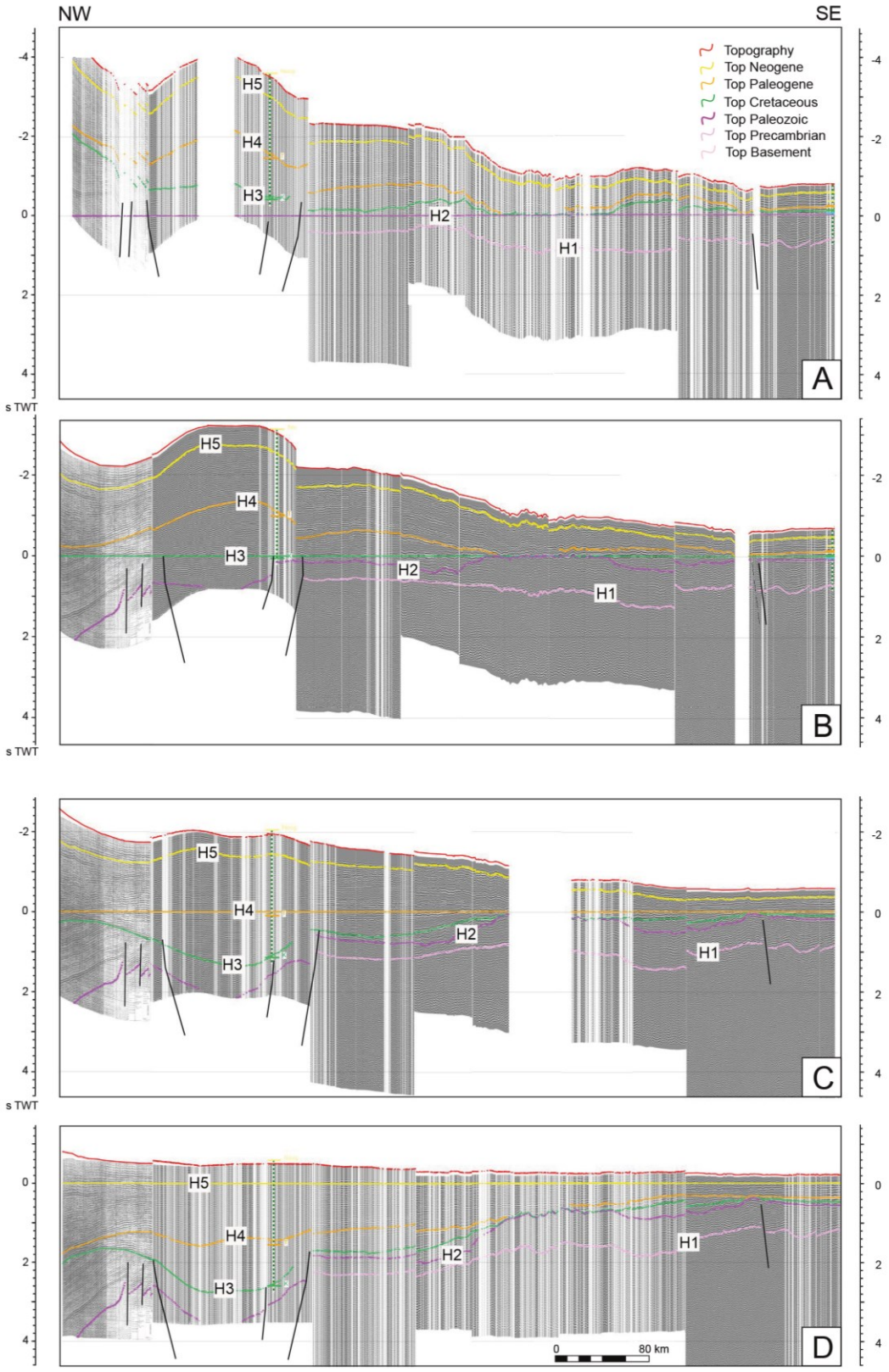
NW
SE
Topography
Top Neogene
Top Paleogene
Top Cretaceous
Top Paleozoic
Top Precambrian
Top Basement
H5
H4
H3
H2
H1
A
B
C
D
s TWT
0
80 km

Figure 3.5: Flattening of the horizons in the North Transect (see location in Fig. 3.2). A- Flattening of H2-Top Paleozoic. B- Flattening of H3-Top Cretaceous. C- Flattening of H4-Top Paleogene. D- Flattening of H5-Top Neogene.

3.3.3. Additional seismic surveys

Here, I describe four additional seismic surveys to complement the seismic transect with lines that were shot between the North and South transects (surveys 33049 & pw_89_40), and two approximately N-S-oriented surveys (TX_209_NS & 45054) to gain more insight regarding the character of the Quirquincho High.

Unit tops were marked following the same parameters as described for the North and South transects, and units generally have the same reflector characteristics. I focus on the description of the morphology observed in the other lines for top and unit characteristics. The locations of these four surveys are shown in Figure 3.6 and the references in Figure 3.7.

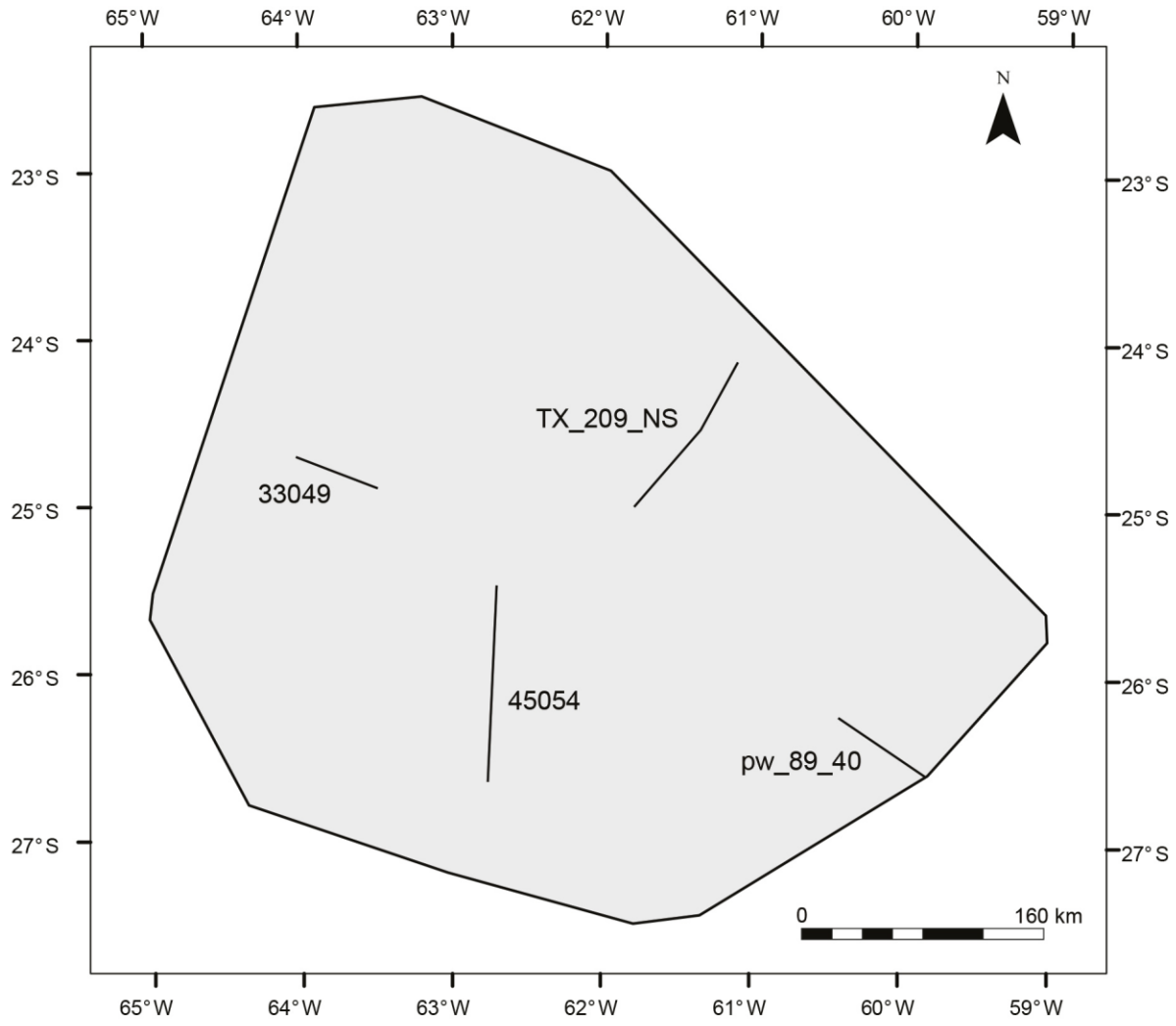

Figure 3.6: Location of additional seismic surveys in the study area.

Line pw_89_40 (Fig. 3.8) helps to constrain the early history of the Chacoparanaense Basin, as does the South transect (Fig. 3.4) in its eastern sector. In this survey, I interpreted five tops, an unconformity, and a major fault. The data from the Pampa Bandera well (Fig. 3.2) allowed correlation of the units with the Paleozoic units. The most notable feature of this survey is a large normal fault of almost 4s TWT vertical extent. This fault dips steeply to the east and it belongs to the northern part of the Las Breñas halfgraben, which was observed in the South

transect (Fig. 3.4). The subsidence of this halfgraben began during the Precambrian and created accommodation space in the crystalline basement for the deposition of Precambrian (U0) and early Paleozoic sediments (U1). The sediments inside the graben are gently folded below the Pampa Bandera well, suggesting compressional inversion at the end of the early Paleozoic. Above the folded sediments there is an unconformity, inside U1-Paleozoic, marked by truncation terminations and horizontal reflectors in the upper part. Truncation terminations suggest erosion. Above the U1-Paleozoic, a 300ms (TWT) thick, U2-Mesozoic reflector is imaged, followed by a U3-Paleogene unit. Covering the complete sequence comprises a thin layer of undifferentiated Neogene and Quaternary (U5) sediments.

The N-S-oriented Survey 45054 (Fig. 3.9) exhibits an unconformity between the U1-Paleozoic and U2, U3, and U4 horizons, marked by onlap terminations. U2- Mesozoic and U3-Paleogene have a wedge shape that thins northward. This agrees with a N-S-oriented profile of the Quirquincho High, where Mesozoic (mainly Cretaceous) sediments occur on both sides of the High. Here, Paleogene sedimentary rocks are not present on top of the High. Whereas Neogene unit (U4) onlaps only in its lower part on the High, the other Neogene strata and the Quaternary (U5) units cover the area uniformly.

Survey TX_90_209 (Fig. 3.10) reveals the same five units as survey 45054. It is oriented S-N and located on the eastern flank of the Quirquincho High. Between U1-Paleozoic and U2-Mesozoic there is an unconformity marked by truncation terminations below and onlap terminations on top. U1- Paleozoic is elevated and folded in the center of the survey, and it is

covered by onlapping, slightly elevated and folded Cretaceous sediments. U3- Paleogene onlaps towards the U2-Cretaceous in the center part of the High. While U4-Neogene and U5-Quaternary are not affected and form a continuous cover.

Seismic survey 33049 (Fig. 3.11) is located in the western part of the area, in between the north and south transect, following an almost W-E orientation. This survey covers part of the Salta Rift Basin. In this area, it is not possible to differentiate Precambrian crystalline basement from the Paleozoic basement (Tarija Basin) associated with the Salta Rift Basin that started deposition during the early Cretaceous. The sedimentary sequence in this area thus starts with Cretaceous sediments (U2) that cover a slightly irregular basement topography. The reflectors are generally horizontal, with some folding and truncations in the upper part. In the east, these units are covered by onlapping Paleogene (U3) strata. Both units, U2 and U3, gently dip westward. U4-Neogene has a slight wedge shape, thickening to the west. Horizon H5-Top Neogene is almost horizontal, and the topography is higher in the west, creating a wedge shape for the Quaternary (U5) deposits.

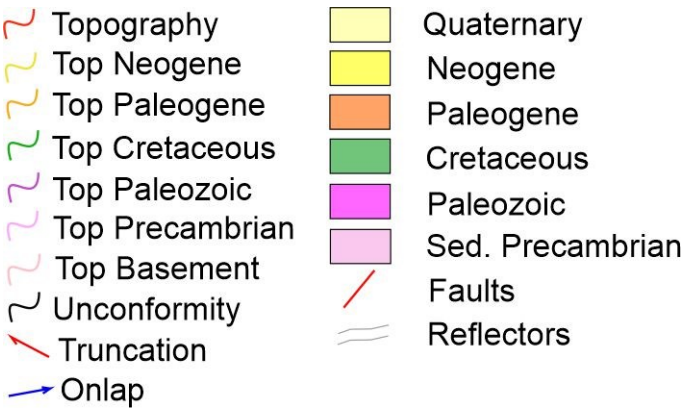

Figure 3.7: Legend for figures 3.8-3.11.

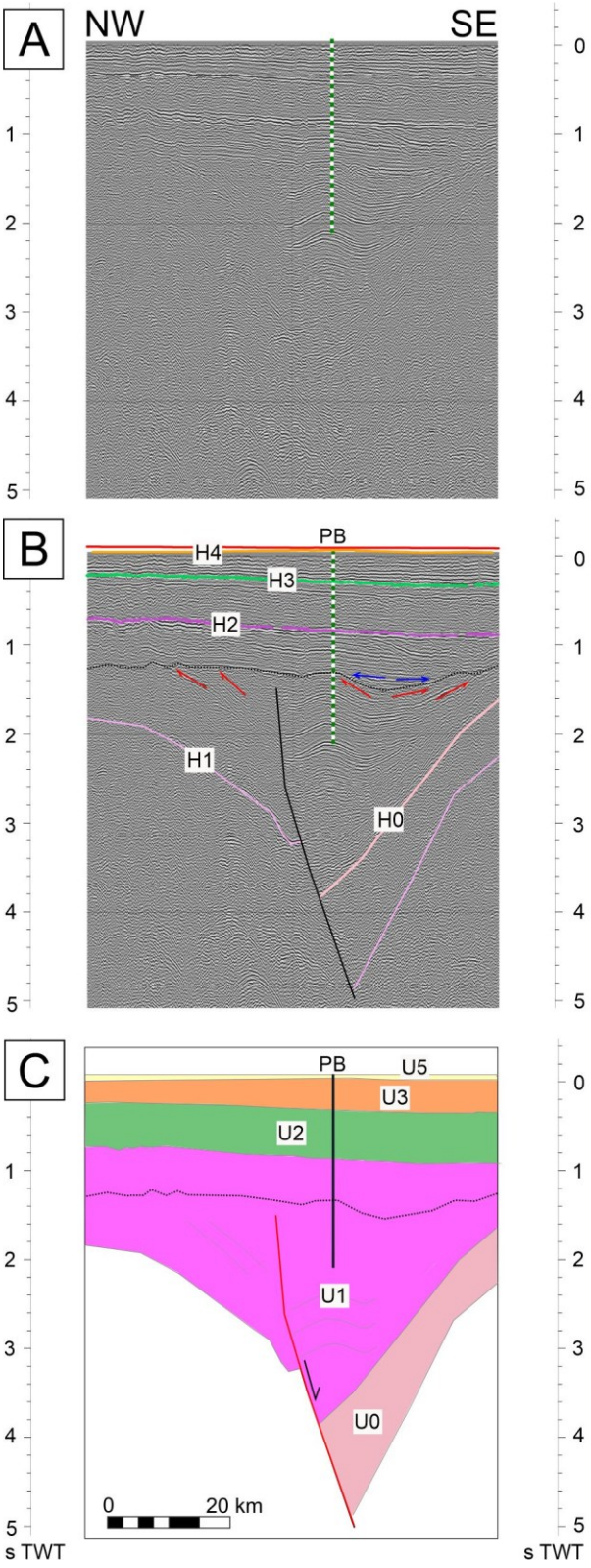

Figure 3.8: Survey pw_89_40. A- uninterpreted seismic line. B- Interpreted color-coded horizons (H1: Top Precambrian basement, H2: Top Paleozoic, H3: Top Cretaceous, H4: Top Paleogene, H5: Top Neogene). C- Geological profile across the interpreted units (U1: Paleozoic, U2: Cretaceous, U3: Paleogene, U4: Neogene, U5: Quaternary). PB: Pampa Bandera borehole.

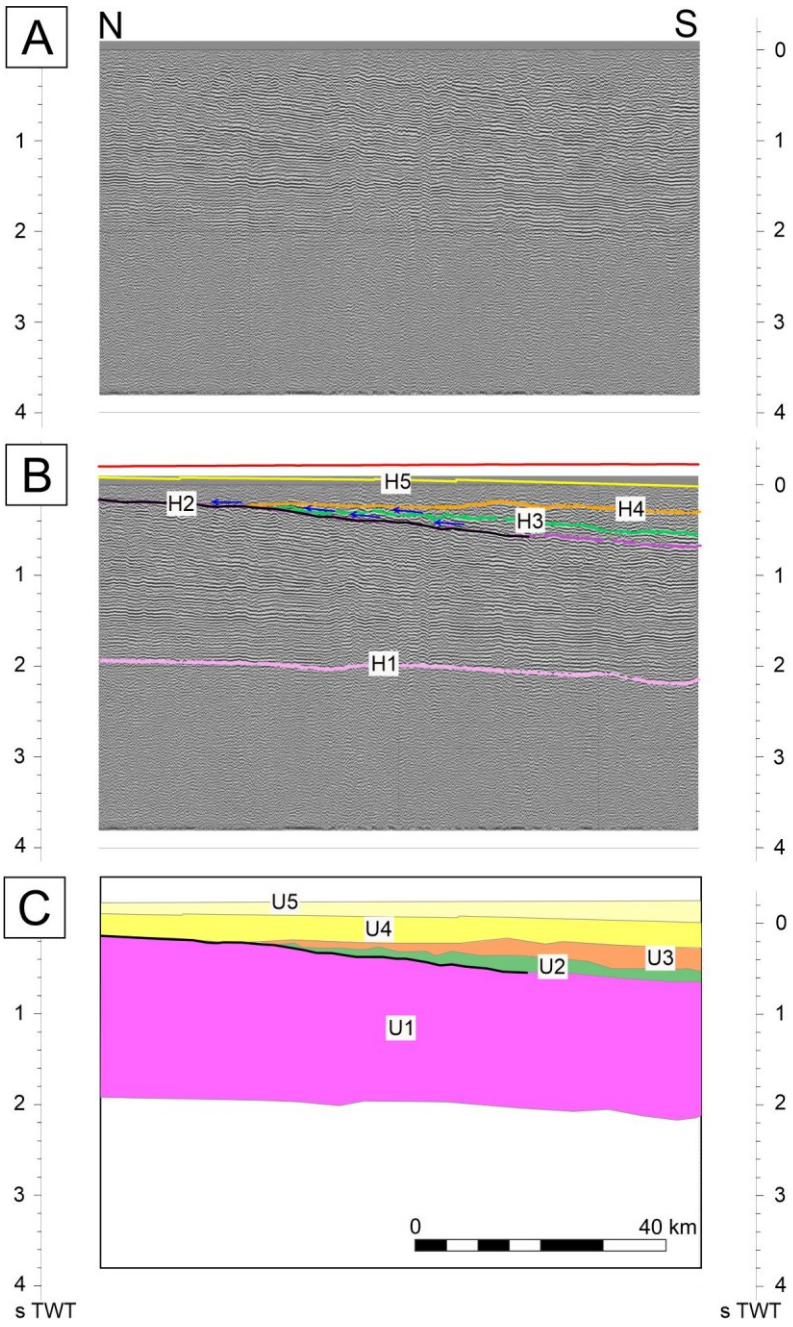

Figure 3.9: Survey 45054. A- uninterpreted seismic line. B- Interpreted color-coded horizons (H1: Top Precambrian basement, H2: Top Paleozoic, H3: Top Cretaceous, H4: Top Paleogene, H5: Top Neogene). C- Geological profile across the interpreted units (U1: Paleozoic, U2: Cretaceous, U3: Paleogene, U4: Neogene, U5: Quaternary).

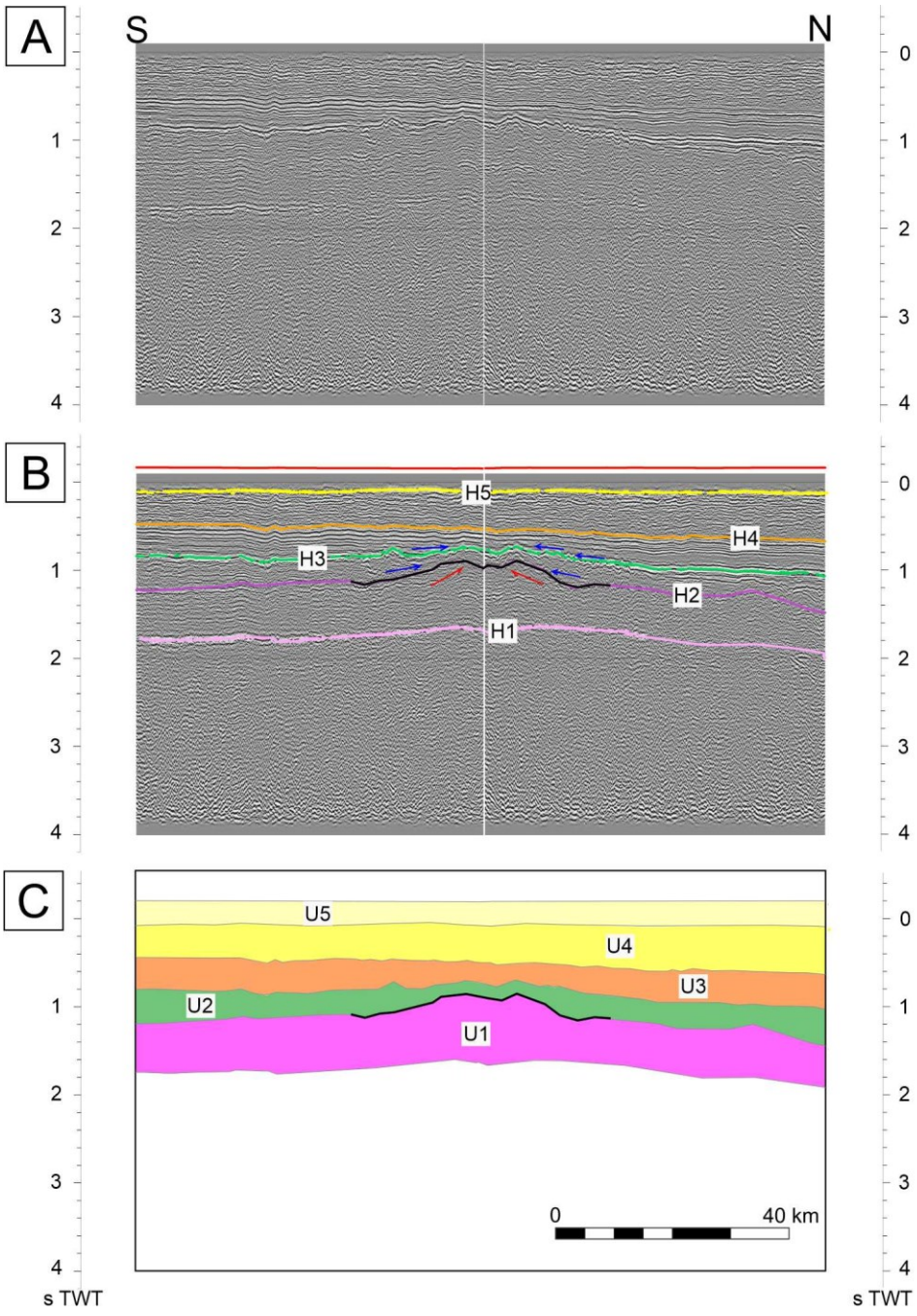

Figure 3.10: Survey TX_90_209. A- uninterpreted seismic line. B- Interpreted color-coded horizons (H1: Top Precambrian basement, H2: Top Paleozoic, H3: Top Cretaceous, H4: Top Paleogene, H5: Top Neogene). C- Geological profile across the interpreted units (U1: Paleozoic, U2: Cretaceous, U3: Paleogene, U4: Neogene, U5: Quaternary). PB: Pampa Bandera borehole.

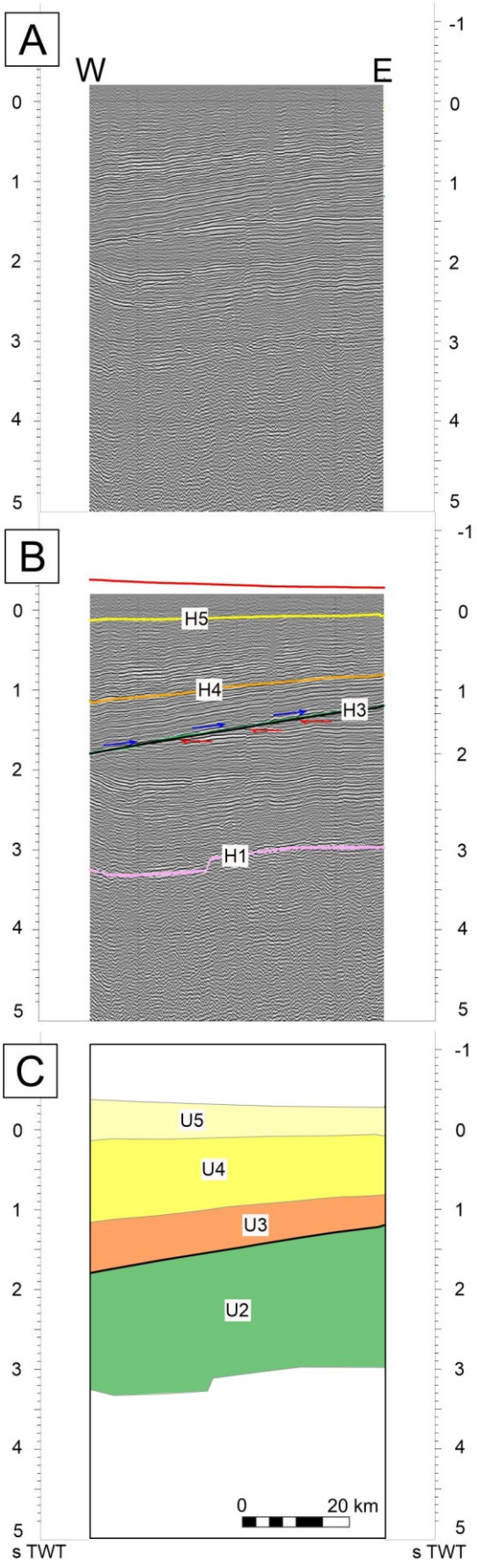

Figure 3.11: Survey 33049. A- uninterpreted seismic line. B- Interpreted color-coded horizons (H1: Top Precambrian basement, H2: Top Paleozoic, H3: Top Cretaceous, H4: Top Paleogene, H5: Top Neogene). C- Geological profile across the interpreted units (U1: Paleozoic, U2: Cretaceous, U3: Paleogene, U4: Neogene, U5: Quaternary). PB: Pampa Bandera borehole.

3.3.4. Depth and isopach maps

After interpolation of reflector horizons in the time domain, I converted the horizons to the depth domain by applying the equation created by the general trend-velocity model (see section 3.2) to each point of the horizons (Fig. 3.12). I exported the coordinates and time (ms) for each interpreted point and applied the equation to obtain depths (m). I used interpolation techniques (standard convergent interpolation and conformal gridding) in PETREL 2016 Schlumberger software to create depth and isopach maps for each unit top from the corresponding depth-converted horizons (Figs. 3.13 & 3.14).

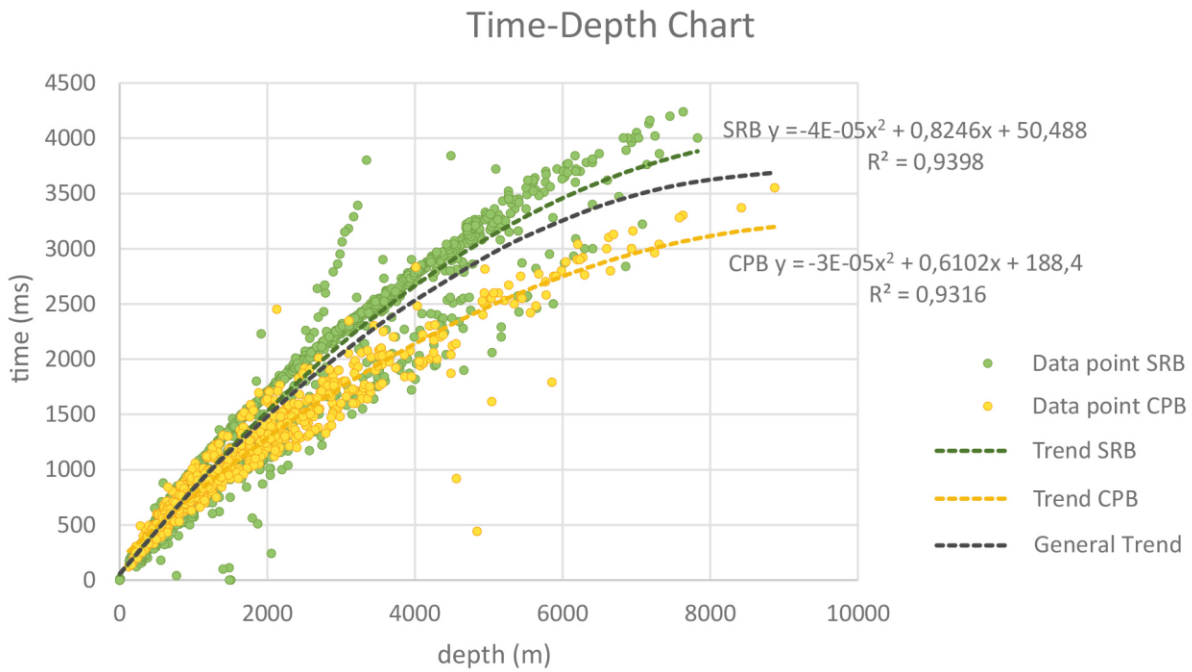

Figure 3.12: Time–depth chart for the wells and seismic profiles of the Salta Rift Basin (SRB) and the Chacoparanaense Basin (CPB). Each data point corresponds to one check-shot. Three trends and equations are generated from the data: an SRB trend for the Salta Rift Basin, a CPB trend for the Chacoparanaense Basin and a general trend for the entire study area.

Description of depth maps

The objective of using depth maps is to illustrate the present-day subsurface position of the top of each stratigraphic unit and to analyze its present-day morphology. I constructed four depth maps for the most relevant and best data-supported unit tops; these are the top of the Precambrian basement (H1), the top of the Paleozoic sediments (H2); the top of the Cretaceous sediments (H3); and the top of the Paleogene sediments (H4). I chose these four horizons to create depth maps because they were the best-identifiable and best-represented horizons based on the seismic and well data across the entire study area; based on their lateral extent and clarity they were thus the most meaningful and feasible horizons for the purpose of this study.

The depth of the Precambrian Top (Fig. 3.13A) varies from 1650m b.s.l. (below sea level), to *ca.* 9150m b.s.l. The deepest sector is located in the northwest of the study area. The great depth at which this reflector is found is due to the tectonic subsidence accommodated by offset along the normal faults of the Salta Rift Basin in its Lomas de Olmedo sub-basin. Subsidence associated with extensional processes also affected the western margin of the study area with depths of 6300 m b.s.l., where the Metán-Alemanía basin is located. For example, to the southeast, the depth of the horizon decreases, showing two elevated areas with approximately NE-SW-orientation; the first one is located around the north-central part of the study area and coincides with the position of the Quirquincho High; the second one, which is close to the eastern

boundary of the study area, is clearly associated with the location of the Pampeano-Chaqueño High.

The Paleozoic Top (Fig. 3.13B) ranges from 250 m a.s.l. (above sea level) to 7550 m b.s.l, with its maximum depth in the northwest of the study area, where the Paleozoic rocks underlie the Lomas de Olmedo depocenter of the Salta Rift. The depth of this horizon rapidly decreases towards an elevated area in the center of the map, which is approximately 150 km wide and oriented NE-SW. To the east, parts of the main elevated area are still visible at the Paleozoic Top, which coincides with the location of the Pampeano-Chaqueño High, however, not as prominently as in the horizon below.

The Cretaceous Top (Fig. 3.13C) lies between 45 m a.s.l. and 6230 m b.s.l. depth. Its deepest sector is located in the northwest, from where it progressively rises toward its highest elevations in the southern portion of the study area.

The depth of the Top Paleogene (Fig. 3.13D) ranges from 630 m a.s.l. to 3260m b.s.l. The deepest area is located to the northwest, and depth decreases gently toward the southeast, except for sectors with minor elevations in the southwest, where Cenozoic mountain ranges exist and associated folding and inversion of structures have occurred, such as in the Sierra de la Candelaria (Arnous et al., 2024).

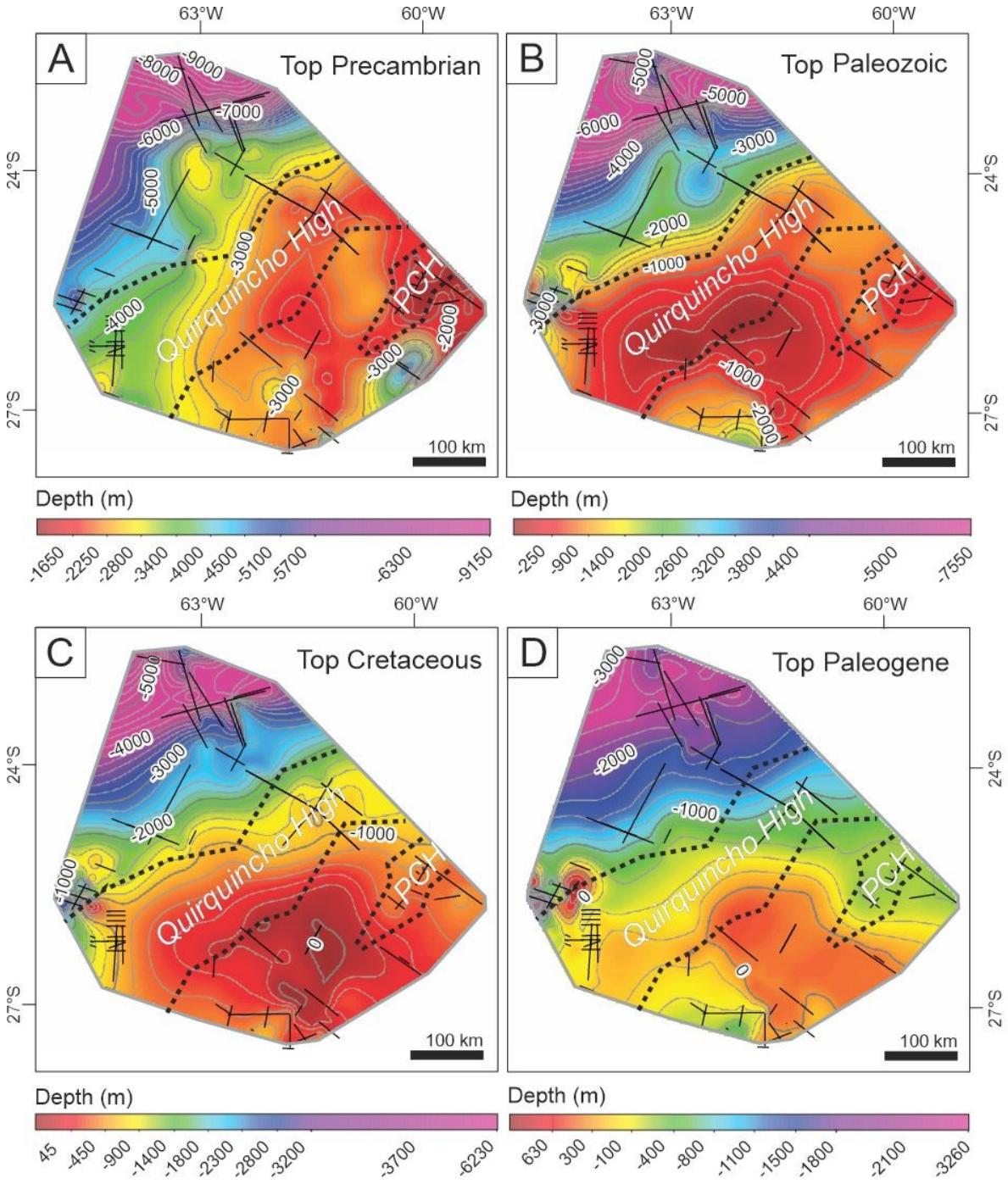

Figure 3.13: Depth map showing the present-day subsurface position and morphology of the top of each stratigraphic unit of horizons 1 to 4: A) H1- Precambrian Top, B) H2- Paleozoic Top, C) H3- Cretaceous Top, D) H4- Paleogene Top. In black location of the 2D seismic surveys. Depth maps were constructed based on seismic interpretations, through interpolations in Petrel 2015 E&P Software (®Schlumberger).

Description of isopach maps

Isopach maps allow to display the spatial distribution of the sediments for each seismically imaged sedimentary unit in the study area.

The Paleozoic unit (U1) thickness distribution ranges from 0m to 4360m (Fig. 3.14A). U1 is thinnest or not detected in the northwest, approximately underneath the Lomas de Olmedo depocenter of the Salta Rift basin, because in this area the Precambrian basement is too deep for a reliable identification in seismic profiles. In addition, in some regions, it is not possible to distinguish between the Paleozoic rocks and the Precambrian basement. Two areas have the greatest sediment thickness; the first and larger one is located in the southwest and has an irregular thickness distribution, whereas the second one is located to the east and corresponds to the offset of the basement surface caused by a normal fault near the location of the Pampa Bandera well (Las Breñas halfgraben). To the west of this area lies an elongated area of reduced sediment thickness with NE-SW orientation; this region corresponds to the position of the Pampeano-Chaqueño High. From Figure 3.14A it can be seen that this area is characterized by a medium thickness of sediments.

The Cretaceous unit (U2) thickness (Fig. 3.14B) ranges from 0 to 2300m; its thickest area is located to the northwest and coincides with the position of the Salta Rift Basin. The thinnest area is elongated and in the center of the analyzed area, and corresponds to the Quirquincho High.

The Paleogene unit (U3) thickness (Fig. 3.14C) spans 0 to 3000m. The thickest region is to the northwest and the thickness decreases to the southeast, with a thickness close to zero in almost half of the study area. Some irregular distributions of sedimentary thickness occur in the southwest, in the area of the Cenozoic La Candelaria range (Arnous *et al.*, 2021; 2024). The general shape of this sedimentary unit is a wedge, thicker to the northwest and pinching out to the southeast.

The Neogene unit (U4) thickness (Fig. 3.14D) ranges from 0 to 4200m, with a greater sediment thickness in the northwest, but gradually decreasing toward the southeast. I observed similar irregularities with regard to the Paleogene map in the southwest. The Neogene exhibits comparable features, but a generally flatter or gentler wedge shape than can be inferred from the Paleogene isopach map.

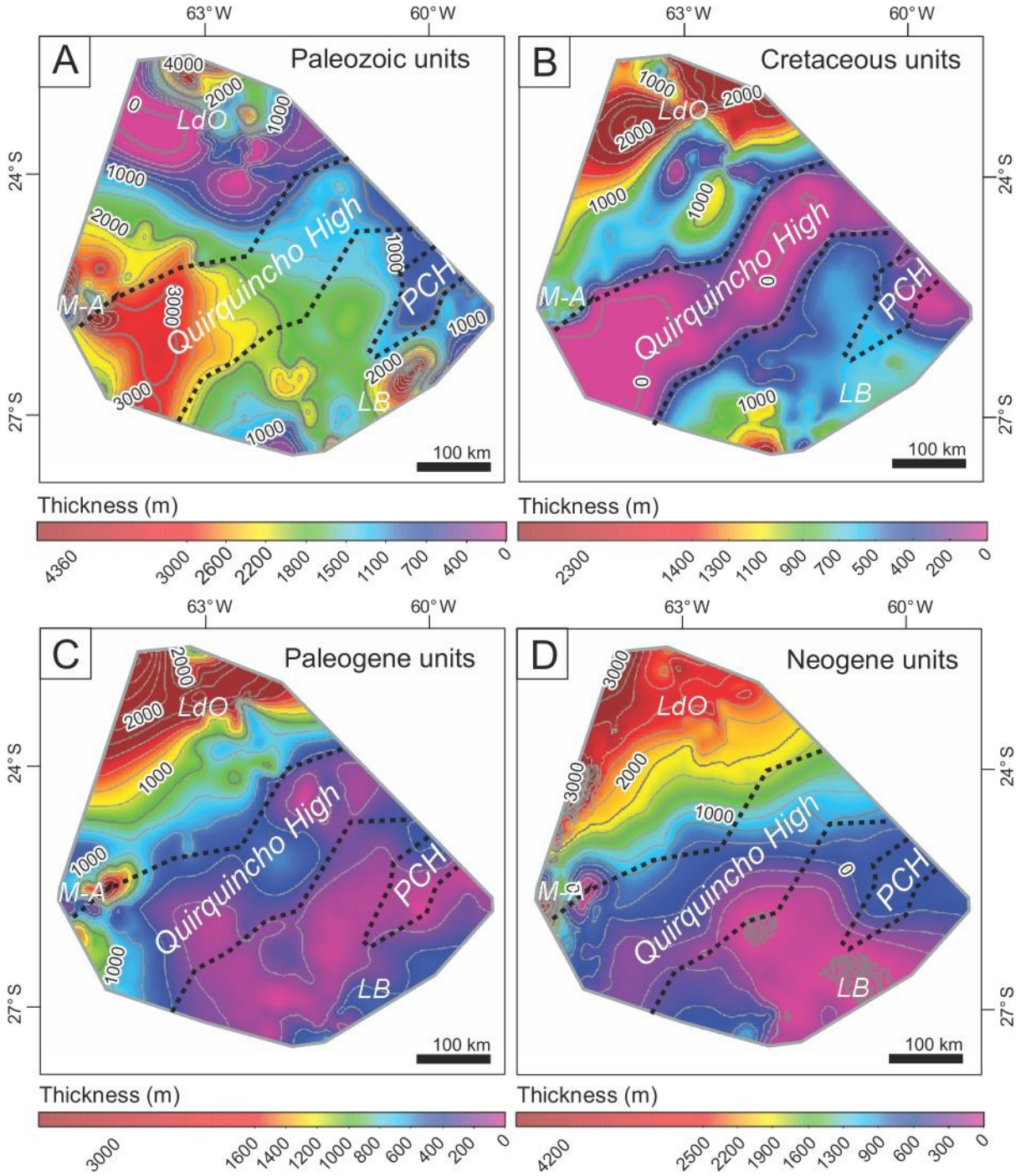

Figure 3.14: Isopach maps showing the thickness distribution of units 1 to 4: A) U1-Paleozoic sediments, B) U2-Cretaceous sediments, C) U3-Paleogene sediments, D) U4-Neogene sediments. LdO: Lomas de Olmedo depocenter; M-A: Metán-Alemanía depocenter; LB: Las Breñas half-graben; PCH: Pampeano-

Chaqueño High. Isopach maps were constructed based on the difference between unit bounding depth maps in Petrel 2015 E&P Software (®Schlumberger).

3.4. Discussion

In this section, I will address the integrated interpretation of the facies relationships associated with the basement highs that were obtained by using different approaches; I will furthermore focus on the timing and possible conceptual models for the origin of the basement highs and their implications for the development of the present-day broken-foreland basin in the adjacent Santa Bárbara System morphotectonic province.

To recapitulate, in the study area, the Quirquincho High has a width that ranges between 115 km in the North and 190 km in the South, a partial length of 470 km that continues outside of the studied area, towards the North and South. Measured in the Top Paleozoic depth map (Fig. 3.13B), the Quirquincho High has a slope of ~0.9% on its NW and the SE-facing flanks. The Pampeano-Chaqueño High has a maximum width of 60 km in the study area, and a length of approximately 160 km, extending farther to the North. Its slope is ~1% on the NW and SE flanks.

3.4.1. Tectono-sedimentary interpretations

The stratal terminations and thickness variations in the seismic transects across the basement highs constrain the timing for the development of the Quirquincho and Pampeano-Chaqueño highs. In the North transect and lines TX_90_209 and 45054, the H1 Precambrian Top and the H2 Paleozoic Top are elevated on the position of the Quirquincho High (Figs. 3.3, 3.9 & 3.10). The U1 Paleozoic seismic unit is slightly thicker beneath the unconformity of the

Quirquincho High than to the west. The truncation of the Paleozoic reflectors marks this unconformity (Figs. 3.9, 3.10 & 3.15). The Cretaceous (U2) and the Paleogene (U3) seismic units onlap towards the Quirquincho High on both, east and west flanks (Figs. 3.9, 3.10 & 3.15). Importantly, the onlap terminations are associated with a thinning of the units until their absence on top of the Quirquincho High.

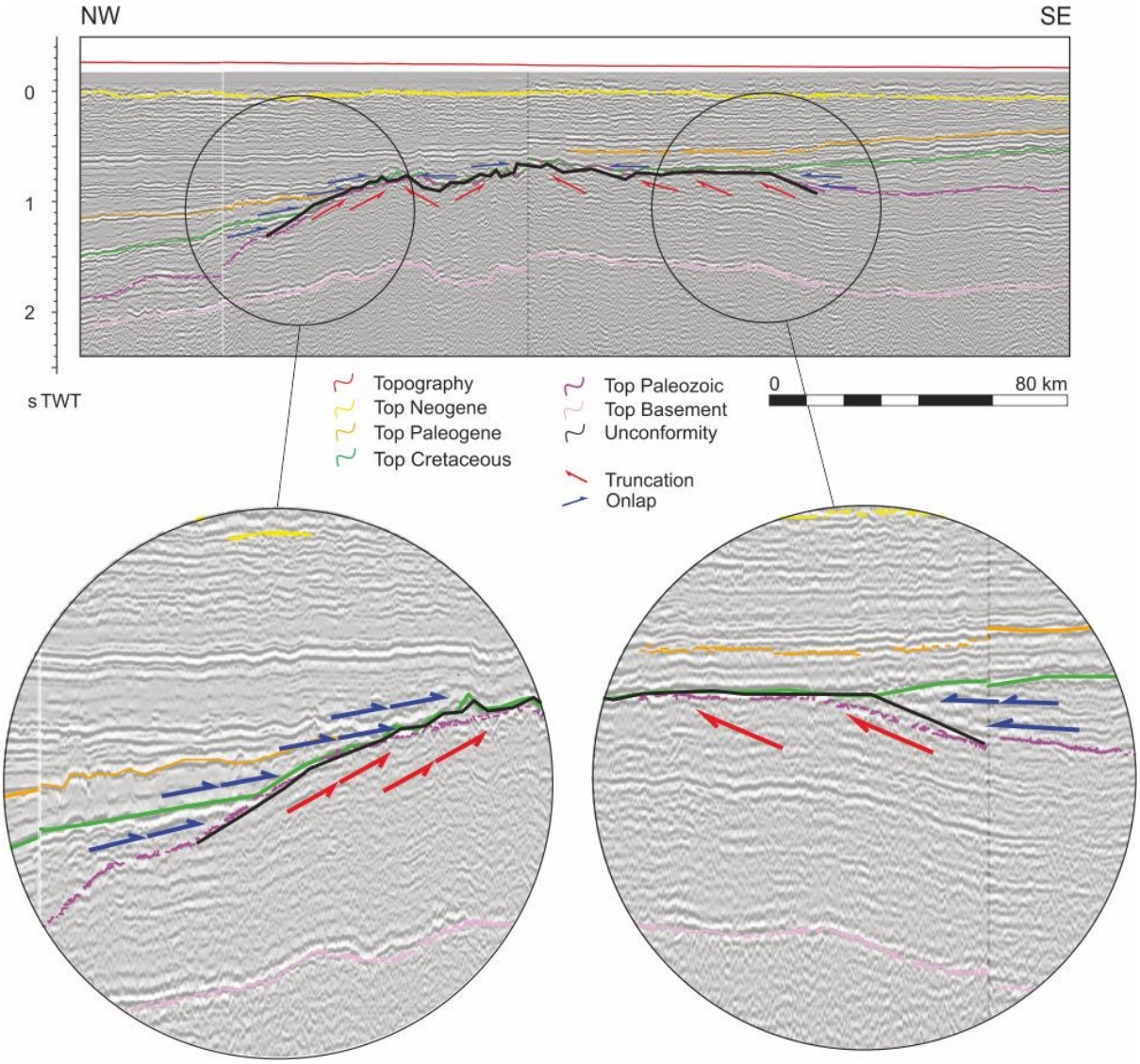

Figure 3.15: Detailed seismic interpretation and stratal terminations in the North Transect (Fig. 3.3), clearly showing the unconformity of the Quirquincho High.

The horizon flattening of the Top Cretaceous H3 (Fig. 3.5B) clearly shows that the Paleozoic seismic unit (U1) was elevated at the time of deposition of the Cretaceous units, representing a positive topographic area in the paleo-landscape with sedimentary onlap to the east and west. The flattening of the Top Paleogene horizon (Fig. 3.5C) documents that the Quirquincho High remained a positive topographic feature during the Paleogene, with sediment onlap against its flanks. This suggests that the Quirquincho High was subject to tectonic uplift during the Cretaceous and remained a positive topographic feature in the landscape when the early Andean foreland basin began to evolve during the Paleogene.

On the isopach map for the Cretaceous unit (Fig. 3.14B), the thickness is minimal (<200 to 0 m) above the Quirquincho High. This thinning and the local absence of Cretaceous sediments on top of the high indicate that this was a non-deposition and/or a bypass sedimentary region. In this sense, the Top Paleozoic depth map (Fig. 3.13B) clearly reveals that this area had positive relief compared to the surrounding areas of the unit.

The combination of i) stratigraphic and structural seismic interpretation; ii) palinspastic restoration derived from horizon flattening; and iii) depth and thickness reconstructions unambiguously documents that the Quirquincho High was a depositional area during the Paleozoic. This is the reason for the greater thickness of the Paleozoic strata in this region compared to neighboring areas (Figs. 3.3 & 3.14A). This character changes during the Mesozoic when the topographic high gained elevation and thus remained a positive topographic element throughout the Cretaceous and Paleogene, as illustrated by the thickness maps (Figs. 3.14B & C).

The truncation terminations suggest exhumation and erosion of the uplifted Paleozoic units (Figs. 3.3, 3.9, 3.10 & 3.15), a diastem with regard to the Cretaceous and Paleogene units, and the onlap termination of their reflectors against the Quirquincho High (Figs. 3.3, 3.9, 3.10 & 3.15). The different thickness maps and characteristics of lateral pinchouts, however, indicate that the uplift of the Quirquincho High must have decreased over time and finally came to a complete halt during the Paleogene. This notion is supported by the uninterrupted deposition of Neogene and Quaternary sediments and the complete burial of the high.

At the eastern end of the North transect (Fig. 3.3), the H1 Precambrian Top and H2 Paleozoic Top are elevated beneath the Pampeano-Chaqueño High unconformity. Here, the Paleozoic seismic unit (U1) exhibits folding of the reflectors, and both Paleozoic and Precambrian levels are affected by an east-dipping normal fault. On top of the Paleozoic, the Mesozoic (U2) strata record thinning with folding and truncation of reflectors that might indicate growth strata associated with the Pampeano-Chaqueño High. At the top of the High, the Paleogene strata (U3) onlap towards both sides. Erosional truncation of horizons and onlap on the top of the Mesozoic horizon mark the unconformity that represents this High.

The structural depth map of the Top Precambrian (Fig. 3.13A), reveals the existence of the Pampeano-Chaqueño High. This relatively elevated irregular topographic feature is oriented NE-SW direction and is smaller in area and elevation compared to the Quirquincho High. The Pampeano-Chaqueño High is also visible in the isopach map of the U1 Paleozoic seismic unit (Fig.3.14A) and by the pronounced thinning of the unit above the High. This stratal configuration

suggests that the Pampeano-Chaqueño High was a slightly elevated topographic feature during the (late?) Paleozoic, controlling the accommodation space of the Paleozoic sediments.

The Cretaceous and Paleocene isopach maps (Figs. 3.14b & C) also document a reduction in thickness near the Pampeano-Chaqueño High, which is compatible with onlap terminations of these units against the topographic feature.

In a proximal position to the Pampeano-Chaqueño High, the reflectors of the Cretaceous seismic unit are folded and truncated by an unconformity (Fig. 3.3). This suggests an active tectonic control of uplift of the Pampeano-Chaqueño High during the deposition of Cretaceous sediments, which was followed by a period of denudation before the accumulation of the Paleogene units started.

Toward the top of the Pampeano-Chaqueño High, the Paleogene seismic unit shows reflectors that gradually onlap against the Cretaceous seismic unit (Fig. 3.3). This suggests that the Pampeano-Chaqueño High remained as an elevated topographic feature during the Paleogene, consequently affecting the stratal architecture of the Paleogene units in the transition between the late stages of extensional processes in the realm of the Salta Rift and sedimentation in the Andean foreland basin.

On top of the seismic stratigraphic sequence above the Pampeano-Chaqueño High follow the Neogene and Quaternary seismic units, which show a flat-lying and tabular configuration of reflectors that entirely covers the Pampeano-Chaqueño High (Fig. 3.3). This indicates that the

uplift of the Pampeano-Chaqueño High and its tectonic control on sedimentation lasted from the late Paleozoic to the Cretaceous and probably extended even into the Paleogene, but it had no effect on subsequent sediment routing and depositional processes.

The morphology of the Quirquincho High as shown on the seismic interpretation of the South transect (Fig. 3.4), is similar to that seen in the North transect (Fig. 3.3). This also emerges from the isopach maps (Fig. 3.15), thus suggesting tectono-sedimentary control along strike with respect to the Paleozoic–Cenozoic sedimentary cover. However, in the South transect, the Cretaceous sediments do not extend to the west of the high; i.e., toward the southwest region of the Salta Rift Basin. In that region, the Cretaceous seismic unit is affected by two N-S-striking conjugated normal faults forming the Metán-Alemanía depocenter (Fig. 3.4). These faults affect the basement and all the seismic units. However, only Cretaceous and Paleogene units are thicker inside the graben than in the surrounding area (i.e., the former rift shoulders areas). During the late Paleogene, the activity of the faults decreased and sediments eventually covered the graben shoulders entirely. This slowdown of the fault-controlled subsidence is compatible with the absence of syn-extensional growth strata and hence the ensuing post-rift or sag stage of the Salta Rift Basin, where thermal subsidence prevailed at least until the Paleocene (Starck, 2011; Marquillas *et al.,* 2005). The distribution of sedimentation during the Paleogene (Figs. 3.5B & C) supports this interpretation and therefore the top of the Cretaceous seismic unit (horizon H3) can be interpreted in the context of a "*breakup unconformity*" (*sensu* Falvey, 1974).

Interestingly, the wedge-shaped geometries of Cretaceous and Paleogene units indicate syn-extensional growth strata due to Cretaceous to Paleogene tectonic reactivation of these faults (*e.g.,* Prosser, 1993; Withjack *et al.,* 2002). In contrast, the Neogene strata have the same thickness within and outside of the graben area. In addition, these strata are folded as the underlying units, suggesting that subsequent to the Neogene deposition, these normal faults were reactivated and positively inverted during the Quaternary. These configurations are thus testimony to basin inversion forced by the compressional stress field in the course of Andean mountain building. In the North transect (Fig. 3.3), a graben located to the west in the Salta Rift Basin, corresponds to the Lomas de Olmedo depocenter. The main differences between the Metán-Alemanía and the Lomas de Olmedo depocenters are rooted in their structural architectures and strike of their principal extensional faults. The Metán-Alemanía depocenter is bounded by ~N-S-striking normal faults, whereas the Lomas de Olmedo basin is bounded by approximately E-W-striking faults. The different orientation of the major normal faults with respect to the Andean regional shortening oriented NE-SW (Marrett & Strecker, 2000) may explain the lack of positive tectonic inversion in the North transect (Fig. 3.3) during the Cenozoic (Iaffa *et al.* 2011, Kley *et al.*, 2005), although Ramos *et al.* (2006) cited limited evidence for reactivation of extensional structures and shortening in the Lomas de Olmedo region that is still active today.

The flattening of the top of Neogene (horizon H5) (Fig. 3.5D) documents a westward-thickening wedge of Neogene seismic unit (U4), which indicates that the general shape of the entire depositional area changes to the geometry of a typical foreland basin, where subsidence

was caused by tectonic and sedimentary loading associated with the uplifting Andes (Horton & Folguera, 2019). The Quaternary sediments show a similar wedge shape geometry in the North transect (Fig. 3.3) and in the South transect (Fig. 3.4), but starting a little more to the east in the latter. In the west, on top of the Cretaceous to Paleogene in the Metán-Alemanía depocenter (Fig. 3.4), the overlying Neogene sediments are folded and exposed at the surface. The less deformed Quaternary deposits outcrop farther to the east, due to the continued compressional tectonism in the Eastern Cordillera (e.g., Garcia *et al.*, 2019; Figueroa Villegas *et al.*, 2020).

3.4.2. Conceptual models of the basement highs

The integration of the geological observations presented in this thesis reveals that the Chaco-Pampean plain covers a complex array of basement topography and depositional geometries involving Paleozoic to Neogene sediments whose stratal relationships and deformation can be probed by geophysical and well data below the Quaternary sedimentary cover.

Basement highs in distal foreland regions or pericratonic areas may occur in a range of tectonic settings and may therefore be caused by a range of geological processes (Peacock & Banks, 2020). In this sense, several hypotheses could explain the tectonic evolution of the Quirquincho and Pampeano-Chaqueño basement highs, which can be addressed by the new structural and seismic stratigraphic information presented in section 3.3. This new information provides valuable spatiotemporal constraints about the tectono-sedimentary evolution of the

Chacoparanaense Basin and allows the elaboration of conceptual models explaining the origins of basement highs in general.

The first hypothesis to be considered is that the Quirquincho and Pampeano-Chaqueño highs may be an integral part of forebulges in a typical foreland basin (*sensu* DeCelles & Giles, 1996). Accordingly, the Quirquincho High might have been generated during the onset of Andean tectonic deformation during the Paleogene (Horton, 2018; Coutand *et al.*, 2001), whereas the Pampeano-Chaqueño High, which is located farther east, might correspond to a Neogene forebulge. This would imply a significant eastward migration of the flexural subsidence profile from the Paleogene to the Neogene. Such a hypothesis would represent a continuous foreland-basin scenario that was later modified by the basement-cored uplifts of the Santa Bárbara morphotectonic province, thus generating a broken foreland dominated by a thick-skin deformation style (Strecker *et al.*, 2012; Del Papa *et al.*, 2013; Zapata *et al.*, 2020; Arnous *et al.*, 2024). However, as my analysis shows, the Cenozoic sediments that cover the basement highs do not exhibit any evidence of contractional deformation in the corresponding locations in the foreland; consequently, in light of the shown depositional geometries and the chronology of deduced events, a Cenozoic forebulge scenario does not apply here.

Another possible cause for the past vertical movements of these highs may be related to the Mesozoic extensional tectonics and associated rift-shoulder uplift during the formation of the Salta Rift Basin and overall subsidence of the Chacoparanaense Basin (Salfity & Marquillas, 1994; Starck, 2011). Such processes have been invoked along the Atlantic margin of North

America (Anell, 2009), at the Rodna Ridge in the United Kingdom (Trice, 2014), or during Cretaceous—Paleogene extensional tectonism before the onset of normal faulting in the Kenya and Southern Ethiopian rifts (Foster & Gleadow, 1996; Torres Acosta *et al.*, 2015; Boone *et al.*, 2019; Erbello *et al.*, 2023). Chronologically, and according to stratigraphic cross-cutting relationships, such a tectonic phase is difficult to reconcile with the genesis of relief of the Quirquincho and Pampeano-Chaqueño highs, and therefore requires other mechanisms that forced late Paleozoic uplift. Nevertheless, the effects of local extensional tectonic activity could have influenced the persistence of the Quirquincho High during the Mesozoic, acting as a peripheral sediment source area for the Salta Rift and Chacoparanaense basins.

In a third alternative, both highs could have been caused by the activity of blind thrusts or reverse faults, associated with a major, westward-dipping crustal detachment during the early stages of development of the Chacoparanaense Basin. However, I could not observe any evidence for structures to support this interpretation either, even taking into account all available geophysical information that would be compatible with a major crustal detachment.

The analysis of the unconformities and lateral pinchouts and terminations, as well as the general morphology of the Quirquincho and Pampeano-Chaqueño basement highs, suggests that both topographic highs were already formed during the late Paleozoic and are thus clearly paleo-tectonic features. In addition, the analyzed data confirm that the Chacoparanaense Basin was a subsiding area with epicontinental marine sedimentation during the late Precambrian and early Paleozoic (Russo *et al.*, 1979; Chebli *et al.,* 1999). However, this first-order assessment needs to

be further examined to link tectonic events or mechanisms that would have been responsible for the uplift of both basement highs in the context of regional geodynamic processes. A viable possibility is that the uplift was caused by flexural loading due to the growth of proto-Andes or Ancient Andes (*sensu* Limarino *et al.* 2023) during the Gondwanic orogeny along the western margin of Gondwana, which lasted from the Carboniferous to the Permian and perhaps continued even during the early Triassic (Ramos, 1999; Heredia *et al.* 2016, 2018; Limarino *et al.* 2023). Such a scenario would imply that the highs might have corresponded to ancient forebulges that evolved during the eastward migration of the Gondwanic deformation front (Fig. 3.16). Chronologically, such a tectonic event would be constrained by the truncation of the Paleozoic strata below the Top Paleozoic unconformity and onlap stratal termination of Mesozoic and Paleogene seismic units against the Paleozoic and Mesozoic seismic units, respectively (Figs. 3.3, 3.4, 3.5, 3.9, 3.10, 3.11, 3.15).

If the hypothetical, fourth scenario suggested above is realistic, the Gondwanan subduction orogen caused the deformation of the continental lithosphere involving two forebulges during the migration of the crustal flexural response associated with tectonic loading (Fig. 3.16). The first, and larger forebulge, would have corresponded to the Quirquincho High, whereas the second, and smaller forebulge, would have corresponded to the Pampeano-Chaqueño High. Importantly, this scenario is consistent with our age observations and onlap relationships and hence provides a reasonable tectonic mechanism for the uplift of these features and the observed stratal relationships. Following DeCelles and Giles (1996), a forebulge is a broad region of flexural uplift and a site of unconformity development, condensation and

stratal thinning. This matches the results of the temporal and stratal relationships regarding the Quirquincho High, which would correspond to a broad, flexurally uplifted region, where an unconformity is observed between truncated Paleozoic strata and condensed Paleogene strata (Figs. 3.3, 3.4, 3.5, 3.9, 3.10, 3.11, 3.15).

Following this line of arguments, the Pampeano-Chaqueño High would have corresponded to a second, areally less pronounced forebulge that developed due to continued flexural migration in combination with the presence of a mechanically weaker, low crustal density zone (section 2.1.1, and Meessen *et al.*, 2018) that was conducive to deformation far away from the Gondwanic deformation front and within the paleo-foreland basin.

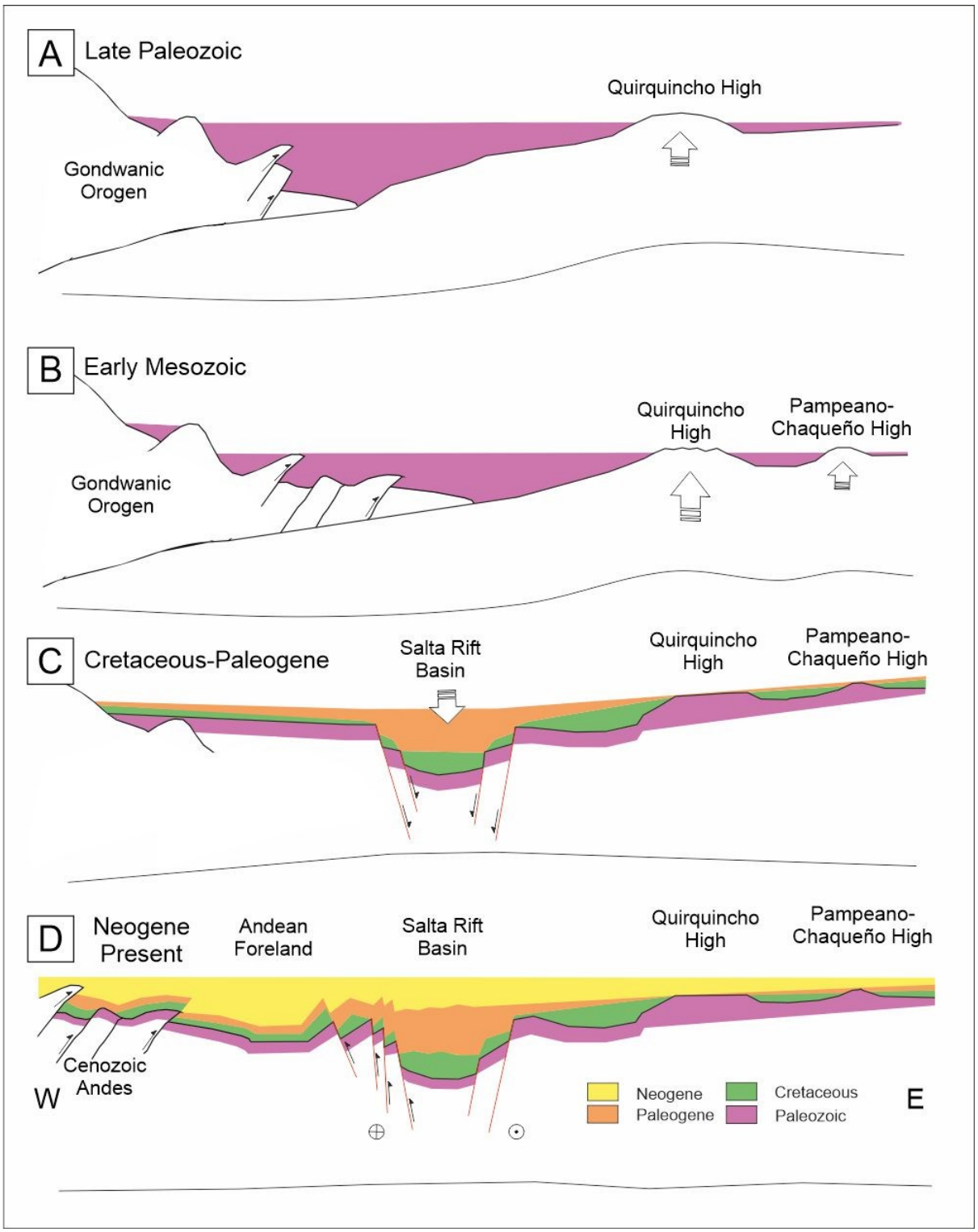

Figure 3.16: Conceptual model of the evolution of the Quirquincho and Pampeano-Chaqueño highs. A) Late Paleozoic: development of the Quirquincho High. B) Early Mesozoic: development of the Pampeano-Chaqueño High and erosion on the Quirquincho High. C) Cretaceous-Paleogene: Development of the Salta Rift Basin and onlapping strata on the high topography. D) Neogene: Andean Foreland setting, progressive

inversion of inherited normal faults, and complete covering of the highs by Neogene and Quaternary sediments.

3.4.3. Influence of the basement highs and comparison with the Cenozoic Andean foreland

The identification of forebulge-like basement highs in the Paleozoic strata of the Chacoparanaense region provides an opportunity to explore how inherited crustal features influence foreland basin development in different tectonic regimes. Assuming that the Quirquincho and Pampeano-Chaqueño highs formed within a flexural regime during the Gondwanan orogeny, this section places the results within a broader geodynamic context. In particular, I compare the Paleozoic foreland architecture with that of the Cenozoic Andean foreland, integrating evidence from analogous regions worldwide to extend the relevance of this case study to other regions.

During the Gondwanan orogeny (the ''Ancient Andes''), the South American plate underwent thin-skinned flexural deformation that produced a classical foreland system (DeCelles & Giles, 1996). This system included a wedge-top (preserved in the modern Frontal Cordillera; Limarino *et al.*, 2023), a foredeep (e.g., Paganzo, Tarija, and San Rafael basins, Limarino *et al.*, 2023), a forebulge (represented by the Quirquincho and Pampeano-Chaqueño highs) and a backbulge zone (represented by the Chacoparanaense basin). The morphotectonic and stratigraphic evidence described above supports the interpretation that these highs were flexurally uplifted during the eastward advance of the Gondwanan deformation front. The presence of regional unconformities, condensation and thinning of overlying strata is consistent with foreland

dynamics and strengthens the interpretation of these features as part of a contiguous, flexural foreland system.

In contrast, the Cenozoic Andean foreland at similar latitudes exhibits a segmented, broken foreland architecture dominated by thick-skinned deformation, where well-defined depozones are absent (Strecker *et al.*, 2011; Del Papa *et al.*, 2013; Zapata *et al.*, 2020). This shift from a continuous to a broken foreland style is interpreted as the result of major changes in lithospheric boundary conditions between the late Paleozoic and the Cenozoic. Following orogenic loading and crustal shortening, the Mesozoic breakup of Gondwana initiated a phase of prolonged extension, leading to the development of the Salta Rift with its three sub-basins between the Cretaceous and the Paleogene (Salfity & Marquillas, 1994; Starck, 2011; Marquillas *et al.*, 2005). Rifting introduced pronounced crustal heterogeneities that modified the mechanical stratigraphy of the crust. When Andean shortening resumed during the Cenozoic, these inherited zones of weakness became focal points for inversion, resulting in distributed crustal shortening and uplift, leading to the formation of the Santa Bárbara broken foreland province.

Recent global syntheses emphasise that both continuous and broken foreland architectures can arise in convergent environments, depending on the pre-existing lithospheric structure (Lacombe & Bellahsen, 2016). The comparison between the Gondwanan and Andean forelands in northwestern Argentina illustrates this principle, illustrating how crustal inheritance can dictate the style and geometry of subsequent foreland evolution.

Numerous global analogues support the interpretation that forebulges and associated flexural features can persist in the geological record and exert a long-term influence on basin evolution. For example, in the western Amazonian foreland of the modern Central Andes, the Iquitos Arch represents an inherited forebulge (Roddaz *et al.*, 2005). Comparable features are also observed in the Sierra Morena of southern Spain, interpreted as a Neogene subaerial forebulge within the Guadalquivir Basin (García-Castellanos *et al.*, 2002), and in the Apulian forebulge of the Adriatic Sea, associated with the Apennine orogeny (de Alteriis, 1995; Billi & Salvini, 2003). The Oman Mountains are also a forebulge formed during the subduction of the Arabian plate under the Eurasian plate (Rodgers & Gunatilaka, 2003). Paleozoic and Mesozoic examples include the Morrowan forebulge of the Alleghanian Orogeny (Lash & Engelder, 2007) in North America, the migrating forebulge within the Cretaceous Western Interior Basin during the Laramide orogeny in North America (White *et al.*, 2002), and the Ediacaran forebulge of the São Francisco Basin in Brazil, where extensional structures provide evidence for flexural uplift and coeval normal faulting (Reis *et al.*, 2017). The tectonic behavior inferred for the Quirquincho High during the Gondwanan orogeny agrees very well with these analogs, supporting the interpretation that similar forebulge dynamics were active in the Gondwanic foreland during the late Paleozoic of South America.

Increasing geophysical and structural evidence in various foreland settings has linked thick-skinned deformation to the reactivation of inherited rift-related faults, similar to what has been observed in the Cenozoic Andean broken foreland regions. Such deformation patterns have been observed in the Ionian segment of the Apennine Belt (Doglioni *et al.*, 1999), the West Duero Basin

associated with the Alpine Pyrenean-Cantabrian orogeny (Martín-González, 2014), and the Cretaceous Subhercynian Basin of Central Europe (Hindle & Kley, 2021). These cases mirror the tectonic evolution of the Andean foreland between 22° and 28°S, where the extensional framework created during the Salta Rift phase conditioned the resulting broken foreland.

Further support for the role of crustal inheritance in shaping the stratal geometries of foreland basins comes from examples in the western United States. In the Uinta region of Utah, domal uplift associated with the Uinta Arch strongly influenced sedimentation patterns in the adjacent foreland basin (Bruhn *et al.*, 1986). Similarly, in the Black Hills of South Dakota and Wyoming, mid–Cretaceous deformation patterns were controlled by pre-existing structural highs (Merewether & Cobban, 1986). The Niobrara Formation and Eagle Sandstone of Montana and South Dakota, for example, record sedimentation processes influenced by uplifted arches that have been interpreted as paleo-forebulges (e.g., Shurr & Rice, 1986).

Taken together, the analysed stratal geometries and the development of high topography in the paleo-foreland of the Gondwanides and comparisons with other orogenic settings highlight how inherited basement highs, such as the Quirquincho and Pampeano-Chaqueño highs, may fundamentally shape foreland development, both as structural barriers and as stratigraphic markers across orogenic cycles. The study presented herein thus contributes to a more nuanced understanding of foreland basin evolution and illustrates the variability of tectonic responses within comparable environments of mountain building. The Chacoparanaense region provides a compelling example of how forebulges can be preserved under different tectonic regimes and

thus provide valuable insights into the interplay between crustal inheritance, ongoing geodynamic processes, and basinwide sedimentary processes, both regionally and globally.

3.5. Conclusion

The subsurface interpretation of the Chacoparanaense Basin in northern Argentina suggests that the morphology, wavelength, and stratal terminations of the Quirquincho High may represent a forebulge resulting from late Paleozoic orogenic processes. Similarly, the Pampeano-Chaqueño High farther east may represent a second-stage of forebulge in orogenic evolution, favored by crustal weakness. All of the analyzed features are now buried below younger sediments, and the observed structures and sedimentary relationships are inherited from late Paleozoic processes. The basement highs persisted as positive topographic elements during the Mesozoic, when the region became an integral part of the Salta Rift province. The third step in the evolution is still active and associated with subsidence and depositional processes of the Andean sedimentary wedge.

The entire history of the Chacopampean plain is reflected by the studied sections, starting with late Precambrian intracratonic extension in Las Breñas halfgraben and continuing with subsidence and marine deposition during most of the Paleozoic. During the late Paleozoic, the area was distally affected by shortening of the Gondwanic orogeny, which caused forebulge uplift of the crust in two different positions: The Quirquincho High and the Pampeano-Chaqueño High. During the Mesozoic Gondwana break-up, the extensional tectonics caused the rifting and formation of the Salta Rift Basin, the subsidence of the Chacoparanaense Basin, and the

Pampeano-Chaqueño and Quirquincho Highs remained positive features, with the regional onlap of the Mesozoic strata towards the highs.

At the beginning of the Cenozoic, subduction of the Nazca plate beneath the South American plate caused the first phase of the Andean deformation. In the Cenozoic, deformation advanced from west to east and resulted in compressional inversion of the western branches of the Salta Rift Basin (Metán-Alemanía branch), while the deformation has not yet reached the Lomas de Olmedo Basin in the eastern sectors of the former rift. The studied Quirquincho and Pampeano-Chaqueño highs and the rest of the Chacoparanaense Basin were gradually covered by the sediments sourced from the orogen, which now form the present-day wedge-shaped Andean Foreland Basin.

Finally, the study offers new insights about the potential of the Quirquincho High for hydrocarbon trap formation due to the onlap stratal terminations, a topic of interest for further research. For this reason, I encourage explorers to study individual tectonic domains in detail to understand the temporal relationships of petroleum systems in their complex tectonic context. Techniques of structural and thermal history reconstruction (organic petrography, fission-track dating, geologic age dating), structural restoration, and basin modelling should be used in an integrated and more detailed manner.

Chapter 4: Basin Modelling of the Chacoparanaense Basin

4.1. Introduction

Basin modelling is the temporal reconstruction of the geologic evolution of a basin, which involves establishing the sequential records of changes that have occurred in a basin over time (e.g., Welte *et al.*, 1997; Allen & Allen, 2013). A sedimentary basin, as we see it today, is the result of the sum of all the geological, geophysical, and geochemical processes that have either influenced distinct sectors of the basin or a basin system as a whole during its geological history (e.g., Welte *et al.*, 1997). Interpreting a basin can be a complex task for geoscientists because evidence of past forcing mechanisms and processes is often incomplete, covered, altered, or even obliterated by more recent geological activity, involving basin inversion (e.g., Welte *et al.*, 1997; Allen & Allen, 2013)

Hydrocarbon exploration is often the main target of basin modelling, which has driven the technological development of this technique over the past decades. Basin modelling will help to understand petroleum formation taking the entire basin history into account, making it a valuable method in terms of exploration targets for economically viable resources (Welte *et al.*, 1997); it is also a powerful technique that enables an assessment of the different effects of tectonism, sedimentary and erosion processes, diagenesis, and sea-level change that have influenced the Earth's crust in the geological past under changing geodynamic and climatic conditions (e.g., Garcia-Castellanos & Cloetingh, 2011).

The basin modelling approach used in this study is a dynamic forward modelling approach in which the controlling processes of basin evolution are computer-modelled to simulate geologic time and create temporal reconstructions of the various elements of basin history. (Welte *et al.*, 1997; Hantschel & Kauerauf, 2009).

The first step in the chosen approach of basin modelling is the collection of regional-scale geological and geophysical data to construct a structural model. The backbone of this structural model is mainly based on the integration of seismic reflection and well data. Basin evolution processes are then modelled computationally, and the results are evaluated against measured calibration values to test the various hypotheses of basin evolution (Welte *et al.*, 1997; Hantschel & Kauerauf, 2009).

Using this technique, I intended to shed light on the geological evolution of the Chacoparanaense Basin. The Chacoparanaense basin is of intracratonic origin (Reinante *et al.*, 2014) and has received sediments since the late Precambrian. Previous studies (e.g., Russo *et al.*,1979; Chebli *et al.*, 1999; Fernandez Garrasino *et al.*, 2005; Reinante *et al.*,2014) have assessed the evolution of the Chacoparanaense Basin based on the stratigraphic record obtained from exploratory drilling and seismic lines. In this thesis, I have reinterpreted a large volume of available and newly released subsurface data, modelled basin-evolutionary processes by taking into account regional geological knowledge, and compared the results with calibration data. Several sets of reasonable geological scenarios were modelled using PetroMod petroleum

systems modelling software (®Schlumberger) concerning different stages of basin history. The six most representative scenarios are presented in section 4.4 and are discussed below.

4.1.1. General characteristics of the Chacoparanaense Basin

The stratigraphy and a review of the state of knowledge of the Chacoparanaense Basin are presented in Chapter 2.2. To follow the work in Chapter 3 on the geological transition between the Chacoparanaense Basin, the Salta Rift, and the Cenozoic Andean foreland basin, the model is developed for the northern part of the Chacoparanaense Basin, covering parts of the provinces of Santiago del Estero and Chaco. The study area includes part of the buried high topography of the Paleozoic Quirquincho High in the northeast (Fig. 1.4; see chapter 1). The study area was selected because it covers part of Quirquincho High in the northeast (Fig. 1.4) and due to its relatively high density of seismic-reflection data and wells, particularly those with calibration data.

The area covers 56,150 km² and includes 954 km of 2D seismic surveys and 12 boreholes with stratigraphic reports, 5 of which have calibration data. This distribution of subsurface data has enabled to generate a reasonable vertical resolution, which is necessary for the creation a viable structural model.

The surface of the study region is flat (>1% slope), with elevations ranging from 56 m a.s.l. in the southeast to 292 m a.s.l. in the northwest (Fig. 4.1). It is an integral part of the present-day

Andean foreland basin, with only Pleistocene and Holocene clastic sediments exposed, except for a very small area where Cretaceous–Paleogene sediments outcrop (Fig 4.2).

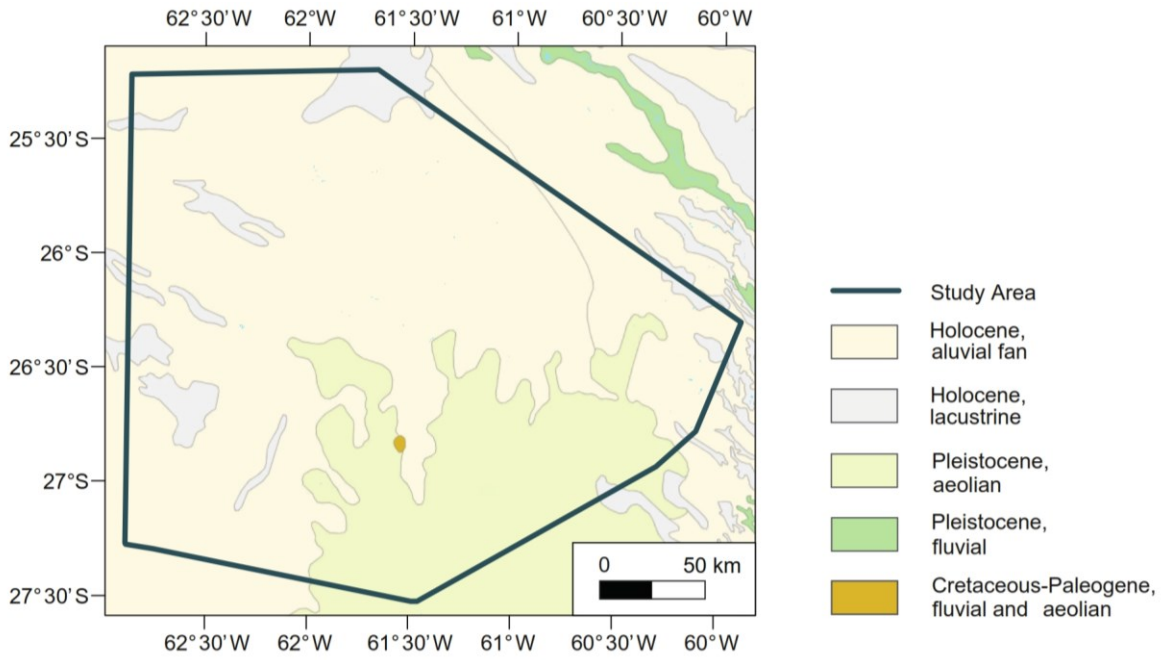

Figure 4.1: Geological map of the study area.

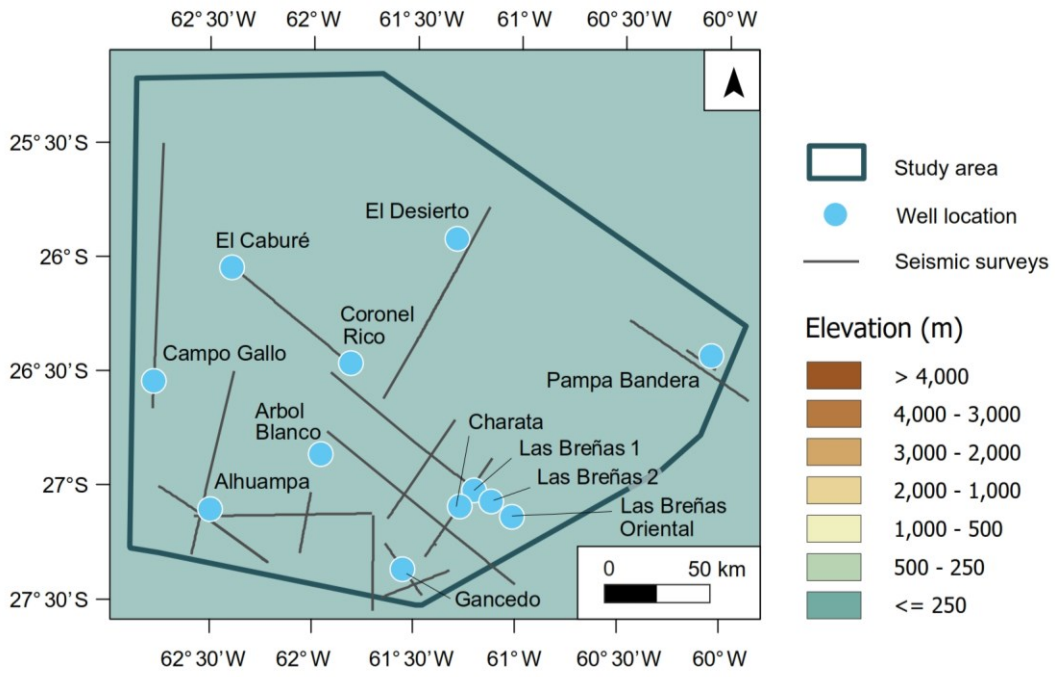

Figure 4.2: Digital Elevation Model (DEM) of the study area, location of seismic surveys and boreholes.

4.1.2. Workflow Outline

The first and most critical step in developing a basin model is creating a conceptual model. The conceptual model is a compilation of the main elements of the basin, suitable for numerical treatment (discretization), placed in a temporal framework (Welte *et al.*, 1997).

Stratigraphic analysis provides the main input to the conceptual model. The history of the basin should be divided into a finite and uninterrupted sequence of events of specific age and duration that describe the evolution of the basin. During each defined period, one of three basic processes was dominant: accumulation of a layer (deposition), non-deposition (hiatus), or uplift

and erosion (unconformity) (Welte *et al*, 1997). To build the geological or conceptual model, I followed these main steps:

- Collection and digitization of all available 2D seismic lines and well reports.
- Selection of the best-quality seismic lines for interpretation.
- Depth-time conversion of well tops according to the velocity law of the Chacoparanaense Basin (see section 3.2- Velocity Models) to correlate seismic lines with well tops.
- Seismic interpretation – in TWT domain- based on reported well tops (Charata, Becker, 1975; El Caburé, Bottcher, 1965; Las Breñas 1, Bottcher, 1974; Coronel Rico, Di Persia, 1969; Pampa Bandera, Knowlton, 1991; El Caburé, Mingramm, 1966a; Arbol Blanco, Mingramm, 1966b; Las Breñas Oriental, Rolleri, 1966; Las Breñas 2, Rolleri, 1967; El Desierto, Rolleri, 1970), using the formation names and their ages as reported in the well reports. 12 seismic horizons were interpreted, and the stratigraphic sequence was divided into 13 units (section 4.2.1).
- Conversion of seismic horizons into depth using the velocity law of the Chacoparanaense Basin (see section 3.3 Depth and thickness maps).
- Interpolation of horizons after seismic interpretation, to produce depth and thickness maps (section 4.2.2).
- Assignment of ages to every interpreted unit and the hiatus and unconformities between them (section 4.2.3).
- Development of simple facies maps for each unit (section 4.2.4).

The different steps are described in detail in the following sections.

4.2. Conceptual Model

The conceptual model represents the current state of the basin, specifically the distribution of strata, structural elements, facies, ages of the horizons and timing of geological events.

Two seismic horizons define each layer of the conceptual model, and its age is defined by the age of these bounding seismic horizons. Discontinuous sedimentary section, marked either by erosional unconformity and/or stratigraphic evidence, may indicate temporal gaps that need to be accounted for by direct or indirect evidence. The facies of a layer vary laterally, representing the main rock types as described by facies maps for each layer.

4.2.1. Seismic Interpretation

The first step for the development of the structural model is the seismic interpretation of all available 2D seismic lines, correlated with information from well reports (chrono-lithostratigraphy).

To obtain a structural model with better vertical resolution than the one presented in Chapter 3, within the precision of the data, I have divided the seismic surveys with twelve seismic horizons into thirteen seismic units based on the denser network of well tops. Each unit includes one or two stratigraphic formations with similar characteristics, and its name is derived from the

corresponding geological system, which is presented in the stratigraphic column of the Chacoparanaense Basin (Fig. 2.1, see chapter 2).

The age of the sediments was determined based on logs of well cuts for each well drilled in the study area. As a first premise, I adopt the ages reported by the authors of these studies (Charata, Becker, 1975; El Caburé, Bottcher, 1965; Las Breñas 1, Bottcher, 1974; Coronel Rico, Di Persia, 1969; Pampa Bandera, Knowlton, 1991; El Caburé, Mingramm, 1966a; Arbol Blanco, Mingramm, 1966b; Las Breñas Oriental, Rolleri, 1966; Las Breñas 2, Rolleri, 1967; El Desierto, Rolleri, 1970). However, the presence of Triassic and Jurassic strata and the challenges in distinguishing them due to the lack of microfossils in the Mesozoic continental deposits is a potential problem in the age assessment (Russo *et al.*, 1989; Chebli *et al.*, 1999; Fernandez Garrasino, 2005) and will be further examined in the section on Modelling Analysis in Chapter 4.5.

In this subsection, I describe seven seismic surveys, selected for their appropriate quality, covering the study area. The seismic surveys have different orientations (Fig. 4.3) and are in most cases within a correlation distance of several boreholes. Interpretation of the horizons was based on correlation with nearby boreholes and subsequent tracking of the horizon reflection pattern.

In survey 44017 (Fig. 4.4), the most prominent feature is a major normal fault striking SE. This fault defines the Las Breñas half-graben, which is intersected perpendicularly by this seismic line. H1 is the top of the crystalline basement (U1). H0 is the top of the late Precambrian metasediments. These sediments were deposited after the opening of the half-graben. This is

followed by a thick wedge of Ordovician sediments (U3), which continues to the NW outside the half-graben. A thin layer of Silurian sediments (U4) lies to the NW. Both the Ordovician and Silurian sediments are overlain by Devonian sediments (U5), seemingly wedged in from the NW. After the deposition of the Devonian sediments, the normal fault bounding the halfgraben appears to have been inverted. The Precambrian–lower Paleozoic sequence is covered by Carboniferous (U6) and Permian (U7) sediments. To the east, where the three wells are located, a pair of conjugate normal faults open a much smaller graben. The graben and surrounding areas are infilled by Jurassic strata (U9) and a thin layer of Cretaceous (U10) sediments. These sediments are superseded by Paleogene sediments (U11), which are thicker in the small graben. A thin layer of undifferentiated Neogene and Quaternary sediments (U12) forms the uppermost layer.

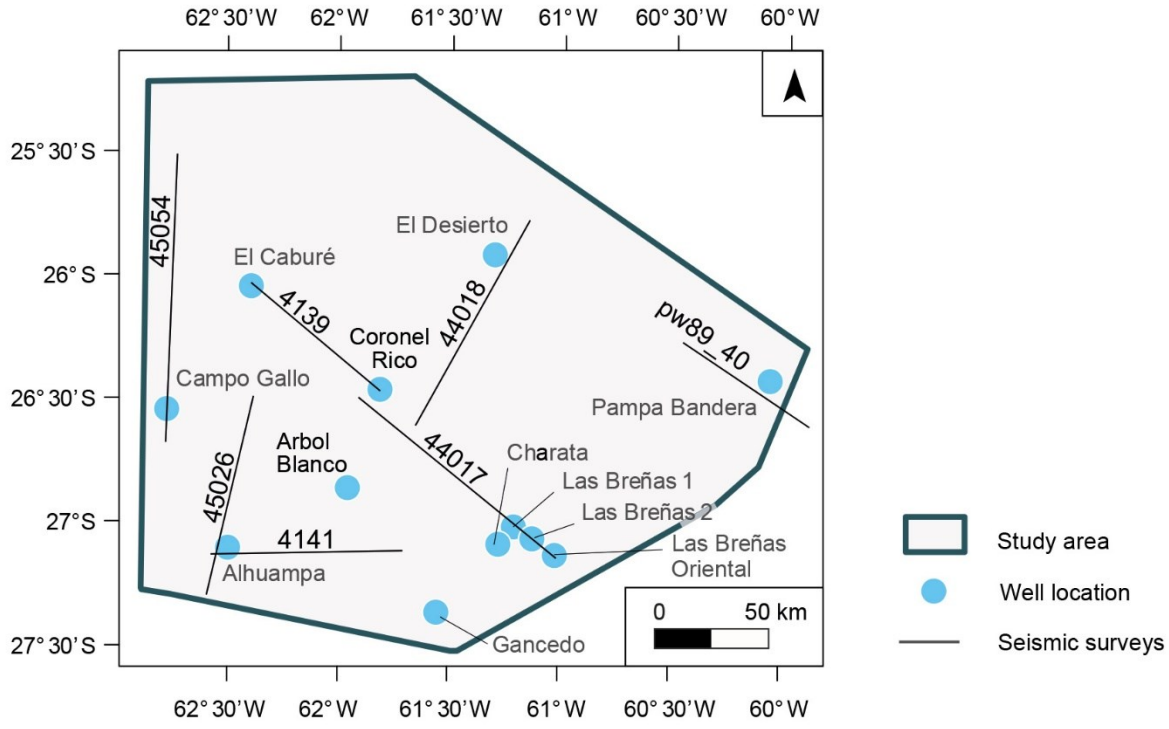

Fig 4.3. Distribution of available data: location of boreholes and seismic lines used for the construction/definition of the conceptual model.

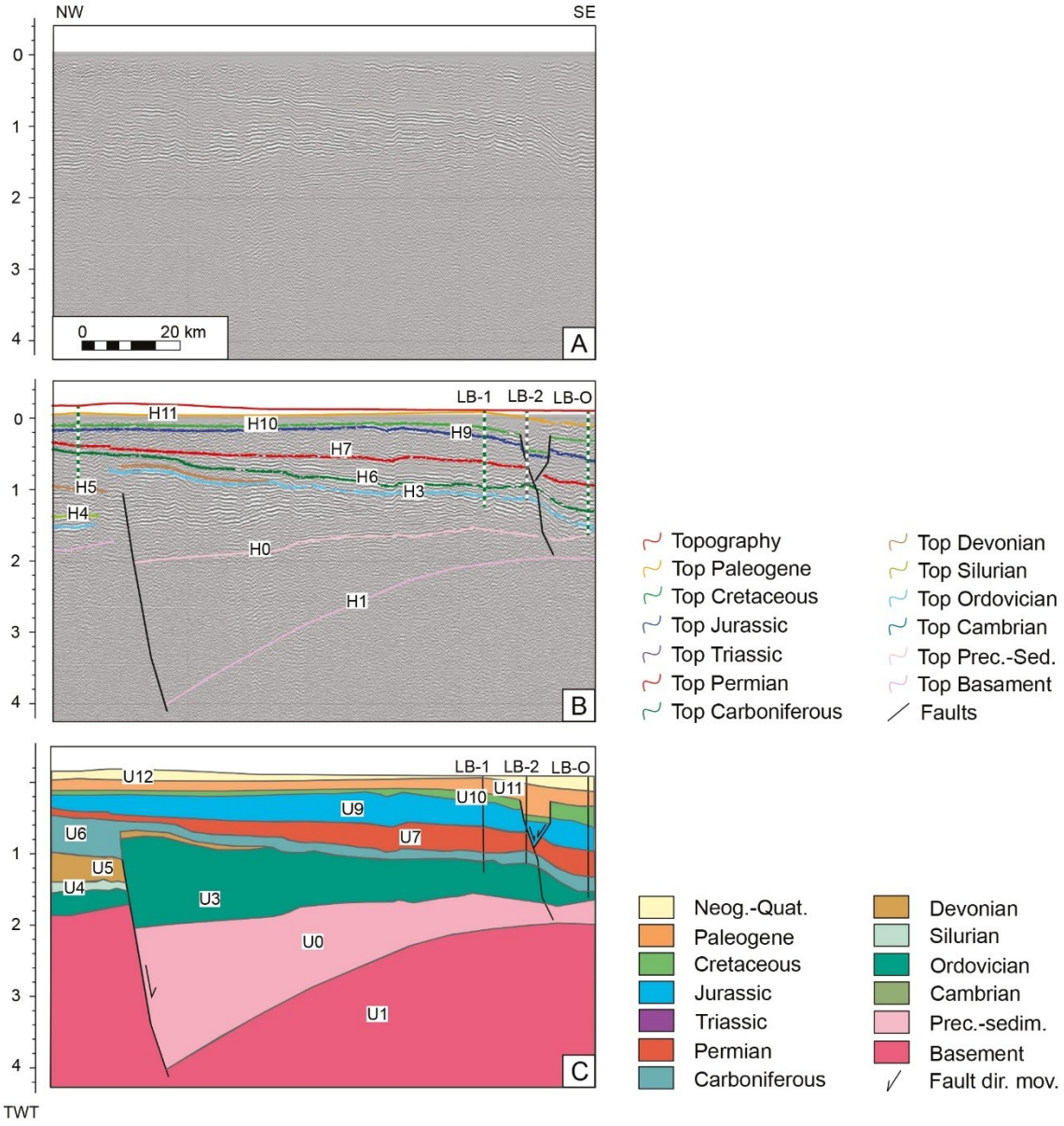

Figure 4.4: Seismic survey 44017. A: uninterpreted seismic line. B: interpreted unit tops: H1: Top Basement, H0: Top Precambrian metasediments, H3: Top Ordovician, H4: Top Silurian, H5: Top Devonian, H6: Top Carboniferous, H7: Top Permian, H9: Top Jurassic, H10: Top Cretaceous, H11: Top Paleogene. C: model of the interpreted units: U1: Basement, U0: Precambrian metasediments, U3: Ordovician, U4: Silurian, U5: Devonian, U6: Carboniferous, U7: Permian, U9: Jurassic, U10: Cretaceous, U11: Paleogene. U12: Undifferentiated Neogene and Quaternary. Wells: LB-1: Las Breñas 1, LB-2: Las Breñas 2, LB-O: Las Breñas Oriental.

Seismic line pw_89_40 (Fig. 4.5) reveals the northern part of the Las Breñas half-graben. It shows the same fault as seismic line 44017 (Fig. 4.4). Deposition begins with late Precambrian sediments (U0) and continues with Cambrian (U2), Ordovician (U3) and Devonian (U5) sediments. All of these units are gently folded around the center of the seismic line, below the Pampa Bandera well. An unconformity, marked by truncation terminations of Ordovician and Devonian (U5) reflectors, interrupts the sedimentary sequence. Above follows an apparently continuous sequence of Carboniferous (U6), Permian (U7), Triassic (U8), Jurassic (U9), Cretaceous (U10), Paleogene (U11) and Neogene, and Quaternary (U12) sediments. The Carboniferous (U6) strata exhibit a wedge-shaped thickening to the NW, and the U7-Permian a complementary wedge-shaped thickening to the SE. The units above (U8 to U12) are almost horizontal.

The W-E oriented seismic survey 4141 (Fig. 4.6) is located in the south of the study area, adjacent to the Alhuampa borehole. The lowest unit is the Precambrian basement (U1), followed by Cambrian (U2) and Ordovician (U3) sediments, partially overlain from the west by Silurian (U4) and Devonian (U5) sediments. Carboniferous (U6) sediments are absent (paraconformity?) and Permian (U7) sediments overlap U3, U4 and U5. This is followed by a thin Triassic layer (U8), a thick Jurassic layer (U9), a thin Cretaceous layer (U10), and a Paleogene layer (U11). The sequence ends with a thick layer of undifferentiated Neogene and Quaternary sediments (U12). All of the horizons are near-horizonal, suggesting a continuous and steady deposition of the sequence, with the only notable feature being the absence of Carboniferous deposits and a less well-developed lateral coverage of Silurian (U4) and Devonian (U5) units, which could be due to the lack of lateral continuity of these units in the region or possible erosion of them.

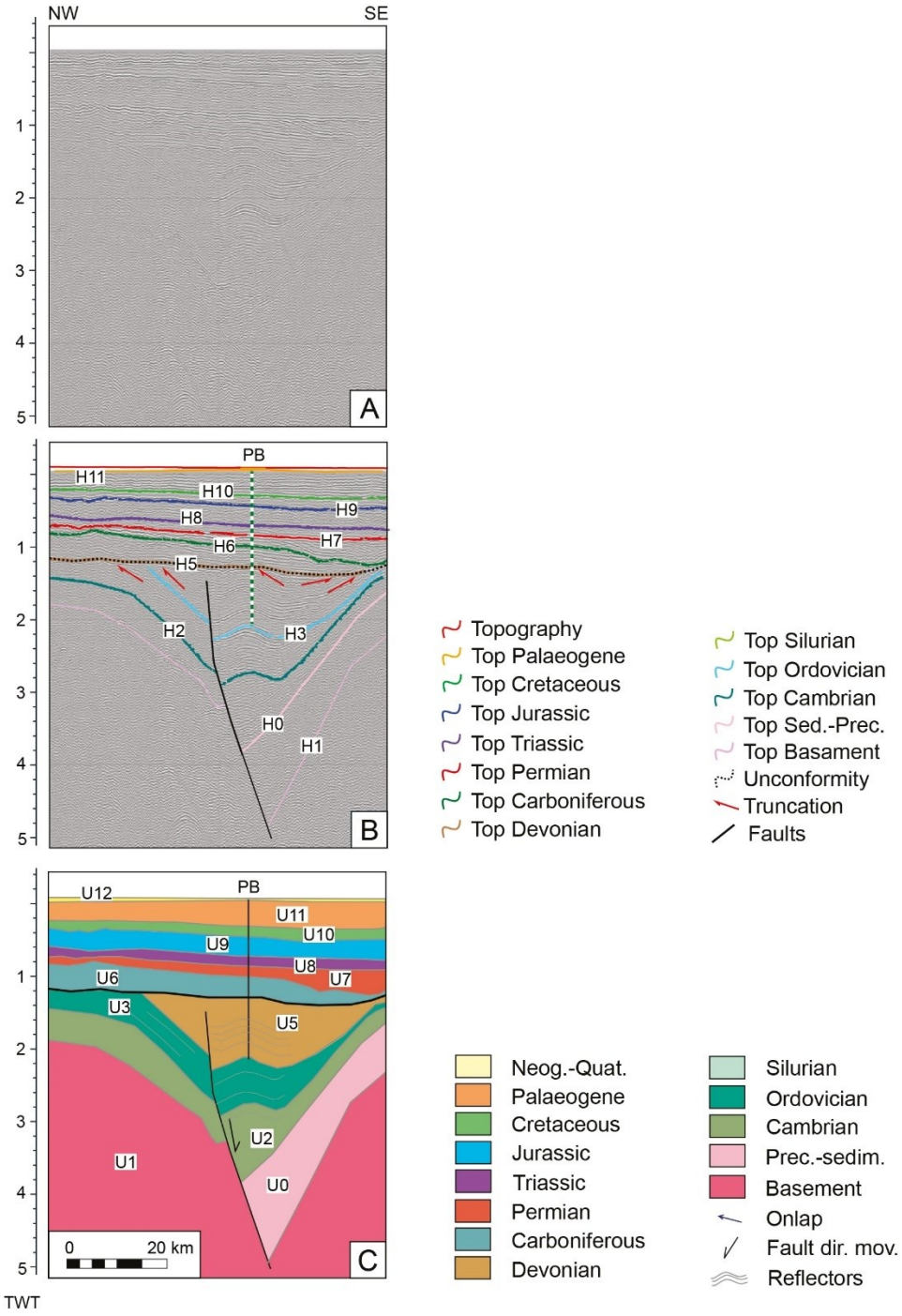

Figure 4.5: Seismic survey pw_89_40. A: uninterpreted seismic line. B: interpreted unit tops: H1: Top Basement, H0: Top Precambrian metasediments, H2: Top Cambrian, H3: Top Ordovician, H5: Top Devonian, H6: Top Carboniferous, H7: Top Permian, H8: Top Triassic, H9: Top Jurassic, H10: Top Cretaceous, H11: Top Paleogene.: C: model of interpreted units: U1: Basement, U0: Precambrian metasediments, U2: Cambrian, U3: Ordovician, U5: Devonian, U6: Carboniferous, U7: Permian, U8:

Triassic, U9: Jurassic, U10: Cretaceous, U11: Paleogene. U12: Undifferentiated Neogene and Quaternary. Well: PB: Pampa Bandera.

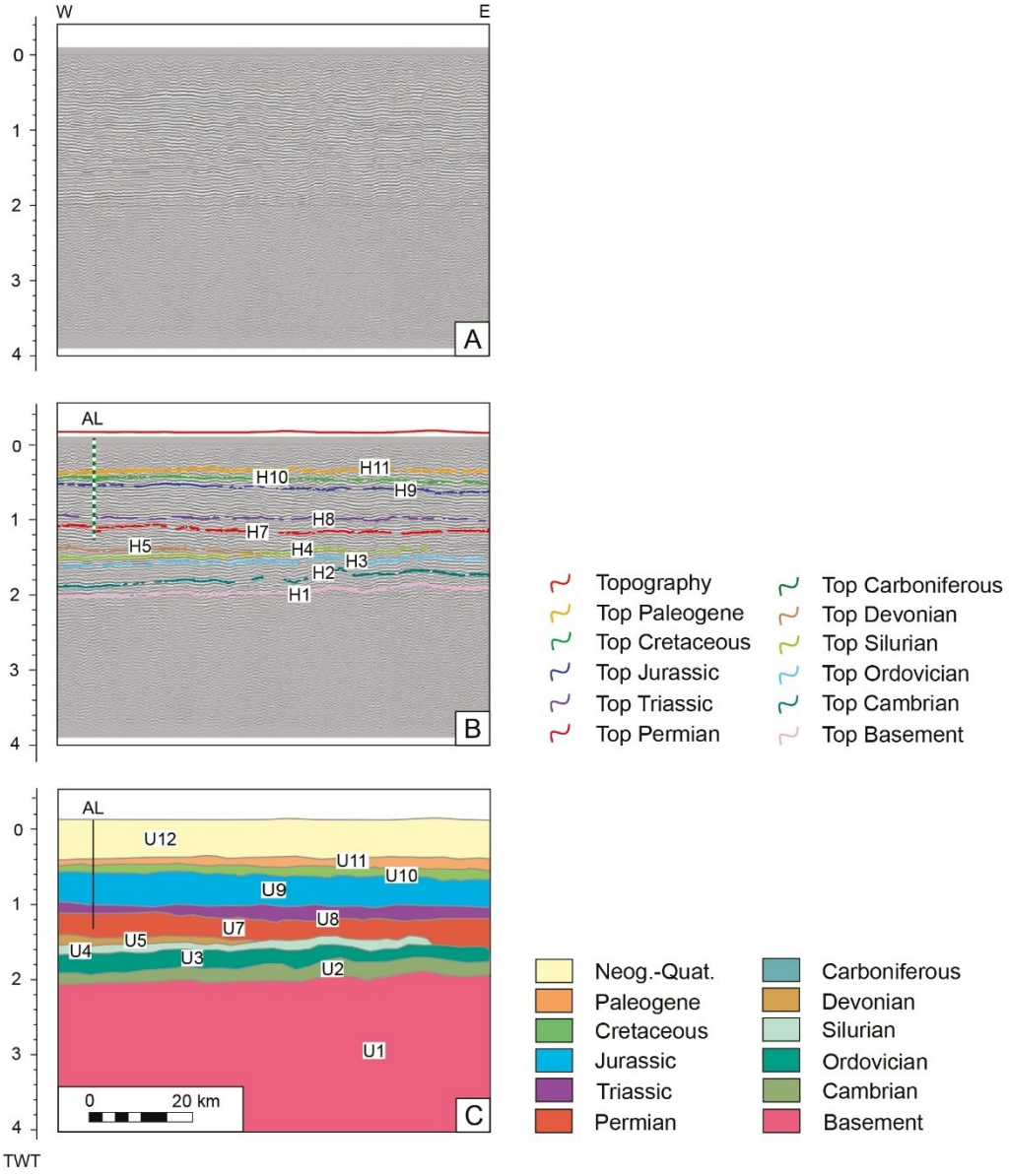

Figure 4.6: Seismic survey 4141. A: uninterpreted seismic line. B: interpreted unit tops: H1: Top Basement, H2: Top Cambrian, H3: Top Ordovician, H4: Top Silurian, H5: Top Devonian, H7: Top Permian, H8: Top Triassic, H9: Top Jurassic, H10: Top Cretaceous, H11: Top Paleogene. C: model of interpreted units: U1: Basement, U2: Cambrian, U3: Ordovician, U4: Silurian, U5: Devonian, U7: Permian, U8: Triassic, U9: Jurassic, U10: Cretaceous, U11: Paleogene, U12: Undifferentiated Neogene and Quaternary. Well: AL: Alhuampa.

Seismic survey 4139 (Fig. 4.7) is NW-SE-oriented and runs between the El Caburé and Coronel Rico wells. The basement (U1) is overlain by Ordovician (U3), a thin layer of Silurian (U4), Devonian (U5) and Carboniferous (U6) sediments. U5 and U6 are slightly wedge-shaped, with the gently tilted, thicker side facing NW. To the SE and center, a thin layer of Permian sediments (U7), terminated by an unconformity, covers U6. The unconformity and the NW dip of U5, U6, and U7 suggest tectonic movement and subsequent erosion, consistent with the uplift proposed for the Quirquincho High to the NW of this survey (see Chapter 3.3 and 3.4). The unconformity is overlain by Cretaceous sediments (U10). To the SE, adjacent to the Coronel Rico well, there is a normal fault that dips to the NW and cuts from the upper part of the Ordovician (U3) to the lower part of the Cretaceous units (U10). The Cretaceous unit (U10) is thicker in the footwall of the fault, suggesting that the fault formed during the early Cretaceous. The Paleogene (U11) lies above and is covered at either end of the line (NW and SE) by a thin layer of Neogene and Quaternary sediments (U12). The shape of U10 and U11 appears to be slightly folded so that U11-Paleogene is exposed in the center of the figure and is only covered on the sides by U12.

Seismic survey 44018 (Fig. 4.8) is oriented SW-NE and located in the immediate vicinity of the Coronel Rico and El Desierto wells. Uniform layers of Ordovician (U3), Silurian (U4), and Devonian (U5) sediments overlie the Precambrian basement (U1). A reverse fault intersects U1 in the center of the survey; U1 and the units above are gently folded over it. The Devonian (U5) is overlain to the SW by a wedge of Carboniferous sediments (U6). A thin layer of Permian sediments (U7) covers U5 and U6, apparently overlapping the fold. This suggests that the faulting and folding predate the Permian and that U7 lies on a paraconformity. U7 is eroded in its upper

part, suggesting an unconformity between U7 and the overlying Cretaceous U10. U10 corresponds to the paleo-topography and is overlain by thin beds of Paleogene (U11) and Neogene and Quaternary (U12) sediments.

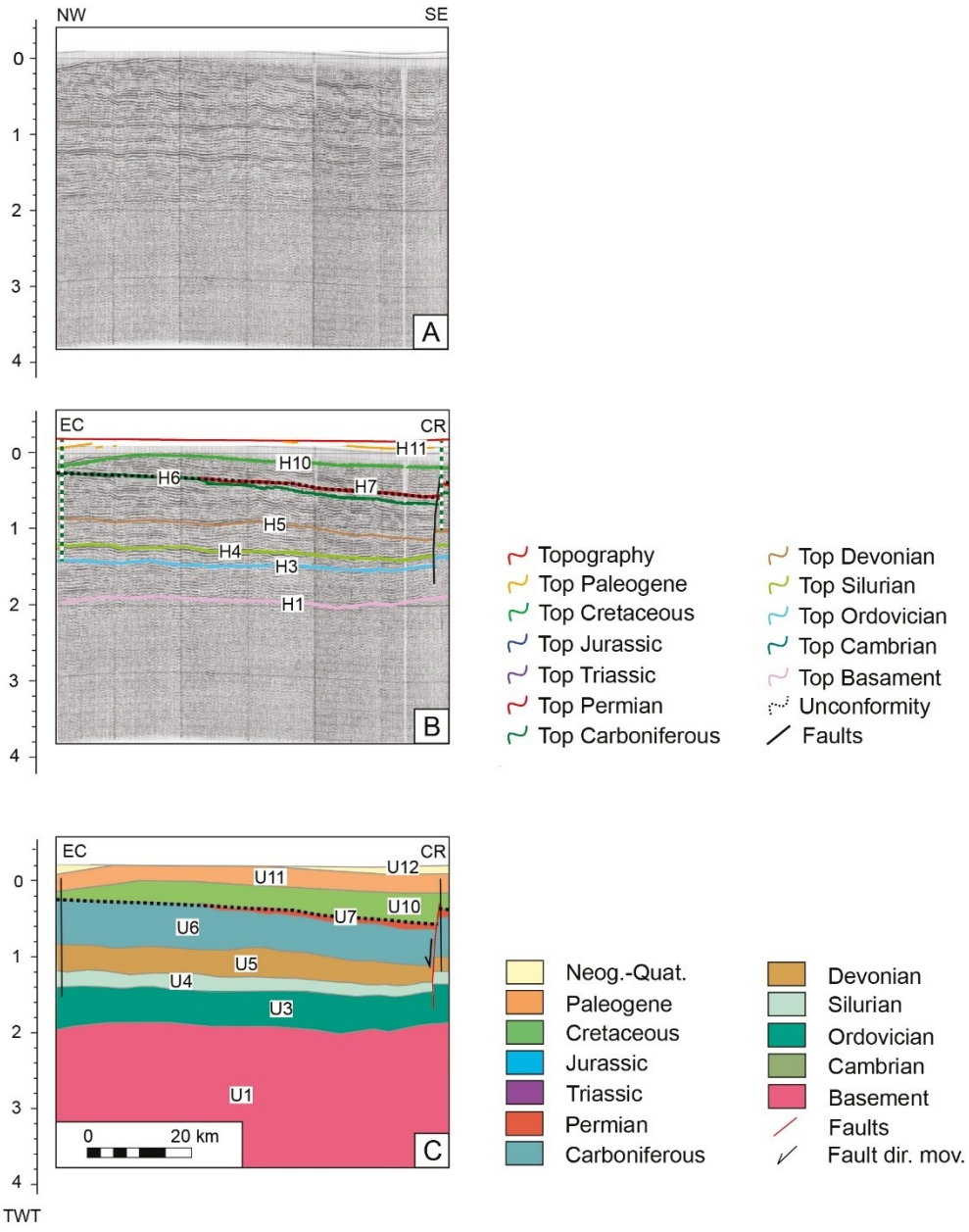

Figure 4.7: Seismic survey 4139. A: uninterpreted seismic line. B: interpreted unit tops: H1: Top Basement, H3: Top Ordovician H4: Top Silurian, H5: Top Devonian, H6: Top Carboniferous, H7: Top Permian, H10: Top Cretaceous, H11: Top Paleogene. C: model of interpreted units: U1: Basement, U3: Ordovician, U4: Silurian, U5: Devonian, U6: Carboniferous, U7: Permian, U10: Cretaceous, U11: Paleogene. U12: Undifferentiated Neogene and Quaternary. Wells: EL: El Caburé, CR: Coronel Rico.

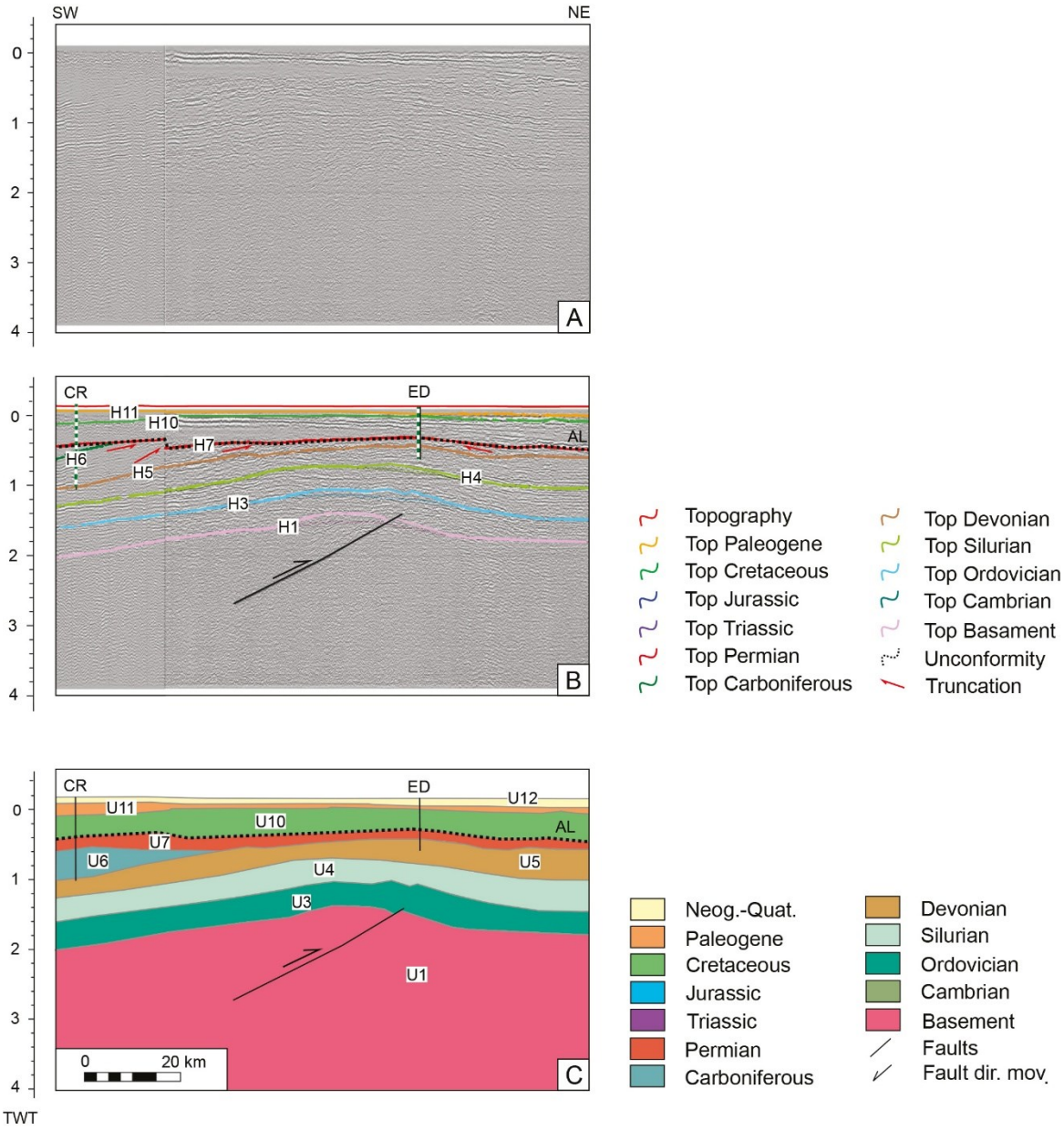

Figure 4.8: Seismic survey 44018. A: uninterpreted seismic line. B: interpreted unit tops: H1: Top Basement, H3: Top Ordovician, H4: Top Silurian, H5: Top Devonian, H6: Top Carboniferous, H7: Top Permian, H10: Top Cretaceous, H11: Top Paleogene, U12: Undifferentiated Neogene and Quaternary. C:

model of interpreted units: U1: Basement, U3: Ordovician, U4: Silurian, U5: Devonian, U6: Carboniferous, U7: Permian, U10: Cretaceous, U11: Paleogene, U12: Undifferentiated Neogene and Quaternary. Wells: CR: Coronel Rico, ED: El Desierto.

Survey 45026 (Fig. 4.9) is located in the SW of the study area and trends nearly N-S close to the Alhuampa borehole. The Precambrian basement (U1) is overlain by Cambrian sediments (U2), which are thicker to the north than to the south. These units are superseded by uniform layers of Ordovician (U3) and Silurian (U4) sediments overlain by Devonian (U5), increasing in thickness to the north. Above follow uniform Permian (U7), Triassic (U8), and Jurassic (U9) sediments. The sequence from U5 to U9 is tilted, being higher to the north, which could be caused by the combination of a depocenter to the north during the Devonian and subsequent deformation and uplift during the Gondwana orogeny. The Top of the Jurassic (U9) is interpreted as an unconformity marked by onlap terminations of Cretaceous (U10) and Paleogene (U11) units at the top, both very thin. The sequence is sealed by Neogene and Quaternary (U12) sediments that filled the pre-existing topography; these sediments define the near-horizontal present-day topography, but in cross section, they comprise a wedge-shaped fill that thickens southward.

Seismic survey 45054 (Fig. 4.10) lies to the west of the study area, also trending N-S, and could be considered a parallel continuation of survey 45026 (Fig. Y10). H1-Top Basement dips very gently to the south, as do H2-Top Cambrian, H3-Top Ordovician, and H4-Top Silurian, all somewhat irregular but parallel to each other. The H5-Upper Devonian is more strongly inclined and forms a wedge-shaped layer of U5 thickening to the north. U6-Carboniferous is also tilted and its top may be eroded to the north, but no truncation terminations are evident. An unconformity exists between the Carboniferous (U6) and the Cretaceous (U10), Paleogene (U11)

and Neogene, and Quaternary (U12) units. This unconformity is marked by onlap terminations of the overlying units to the north. U10-Cretaceous covers the south and center of the line. U11-Paleogene strata cover a slightly greater region towards the N, with both units, U-10 and U-11, onlapping and very thin. U12-Neogene and Quaternary sediments are quite thick and constitute the present-day land surface, which is characterized by flat topography. The position of this seismic reflection line coincides with the southern flank of the Quirquincho High. During the middle Paleozoic, the depocenter was probably farther north, and the subsequent uplift of the Quirquincho High resulting from the Gondwanic orogeny caused the unconformity above U6 and the onlap of U10, U11, and U12.

A first look at the stratal relationships and imaged structures reveals several important observations. One of the first-order structures that had developed in the basin is the Las Breñas half-graben in the east during the late Precambrian. Dominated by a large normal fault, this half-graben received sediments during the late Precambrian and early Paleozoic, until the Devonian, when the fault was partially inverted as a thrust and the overlying sediments were folded and eroded. The sedimentary sequence continues upward to an angular unconformity between the Permian and Cretaceous sediments, with maximum expression in the North, gradually decreasing until the sedimentation becomes continuous, without unconformity, in the southeast.

The Cretaceous and Paleogene strata onlap against this unconformity, and the undifferentiated Quaternary and Neogene sediments complete the sequence.

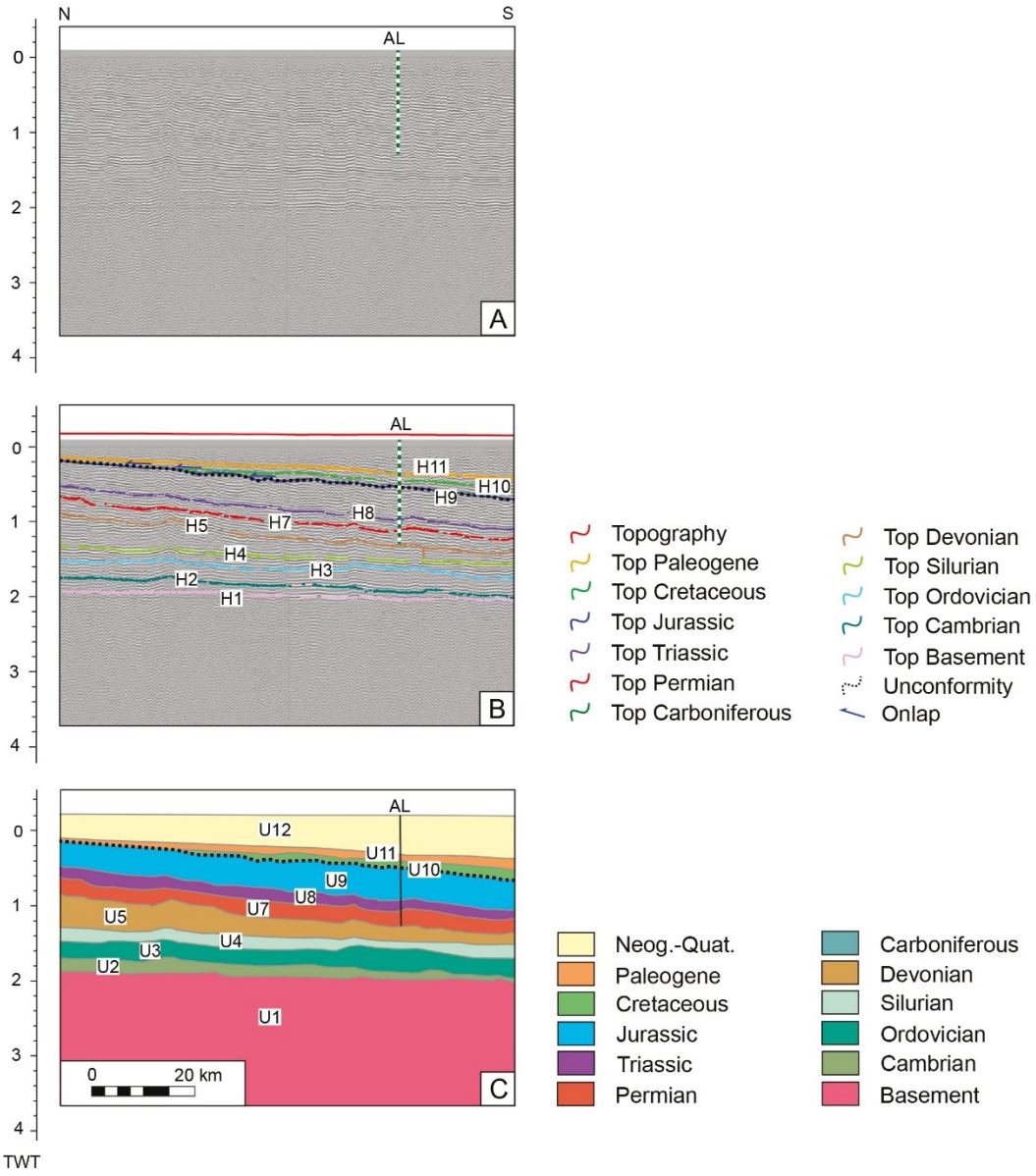

Figure 4.9: Seismic survey 45026. A: uninterpreted seismic line. B: interpreted unit tops: H1: Top Basement, H2: Top Cambrian, H3: Top Ordovician, H4: Top Silurian, H5: Top Devonian, H6: Top Carboniferous, H7: Top Permian, H8: Top Triassic, H9: Top Jurassic, H10: Top Cretaceous, H11: Top Paleogene. C: model of the interpreted units: U1: Basement, U2: Cambrian, U3: Ordovician, U4: Silurian, U5: Devonian, U6: Carboniferous, U7: Permian, U8: Triassic, U9: Jurassic, U10: Cretaceous, U11: Paleogene, U12: Undifferentiated Neogene and Quaternary. Well: AL: Alhuampa.

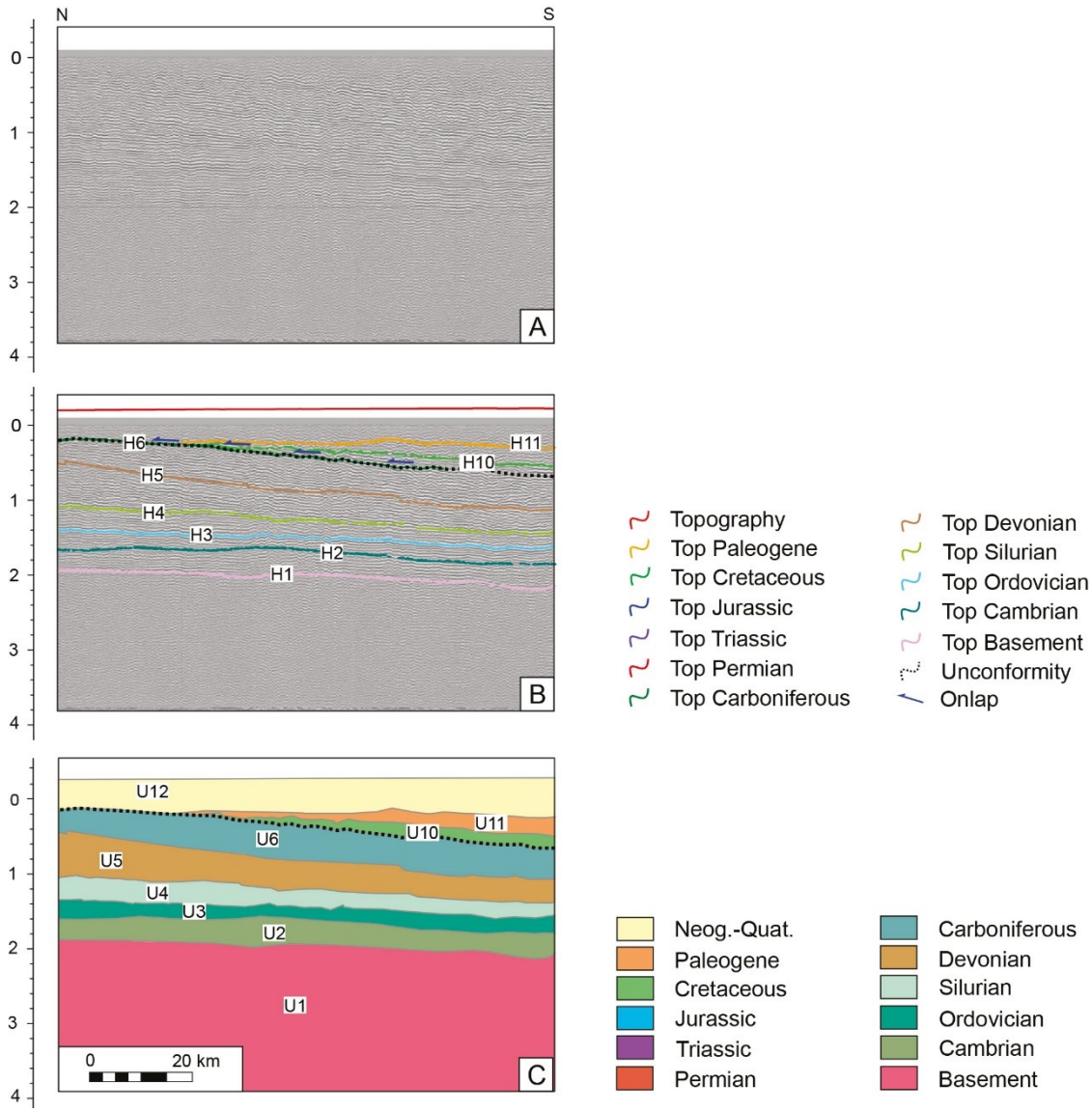

Figure 4.10: Seismic survey 45054. A: uninterpreted seismic line. B: interpreted unit tops: H1: Top Basement, H2: Top Cambrian, H3: Top Ordovician, H4: Top Silurian, H5: Top Devonian, H6: Top Carboniferous, H10: Top Cretaceous, H11: Top Paleogene. C: model of the interpreted units: U1: Basement, U2: Cambrian, U3: Ordovician, U4: Silurian, U5: Devonian, U6: Carboniferous, U10: Cretaceous, U11: Paleogene, U12: Undifferentiated Neogene and Quaternary.

4.2.2 Depth and thickness maps

The seismic horizons interpreted on the 2D seismic lines were converted from time to depth domain (see Sections 3.2 and 3.3, Depth and Isopach Maps) using the equation calculated for the Chacoparanaense Basin (Fig. 3.12), instead of the general trend line for both basins used for the maps in Chapter 3. The equation for the general trend works better at a multi-basin scale, while the equation for the Chacoparanaense Basin provides optimal results for the study area of this chapter, which is only inside this basin.

I imported all of the horizons interpreted in the seismic lines, in depth-converted format, into Petrel 2015 E&P software (®Schlumberger). I interpolated the horizons using several methods, such as convergent interpolation and conformal gridding, to produce depth maps for each geological unit. In the study area for basin modelling (blue polygon in Fig. 1.4), the higher data density compared to the study area of Chapter 3 (red polygon in Fig. 1.4) results in much better resolution and allowed to improve the model from 5 horizons interpreted in Chapter 3, to 13 horizons in this chapter 4.

The higher vertical resolution in combination with the introduction of erosional and non-depositional horizons required an iterative interpolation of the horizons to eliminate unwanted intersections of horizons of the 3D-model.

Depth maps

Figures 4.11 and 4.12 display the resulting depth maps. These maps form the backbone of the conceptual model, providing the present-day 3D structure of the basin to model.

The basement (Precambrian Top) reaches a maximum depth of 8360 m below sea level (m b.s.l) in the area of the Las Breñas half-graben (Fig. 4.11 A). The minimum depth is 2288 m b.s.l., located in the central-eastern part of the study area. The Cambrian Top (Fig. 4.11 B), Ordovician Top (Fig. 4.11 C), and Silurian Top (Fig. 4.11 D) have approximately the same disposition, but with depths between 6331-1248 m b.s.l., 4487-810 m b.s.l and 3117-798 m b.s.l., respectively.

On the Devonian Top map (Fig. 4.11 E), the minimum depth of 508 m b.s.l has moved northward. The zones of minimum depth of the Carboniferous (Fig. 4.11 F), Permian (Fig. 4.12 A), and Triassic Top (Fig. 4.12 B), move progressively to the west, and the deeper area progressively locates in the southeast, towards the northern part of the main depocenter of the Chacoparanaense Basin, located southwards of the study area, in the northern part of the Santa Fe Province (Chebli *et al.*, 1999).

The Cretaceous Top (Fig. 4.12 D) and Paleogene Top (Fig. 4.12 E) maps show a depth distribution that is becoming increasingly similar to the present-day topography (Fig. 4.12 F), with higher elevations (236 m a.s.l.) in the west, a subtle slope, and lower elevations (80 m a.s.l.) toward the southeast of the study area.

Isopach maps (Figs. 4.13 & 4.14) are not imported into PetroMod for modelling purposes, but are very useful for illustrating sediment distribution during each geological period or unit, tracking the migration of depocenters, which thus helps to understand the geological evolution of a basin. When combined with seismic observations, the modeling data can thus aid in developing a clearer depiction of areas where deposition, hiatus, and erosion occurred.

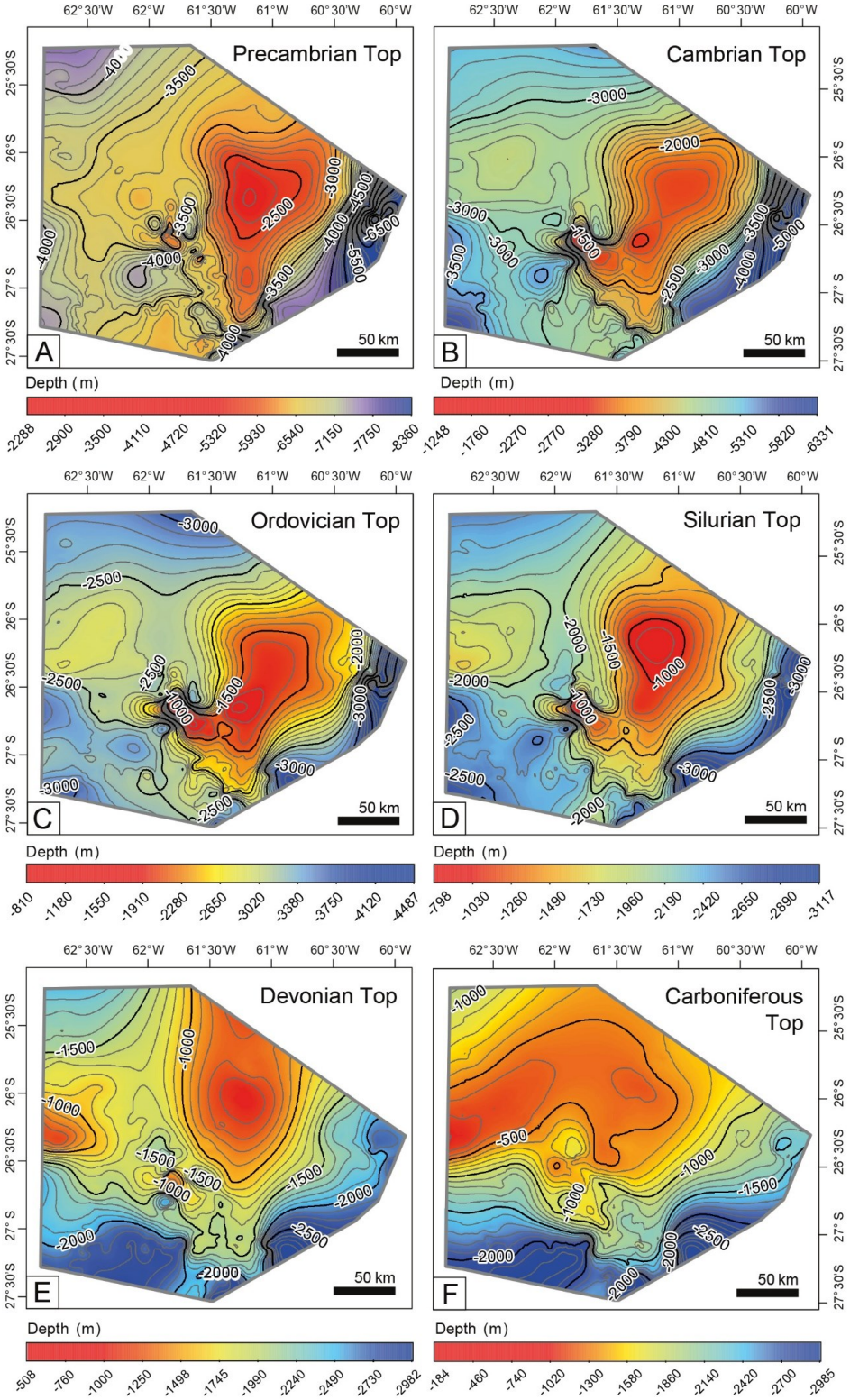
Precambrian Top
A
Cambrian Top
B
Ordovician Top
C
Silurian Top
D
Devonian Top
E
Carboniferous Top
F
50 km
Depth (m)
62°30'W
62°W
61°30'W
61°W
60°30'W
60°W
25°30'S
26°S
26°30'S
27°S
27°30'S

Figure 4.11: Depth map showing the present-day subsurface position and morphology of the top of each stratigraphic unit of horizons 1 - 6: A) H1- Precambrian Top, B) H2- Cambrian Top, C) H3- Ordovician Top, D) H4- Silurian Top, E) H5- Devonian Top, F) H6- Carboniferous Top. Depth maps were constructed based on seismic interpretations, through interpolations in Petrel 2015 E&P Software (®Schlumberger).

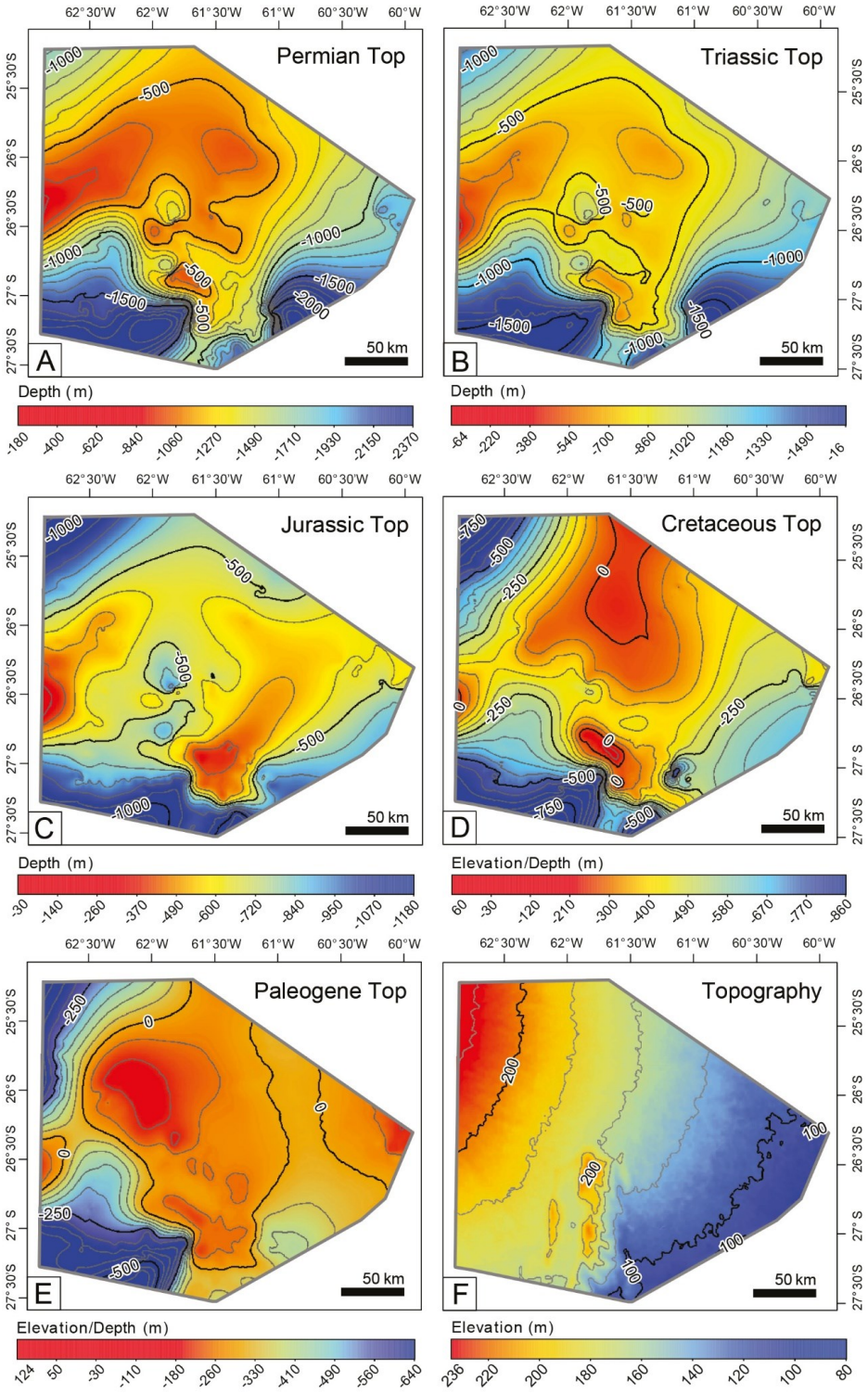

Figure 4.12: Depth map showing the present-day subsurface position and morphology of the top of each stratigraphic unit of horizons 7 - 12: A) H7- Permian Top, B) H8- Triassic Top, C) H9- Jurassic Top, D) H10- Cretaceous Top, E) H11- Paleogene Top, F) H12- Neogene and Quaternary Top (Topography). Depth maps

were constructed based on seismic interpretations, through interpolations in Petrel 2015 E&P Software (®Schlumberger).

Isopach/thickness maps

Cambrian (Fig. 4.13 A), Ordovician (Fig. 4.13 B), Silurian (Fig. 4.13 C), and Devonian (Fig. 4.13 D) thickness maps show the main thickness in the Las Breñas half-graben, with secondary depocenters changing position through time. The maximum thickness of these units is in the order of 1-2 km each, with the older and deeper units being thicker.

Carboniferous sediments (Fig. 4.13 E) range in thickness from 0 m in the southeast to 1012 m in the northwest. The Permian unit (Fig. 4.13 F) is very thin or it is partially absent in the northwest, but it increases to 1032 m in the southeast. The Triassic (Fig. 4.14 A) and Jurassic (Fig. 4.14 B) maps show a similar distribution, with a larger area where these units are completely absent.

The Cretaceous unit (Fig. 4.14 C) varies in thickness from 655 to 32 m and follows a different distribution from the units below. The thickness of the Paleogene sediments (Fig. 4.14 D) ranges from 3 to 610 m, with the thickest area in the south (toward the north of the main depocenter in the Santa Fe Province, Chebli *et al.*, 1999). Neogene and Quaternary sediments (Fig. 4.14 E) have been grouped because of the difficulty in properly differentiating them in the drill reports. They range from 0 m in the east to 790 m in the south, and an additional area of greater thickness in the west.

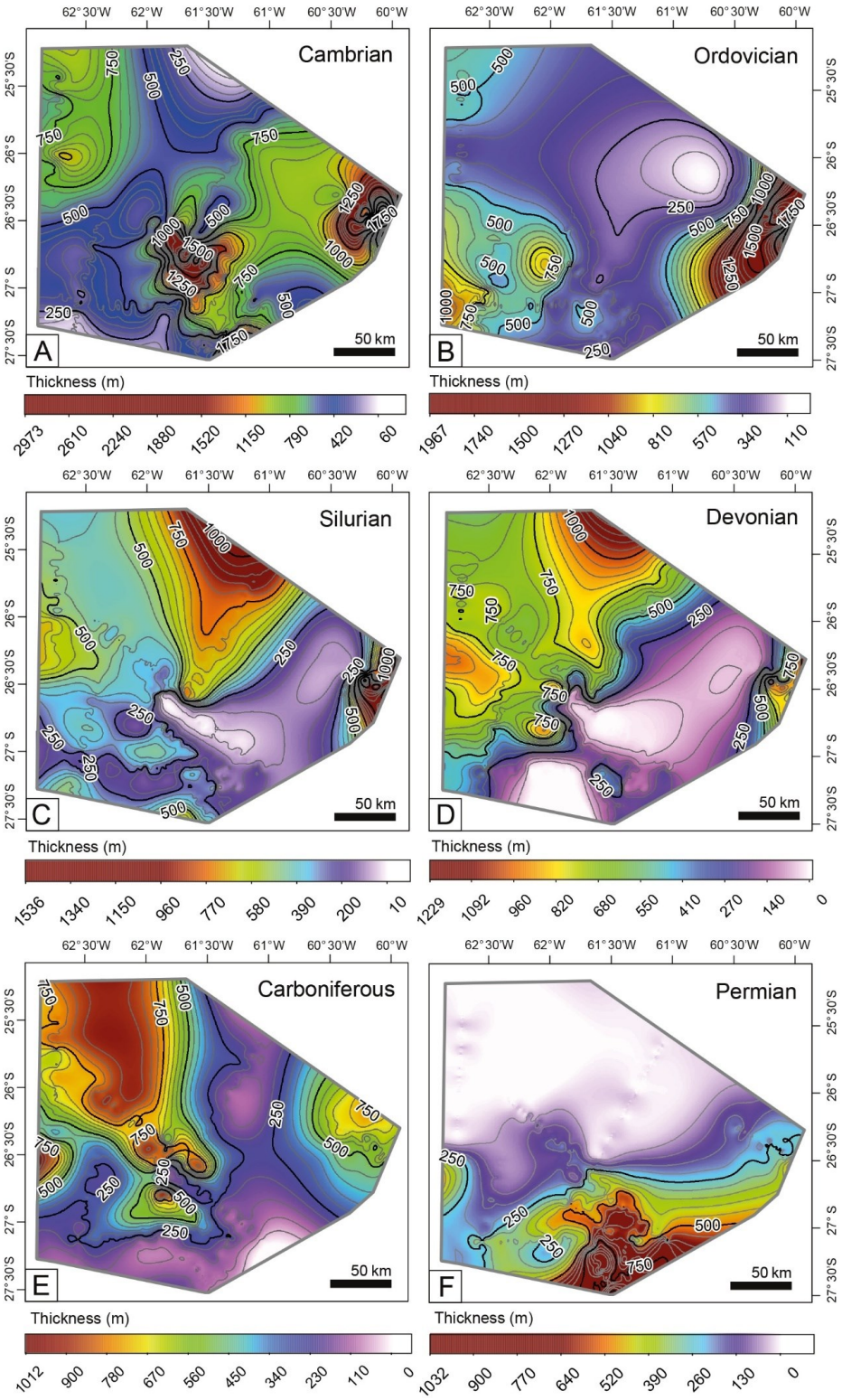

Figure 4.13: Isopach maps showing the thickness distribution of units 1 to 6: A) U1- Cambrian, B) U2- Ordovician, C) U3- Silurian, D) U4- Devonian, E) U5- Carboniferous, F) U6- Permian. Isopach maps were

constructed based on the difference between unit bounding depth maps in Petrel 2015 E&P Software (®Schlumberger).

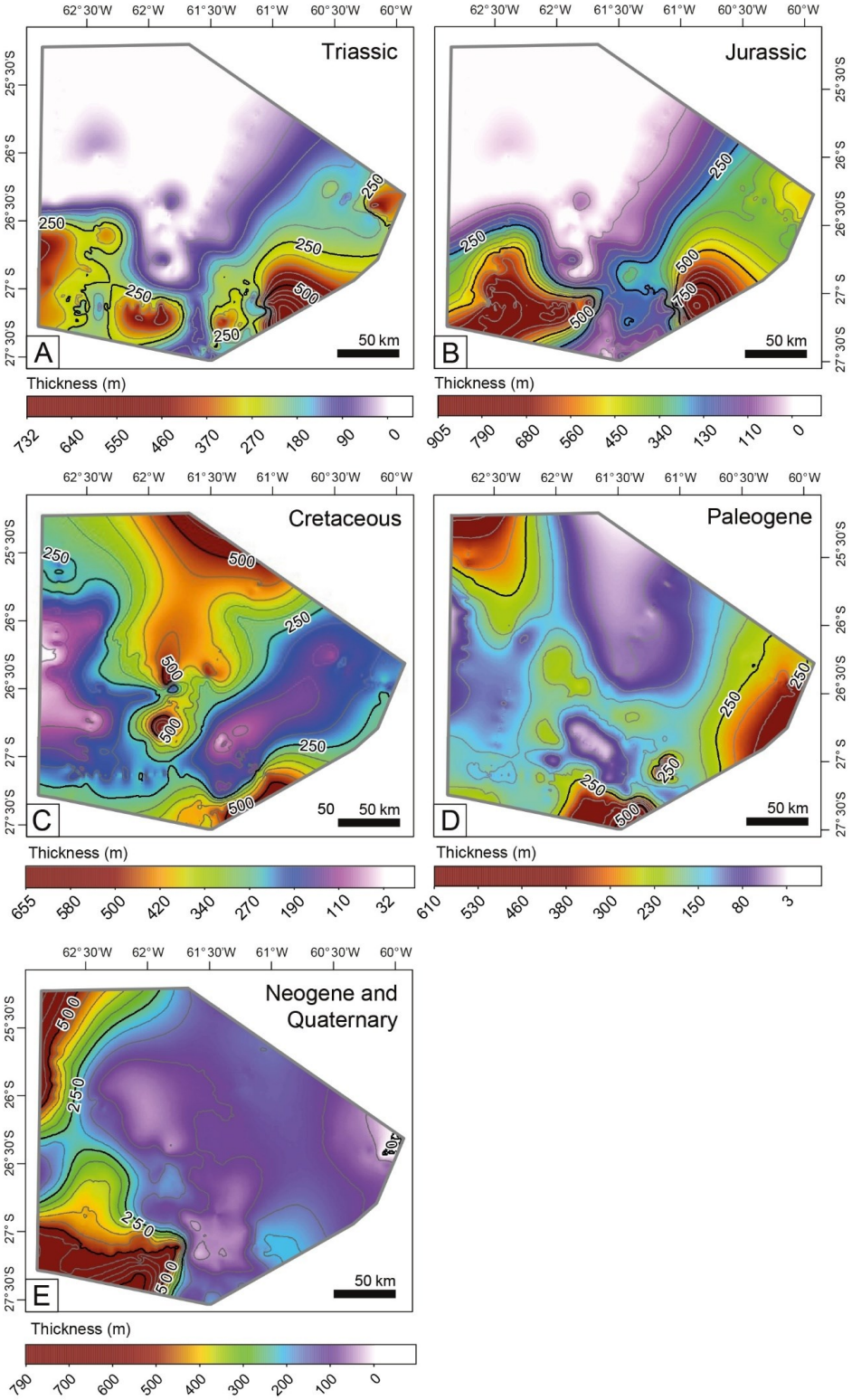

Figure 4.14: Isopach maps showing the thickness distribution of units 7 to 11: A) U7- Triassic, B) U8- Jurassic, C) U9- Cretaceous, D) U10- Paleogene, E) U11- Neogene and Quaternary. Thickness maps were constructed by calculating the difference between unit bounding depth maps in Petrel 2015 E&P Software (®Schlumberger).

4.2.3 Age assignment

All horizon tops have assigned ages based on well reports tied to seismic lines (see Chapter 4.2.1). However, it is still necessary to identify interpretational gaps (hiatuses and erosional phases) in the depositional history and assign corresponding ages to them.

Seismic interpretations and thickness maps reveal two major unconformities. The first is an angular unconformity in survey pw_89_40 (Fig. 4.5) between Devonian and Silurian sediments. Since this unconformity is restricted to the Las Breñas half-graben and is not identifiable in thickness maps, it was not included in the model.

The second unconformity occurs between the Permian and the Cretaceous and is visible in seismic lines 4139 (Fig. 4.7), 45026 (Fig. 4.9), and 45054 (Fig. 4.10) as an onlap termination of the Cretaceous unit (U10) onto the Permian unit (U7), with the Triassic (U8) and Jurassic (U9) sediments absent. In seismic line 44018 (Fig. 4.8), the onlap of the Cretaceous (U10) is still visible, but Triassic (U8) and Jurassic (U9) sediments are present.

Table 1: Age assignment of horizons, corresponding layers, and interpreted non-depositional events.

Age (Ma)	Interpreted Horizon	Layer
0	Top Quaternary	Neogene
23	Top Paleogene	Paleogene
66	Top Cretaceous	Cretaceous
145	Top Jurassic	Jurassic
160		Hiatus
210	Top Triassic	Triassic
220		Permo–Triassic Erosion
250		Eroded Permian
270	Top Permian	Permian
300	Top Carboniferous	Carboniferous
359	Top Devonian	Devonian
419	Top Silurian	Silurian
444	Top Ordovician	Ordovician
485	Top Cambrian	Cambrian
541	Top Precambrian	Precambrian

Thickness maps reveal a significant variation in the thickness of the Permian (Fig. 4.13 F), Triassic (Fig. 4.14 A), and Jurassic (Fig. 4.14 B) units from southeast to northwest. The zero-thickness distribution of these units coincides with the elevated area of the Quirquincho High (Fig. 1.4), suggesting that the uplift of this high was linked to a period of non-deposition.

This non-depositional period, represented by the second unconformity, has been divided into two phases. The first phase, a possible erosion event, occurred from the late Permian to the middle Triassic. Based on the maximum drilled thickness of Permian and Triassic strata, erosion of at least 1,200 m is estimated in areas where late Paleozoic and early Mesozoic rocks were completely removed. The eroded material thickness reconstruction assumes that Permian and Triassic sediment thickness was originally nearly uniform and tabular across the study area, with erosion being the sole cause of the significant thickness difference between the northwest and southeast regions (Fig. 4.13 F, 4.14 A). Figure 4.15 presents the resulting erosion map, assuming a homogeneous initial thickness for the Permian and Triassic layers. The map indicates maximum erosion in the northwest, over Quirquincho High (see Chapter 3.3), decreasing to zero erosion (or preserved Permian and Triassic thickness) in the southeast.

The second phase, linked to Mesozoic tectonic movements associated with the opening of the Atlantic Ocean, is marked by gaps in the sedimentary record, with the absence of Upper Triassic and Jurassic strata. The estimated erosion for this event could reach 900 m or more, based on the remaining thickness of the Triassic and Jurassic strata. However, seismic interpretations reveal onlap features toward the Quirquincho High, which suggests that large-

scale erosion was unlikely. Instead, these features point to sedimentary condensation or non-deposition during the Mesozoic (see Chapter 3.4).

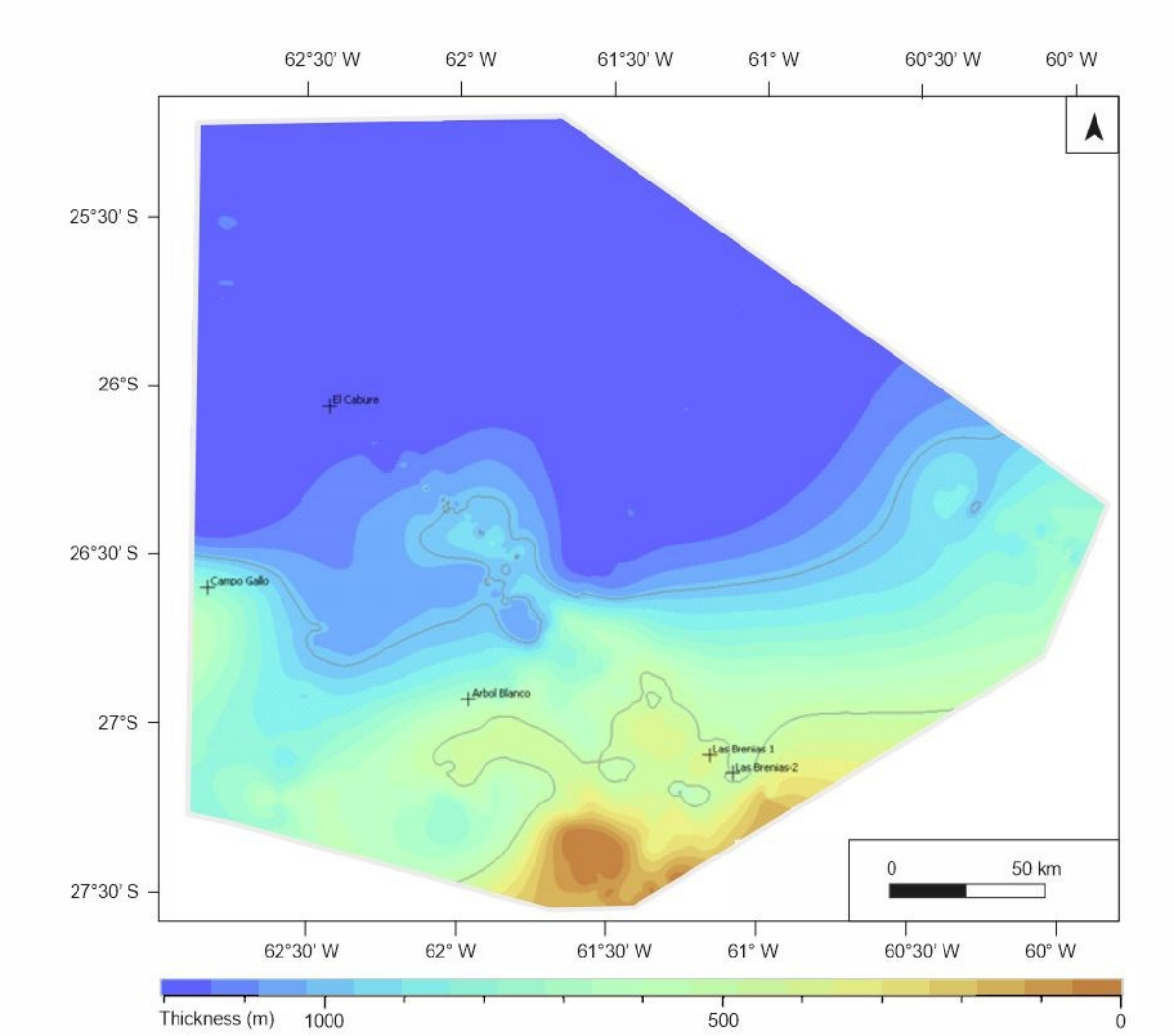

Fig. 4.15: Erosion Map showing the amount of Permo–Triassic erosion from 250-220 Ma. Calculated based on the maximum thickness of the Permian and Triassic units (Figs. 4.13F & 4.14A) and considering uniform deposition.

4.2.4 Facies maps

In addition to defining the geometry and thickness of each model layer, it is essential to assign facies and their corresponding lithologies. Facies distributions vary laterally within the study area, and the assigned lithologies reflect these variations depending on the available data and resolution of each unit. Generally, resolution decreases with depth as fewer wells penetrate the deeper units. Table 2 presents the simplified lithologies used in the facies maps, while Table 3 lists all formation tops reached by each well, with depths in meters below sea level (m b.s.l.).

Defining the rock type for each model cell is a critical parameter, as lithology determines key properties such as thermal conductivity, heat capacity, radiogenic heat production, mechanical behavior (including initial and minimum porosity, compaction characteristics, and compressibility, which influence sediment behavior under overburden loading), and fluid flow properties such as permeability and seal effectiveness, which are crucial for modelling fluid migration (Hantschel & Kauerauf, 2009). In this study, thermal and mechanical property analyses were not possible due to the lack of available samples, and well reports were the primary data source. Therefore, I assigned the respective predefined lithologies, as provided by the PetroMod petroleum systems modelling software (®Schlumberger), to define the thermal, mechanical, and fluid flow properties of the lithologies assigned to the modelled layers.

Table. 2: Facies definition with assigned lithologies.

Facies	Assigned model lithology	Color
Quaternary shaly sand	Sandstone (typical)	
Quaternary silty shale	Shale (organic lean, silty)	
Paleogene Shale	Shale (organic lean, sandy)	
Paleogene shaly sand	Sandstone (clay-rich)	
Cretaceous shale & silt	Siltstone (organic lean)	
Cretaceous shaly sand	Sandstone (clay-rich)	
Cretaceous sand	Sandstone (typical)	
Jurassic shale	Shale (typical)	
Triassic shale	Shale (typical)	
Permian sandy shale	Shale (organic lean, sandy)	
Permian shaly sand	Sandstone (arkose, clay-rich)	
Carboniferous sandstone	Sandstone (subarkose, clay-rich)	
Devonian silt	Siltstone (organic lean)	
Devonian sand	Sandstone (typical)	
Devonian shale & sand	Sandstone (arkose, clay-rich)	
Silurian shale	Shale (typical)	
Silurian silt	Siltstone (organic lean)	
Silurian sandstone	Sandstone (typical)	
Ordovician silt	Siltstone (organic lean)	
Cambrian sandstone	Sandstone (quartzite, very quartz-rich)	
Precambrian	Upper crust (continental, granite)	

Table 3: Formations drilled in each well. Each column corresponds to a drilled well, and each row to a formation. The values are the depth below sea level (m b.s.l.) at which each formation was drilled in the corresponding well.

	Well	Alhuampa	Árbol Blanco	Campo Gallo	Coronel Rico	Charata	El Caburé	El Desierto	Gancedo	Las Breñ 1
Age	**Formation**	m b.s.l.	m b.s.l.	m b.s.l.	m b.s.l.	m b.s.l.	m b.s.l.	m b.s.l.	m b.s.l.	m b.s.l.
Quaternary	**Chaco + Pampa**	-160	-152				-185	-138	-103	
Neogene	**Paraná - Entre Ríos**	125	-50		-178					
Paleogene	**Chaco**	242	-34		-88	-102	75	-33	22	
Cretaceous	**Mariano**	370	142	50	102		95	12	363	
	Boedo									
Jurassic	**Tacuarembó**	542	504	122		118			747	-103
Triassic	**Buena**	1317		200					815	
	Vista									
Permian	**Chacabuco**		628						919	851
	Charata	1552	795	493	332	718			1212	1056
Carboniferous	**Sachayoj**	-160	1076	773	522	1328	545	210	1782	1666
Devonian	**Rincón**			1610			1003	437		
	Caburé			1997	1472		1379	567		
Silurian	**Copo**		2291				1863			
	Zapla		2543				2261			
Ordovician	**Las Breñas**		2554				2295		2505	
	Pirané		2873							
Cambrian	**Árbol Blanco**		3335							

Ages were assigned based on Russo *et al.* (1979) and are following Fig. 2.1. Sources: Charata, Becker, 1975; El Caburé, Bottcher, 1965; Las Breñas 1, Bottcher, 1974; Coronel Rico, Di Persia, 1969; Pampa Bandera, Knowlton, 1991; El Caburé, Mingramm, 1966a; Arbol Blanco, Mingramm, 1966b; Las Breñas Oriental, Rolleri, 1966; Las Breñas 2, Rolleri, 1967; El Desierto, Rolleri, 1970.

Facies maps (Figs. 4.16 and 4.17) were constructed using well reports, based on the primary lithology encountered in each borehole, combined with general manual interpolation. While simple, these maps effectively illustrate lateral lithological variations. The accuracy of facies maps decreases with depth since not all formations are documented in every well due to limited drilling depths.

The Cambrian facies map (Fig. 4.16A) was assigned a quartzitic sandstone unit, based on the only well deep enough to reach it (Arbol Blanco well). The Ordovician unit (Fig. 4.16B), drilled by four wells, consists predominantly of sandstone with minor shale. The Silurian unit (Fig. 4.16C), identified in three wells, reveals a transition from sandstone in the south to siltstone and shale towards the north. The Devonian unit (Fig. 4.16D), identified in five wells, exhibits three distinct lithological zones: a sandstone-dominated region, a siltstone-dominated region, and an area with interbedded sand and shale. The Carboniferous unit (Fig. 4.16E), drilled in ten wells, is characterized by a relatively uniform distribution of sandstone and shale interbeds. The Permian unit (Fig. 4.16F), based on data from seven wells, shows a south-to-north variation, with

predominantly shale and minor sandstone in the southern sector, transitioning to mainly sandstone with minor shale in the north.

The Triassic unit (Fig. 4.17B), documented in only two well reports, is described as consisting mainly of siltstone with some sandstone. The Jurassic unit (Fig. 4.17C), drilled in seven wells, is predominantly composed of sandstone with minor shale, displaying an almost uniform distribution. The Cretaceous unit (Fig. 4.17D), based on nine wells, exhibits a lithological zonation with sandstone-dominated facies in the southwest, a transitional mixed zone, and shale/siltstone-dominated facies in the northeast. The Paleogene unit (Fig. 4.17E) also exhibits a zonation, with predominantly shale in the northwest and southeast, and a sandstone-dominated region in between. The Neogene–Quaternary unit (Fig. 4.17F), described in eight well reports, shows a north-to-south variation, with a northern zone characterized by sandstone with minor shale, followed by a central sandstone-dominated region, and a southern zone with interbedded shale and siltstone.

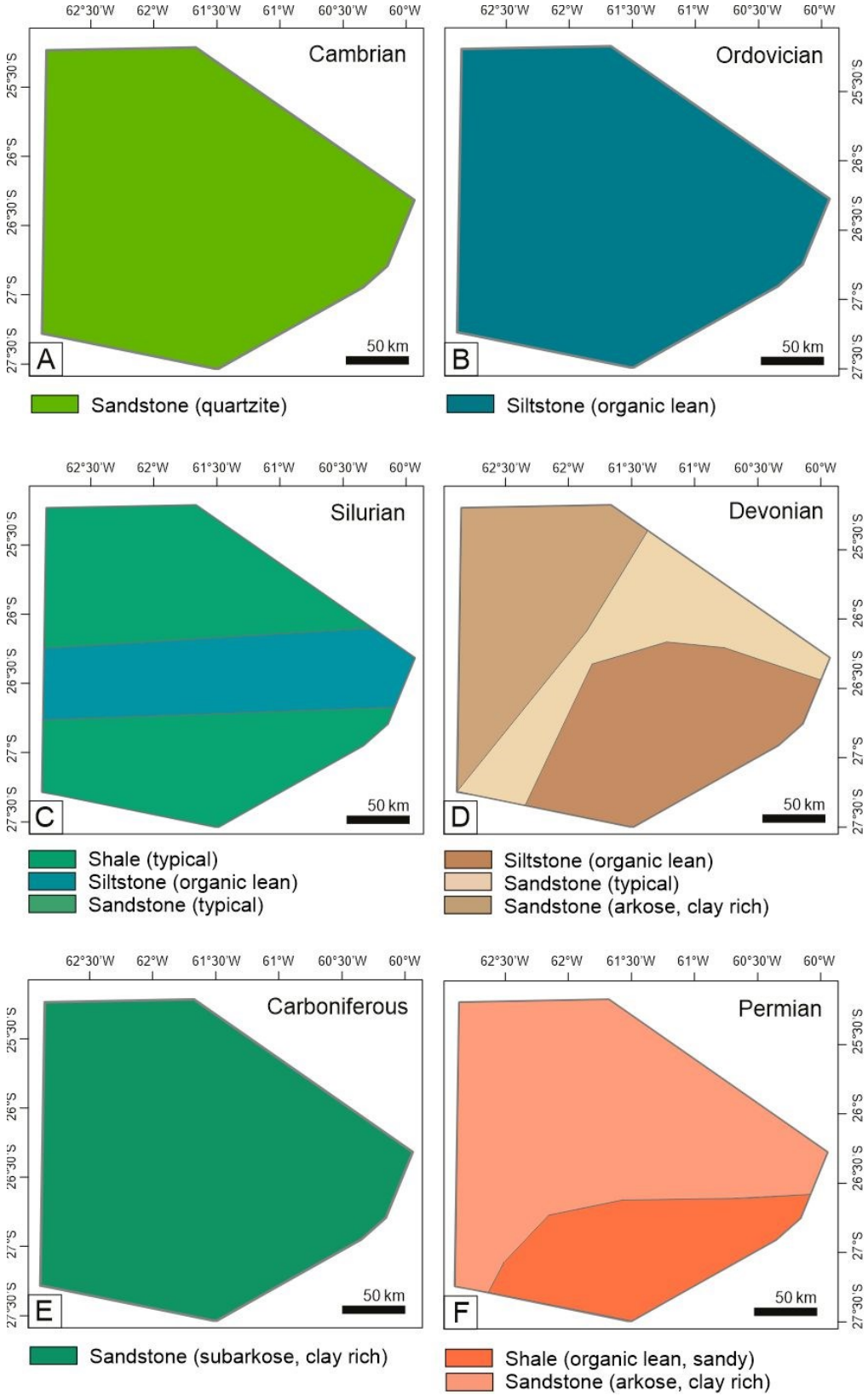
62°30'W
62°W
61°30'W
61°W
60°30'W
60°W
25°30'S
26°S
26°30'S
27°S
27°30'S
Cambrian
A
50 km
Sandstone (quartzite)
Ordovician
B
50 km
Siltstone (organic lean)
Silurian
C
50 km
Shale (typical)
Siltstone (organic lean)
Sandstone (typical)
Devonian
D
50 km
Siltstone (organic lean)
Sandstone (typical)
Sandstone (arkose, clay rich)
Carboniferous
E
50 km
Sandstone (subarkose, clay rich)
Permian
F
50 km
Shale (organic lean, sandy)
Sandstone (arkose, clay rich)

Figure 4.16: Facies maps showing lithology distribution of units 1 to 6: A) U1- Cambrian, B) U2- Ordovician, C) U3- Silurian, D) U4- Devonian, E) U5- Carboniferous, F) U6- Lower Permian (preserved). Facies maps were constructed using the drilled lithologies in each well and unit (see Table 1).

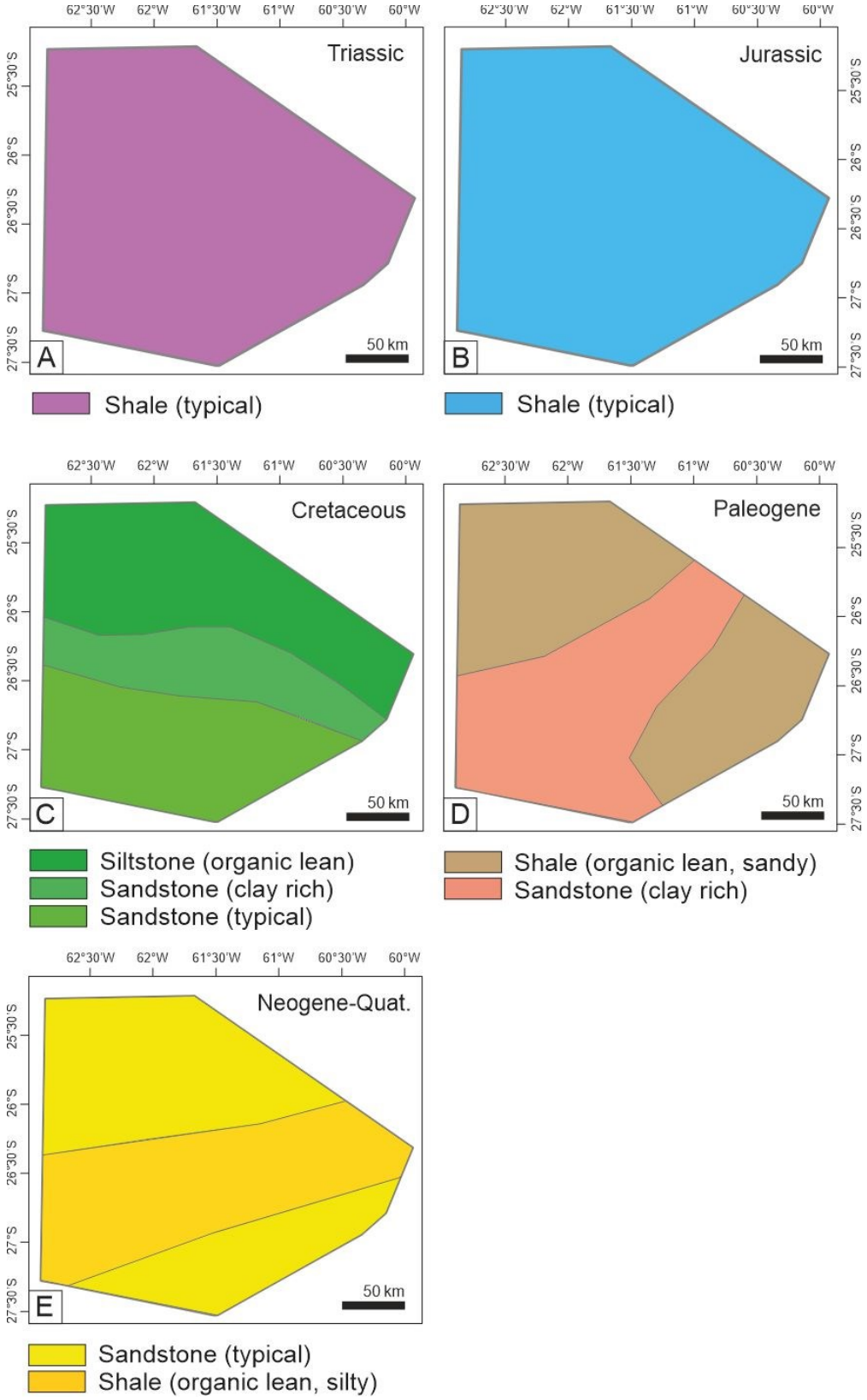
62°30'W
62°W
61°30'W
61°W
60°30'W
60°W
25°30'S
26°S
26°30'S
27°S
27°30'S
Triassic
A
50 km
Shale (typical)
Jurassic
B
50 km
Shale (typical)
Cretaceous
C
50 km
Siltstone (organic lean)
Sandstone (clay rich)
Sandstone (typical)
Paleogene
D
50 km
Shale (organic lean, sandy)
Sandstone (clay rich)
Neogene-Quat.
E
50 km
Sandstone (typical)
Shale (organic lean, silty)

Figure 4.17: Facies maps showing lithology distribution of units 7 to 11: A) U7- Triassic, B) U8- Jurassic, C) U9- Cretaceous, D) U10- Paleogene, E) U11- Neogene and Quaternary. Facies maps were constructed using the drilled lithologies in each well and unit (see Table 1).

4.3 Boundary conditions

The main boundary conditions that must be defined to model the basin relate to heat, pressure, and fluid flow analysis throughout the simulated geologic history. Some of the thermal, pressure, and fluid flow properties are related to rock type and are defined when the facies are assigned to each cell of the model (Hantschel & Kauerauf, 2009). However, other properties, such as heat flow, surface temperature, and water depth, are independent of the sedimentary cover and are related to the lower and upper boundaries of the basin. The bottom, or basement, defines the basal heat flow of the basin (Neumann boundary condition; Hantschel & Kauerauf, 2009; Allen & Allen, 2013), and the upper boundary, or surface interface (Dirichlet boundary; Hantschel & Kauerauf, 2009; Allen & Allen, 2013), is a constant value and is related to the contact with the atmosphere or water layer.

4.3.1. Heat flow

Basal heat flow determines the input/inflow of heat from the bottom into the model and thus determines the temperature evolution in the basin and organic matter maturation over geological time. It may vary in time and spatially, making its reconstruction over time critical for the modelling process (Welte *et al.*, 1997).

For present-day heat flow, I adopted an average regional value of 56 mW/m², based on the maps published by Collo *et al.* (2008), which were derived from corrected bottom-hole temperatures (BHT). For more details on the data and methods, I refer to their publication

(Collo *et al.*, 2008). This value was used as the lower boundary condition, representing heat flow input from the basement.

To reconstruct past heat flow values, I applied basin analogies to model tectonic phases with similar plate tectonic settings (Welte *et al.*, 1997). Model calibration will determine whether the selected heat flow pattern aligns with the basin's evolution or if alternative hypotheses need to be tested. The temporal evolution of heat flow was modelled according to several hypotheses, primarily constrained by vitrinite reflectance measurements from five boreholes across the study area. The initial models assumed a conservative, time-averaged heat flow of 56 mW/m², while subsequent models incorporated Permo–Triassic heat flow peaks reaching 90 mW/m². Each hypothesis will be presented and discussed in the Modelling Results in Section 4.4. While the heat flow peaks illustrate the general regional trend over time, exact values may vary slightly due to lateral lithological differences.

4.3.2 Paleowaterdepth/ bathymetry

The topography and bathymetry of the basin throughout its geologic history serve as boundary conditions for the determination of the temperature at the sediment surface, but the data required for accurate reconstruction are often unavailable.

In the model used here, I attempted 3D decompaction using backstripping tools in 3D Move Structural Geology Modelling Software (®Petex), but the results were highly inconsistent. Therefore, I relied on paleogeographic evolution inferred from sedimentary

facies and fossil content (Russo *et al.*, 1989; Chebli *et al.*, 1999). These studies indicate a shallow marine environment (less than 200 m water depth) during the Paleozoic and predominantly continental deposition throughout the Mesozoic and Cenozoic, except for the early Neogene Paranaense marine ingression, which involved very shallow water depths (Russo *et al.*, 1989).

A precise paleobathymetric reconstruction is most relevant for hydrocarbon migration modelling, as it affects the layer geometries of the model. However, since this is not the focus of this thesis and is less critical for reconstructing the basin's burial and thermal history, because water depth variations over time have minimal impact on temperature and pressure calculations. Consequently, a simplified water depth reconstruction based on sedimentary and fossil evidence is sufficient for the modelling performed here, which primarily focuses on the burial history and thermal maturity of the basin.

4.3.3 Surface temperature

Surface temperature is important for the modeling of the temperature evolution of the sediments deposited in a basin, as it defines its temperature at the top of the model. Surface temperature is influenced by latitude, ocean currents, long-term climatic changes, and seasonal variations.

By definition of the PetroMod modelling tool, the temperature at the sediment-water/atmosphere interface represents the upper temperature boundary, and since the

temperature at the sediment-water interface also depends on water depth, the average surface temperature is corrected for water depth. In addition, the average surface temperature is influenced by long-term climate-driven changes in surface water temperature. Therefore, long-term average surface temperatures should be considered for the determination of the temperature at the sediment surface, together with changes in water depth through geologic ages. Wygrala (1989) synthesized the surface temperature trends from Frakes (1979) into a time-latitude plot (Figure 4.18) that provides valuable temperature estimates for shallow-water sediments according to global climate zones. The graph, based on Wygrala (1989), plots global mean surface temperatures at sea level through geologic time, highlighting variations across latitudes and geological epochs.

The upper boundary conditions used in this conceptual model, i.e., the evolution of water depth and surface temperature, are estimated from published data, deposited sediments, and PetroMod's internal tool for estimating surface temperature at the time of deposition (Wygrala, 1989; Hantschel & Kauerauf, 2009).

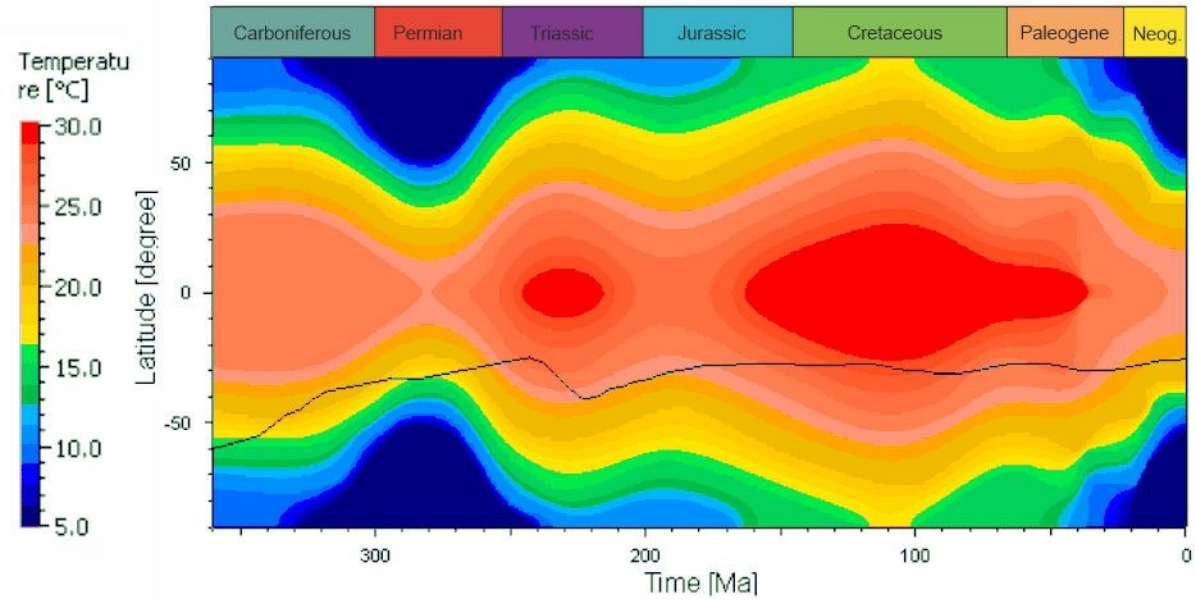

Fig. 4.18: The black line shows the evolution of the mean temperature at 24° South from the Carboniferous until the present using the integrated PetroMod database (Wygrala, 1989).

4.4 Modelling results

Once the conceptual model and boundary conditions were established, they were implemented in PetroMod (®Schlumberger). The Chacoparanaense Basin model covers a total area of 56,150 km², reaches depths exceeding 8 km, includes 13 sedimentary layers, and has been divided into approximately 3.66 million cells for computation in the modelling tool.

The processes of simulation, optimization, and calibration are essential to ensure that basin models accurately represent geological processes. The simulation generates outputs such as layer thickness, porosity, temperature, and maturity, which are then compared to observed data to assess the model's validity. If significant discrepancies arise, model calibration involves adjusting input parameters—such as initial porosity, basal heat flow or

erosion rates—within geologically reasonable ranges to improve the match between the model and measured data while testing parameter sensitivity to identify the most influential factors. Calibration validates the model by comparing key outputs, such as temperature profiles and vitrinite reflectance, to measured data, particularly for thermal history. Together, these steps enhance the model's reliability for reconstructing basin evolution and predicting subsurface conditions (Hantschel & Kauerauf, 2009).

Several simulations of the Chacoparanaense Basin were performed, with the six most significant presented in this section. Calibration was conducted by extracting 1D profiles from the 3D model at five borehole locations containing measured vitrinite reflectance values. Following this comparison, boundary conditions and estimated amounts of erosion were iteratively adjusted to obtain acceptable solutions for discussion. Vitrinite reflectance was calculated using the method of Sweeney & Burnham (1990).

4.4.1 Model 1

In the initial runs, both unconformities in the geologic record were treated as non-depositional periods to see if erosion in the Permo–Triassic and Jurassic was necessary at all or not. For simplicity, the model assumes uniform heat flow through time, based on present-day heat flow. The uniform heat flow used at the base of the model was 56 mW/m², resulting in a surface heat flow of 56 mW/m² (Fig. 4.19). Figure 4.19 shows the constant basal heat flow of 56 mW/m² applied to the Devonian rocks (black line), and the temperature these rocks reach (blue line) through geological time, showing an increased temperature of the Devonian rocks with burial.

Figure 4.20 shows the calculated vitrinite reflectance trend and the measured data in the El Caburé and Arbol Blanco boreholes (see location in Fig. 4.2) for Model 1. The large discrepancy between the calculated and measured values (approximately 0.5 %Ro difference) shows that the model is too immature and needs modifications.

Figure 4.21 shows the burial history for all of the basin layers in the study area. Burial was continuous and rapid until the Permian, and there was a non-depositional/no-burial period between the Permian and the Jurassic. In the Cretaceous, deposition started again, and burial continued until the present day. The colors in the diagram represent the maturity range reached (calculated vitrinite reflectance), and in this model, the maturity is very low (blue and green colors).

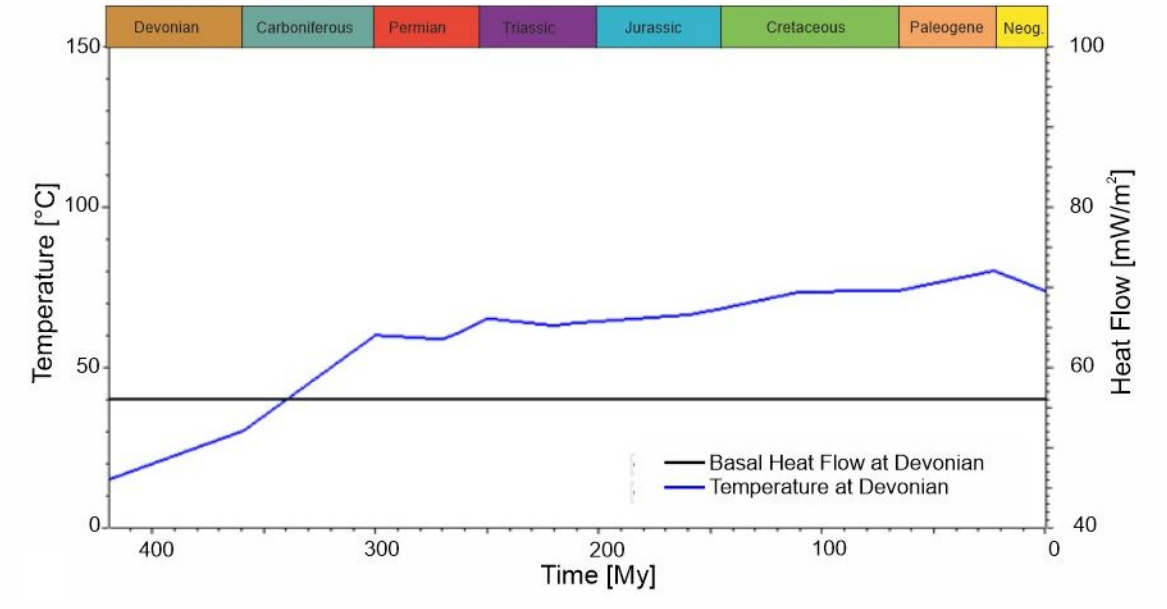

Figure 4.19: Heat flow and temperature history for Model 1: constant heat flow (black line), temperature evolution through time (blue line), rapid burial and no erosion.

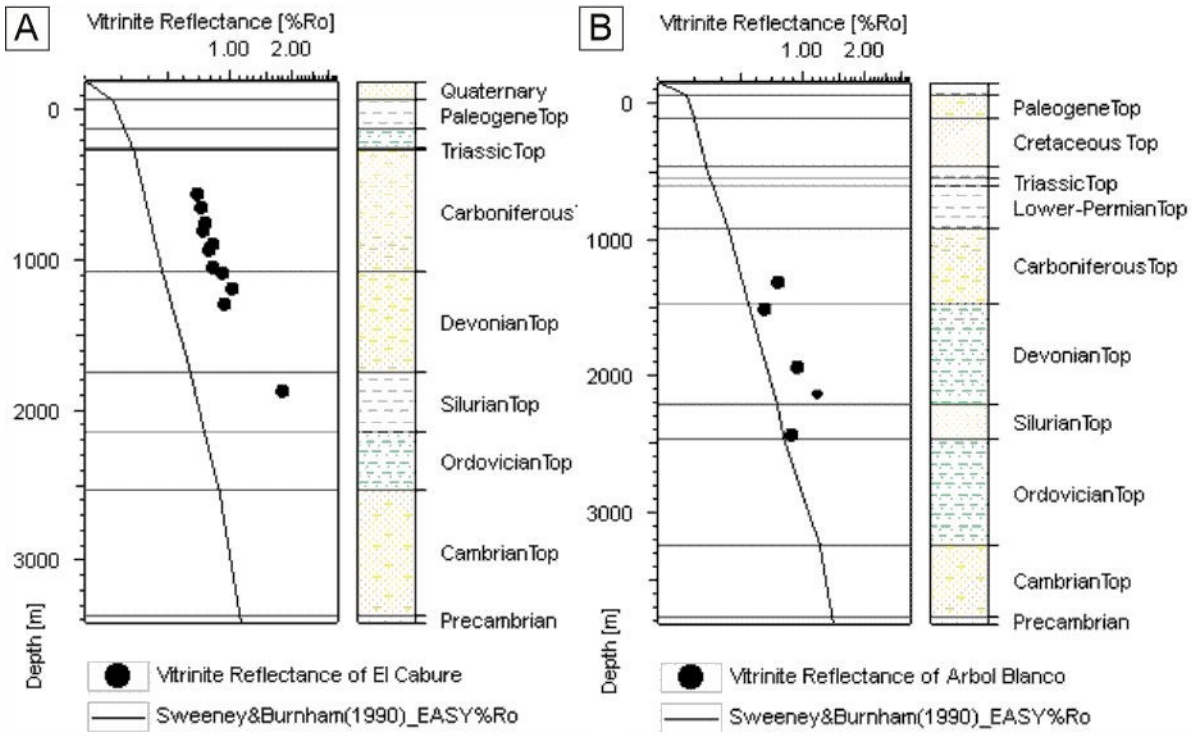

Figure 4.20: Maturity at El Caburé and Arbol Blanco boreholes for Model 1: constant heat flow and no erosion.

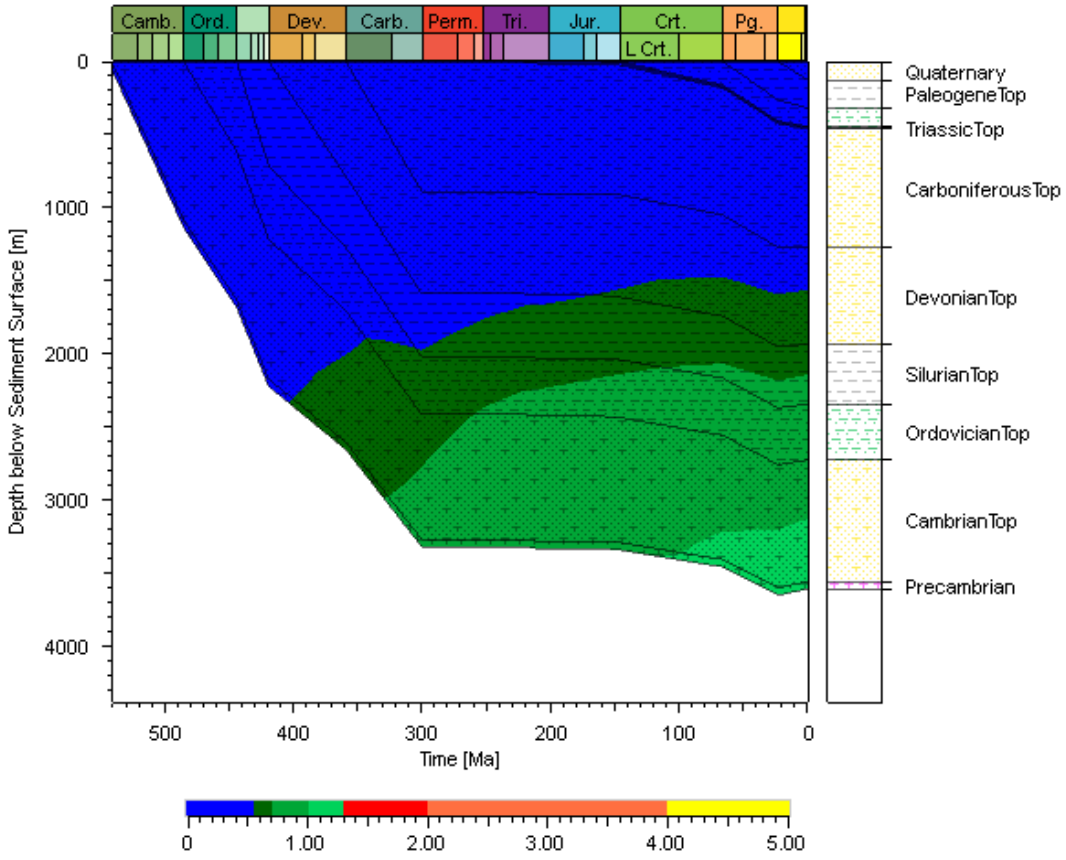

Figure 4.21: Burial history and calculated maturity for Model 1: constant heat flow and no erosion.

4.4.2 Model 2

In Model 2, as in Model 1, both known unconformities were treated as non-depositional periods to see if erosion in the Permo–Triassic and Jurassic was necessary at all or not. The model assumes a heat flow peak of 88 mW/m² for the Permo–Triassic boundary, (Fig. 4.22). Figure 4.22 shows the heat flow variation applied to the Devonian rocks (black line) and the temperature these rocks reach (blue line) through geological time, showing an increased temperature of the Devonian rocks with burial, with maximum values at the time of the heat flow peak (Permo–Triassic boundary).

Figure 4.23 shows the calculated vitrinite reflectance trend and the measured data in the El Caburé and Arbol Blanco boreholes (see location in Fig. 4.2) for Model 2. In this model, there is still a large discrepancy between the calculated and measured values, especially for the El Cabure well, which shows that Model 2, even with the addition of heat flow, is still too immature and needs modifications.

Figure 4.24 shows the burial history for all the layers of the basin in the study area. The burial was continuous and fast until the Permian, and there was a non-depositional/no-burial period between the Permian and the Jurassic. In the Cretaceous, deposition and burial started again and continued until the present day. The shape of the burial curves is the same as in Model 1, but due to the increased amount of heat, the maturity of the rocks (calculated vitrinite reflectance) is higher than in Model 1.

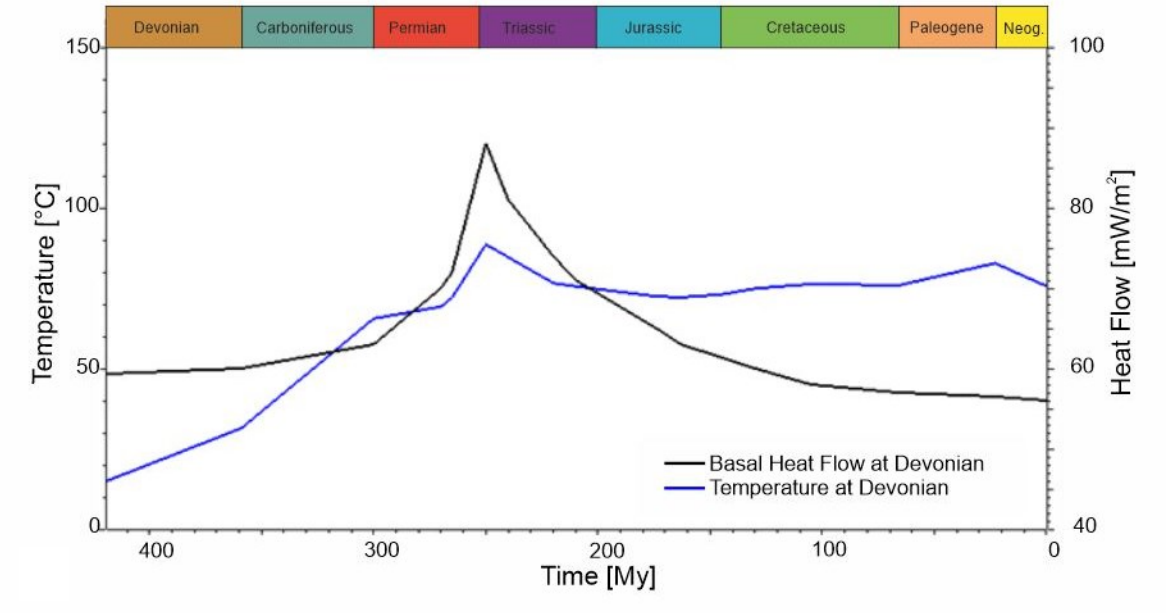

Figure 4.22: Heat flow and temperature history for Model 2: heat flow peak in the Permo–Triassic boundary (black line), temperature variation through time (blue line), rapid burial and no erosion.

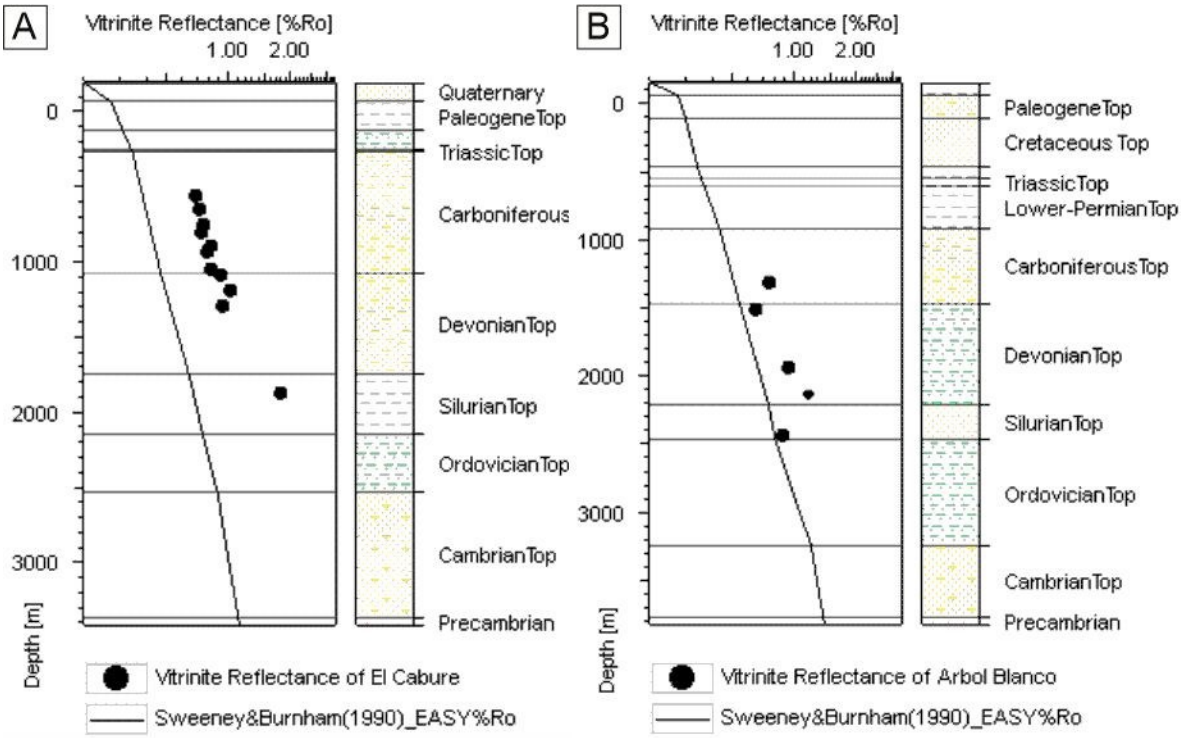

Figure 4.23: Maturity at A)El Caburé and B)Arbol Blanco boreholes for Model 2: Permo–Triassic heat flow peak and no erosion.

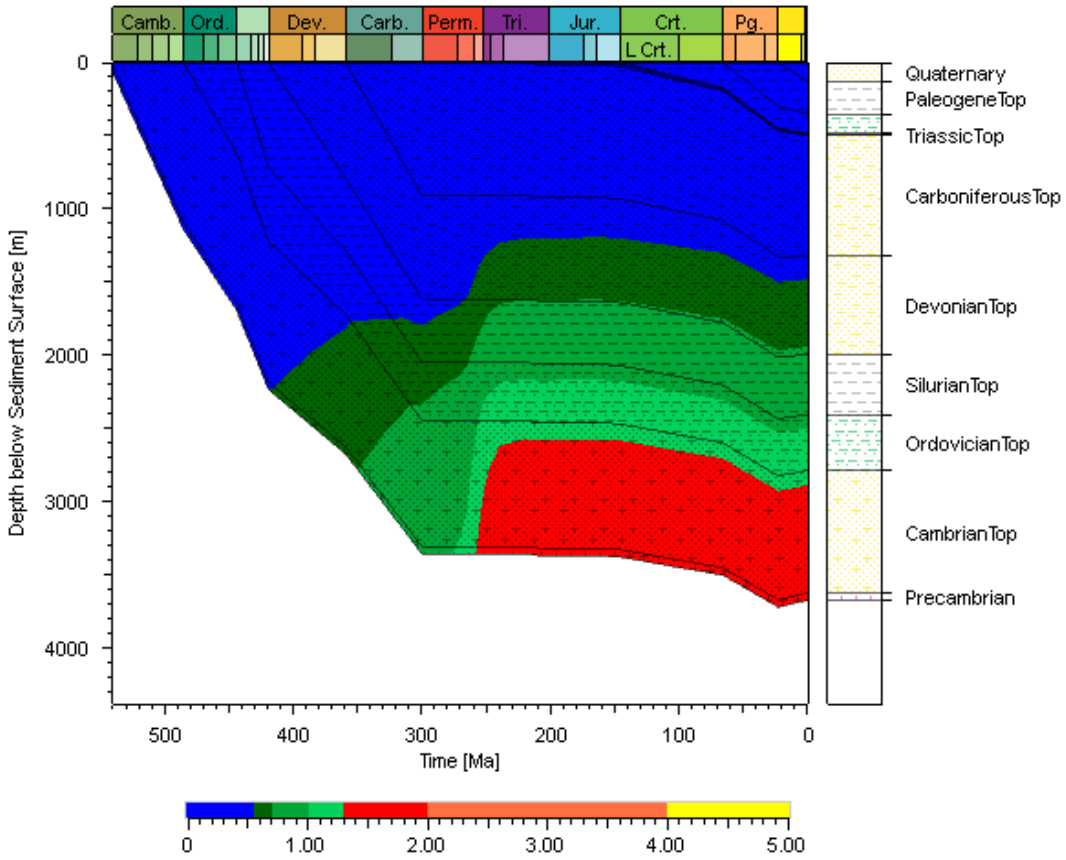

Figure 4.24: Burial history and calculated maturity for Model 2: Permo–Triassic heat flow peak and no erosion.

4.4.3 Model 3

Model 3 considers, as Model 1, a constant heat flow of 56 mW/m² through all geological periods (Fig. 4.25). Model 3 assumes that the burial was continuous until the Permian, including more sediments deposited during the late Permian (eroded Permo–Triassic, Fig. 4.15), followed by a long hiatus period from the early Triassic to the middle Jurassic, and a rapid erosion of late Permian sediments in the early Cretaceous (Fig. 4.27). The additional sediments later eroded have a variable thickness (see erosion map – Fig. 4.15), considering the total sedimentation during the Permian and the corresponding strata as a uniform layer.

Figure 4.26 shows the calculated vitrinite reflectance trend and the measured data in the El Caburé and Arbol Blanco boreholes (see location in Fig. 4.2) for Model 3. The results show Model 3 is still immature. The difference between calculated and measured vitrinite reflectance ranges is smaller than in Model 1, indicating an improvement with the addition of sedimentary thickness and erosion, but it is not yet a valid scenario. Figure 4.26 shows the burial history for all the basin layers, including the early Cretaceous erosion event, and displays higher maturity than previous models.

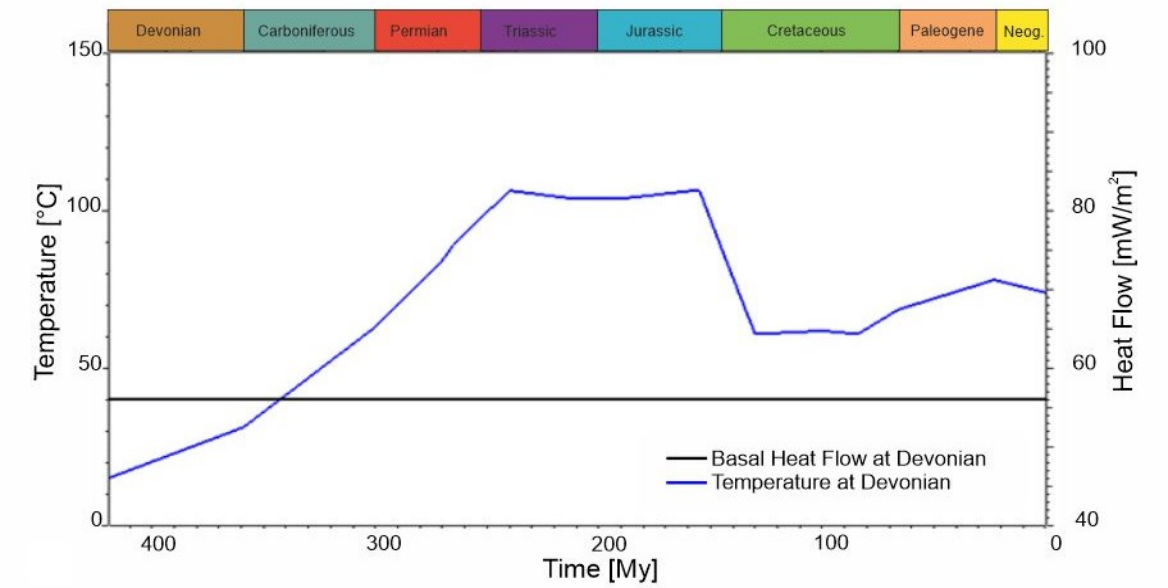

Figure 4.25: Heat flow and temperature history for model 3: constant heat flow (black line), temperature variation through time (blue line), rapid burial and early Cretaceous erosion.

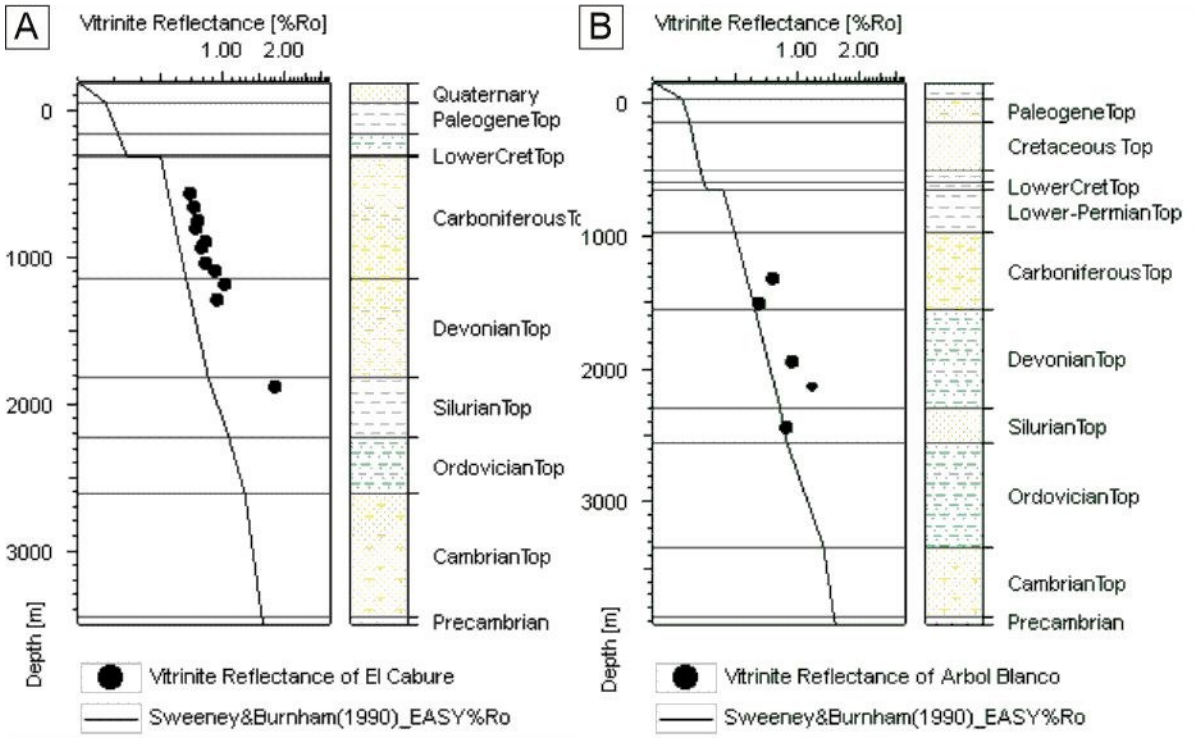

Figure 4.26: Maturity at A)El Caburé and B)Arbol Blanco boreholes assuming a constant heat flow and early Cretaceous erosion.

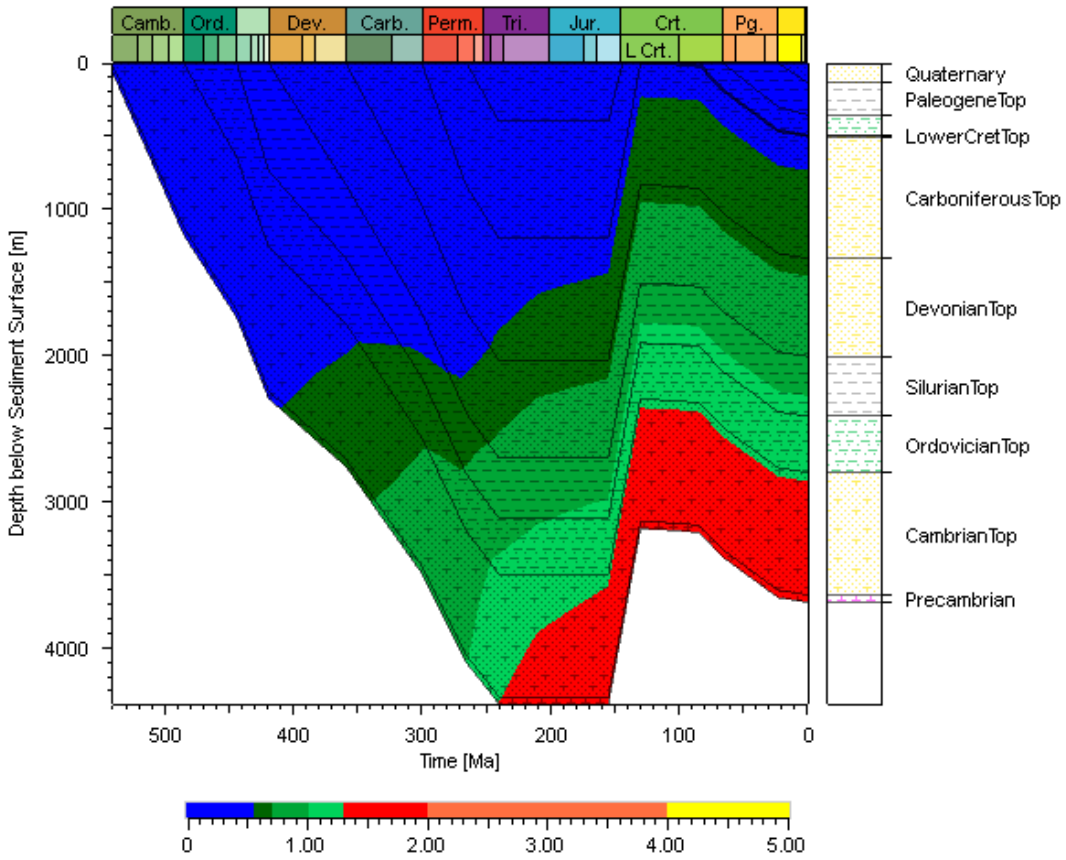

Fig 4.27: Burial history and calculated maturity for model 3: constant heat flow and early Cretaceous erosion.

4.4.4 Model 4

Model 4 assumes a heat flow peak of 87 mW/m^2 in the Permian–Triassic boundary (Fig. 4.28), and continuous burial from the Cambrian to the middle Permian, including the deposition of the extra layer eroded Permo–Triassic (Fig 4.15), but with the difference that this erosion event occurs almost immediately after the end of deposition of Permian sediments, in the early Triassic (Fig. 4.30). The maximum burial and the heat flow peak must coincide to increase the maturity of the buried sediments.

As a result, the maturity calculated in El Caburé and Arbol Blanco wells (Fig. 4.29) reaches values that have a fair correlation with the measured values. Consequently, this model is one of the viable representations of basin history. Nevertheless, other possible scenarios need to be tested and discussed. Models 5 and 6 show variations of model 4, increasing the length of the maximum burial period and decreasing the heat flow peak.

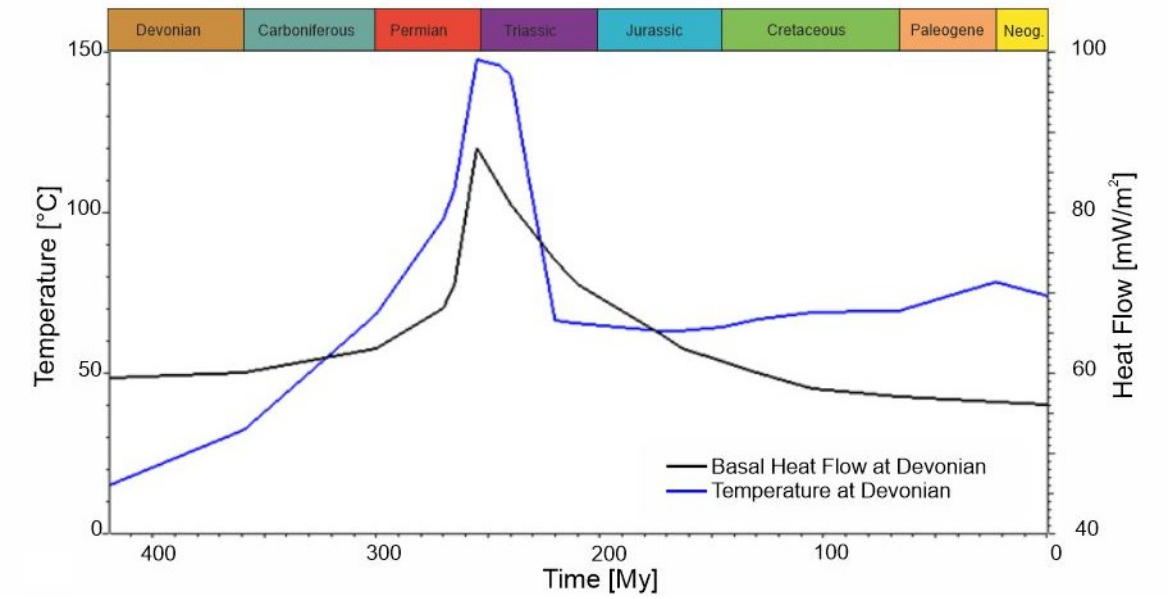

Figure 4.28: Heat flow and temperature for Model 4: Permo–Triassic (higher) heat flow peak and early Triassic erosion.

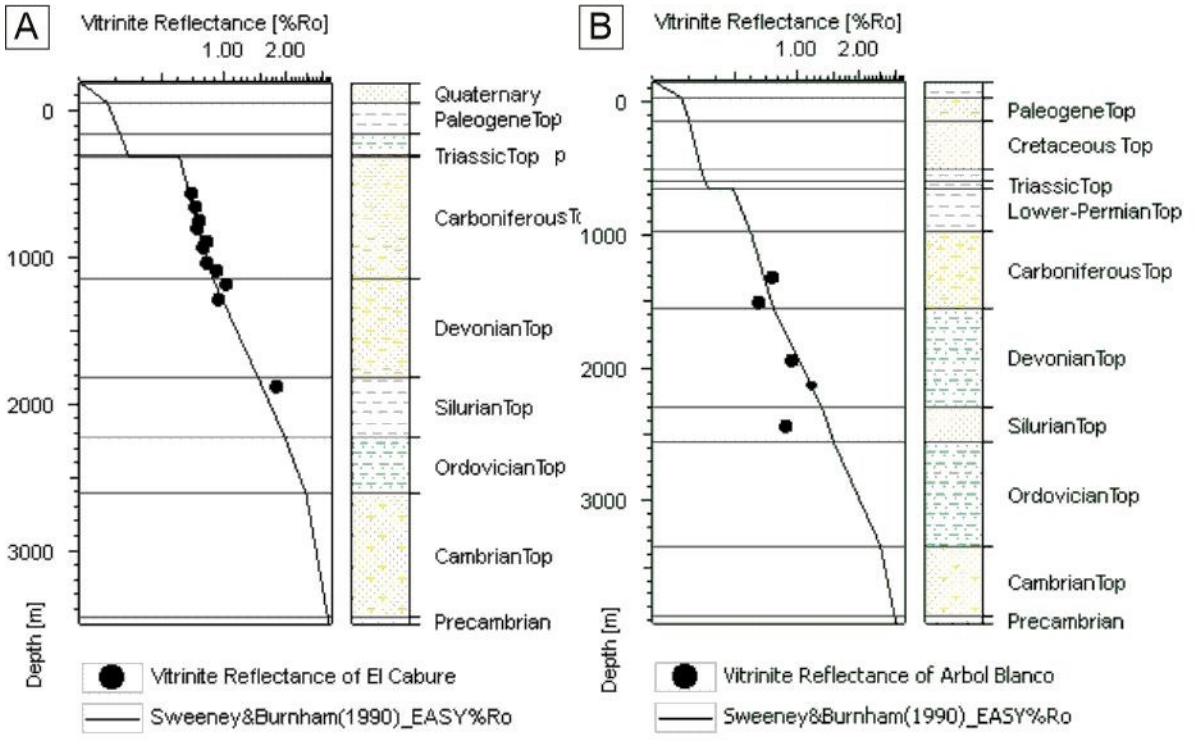

Figure 4.29: Maturity at A)El Caburé and B)Arbol Blanco wells for Model 4: Permo–Triassic (higher) heat flow peak and early Triassic erosion.

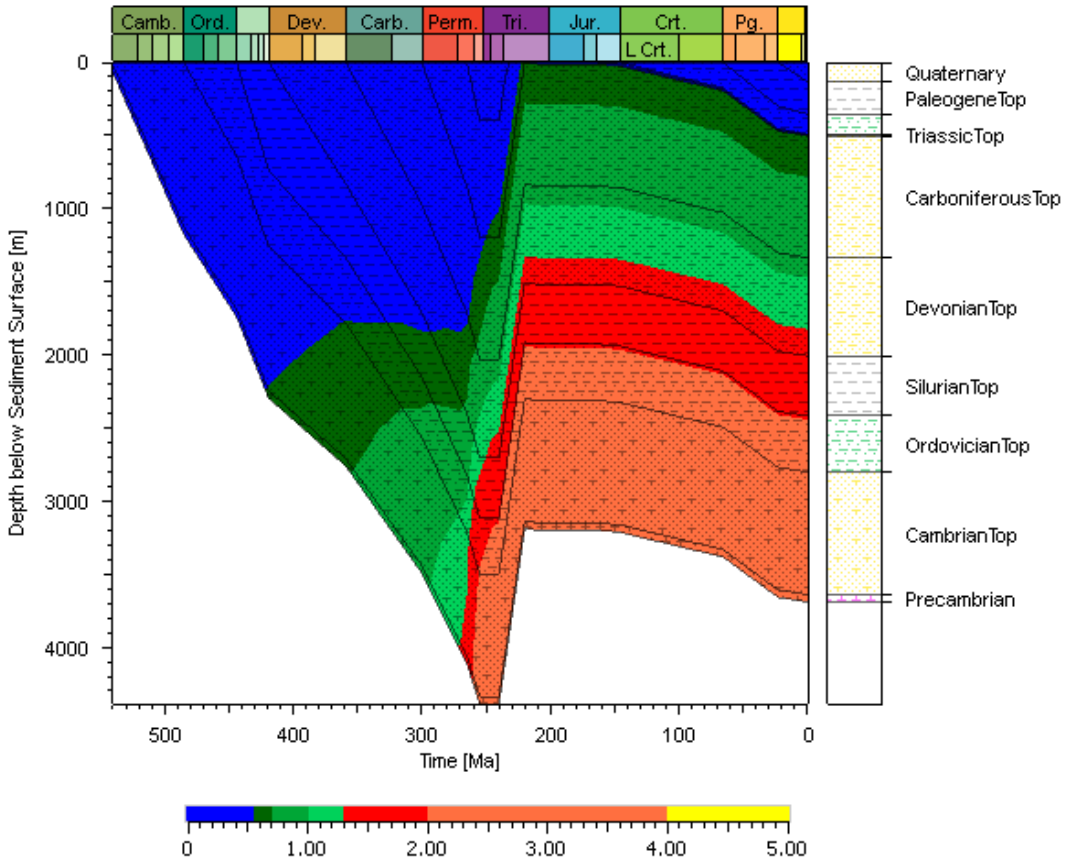

Fig 4.30: Burial history and calculated maturity for Model 4: Permo–Triassic (higher) heat flow peak and early Triassic erosion.

4.4.5. Model 5:

Model 5 assumes a slightly lower heat flow peak (84 mW/m²) also at the Permian–Triassic boundary (Fig. 4.31). The burial for Model 5 is continuous from the Cambrian to the middle Permian, followed by a hiatus or quiescence period until the late Triassic and erosion in middle Jurassic times (Fig. 4.33).

The vitrinite reflectance results (Fig. 4.32) for both wells show a fair correlation, with the main difference with Model 4 being that a longer burial period requires a slightly lower heat flow peak to achieve the same maturation values. Model 5 could also be considered appropriate for representing the basin history.

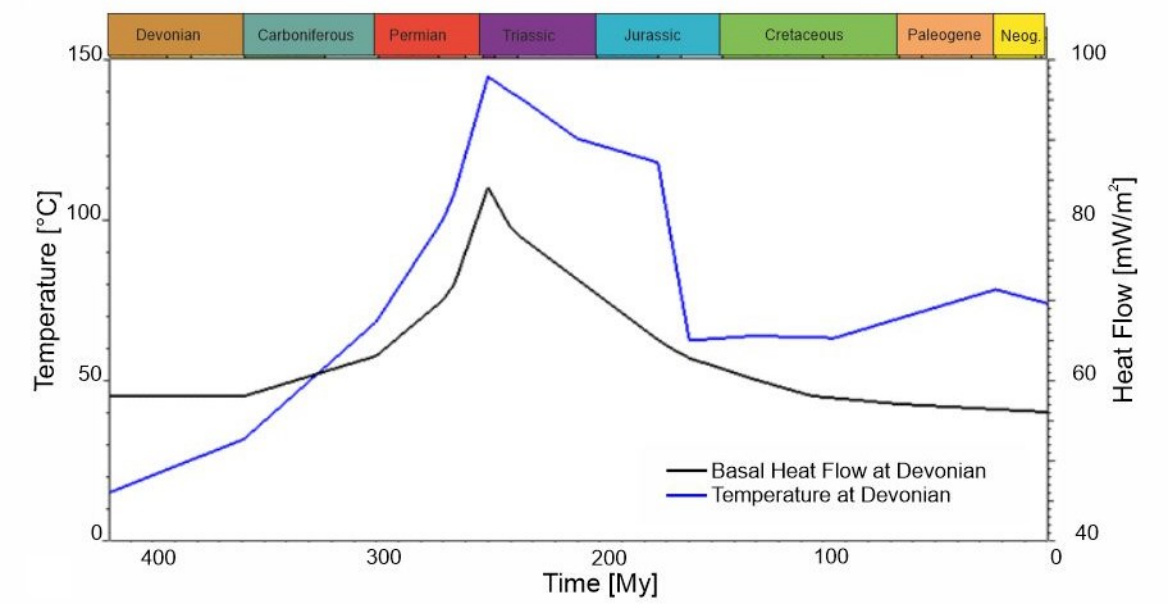

Figure 4.31: Heat flow and temperature for Model 5: Permo–Triassic (medium) heat flow peak and middle Jurassic erosion.

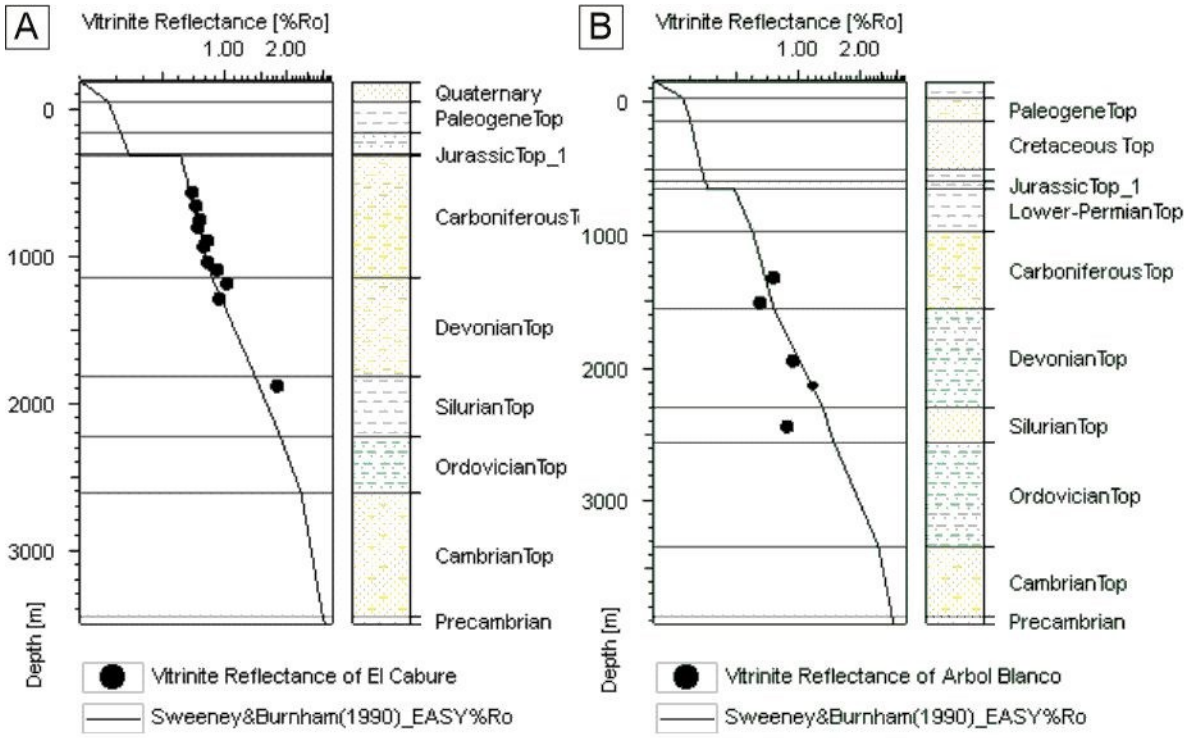

Figure 4.32: Maturity at A)El Caburé and B)Arbol Blanco wells for Model 5: Permo–Triassic (medium) heat flow peak and middle Jurassic erosion.

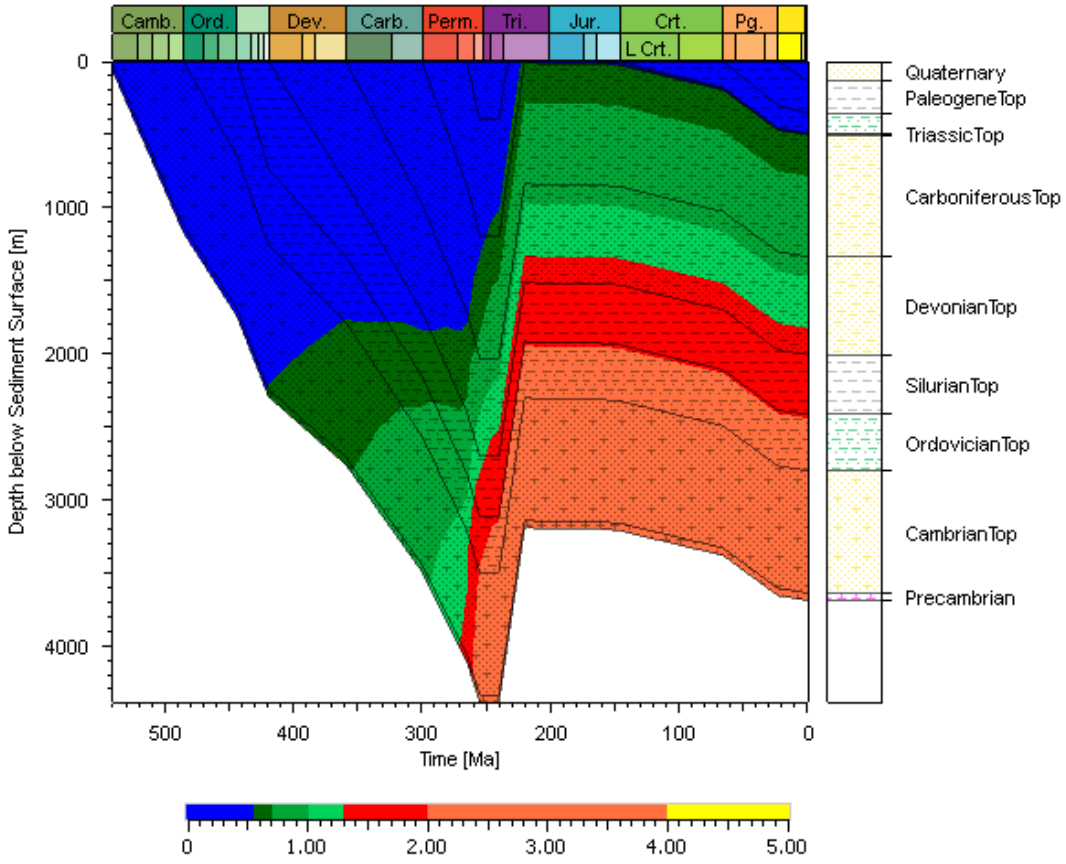

Fig 4.33: Burial history and calculated maturity for Model 5: Permo–Triassic (medium) heat flow peak and middle Jurassic erosion.

4.4.5 Model 6

Model 6 considers an increased heat flow, with a maximum value of 74 mW/m² in the Triassic, but differs from previous models because the increase of heat flow is not punctual and instead decreases gently during the Mesozoic period (Fig. 4.34). The burial history (Fig. 4.36) considers a constant burial from the Cambrian to the early Triassic, including the deposition of the eroded Permo–Triassic extra layer (Fig. 4.15) and a rapid erosion event in the early Cretaceous.

The results calculated against measured vitrinite reflectance (Fig. 4.35) for both wells show a good correlation, indicating that Model 6 also represents a possible scenario for basin history, in which a lower value of maximum heat flow is needed with a longer period of maximum burial and high heat flow.

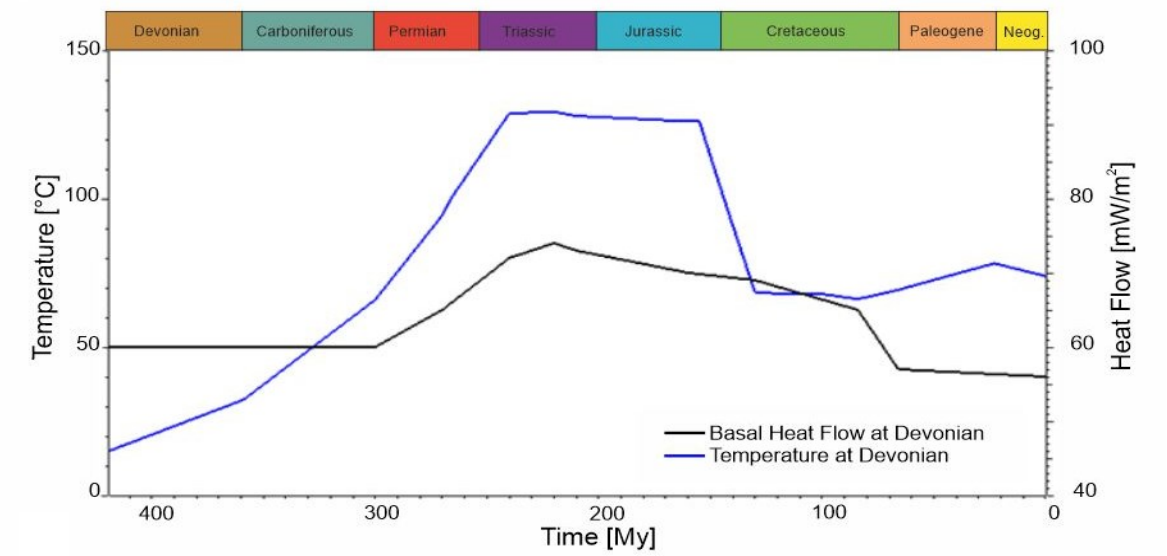

Figure 4.34: Heat flow and temperature for Model 6: Mesozoic (lower) heat flow increase and early Cretaceous erosion.

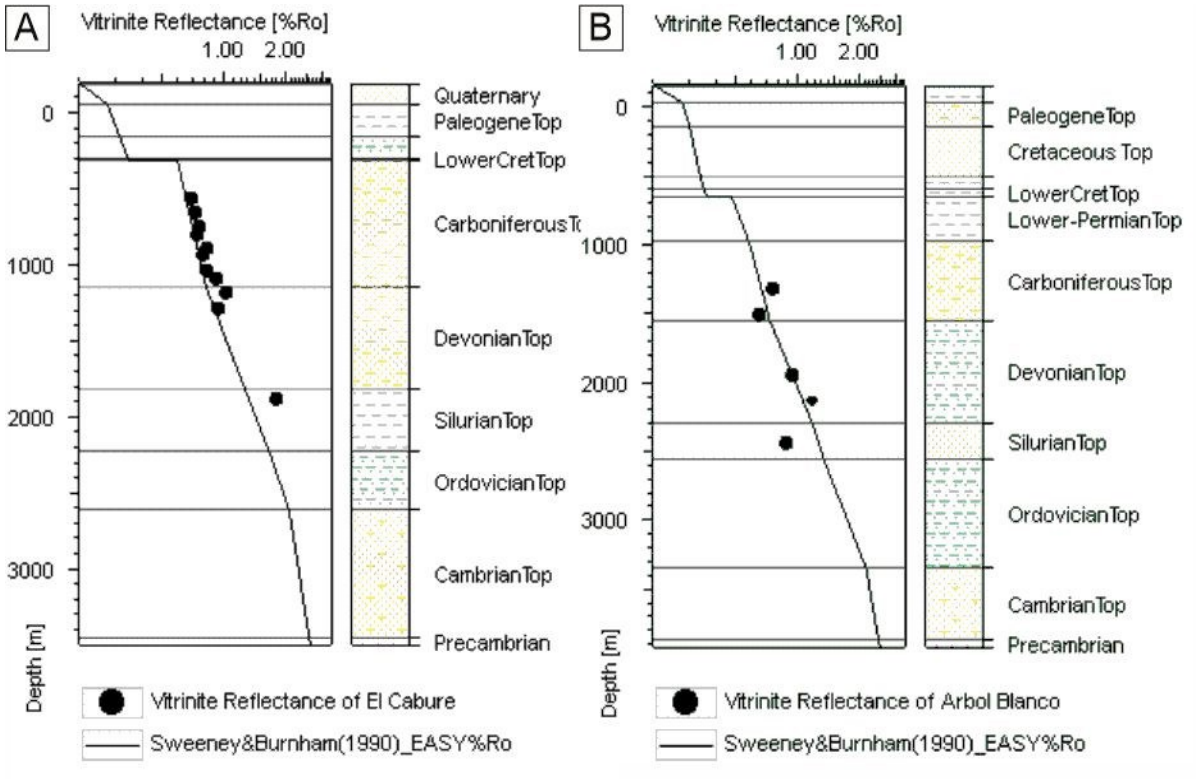

Figure 4.35: Maturity at A)El Caburé and B)Arbol Blanco wells for Model 6: Mesozoic (lower) heat flow increase and early Cretaceous erosion.

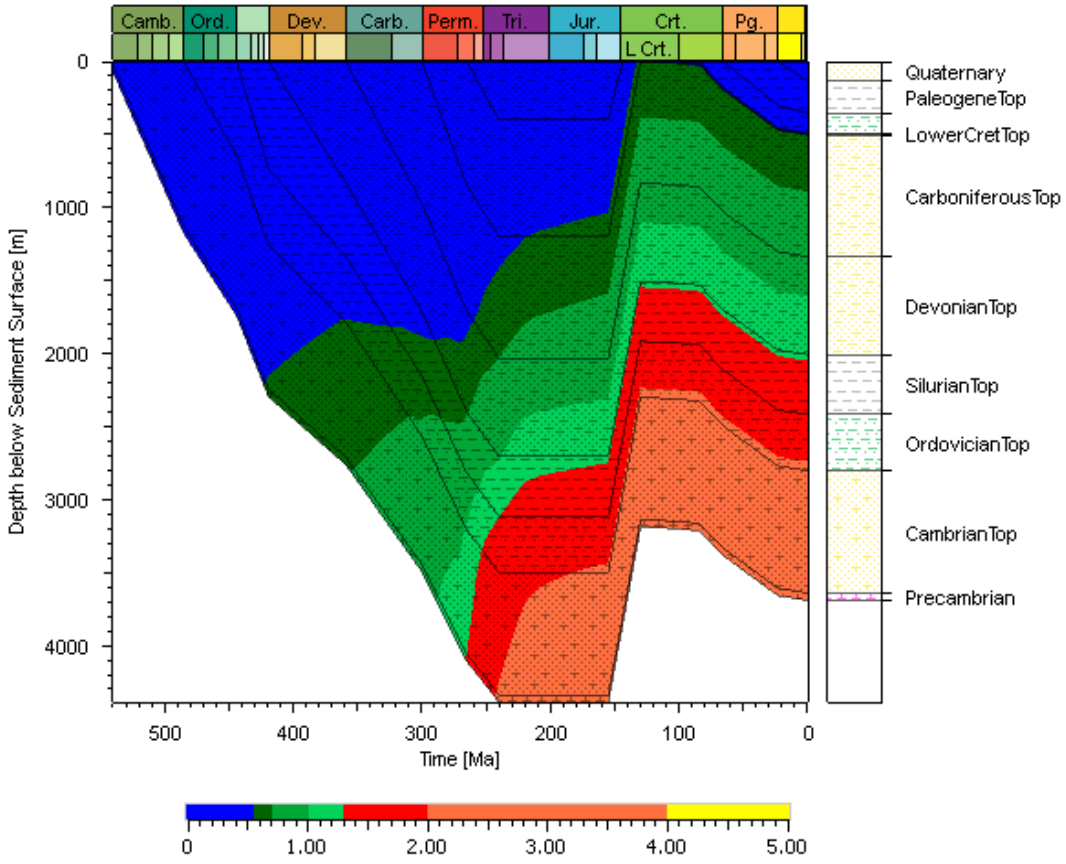

Fig 4.36: Burial history and calculated maturity for Model 6: Mesozoic (lower) heat flow increase and early Cretaceous erosion.

4.5. Modelling Analysis.

Above, I described six of the most representative models for the thermal history of the Chacoparanaense Basin. The key question that remains, however, is which of these models best represents the geological evolution of the basin in a realistic manner and based on the integration of geological background and modelling results.

Analysis of seismic lines (Figs. 4.4 to 4.10) and isopach maps (Figs. 4.13 & 4.14) reveals the presence of an unconformity that occurs after the deposition of the Permian sedimentary record and before the onset of Cretaceous sedimentation (see Section 4.2.3). This unconformity is treated conservatively in Models 1 and 2, interpreted as either a period of non-deposition or a hiatus, with no additional sedimentation or erosion. These missing deposits are not preserved in the stratigraphic record and can only be estimated. Model 1 assumes a constant heat flow equal to the present value (56 mW/m²; Collo *et al.*, 2008), while Model 2 incorporates an increased heat flow (88 mW/m²) at the Permo–Triassic boundary, corresponding to the time of the unconformity. Despite the thermal input, both models predict thermal maturities that are significantly lower than those indicated by the measured vitrinite reflectance data (Figs. 4.20 & 4.23), suggesting that the preserved stratigraphic column, even under elevated heat flow, cannot account for the observed thermal maturity.

Model 3 takes a different approach, maintaining the current heat flow (56 mW/m²; Collo *et al.*, 2008) throughout the history of the basin, while introducing an additional Permo–Triassic sedimentary package (now eroded; Fig. 4.15), followed by a quiescent period and

rapid erosion during the early Cretaceous. This interpretation reflects the unconformity described above. However, the results of Model 3 also fail to agree with the measured age data and produce values that are too low.

Comparison of Models 1, 2, and 3 suggests that both additional sedimentation (now eroded) and increased heat flow are required to adequately simulate the thermal evolution of the basin. Models 4, 5, and 6 test different combinations of increased heat flow and timing of erosion for the Permo–Triassic sediments. Model 4 applies the highest peak heat flow (88 mW/m^2), a brief period of tectonic quiescence, and erosion during the early Triassic. Model 5 shows a slightly lower peak (84 mW/m^2), a longer quiescence and erosion during the middle Jurassic. Model 6 shows the lowest heat flow increase of the three, coupled with a longer quiescence and erosion during the early Cretaceous.

All three models (4, 5, and 6) produce vitrinite reflectance values in agreement with the measured data, making them viable scenarios for the thermal history of the basin. They are consistent in indicating that additional sedimentary sequences were deposited and later eroded, and that higher heat fluxes than present-day values affected the basin during maximum burial. This eroded package must have been more extensive at the El Caburé well site than at Arbol Blanco, consistent with the absence of Permian, Triassic, and Jurassic units in the northwestern sector as indicated on the thickness maps (Figs. 4.13F, 4.14A & 4.14B). As discussed above, the lateral thinning and disappearance of these units, coupled with the overlying Cretaceous sediments, define a clear regional unconformity.

The requirement for increased sedimentation, burial and subsequent erosion to reconcile model results with observed data is strongly supported by the geological evidence. Although the exact volume of eroded material remains uncertain and may be subject to adjustment, its spatial distribution (Figure 4.15) must reflect thicker deposits in the north-west and thinning towards the south-east.

Regarding thermal evolution, the model results indicate that a higher heat flow is necessary during the maximum burial. Although absolute values of paleothermal heat flow may vary, the general trend is supported by tectonic and thermal history. Heat flow reconstruction is inherently challenging (e.g., Welte *et al.*, 1997; Hantschel & Kauerauf, 2009) and is typically guided by tectonic context and model calibration, as demonstrated here. While the reconstructed heat flux curve provides a minimum scenario to explain present-day maturity, additional thermal events - either before maximum burial or after erosion - could have occurred without significantly affecting organic matter maturity. Thus, these models represent a baseline thermal scenario consistent with the available data, while allowing for the potential for additional, unrecorded thermal perturbations.

Changes in heat flow are closely linked to shifts in tectonic regimes (Welte *et al.*, 1997). The Chacoparanaense Basin, an intracratonic basin from the late Precambrian to the Paleogene, eventually became an integral part of the Andean foreland during the Neogene. These tectonic phases suggest an overall stable subsidence history (Yalçin & Welte, 1988; Yalçin *et al.*, 1997), although large-scale tectonic events may have temporarily altered the

thermal regime. Several studies (e.g., Kay *et al.*, 1989; Spalletti *et al.*, 2008; Rocha-Campos *et al.*, 2011; Poma *et al.*, 2014; Rocher *et al.*, 2015; Sato *et al.*, 2015; Riel *et al.*, 2018) propose a Permo–Triassic thermal anomaly along the western margin of Gondwana, driven by slab steepening and associated magmatism, which may have increased regional heat flow. Although the Chacoparanaense Basin was located some distance from the active margin, the thermal influence was likely sufficient to increase temperatures and contribute to the observed maturity.

Taking all these elements into account, Model 4 emerges as the most consistent scenario, with both geological and geothermal constraints. Importantly, it is characterised by an intense heat flow peak that coincides with the timing proposed by several authors for the Permo–Triassic thermal event (e.g., Kay *et al.*, 1989; Rocha-Campos *et al.*, 2011; Sato *et al.*, 2015). Furthermore, the timing of erosion in this model - during the Triassic - is well aligned with the deduced uplift of the Quirquincho High (see Chapter 3), which is associated with a regional unconformity and an eroded area identified in the stratigraphic and seismic records. This supports the notion of a Paleozoic forebulge associated with the tectonic evolution of the ancestral Andes (see Section 3.4) and reinforces Model 4 as a geologically plausible reconstruction of the thermal and structural history of the basin.

The argument of some authors concerning the lack of certainty in the definition of Triassic and Jurassic units (e.g., Russo *et al.*,1979; Chebli *et al.*, 1999; Fernandez Garrasino *et al.*, 2005; Reinante *et al.*,2014) due to the absence of sufficient age indicators (e.g.,

microfossils) is interesting in light of the new findings. This lacuna coincides with the observed erosion period and posterior hiatus, suggesting the possibility that the sediments considered to Triassic and Jurassic could actually be part of the continental Cretaceous deposits, indicating a pause in sedimentation during the early Mesozoic after a significant change from marine to continental depositional environments had occurred.

4.6. Hydrocarbon potential

The evaluation of hydrocarbon (HC) potential in the Chacoparanaense Basin was carried out using the results from Model 4, identified as the most geologically and thermally consistent scenario. The analysis focused on three stratigraphic units with possible source rock potential in the region: the Carboniferous, Devonian, and Silurian. For each of these units, the Transformation Ratio (TR), total organic carbon (TOC) values, thickness, and facies distribution were examined in detail to assess their generation potential. This integrated approach provides a comprehensive understanding of the basin's HC prospectivity.

4.6.1 Transformation Ratio

The transformation ratio (TR) is a critical parameter in petroleum system modelling, representing the proportion of kerogen that has been thermally converted to hydrocarbons. It reflects the generative evolution of the source rock from initial maturity, through peak oil and gas generation, to over-maturity (Tissot & Welte, 1984; Peters *et al.*, 2005). TR values of less than 5% indicate immature source rocks that have only begun to generate hydrocarbons,

while values above 95% reflect almost complete transformation, typically associated with overmature conditions and only residual dry gas potential. Intermediate TR values (e.g., 20-80%) signal active hydrocarbon generation and potential expulsion, and are often correlated with peak oil and wet gas windows (Pepper & Corvi, 1995). Besides providing information about the maturity of the source rock, the TR integrates the kerogen-dependent rate of the transformation. This factor is important because, depending on the kerogen type, for the same values of vitrinite reflectance maturity, the hydrocarbon generation varies (Jarvie *et al.*, 2007; Jarvie, 2012). Interpretation of TR values is important for the assessment of both conventional and unconventional hydrocarbon potential within a basin.

Transformation ratio (TR) maps were calculated for the Carboniferous, Devonian, and Silurian intervals using standard kinetic parameters for kerogen type II, selected based on the depositional environment and geochemical characteristics of the source rocks (Tegelaar & Noble, 1994). Type II kerogen is the most common in marine settings, formed primarily from autochthonous planktonic and microbial organic matter deposited under anoxic to suboxic conditions (Tissot & Welte, 1984; Peters *et al.*, 2005). This type of kerogen is known for its oil-prone behavior, with the potential for wet gas generation at higher levels of thermal maturity. In contrast, type I kerogen, typically found in lacustrine environments, originates predominantly from algal material and is highly oil-prone but less common in marine sequences. Type III kerogen, by comparison, is derived from terrestrial plant debris and is predominantly gas-prone, characteristic of deltaic or continental depositional systems (Hunt, 1996; Peters *et al.*, 2005). Given the marine origin of the Paleozoic units in the study area,

kerogen type II provides a geologically consistent basis for TR modelling and better reflects the expected hydrocarbon generation behavior.

The Carboniferous (Fig. 4.37) has negligible TR values across most of the basin, suggesting that it remains thermally immature and has not generated significant hydrocarbons. This suggests limited current exploration potential for the Carboniferous rocks in our study area. A small area of anomalously high TR in the SE may represent a modelling artefact.

The Devonian (Fig. 4.38) source rock has moderate to high TR values that increase towards the NE, suggesting that it has undergone significant hydrocarbon generation, probably within the oil-wet gas window (Pepper & Corvi, 1995; Peters *et al.*, 2005). If organic-rich, this unit may have unconventional potential as a self-generating reservoir (e.g., shale oil or accumulation of tight gas in the siltstone and sandstone facies), particularly if TOC, porosity, and hydrocarbon saturation are favorable. In addition, its generative performance suggests that it could have contributed to oil migration, but there are no findings in the drilled wells that support an accumulation in conventional reservoirs in the basin.

The Silurian (Fig. 4.39) unit is characterized by very high TR values, indicating that it is over-mature and has largely exhausted its hydrocarbon potential. Such high TR values are typical of source rocks that have passed peak oil production and are now in the dry gas window (Peters *et al.*, 2005; Jarvie *et al.*, 2007). However, the SE sector of the basin may still

be actively producing hydrocarbons. Although the Silurian has limited remaining generating capacity, it may still hold unconventional dry gas potential (Jarvie, 2012).

Plots of TR vs. Time extracted for single wells (Fig. 4.40) show that the only generation occurred during the maximal burial, in the Permo–Triassic boundary, and there is no later or current generation of hydrocarbons.

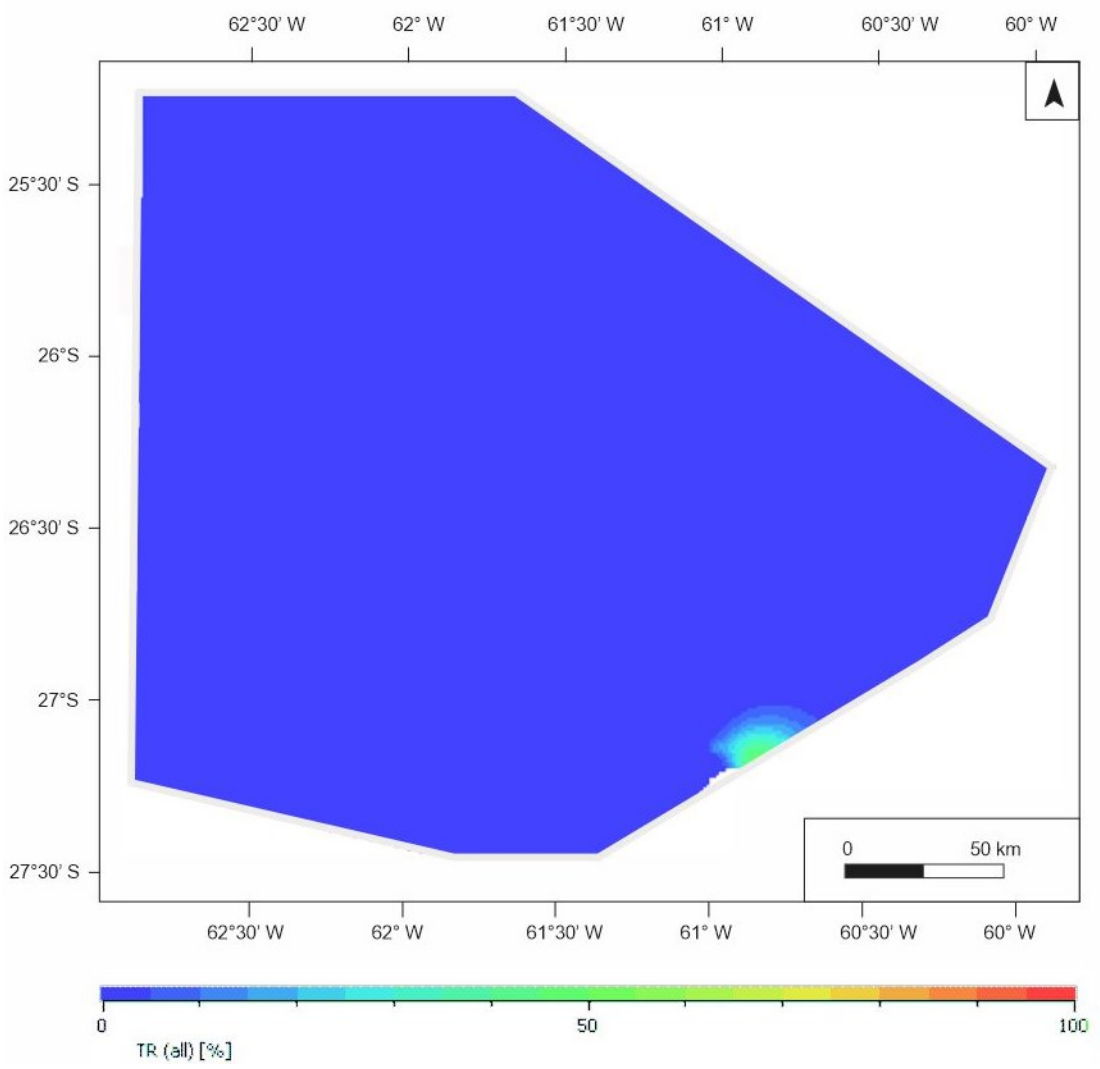

Figure 4.37: Transformation ratio (TR%) calculated for the Carboniferous unit using kerogen Tegelaar Type II Texas (shale) (Tegelaar & Noble, 1994).

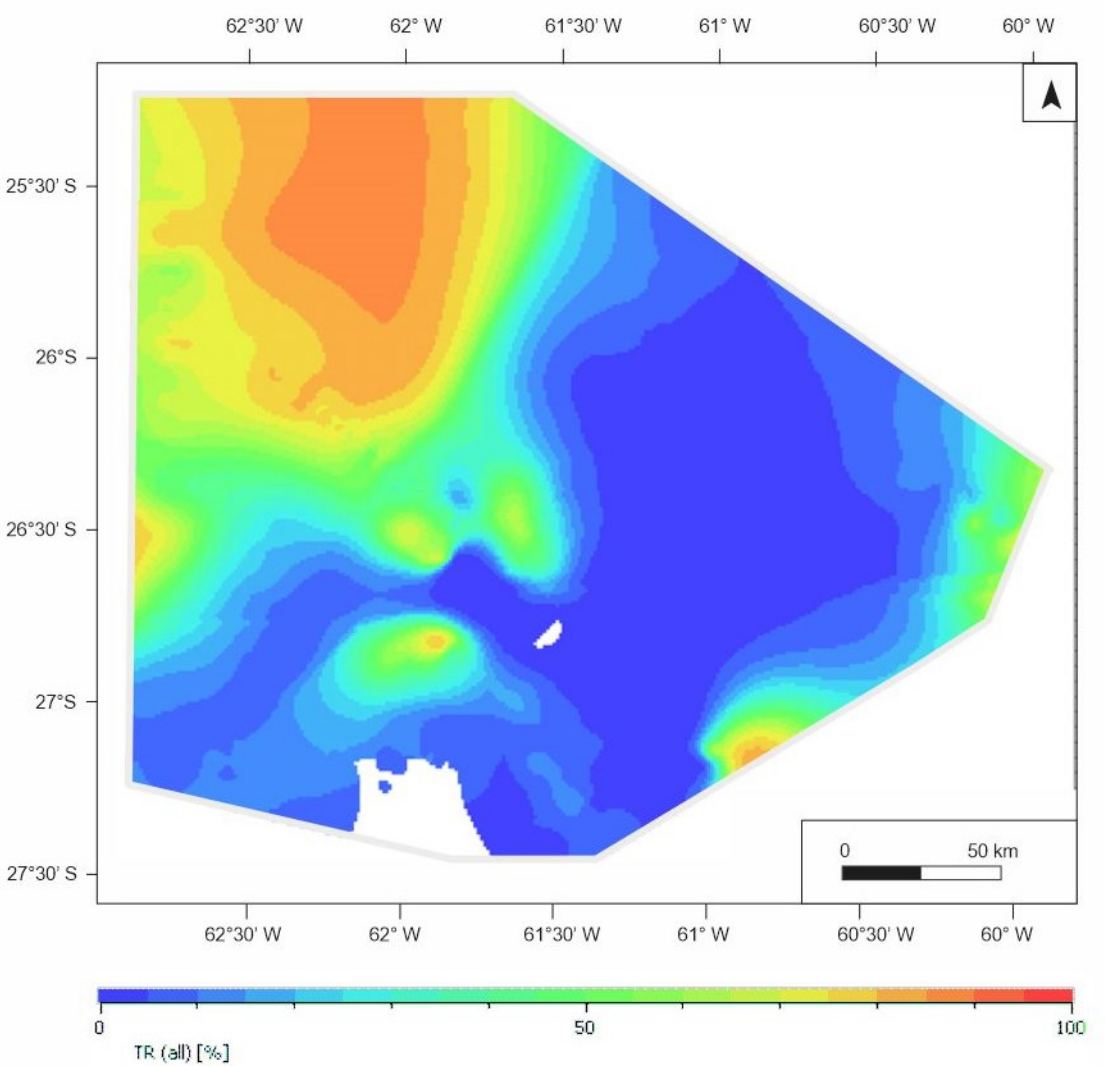

Figure 4.38: Transformation ratio (TR%) calculated for the Devonian unit using kerogen Tegelaar Type II Oklahoma (Woodford shale) (Tegelaar & Noble, 1994).

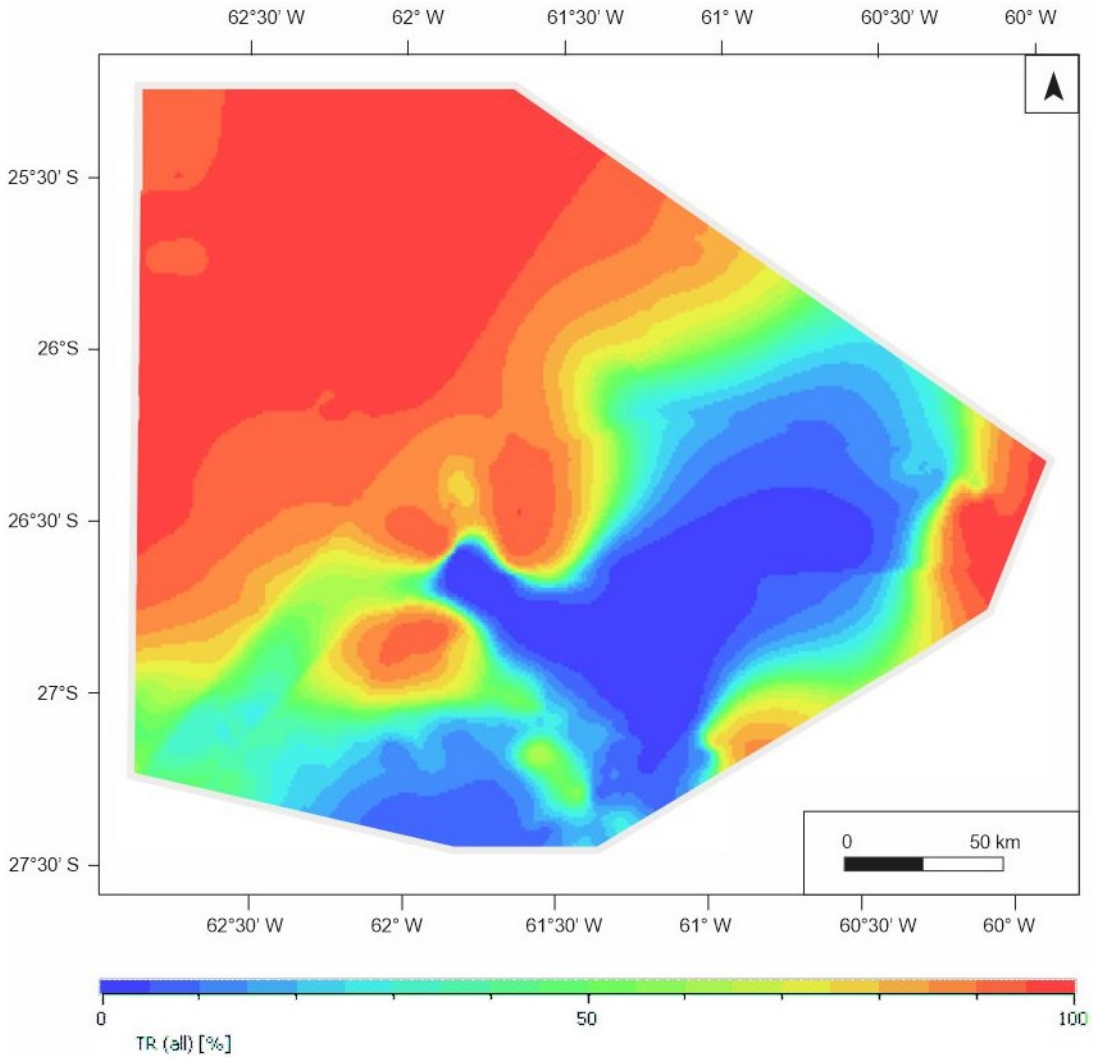

Figure 4.39: Transformation ratio (TR%) calculated for the Silurian unit using kerogen Abu-Ali Type II Quasiba (Silurian shale) (Tegelaar & Noble, 1994).

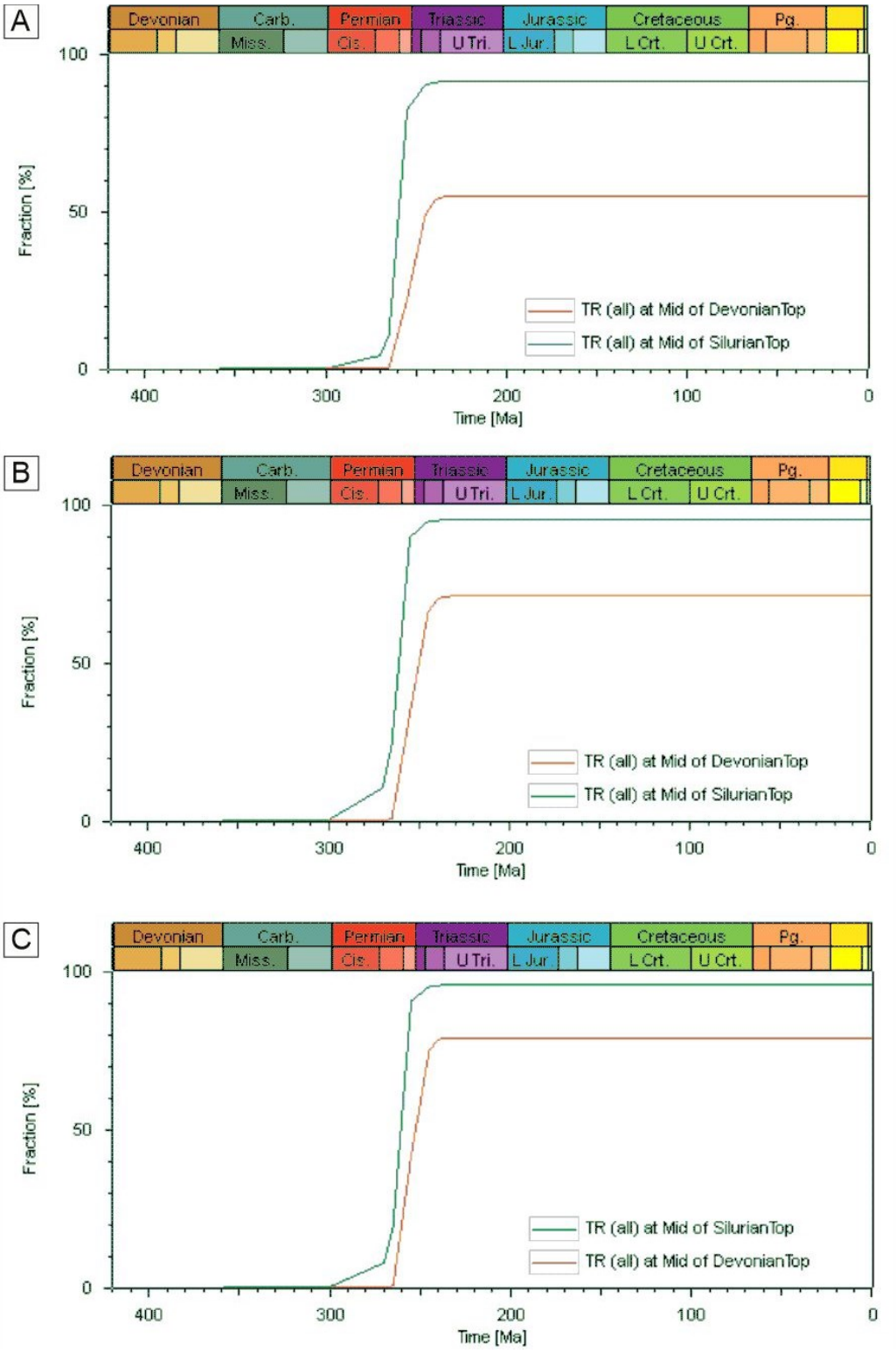

Figure 4.40: Transformation ratio (TR%) vs. time for A) Arbol Blanco, B) Campo Gallo, and C) El Caburé boreholes. The brown line shows TR for Devonian potential source rock using “Devonian Oklahoma”

type II kinetics. The green line shows TR for Silurian potential source rock using “Silurian Qusaiba” type II kinetics (Tegelaar & Noble, 1994; Abu & Ali, 1999).

4.6.2. TOC analysis

Total Organic Carbon (TOC) was evaluated in 4 wells to assess the organic richness of the Silurian, Devonian and Carboniferous units in the study area. TOC is a critical parameter in source rock evaluation and serves as a proxy for hydrocarbon generation potential. While TOC neither indicates maturity nor timing and extend of hydrocarbon generation, values above certain thresholds are essential to classify source rocks as fair (>0.5 wt%), good (>1 wt%), or excellent (>2 wt%) in terms of richness (Tissot & Welte, 1984; Peters *et al.*, 2005; Jarvie, 2012).

The Carboniferous unit shows considerable heterogeneity between drill holes. While El Caburé and Arbol Blanco have average TOC values of 0.52 wt% and 1 wt%, respectively, locally exceeding the minimum generative threshold, Campo Gallo has consistently very low TOC values (~0.22 wt%), with some measurements as low as 0.04 wt%. Despite a few enriched samples (e.g., max 3.08 wt% in Arbol Blanco), the overall distribution suggests limited source potential, with much of the interval likely below the richness required for significant generation. Combined with the previous assessment of immature thermal maturity and low transformation ratio (TR), the Carboniferous interval can be considered non-prospective as a source rock, although its potential as a tight reservoir could be reassessed if structurally charged by the underlying units.

The Devonian shows moderate TOC values in all boreholes. El Caburé has the highest average (0.58 wt%) and a maximum of 1 wt%, while Arbol Blanco and Campo Gallo have slightly lower averages (0.62 wt% and 0.44 wt%, respectively). Although these values are below the "good" threshold for classic shale plays, they exceed the 0.5 wt% limit in several samples, suggesting good to marginal source potential, particularly in zones where TR indicates how much of the organic matter was converted into hydrocarbons and when that transformation took place, indicating that the TOC could be originally higher. The Devonian may warrant further geochemical evaluation (e.g., Rock-Eval pyrolysis) to assess hydrogen index (HI) and kerogen quality, particularly in siltstone and mixed lithofacies zones that may act as hybrid source-reservoirs (Jarvie *et al.*, 2007; Loucks & Ruppel, 2007).

The Silurian unit, although represented by a limited number of samples in this dataset, shows geochemically promising features where available. At El Caburé, TOC values range from 0.39 to 1.27 wt% (average 0.52 wt%), indicating moderate to good organic richness. Although not as enriched as global analogues such as the Qusaiba Formation in Saudi Arabia (which can exceed 4-5 wt% TOC) or the Llandovery-age shales in North Africa and Canada (Jenkins *et al.*, 1997; Lüning *et al.*, 2000), these values nevertheless support the presence of a viable source interval within this stratigraphic level.

Importantly, these results are consistent with previous results from Transformation Ratio (TR) analysis, which indicated that the Silurian has already generated most of its hydrocarbon charge. In such overmature or post-generation conditions, the presence of residual TOC (organic matter that has not been expelled as hydrocarbons) can be a key factor in assessing

unconventional gas potential. Residual organic matter may still contain significant amounts of adsorbed gas, particularly methane, trapped in micropores of the kerogen or associated with clay minerals (Jarvie, 2012).

Although the Silurian interval is past peak generation, its retained organic richness and geological context suggest that it may be a candidate for unconventional shale gas or tight gas exploration and should be further explored in the SE part of the study area, where it has not reached maximum TR values. Retained organic richness indicates that this source rock had even better TOC values before maximum burial and generation of hydrocarbons (maximum TR in Fig. 4.40).

4.6.3. Maturity – Vitrinite Reflectance

The Devonian unit, based on the vitrinite reflectance (%Ro) map (Fig. 4.41), has maturity values predominantly between 0.6% and 1.2% Ro, with localised areas to the east and south-east exceeding 1.3%Ro. This distribution suggests that the Devonian is predominantly within the oil window to early gas window maturity range (0.6-1.3%Ro. These maturity levels are consistent with transformation ratio (TR) values observed in the same interval, reinforcing the idea of moderate to advanced thermal evolution. In particular, the central and western sectors (including wells such as Campo Gallo, Coronel Rico and Arbol Blanco) fall within this maturity window and are associated with moderate total organic carbon (TOC) levels, typically around 0.4-0.6 wt%. These characteristics support the potential of the Devonian as a conventional source rock in these areas. Conversely, the easternmost

parts of the basin, such as the Pampa Bandera, appear to be late mature and have probably expelled most of their hydrocarbons. However, these zones may still have residual gas potential, particularly if kerogen quality and pressure conditions are favorable.

For the Silurian unit (Fig. 4.42), their vitrinite reflectance description suggests a very mature to over-mature system, particularly in the northwest and near Arbol Blanco and Pampa Bandera, where Ro values reach approximately 2.0%. This observation is in good agreement with calculated TR values and TR vs. Time, indicating that the Silurian has passed the peak of oil generation and could have entered a phase of extensive hydrocarbon expulsion. A narrow transition zone marked by ~1% Ro outlines the peak oil generation along the boundary between the overmature and immature areas.

This maturity pattern is consistent with analogous Silurian source rocks elsewhere in South America, such as the Lipeón Formation in northwestern Argentina and the Fuentemolinos and Los Espejos formations in the Precordillera, which have been described as effective regional source rocks (Gallagher & Lamadrid, 2015; Zappettini & López-Gamundí, 1995).

The implications for unconventional exploration are significant, especially in the Silurian. The combination of high thermal maturity (Ro > 2%), residual TOC values around 0.5 wt% (e.g., El Caburé area), and significant thicknesses up to 1500 m in both the northwestern and southeastern sectors supports the potential for a dry gas-prone unconventional shale play. The presence of residual TOC in overmature stages implies that gas may remain adsorbed

within the organic matrix or trapped as free gas in pore spaces and fractures. In addition, the high level of thermal maturity may have generated overpressure and micro-fracture formation, creating natural microfractures that enhance gas storage and deliverability. If coupled with favorable mineralogy (such as quartz-rich or brittle compositions) and suitable structural settings for hydraulic stimulation, these features could make the Silurian a viable target for shale gas development (Jarvie, 2012; Loucks & Ruppel, 2007).

4.6.4. Integrated potential

The maturity maps, TOC data, and calculated transformation ratios (TR) provide a consistent framework for assessing the generation potential of each stratigraphic unit. The Devonian unit, although generally mature (0.6-1.2% Ro), has moderate TOC values (~0.4-0.6 wt%) and variable lithologies. Its hydrocarbon potential is constrained by low organic richness and relatively thin organic-rich intervals, limiting its capacity as an important source, but with potential as a secondary source rock. The Silurian unit, in contrast, shows clear evidence of extensive past hydrocarbon generation, with TR values close to 100% and vitrinite reflectance exceeding 2.0% Ro over wide areas. Despite being overaged, residual TOC values (~0.5 wt%) and favourable lithology in some zones suggest that it could retain gas in place, particularly in thicker parts of the basin. In particular, the thickness of the Silurian varies considerably, with the highest accumulations (up to 1500m) occurring in the northwest and east (Las Breñas half-graben), coinciding with areas of high maturity and gas potential. In the central region, where both maturity and thickness decrease, the potential of the unit is more limited. In contrast,

the Carboniferous unit, although dominated by sandstone lithologies that may be favourable for reservoir quality, lacks sufficient maturity and shows little evidence of hydrocarbon generation across the study area. Its low TR values and immaturity make it unsuitable as a source rock, and its potential as a tight reservoir is limited without an associated effective charge. This integration highlights the importance of considering maturity, TOC and thickness together, as productive unconventional plays typically require not only mature source rocks but also sufficient thickness to sustain economic production volumes (Jarvie, 2012; Loucks & Ruppel, 2007).

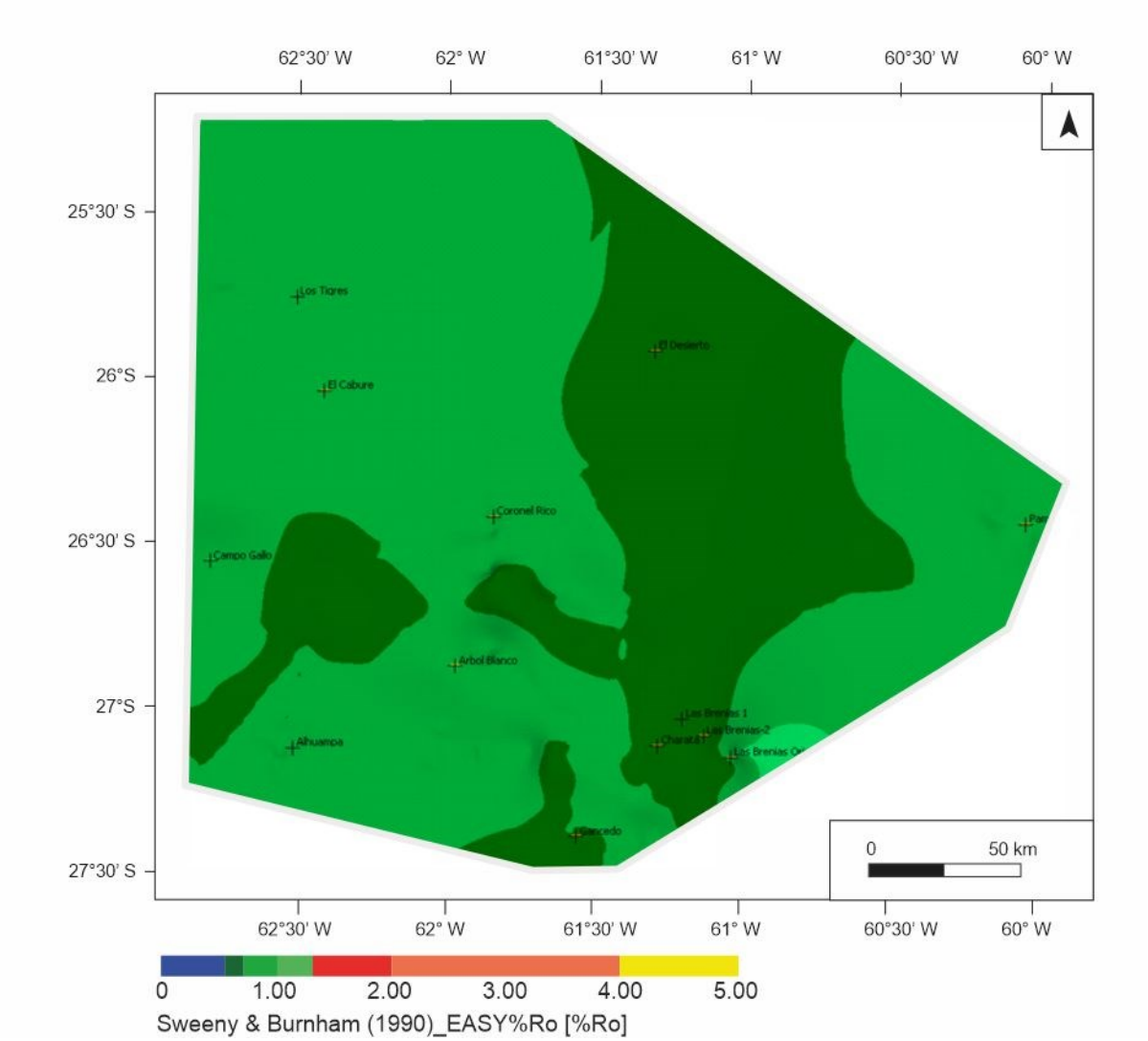

Figure 4.41: Vitrinite reflectance map of the Devonian unit.

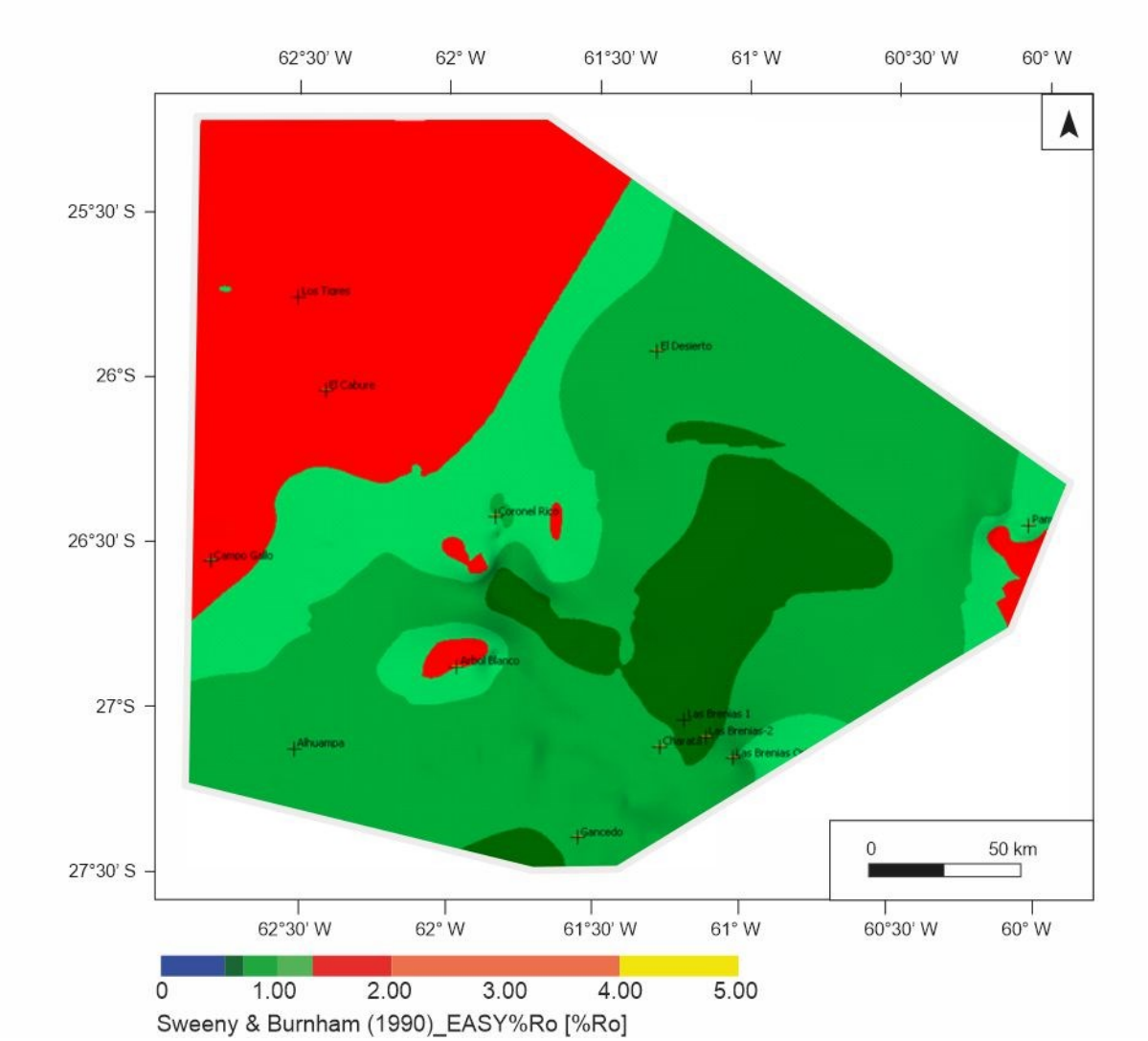

Figure 4.42: Vitrinite reflectance map on the Silurian unit.

4.7. Conclusions

Seismic interpretation and interpolation of horizons into depth and thickness maps depict the protracted depositional and erosional history of the Chacoparanaense Basin. The analysis carried out in this study allowed the construction of a very detailed 3D structural model, which is suitable for reconstructing the thermal and sedimentary history of the basin.

The evolution of the northern Chacoparanaense Basin began with the development of the Las Breñas half-graben during the late Precambrian, which later experienced an inversion episode during the Devonian. Subsequently, the basin evolved into an intracratonic setting, with marine conditions during the Paleozoic and continental environments during the Mesozoic. The obtained results suggest a significant uplift and erosion event in the north-west of the study area, coinciding with the position of the Paleozoic Quirquincho High. Additional Permo–Triassic sediments were probably deposited but not preserved due to Triassic erosion, supporting the hypothesis of the elevation of a late Paleozoic–Triassic forebulge discussed in Chapter 3. Following this erosional episode, a period of tectonic quiescence resulted in a marked hiatus between Paleozoic and Mesozoic deposits, accompanying the transition from a marine to a continental depositional environment. During the Paleogene, the basin was subjected to a cycle of transgression and regression, and in the Neogene, its subsidence regime changed as it became an integral part of the Cenozoic Andean foreland.

The thermal evolution of the basin reflects a more complex history than subsidence alone would suggest. Basin models indicate that a peak in heat flow at the Permo–Triassic

boundary - associated with geodynamic processes at the south-eastern margin of Gondwana - also affected the Chacoparanaense region.

The integrated assessment of thermal maturity, transformation ratio (TR), and total organic carbon (TOC) across stratigraphic units provides a comprehensive framework for hydrocarbon potential in what has historically been considered a frontier exploration area. The Carboniferous unit, although lithologically favorable to be a reservoir rock due to its sandstone composition, remains thermally immature and lacks generative capacity, making it unsuitable as a source rock. The Devonian unit is moderately mature (0.6-1.2% Ro) over much of the basin, with TOC values ranging from 0.4 to 0.6 wt% in siltstone- and clay-rich intervals. This supports a modest conventional hydrocarbon potential, particularly in the central and western regions. However, due to variable lithologies and limited organic richness, only selected intervals may warrant further evaluation, particularly as hybrid source-reservoir systems. In contrast, the Silurian unit offers the most promising characteristics for unconventional development. It is thermally mature (Ro > 2%) over much of the basin, with residual TOC values (~0.5 wt%) and significant thicknesses (up to 1500 m) in the north-western and eastern sectors. If favorable mineralogy (e.g., quartz-rich, brittle zones) and structural conditions for stimulation exist, the Silurian may represent a viable target for shale gas exploration. While conventional prospects are limited overall, the basin retains significant unconventional potential, particularly within the Silurian interval.

5. Conclusions

This thesis has shown that beneath the apparently monotonous Chacopampean Plain exists evidence for a rich geological history, dating back to the late Precambrian, which records a complex evolution of localized, early-stage extensional processes that were followed by regional subsidence during marine and continental sedimentation, erosion, and long-wavelength deformation. The evolution of the Chacopampean Plain involved three distinct sedimentary basins and two distinct basement highs, of which the Quirquincho High is the most important. The Paleozoic and Mesozoic basinwide processes have also had an influence on the subsequent development of the Cenozoic Andean foreland basin and highlight the long-lasting influence of inherited geological structures and sedimentary characteristics on the most recent geological evolution.

By digitising and reinterpreting an extensive data set of seismic lines, well reports and logs, I was able to reconstruct the geological history beneath the Chacopampean Plain, with particular emphasis on the formation of the buried Quirquincho High. The morphology of the Quirquincho High extends in width between 115 km in the north and 190 km in the south, with a partial length of 470 km extending beyond the covered area. It has an inclination of ~0.9% on its northwest, farther east reaches a maximum width of 60 km within the study area, and extends about 160 km further north, with a similar slope of ~1%.

The well-connected seismic interpretations unambiguously show that the Quirquincho High was already elevated in the early Mesozoic and remained a positive topographic feature until the Paleogene, when strata began to onlap its top. This trend has continued until the present-day and resulted in the current depositional and morphological characteristics of the Chacopampean Plain. As discussed in Chapter 3, the elevation of the Quirquincho High was primarily due to flexure of the crust in the foreland of the ancestral Andes or during the Gondwana orogeny, which occurred from the late Paleozoic to the early Mesozoic. Given the overall paleogeographic relationships and the deformational and depositional characteristics. In the area of the Quirchincho High, this feature is interpreted as an ancient forebulge. In this context, the Pampeano-Chaqueño High farther east is interpreted as a second, smaller forebulge, influenced by crustal weakness inherited from the suture between the Pampia and Rio de la Plata cratons.

In Chapter 4, I refined the different steps of basin evolution through basin modelling, which indicated continuous sedimentation in the Las Breñas half-graben from the late Precambrian throughout the Palaeozoic and until the early Triassic. During this protracted period, the Quirquincho High began to emerge as an elevated feature that became subjected to erosion during the Triassic. Following this erosional episode, the basin transitioned to a period of tectonic quiescence, characterised by a hiatus in both erosion and sedimentation; this transition signalled the changeover from a marine to a continental environment by the Cretaceous.

During the Cretaceous, the Salta Rift Basin formed on the opposite side of the Quirquincho High, as part of extensional tectonism associated with the opening of the South Atlantic Ocean. early Cretaceous rifting led to normal faulting, followed by post-rift thermal subsidence in the late Cretaceous and Paleogene. During the Neogene, Andean shortening reached the Metán-Alemanía and Tres Cruces depocenters of the Salta Rift Basin, leading to structural inversion of the graben-bounding normal faults. Although limited inversion has occurred in the Lomas de Olmedo depocenter farther east, in the analysed sections in this study, it is concluded that this sub-basin of the Salta Rift was not inverted to the same degree as the other Cretaceous basins. This may be due to its distal location with respect of the Andean orogen and unfavorable fault orientations.

The lack of reactivation of the Quirquincho and Pampeano-Chaqueño highlands during the Andean orogeny raised the question of why the ancient foreland structures similar to those of the present Andes were not reactivated. The answer lies in the Salta Rift Basin, where normal faults focused much of the Andean strain, facilitating the development of thick-skinned tectonics that contributed to the formation of the Santa Bárbara broken foreland system. As a result, the tectonic style of flexural deformation and a contiguous foreland system that characterized the Ancestral Andes was not continued during Cenozoic Andean mountain building and a broken foreland evolved due to the overprint of changing geodynamic boundary conditions and the corresponding evolution of extensional provinces that were subsequently reactivated compressionally.

Nevertheless, the presence of both inherited basement highs influenced the long-term basin geometry and distribution of sediments. The Quirquincho High disrupted the continuity of the Paleozoic basin, separating the Tarija Basin in the northwest from the Chacoparanaense Basin in the southeast. This division led to different sedimentary depositional processes on each side during the Cretaceous. While the Chacoparanaense Basin continued to receive sediments at a relatively low rate, the Tarija Basin formed the basement for the Salta Rift Basin. The Pampeano-Chaqueño High further segmented the Cretaceous depocenters within the Chacoparanaense Basin and acted as a source area after its erosion during the early Mesozoic.

The Salta Rift Basin has been extensively explored for hydrocarbons and is currently being exploited primarily for gas. While there is extensive literature on the burial and thermal history of the Salta Rift, the Chacoparanaense Basin has remained less explored, with limited understanding of its sedimentary history. Through detailed seismic interpretation in Chapter 4, I was able to identify an important unconformity between the Permian and Cretaceous units, which was later confirmed as an erosional unconformity by basin modelling. This erosion, particularly towards the Quirquincho High, removed a significant part of the Permo–Triassic units during the Triassic, immediately following the uplift of the High.

The period of maximum burial coincides with a peak in heat flow associated with the Permo–Triassic thermal anomaly along the western margin of Gondwana, which increased basal heat flow in the Chacoparanaense Basin. Although other thermal events may have

occurred during the history of the basin, they did not significantly affect the maturation of potential source rocks.

The integrated assessment of thermal maturity, transformation ratio (TR) and total organic carbon (TOC) across stratigraphic units provides a comprehensive framework for evaluating hydrocarbon potential in what has historically been considered an unexplored frontier. The Carboniferous and upper stratigraphic units are thermally immature and unsuitable as source rocks, although they may serve as good reservoirs if sufficiently charged by hydrocarbons from deeper units. However, there are no known oil or gas accumulations in these units. The Devonian unit shows moderate maturity over much of the basin, with limited organic richness. As a result, only certain intervals may be of economic interest. In contrast, the Silurian unit shows the most promising characteristics, with thermal maturity (Ro > 2%), significant TOC values and thicknesses up to 1500 m in the north-western and eastern sectors. If the mineralogy is favourable (e.g., quartz-rich, brittle zones) and the structural conditions for stimulation are met, the Silurian may represent a viable target for shale gas exploration.

In conclusion, while the Chacoparanaense Basin is not a promising conventional reservoir, the Silurian strata deserve further exploration regarding their unconventional potential. Importantly, and with regard to the overall history of the buried basin the results of this study provide new insights into the buried structures, sedimentary and erosional processes as well as the tectonic history of the Chacopampean Plain, particularly the

Quirquincho High, suggesting that these inherited structures have significantly influenced the development of both the continuous and broken foreland styles.

References

Abu-Ali, M. A., Rudkiewicz, J. L. L., McGillivray, J. G., & Behar, F. (1999). Paleozoic petroleum system of central Saudi Arabia. GeoArabia, 4(3), 321-336.

Allen, P. A., & Allen, J. R. (2013). Basin Analysis: Principles and Applications to Petroleum Play Assessment (3rd ed.). Wiley-Blackwell.

Allmendinger, R. W., Isacks, B. L., Jordan, T.E. y Kay, S. M. (1997). The evolution of the Altiplano – Puna plateau of the Central Andes. Annual Reviews of Earth and Planetary Sciences, 25, 139–174.

Allmendinger, R. W., Ramos, V. A., Jordan, T. E., Palma, M., & Isacks, B. L. (1983). Paleogeography and Andean structural geometry, northwest Argentina. Tectonics, 2(1), 1-16.

Alvarado, P., Beck, S., & Zandt, G. (2007). Crustal structure of the south-central Andes Cordillera and backarc region from regional waveform modelling. Geophysical Journal International, 170(2), 858-875.

Ammirati, J. B., Mackaman-Lofland, C., Zeckra, M., & Gobron, K. (2022). Stress transmission along mid-crustal faults highlighted by the 2021 Mw 6.5 San Juan (Argentina) earthquake. Scientific Reports, 12(1), 17939.

Arnous, A. (2021). Paleosismología y neotectónica del antepaís fragmentado en el extremo sureste del Sistema Santa Bárbara, Noroeste Argentino (Doctoral dissertation, Dissertation, Potsdam, Universität Potsdam, 2021).

Arnous, A., Garc.a, V. H., Pingel, H., Giambiagi, L., & Strecker, M. R. (2024). Kinematic evolution of the Santa B.rbara System in the foreland of the Central Andes of northwestern Argentina (26ÅãS). Tectonics, 43, e2023TC008195. https://doi.org/10.1029/2023TC008195

Assumpção Assumpção, M., Feng, M., Tassara, A., & Julià, J. (2013). Models of crustal thickness for South America from seismic refraction, receiver functions and surface wave tomography. Tectonophysics, 609, 82-96.*et al.* (2013)

Axen, G. J., van Wijk, J. W., & Currie, C. A. (2018). Basal continental mantle lithosphere displaced by flat-slab subduction. Nature Geoscience, 11(12), 961-964.

Barazangi, M., & Isacks, B. L. (1976). Spatial distribution of earthquakes and subduction of the Nazca plate beneath South America. Geology, 4(11), 686-692.

Barcelona, H., Peri, G., Tobal, J., Sagripanti, L., & Favetto, A. (2014). Tectonic activity revealed by morphostructural analysis: Development of the Sierra de la Candelaria range, northwestern Argentina. Journal of South American Earth Sciences, 56, 376-395. https://doi.org/10.1016/j.jsames.2014.10.002

Barredo, S., & Stinco, L. (2014). Unconventional Reservoir Geology of the Neuquén Basin Argentina. In SPE Annual Technical Conference and Exhibition (pp. SPE-170905). SPE.

Becker, D. (1975). Stratigraphy report of the well YPF.CHA.CH-1 (Charata 1, Chaco, Argentina) YPF S.A. Unpublished report.

Bevis, M., & Isacks, B. L. (1984). Hypocentral trend surface analysis: Probing the geometry of Benioff zones. Journal of Geophysical Research: Solid Earth, 89(B7), 6153-6170.

Billi, A., & Salvini, F. (2003). Development of systematic joints in response to flexure-related fibre stress in flexed foreland plates: the Apulian forebulge case history, Italy. Journal of Geodynamics, 36(4), 523-536.

Bird, P. (1984). Laramide crustal thickening event in the Rocky Mountain foreland and Great Plains. Tectonics, 3(7), 741-758.

Bird, P. (1998). Kinematic history of the Laramide orogeny in latitudes 35–49 N, western United States. Tectonics, 17(5), 780-801.

Bishop, B. T., Beck, S. L., Zandt, G., Wagner, L. S., Long, M. D., & Tavera, H. (2018). Foreland uplift during flat subduction: Insights from the Peruvian Andes and Fitzcarrald Arch. Tectonophysics, 731, 73-84.

Bjorlykke, K. (2010). Petroleum geoscience: From sedimentary environments to rock physics. Springer Science & Business Media.

Blake Jr, M. C., Campbell, R. H., Dibblee Jr, T. W., Howell, D. G., Nilsen, T. H., Normark, W. R., Vedder, J. C. & Silver, E. A. (1978). Neogene basin formation in relation to plate-tectonic evolution of San Andreas fault system, California. AAPG Bulletin, 62(3), 344-372.

Blisniuk, P. M., Sonder, L. J., & Lillie, R. J. (1998). Foreland normal fault control on northwest Himalayan thrust front development. Tectonics, 17(5), 766-779.

Bookhagen, B., & Strecker, M. R. (2008). Orographic barriers, high-resolution TRMM rainfall, and relief variations along the eastern Andes. Geophysical Research Letters, 35(6).

Boone, S. C., Balestrieri, M. L., Kohn, B. P., Corti, G., Gleadow, A. J. W., & Seiler, C. (2019). Tectonothermal evolution of the Broadly Rifted Zone, Ethiopian Rift. Tectonics, 38(3), 1070–1100. https://doi.org/10.1029/2018TC005210

Bossi, G., & Palma, R.M. (1982). Reconsideración de la estratigrafía del valle de Santa María, provincia de Catamarca, Argentina.V Congr. Lationoamericano Geol., Buenos Aires, Argentina, 155–172.

Bottcher, G. (1965). Stratigraphy report of the well, YPF.SE.EC.x-1 (Santiago del Estero, Argentina). YPF S.A. Unpublished report.

Bottcher, G. (1974). Stratigraphy report of the well YPF.CHA.LB-1 (Chaco, Argentina). YPF S.A. Unpublished report.

Bradley, D. C., & Kidd, W. S. F. (1991). Flexural extension of the upper continental crust in collisional foredeeps. Geological Society of America Bulletin, 103(11), 1416-1438.

Bruhn, R. L., Picard, M. D., & Isby, J. S. (1986). Tectonics and sedimentology of Uinta arch, western Uinta Mountains, and Uinta Basin.

Bruhn, R. L., Picard, M. D., & Isby, J. S. (1986). Tectonics and sedimentology of Uinta arch, western Uinta Mountains, and Uinta Basin.

Burkhard, M., & Sommaruga, A. (1998). Evolution of the western Swiss Molasse basin: structural relations with the Alps and the Jura belt. Geological Society, London, Special Publications, 134(1), 279-298.

Cahill, T., & Isacks, B. L. (1992). Seismicity and shape of the subducted Nazca plate. Journal of Geophysical Research: Solid Earth, 97(B12), 17503-17529.

Campos, H., & Mann, P. (2015). Tectonostratigraphic evolution of the Northern Llanos Foreland Basin of Colombia and implications for its hydrocarbon potential.

Cardozo, N., & Jordan, T. (2001). Causes of spatially variable tectonic subsidence in the Miocene Bermejo Foreland Basin, Argentina. Basin Research, 13(3), 335-357.

Carlotto Caillaux, V. S. (2013). Paleogeographic and tectonic controls on the evolution of Cenozoic basins in the Altiplano and Western Cordillera of southern Peru.

Carrapa, B., Adelmann, D., Hilley, G., Mortimer, E., Strecker, M. R. & Sobel, E. R. (2005). Oligocene uplift, establishment of internal drainage and development of plateau morphology in the southern Central Andes. Tectonics, 24, TC4011.

Carrapa, B., Bywater-Reyes, S., DeCelles, P. G., Mortimer, E., & Gehrels, G. E. (2012). Late Eocene-Pliocene basin evolution in the Eastern Cordillera of northwestern Argentina(25 degree-26 degree S): regional implications for Andean orogenic wedge development. Basin Research, 24(3), 249-268.

Carrapa, B., Hauer, J., Schoenbohm, L., Strecker, M. R., Schmitt, A. K., Villanueva, A., & Sosa Gomez, J. (2009). Dynamics of deformation and sedimentation in the northern Sierras Pampeanas: An integrated study of the Neogene Fiambalá basin, NW Argentina. Geological Society of America Bulletin, 120(11-12), 1518-1543.

Carrera, N., & Muñoz, J. A. (2008). Thrusting evolution in the southern Cordillera Oriental (northern Argentine Andes): Constraints from growth strata. Tectonophysics, 459(1-4), 107-122.

Carrera, N., Muñoz, J. A., Sábat, F., Mon, R. & Roca, E. (2006). The role of inversion tectonics in the structure of the Cordillera Oriental (NW Argentinean Andes). Journal of Structural Geology, 28, 1921–1932.

Cediel, F., Shaw, R. P., & Cáceres, C. (2003). Tectonic assembly of the northern Andean Block. In Petroleum basins of South America (pp. 183-201). AAPG Memoir 62.

Charrier, R., Ramos, V. A., Tapia, F., & Sagripanti, L. (2015). Tectono-stratigraphic evolution of the Andean Orogen between 31 and 37 S (Chile and Western Argentina). Geological Society, London, Special Publications, 399(1), 13-61.

Chase, C. G., Sussman, A. J., & Coblentz, D. D. (2009). Curved Andes: Geoid, forebulge, and flexure. Lithosphere, 1(6), 358-363.

Chebli, G., Mozetic, M., Rossello, E., & Bühler, M. (1999). Cuencas sedimentarias de la llanura Chacopampeana. Geología Argentina anales, 29, 627-644.

Chernicoff, C. J., & Zappettini, E. O. (2004). Geophysical evidence for terrane boundaries in south-central Argentina. Gondwana research, 7(4), 1105-1116.

Chiang, C. S., Yu, H. S., & Chou, Y. W. (2004). Characteristics of the wedge-top depozone of the southern Taiwan foreland basin system. Basin Research, 16(1), 65-78.

Cloetingh, S. A. P. L., Burov, E., Matenco, L., Toussaint, G., Bertotti, G., Andriessen, P. A. M., ... & Spakman, W. (2004). Thermo-mechanical controls on the mode of continental collision in the SE Carpathians (Romania). Earth and Planetary Science Letters, 218(1-2), 57-76.

Coakley, B. J., & Watts, A. B. (1991). Tectonic controls on the development of unconformities: the North Slope, Alaska. Tectonics, 10(1), 101-130.

Cobbold, P.R., Rossello, E.A., Roperch, P., Arriagada, C., Gómez, L.A., Lima, C. (2007). Distribution, timing, and causes of Andean deformation across South America. In: Ries, A.C., Butler, R.W.H., Graham, R.H. (eds.), Deformation of the continental crust: The legacy of Mike Coward. Geological Society of London, Special Publications, 272, 321-343.

Collo, G., Ezpeleta, M., Dávila, F. M., Giménez, M., Soler, S., Martina, F., ... & Schiuma, M. (2018). Basin thermal structure in the Chilean-Pampean flat subduction zone. The evolution of the Chilean-argentinean Andes, 537-564.

Coney, P. J., & Reynolds, S. J. (1977). Cordilleran benioff zones. Nature, 270(5636), 403-406.

Constenius, K. N. (1996). Late Paleogene extensional collapse of the Cordilleran foreland fold and thrust belt. Geological Society of America Bulletin, 108(1), 20-39.

Cordani, U. G., & Sato, K. (1999). Crustal evolution of the South American Platform, based on Nd isotopic systematics on granitoid rocks. Episodes Journal of International Geoscience, 22(3), 167-173.

Cordani, U. G., Pimentel, M. M., De Araújo, C. E. G., Basei, M. A. S., Fuck, R. A., & Girardi, V. A. V. (2013). Was there an Ediacaran Clymene ocean in central South America?. American Journal of Science, 313(6), 517-539.

Coutand, I., Cobbold, P. R., de Urreiztieta, M., Gautier, P., Chauvin, A., Gapais, D., Rossello, E.A. & López-Gamundí, O. (2001). Style and history of Andean deformation, Puna plateau, northwestern Argentina. Tectonics, 20(2), 210-234.

Crampton, S. L., & Allen, P. A. (1995). Recognition of forebulge unconformities associated with early stage foreland basin development: example from the North Alpine Foreland Basin. AAPG bulletin, 79(10), 1495-1514.

Cuong, T. X., & Warren, J. K. (2009). Bach ho field, a fractured granitic basement reservoir, Cuu Long Basin, offshore SE Vietnam: A “buried-hill” play. Journal of Petroleum Geology, 32(2), 129-156.

Dávila, F. M., & Carter, A. (2013). Exhumation history of the Andean broken foreland revisited. Geology, 41(4), 443-446.

de Almeida, F. F. M., de Brito Neves, B. B., & Carneiro, C. D. R. (2000). The origin and evolution of the South American Platform. Earth-Science Reviews, 50(1-2), 77-111.

de Alteriis, G. (1995). Different foreland basins in Italy: examples from the central and southern Adriatic Sea. Tectonophysics, 252(1-4), 349-373.

DeCelles, P. G. (2004). Late Jurassic to Eocene evolution of the Cordilleran thrust belt and foreland basin system, western USA. American Journal of Science, 304(2), 105-168.

DeCelles, P. G., & Giles, K. A. (1996). Foreland basin systems. Basin research, 8(2), 105-123.

DeCelles, P., Carrapa, B., Horton, B., & Gehrels, G. (2011). Cenozoic foreland basin system in the central Andes of northwestern Argentina: Implications for Andean geodynamics and modes of deformation. Tectonics 30: 6, 2011.

DeCelles, P.G. & DeCelles P.C.(2001) Rates of shortening, propagation, underthrusting, and flexural wave migration in continental orogenic systems. Geology; 29 (2): 135–138

DeCelles, P.G. (2011). Foreland basin systems revisited: Variations in response to tectonic settings. Busby, C., & Pérez, A. A. (Eds.). (2011). Tectonics of sedimentary basins: recent advances. Wiley-Blackwell, 405-426.

del Papa, C., Babot, J., Dahlquist, J., López, D.G., Deraco, V., Herrera, C., Bertelli, S., Rougier, G.W., Giannini, N.P. (2022). Toward a chronostratigraphy of the Paleocene-Eocene sedimentary record in northwestern Argentina. Journal of South American Earth Sciences, 113, 103677. ISSN 0895-9811, https://doi.org/10.1016/j.jsames.2021.103677.

Del Papa, C., Hongn, F., Powell, J., Payrola, P., Do Campo, M., Strecker, M. R., ... & Pereyra, R. (2013). Middle Eocene-Oligocene broken-foreland evolution in the Andean Calchaqui Valley, NW Argentina: insights from stratigraphic, structural and provenance studies. Basin Research, 25(5), 574-593.

Del Papa, C., Kirschbaum, A., Powell, J., Brodd, A., Hongn, F. & Pimentel, M. (2010). Sedimentological, geochemical and paleontological insights applied to continental omission surfaces: A new approach for reconstructing an eocene foreland basin in NW Argentina. Journal of South American Earth Sciences, Volume 29 (2), 327-345.

Demko, T. M., Currie, B. S., & Nicoll, K. A. (2004). Regional paleoclimatic and stratigraphic implications of paleosols and fluvial/overbank architecture in the Morrison Formation (Upper Jurassic), Western Interior, USA. Sedimentary Geology, 167(3-4), 115-135.

Di Persia, C.A. (1969). Stratigraphy report of the well YPF.SE.CR.x-1 (Santiago del Estero, Argentina). YPF S.A. Unpublished report.

Di Persia, C.A. (1970). Stratigraphy report of the well YPF.SE.LH.x-1 (Santiago del Estero, Argentina). YPF S.A. Unpublished report

Dickinson, W. R. (1974). Tectonics and sedimentation. SEPM Society for Sedimentary Geology.

Dickinson, W. R. (1979). Mesozoic forearc basin in central Oregon. Geology, 7(4), 166-170.

Dickinson, W. R. (2004). Evolution of the North American cordillera. Annu. Rev. Earth Planet. Sci., 32(1), 13-45.

Dickinson, W. R., & Snyder, W. S. (1978). Plate tectonics of the Laramide orogeny. Geological Society of America Memoirs, 151, 355-366.

Doglioni, C., Merlini, S., & Cantarella, G. (1999). Foredeep geometries at the front of the Apennines in the Ionian Sea (central Mediterranean). Earth and Planetary Science Letters, 168(3-4), 243-254.

Eakin, C. M., Lithgow-Bertelloni, C., & Dávila, F. M. (2014). Influence of Peruvian flat-subduction dynamics on the evolution of western Amazonia. Earth and Planetary Science Letters, 404, 250-260.

El Sharawy, M. (2015). Fractured basement reservoir identification using geophysical well log data, Gulf of Suez, Egypt. Pelagia Research. Adv Appl Sci Res, 6(8), 17-35.

Erbello, A., Colleps, C., Melnick, D., Sobel, E. R., Bookhagen, B., Pingel, H., *et al.* (2023). Magma-assisted continental rifting: The Broadly Rifted Zone in SW Ethiopia, East Africa. Tectonics, 42, e2022TC007651. https://doi.org/10.1029/2022TC007651

Escalona, A., & Mann, P. (2006). An overview of the petroleum system of Maracaibo Basin. AAPG bulletin, 90(4), 657-678.

Falconier, J. D. (1931). Terrenos Gondwánicos del departamento Tacuarembó. Memoria explicativa del mapa geológico, Vol. 15. Instituto Geológico del Uruguay, Montevideo.

Fernández Garrasino, C., Laffitte, G., Villar, H. (2005). Cuenca Chacoparanaense. 6° Congreso de Exploración y Desarrollo de Hidrocarburos, Frontera Exploratoria de la Argentina (Mar del Plata, Argentina), Proceedings (pp. 97-114).

Figueroa, S., Weiss, J. R., Hongn, F., Pingel, H., Escalante, L., Elías, L., ... & Strecker, M. R. (2021). Late Pleistocene to recent deformation in the thick-skinned fold-and-thrust belt of northwestern Argentina (central Calchaquí Valley, 26 S). Tectonics, 40(1), e2020TC006394. https://doi.org/10.1029/2020TC006394

Flemings, P. B., & Jordan, T. E. (1989). A synthetic stratigraphic model of foreland basin development. Journal of Geophysical Research: Solid Earth, 94(B4), 3851-3866.

Ford, M., Williams, E. A., Artoni, A., Vergés, J., & Hardy, S. (1997). Progressive evolution of a fault-related fold pair from growth strata geometries, Sant Llorenç de Morunys, SE Pyrenees. Journal of structural Geology, 19(3-4), 413-441.

Foster, D. A., and A. J. W. Gleadow (1996), Structural framework and denudation history of the flanks of the Kenya and Anza Rifts, East Africa,Tectonics, 15(2), 258–271, doi:10.1029/95TC02744.

Frakes, L. A. (1979). Climates throughout Geologic Time. Elsevier, Amsterdam.

Fuentes, R., Sempere, T., Aguado, R., Baudino, R., & Vega, L. (2009). Tarija Basin, Southern Bolivia: A lacustrine basin in a magmatic arc setting. In Sedimentary basins of South America (pp. 395-414). Springer, Berlin, Heidelberg.

Gallagher, T. M., & Lamadrid, H. M. (2015). An in situ shelly fauna from the lower Paleozoic Zapla diamictite of northwestern Argentina: Implications for the depositional environment and age of the Zapla diamictite. Journal of South American Earth Sciences, 64, 1–10. ScienceDirect

Galliski, M. A., and J. G. Viramonte (1988), The Cretaceous paleorift in northwestern Argentina: A petrologic approach, Journal of South American Earth Sciences, 1(4), 329-342, doi:https://doi.org/10.1016/0895-9811(88)90021-1

Garcia Bautista, D. F., Vaz dos Santos Neto, E., & Penteado, H. L. D. B. (2015). Controls on petroleum composition in the Llanos basin, Colombia: Implications for exploration. AAPG bulletin, 99(8), 1503-1535.

Garcia, V. H., Hongn, F., Yagupsky, D., Pingel, H., Kinnaird, T., Winocur, D., *et al.* (2019). Late Quaternary tectonics controlled by fault reactivation. Insights from a local transpressional system in the intermontane Lerma valley, Cordillera Oriental, NW Argentina. Journal of Structural Geology, 128, 103875. https://doi.org/10.1016/j.jsg.2019.103875

Garcia-Castellanos, D., & Cloetingh, S. (2011). Modeling the interaction between lithospheric and surface processes in foreland basins. Tectonics of sedimentary basins: Recent advances, 152-181.

Garcia-Castellanos, D., Fernandez, M., & Torné, M. (2002). Modeling the evolution of the Guadalquivir foreland basin (southern Spain). Tectonics, 21(3), 9-1.

Gianni, G. M., García, H. P., Pesce, A., Lupari, M., González, M., & Giambiagi, L. (2020). Oligocene to present shallow subduction beneath the southern Puna plateau. Tectonophysics, 780, 228402.

Grier, M.E., Salfity, J.A, y Allmendinger, R.W. (1991). Andean reactivation of the Cretaceous Salta rift, northwestern Argentina. Journal of South American Earth Sciences, 4: 351-372.

Grujic, D., Coutand, I., Bookhagen, B., Bonnet, S., Blythe, A., & Duncan, C. (2006). Climatic forcing of erosion, landscape, and tectonics in the Bhutan Himalayas. Geology, 34(10), 801-804.

Gupta, S., & Allen, P. A. (2000). Implications of foreland paleotopography for stratigraphic development in the Eocene distal Alpine foreland basin. Geological Society of America Bulletin, 112(4), 515-530.

Gutscher, M. A., Spakman, W., Bijwaard, H., & Engdahl, E. R. (2000). Geodynamics of flat subduction: Seismicity and tomographic constraints from the Andean margin. Tectonics, 19(5), 814-833.

Hain, M. P., Strecker, M. R., Bookhagen, B., Alonso, R. N., Pingel, H., & Schmitt, A. K. (2011). Neogene to Quaternary broken foreland formation and sedimentation dynamics in the Andes of NW Argentina (25 S). Tectonics, 30(2).

Hantschel, T., & Kauerauf, A. I. (2009). Fundamentals of basin and petroleum systems modeling. Springer Science & Business Media.

Heredia, N., García-Sansegundo, J., Farias Arquer, P.J., Alonso Alonso, J.L., Gallastegui Suárez, J., Méndez Bedia, M.I., Rubio Ordóñez, Á. (2016). Evolución Geodinámica de los Andes argentinochilenos y la Península Antártica durante el Neoproterozoico tardío y el Paleozoico. Trabajos de Geología, 36.

Heredia, N., García-Sansegundo, J., Gallastegui, G., Farias, P., Giacosa, R., Hongn, F., Ramos, V.A. (2018). The pre-andean phases of construction of the southern Andes basement in neoproterozoic–paleozoic times. Folguera, A. *et al.* (ed.). The Evolution of the Chilean-Argentinean Andes. Springer, 111-131.

Heuret, A., & Lallemand, S. (2005). Plate motions, slab dynamics and back-arc deformation. Physics of the Earth and Planetary Interiors, 149(1-2), 31-51.

Hilley, G. E., & Strecker, M. R. (2005). Processes of oscillatory basin filling and excavation in a tectonically active orogen: Quebrada del Toro Basin, NW Argentina. Geological Society of America Bulletin, 117(7-8), 887-901.

Hilley, G.E., Blisniuk, P.M. and Strecker, M.R. (2005). Mechanics and erosion of basement-cored uplift provinces. J. Geophys. Res., 110 B12409, doi: 10.1029/2005JB003704.

Hindle, D., & Kley, J. (2021). The Subhercynian Basin: an example of an intraplate foreland basin due to a broken plate. Solid Earth, 12(10), 2425-2438.

Hongn, F. D., Heit, B., & Caffe, P. J. (2005). Tectono-stratigraphic evolution of the Salta Rift Basin (NW Argentina): Implications for the Andean foreland deformation. Tectonophysics, 399(1-4), 221-250.

Hongn, F., Mon, R., Petrinovic, I., Del Papa, C., & Powell, J. (2010). Inversion y reactivacion tectonicas cretacicocenozoicas en el Noroeste Argentino: influencia de las heterogeneidades del basamento neoproterozoico-paleozoico inferior. Revista de la Asociacion Geologica Argentina, 66(1–2), 38–53. https://revista.geologica.org.ar/raga/article/view/841

Horton, B. (2018). Tectonic regimes of the Central and Southern Andes: Responses to variations in plate coupling during subduction. Tectonics, 37(2), 402–429. https://doi.org/10.1002/2017tc004624

Horton, B. K., Capaldi, T. N., Mackaman-Lofland, C., Perez, N. D., Bush, M. A., Fuentes, F., & Constenius, K. N. (2022). Broken foreland basins and the influence of subduction dynamics, tectonic inheritance, and mechanical triggers. Earth-Science Reviews, 234, 104193.

Horton, B.K. (2018). Tectonic regimes of the central and southern Andes: Responses to variations in plate coupling during subduction. Tectonics, 37, 402-429.

Horton, B.K., DeCelles, P.G. (1997). The modern foreland basin system adjacent to the Central Andes. Geology, 25, 895-898.

Horton, B.K., Folguera, A. (2022). Tectonic inheritance and structural styles in the Andean fold-thrust belt and foreland basin. In Zamora, G., & Mora, A. (Eds.). Andean Structural Styles (pp. 3-28). Elsevier.

Howell, J. A., Schwarz, E., Spalletti, L. A., & Veiga, G. D. (2005). The Neuquén basin: an overview. Geological Society, London, Special Publications, 252(1), 1-14.

Hunt, J. M. (1996). Petroleum geochemistry and geology (2nd ed.). W. H. Freeman.American Chemical Society Publications

Iaffa, D. N., Sábat, F., Muñoz, J. A., Mon, R. y Gutierrez, A. A. (2011). The role of inherited structures in a foreland basin evolution. The Metán Basin in northwest Argentina. Journal of Structural Geology, 33, 1816–1828. https://doi.org/10.1016/j.jsames.2014.10.002

Ibarra, F., Prezzi, C. B., Bott, J., Scheck-Wenderoth, M., & Strecker, M. R. (2021). Distribution of temperature and strength in the Central Andean lithosphere and its relationship to seismicity and active deformation. Journal of Geophysical Research: Solid Earth, 126(5), e2020JB021231.

Jarvie, D. M. (2012). Shale resource systems for oil and gas: Part 1—Shale-gas resource systems. In J. A. Breyer (Ed.), Shale reservoirs—Giant resources for the 21st century (AAPG Memoir 97, pp. 69–87). American Association of Petroleum Geologists.ResearchGate

Jarvie, D. M., Hill, R. J., Ruble, T. E., & Pollastro, R. M. (2007). Unconventional shale-gas systems: The Mississippian Barnett Shale of north-central Texas as one model for thermogenic shale-gas assessment. AAPG Bulletin, 91(4), 475–499.

Jenkins, C. D., Pepper, A. S., & Corvi, P. J. (1997). Quantitative modeling of petroleum generation and expulsion. Marine and Petroleum Geology, 14(6), 731–748.

Jordan, T. E. (1981). Thrust loads and foreland basin evolution, Cretaceous, western United States. AAPG bulletin, 65(12), 2506-2520.

Jordan, T. E., & Allmendinger, R. W. (1986). The Sierras Pampeanas of Argentina; a modern analogue of Rocky Mountain foreland deformation. American Journal of Science, 286(10), 737-764.

Jordán, T. E., Isacks, B. L., Allmendinger, R. W., Brewer, J. A., Ramos, V. A., & Ando, C. J. (1983). Andean tectonics related to geometry of subducted Nazca plate. Geological Society of America Bulletin, 94(3), 341-361.

Kay, S. M., Mpodozis, C., Ramos, V. A., & Munizaga, F. (1989). Late Paleozoic to early Mesozoic evolution of the Gondwana margin: Evidence from Chilean and Argentine geology. Tectonophysics, 161(1–2), 1–17.

Kay, S. M., Ramos, V. A., Mpodozis, C., & Sruoga, P. (1989). Late Paleozoic to Jurassic silicic magmatism at the Gondwana margin: Analogy to the Middle Proterozoic in North America?. Geology, 17(4), 324-328.

Kley, J., & Monaldi, C. R. (2002). Tectonic inversion in the Santa Barbara System of the central Andean foreland thrust belt, northwestern Argentina. Tectonics, 21(6), 1061. https://doi.org/10.1029/2002TC902003

Kley, J., Monaldi, C. R., & Salfity, J. A. (1999). Along-strike segmentation of the Andean foreland: Causes and consequences. Tectonophysics, 301(1–2), 75–94. https://doi.org/10.1016/S0040-1951(98)90223-2

Kley, J., Rossello, E. A., Monaldi, C. R., & Habighorst, B. (2005). Seismic and field evidence for selective inversion of Cretaceous normal faults, Salta rift, northwest Argentina. Tectonophysics, 399(1–4), 155–172. https://doi.org/10.1016/j.tecto.2004.12.020

Knowlton, K. B. (1991). Informe final de Pozo PP.CC.PB.x-1001 (Pampa Bandera, Chaco, Argentina). Unpublished report for Pluspetrol S.A.

Lacombe, O., & Bellahsen, N. (2016). Thick-skinned tectonics and basement-involved fold–thrust belts: insights from selected Cenozoic orogens. Geological Magazine, 153(5-6), 763-810.

Lash, G. G., & Engelder, T. (2007). Jointing within the outer arc of a forebulge at the onset of the Alleghanian Orogeny. Journal of Structural Geology, 29(5), 774-786.

Lash, G. G., & Engelder, T. (2007). Jointing within the outer arc of a forebulge at the onset of the Alleghanian Orogeny. Journal of Structural Geology, 29(5), 774-786.

Limarino, C. O., Heredia, N., Spalletti, L. A., Busquets, P., Colombo, F., Méndez-Bedia, I. & Césari, S. N. (2023). Stratigraphy and tectosedimentary evolution of the late Paleozoic Ancestral Andes between 33° and 25° SL. Journal of South American Earth Sciences, 121, 104116.

Liu, L., Spasojevic, S., & Gurnis, M. (2008). Reconstructing Farallon plate subduction beneath North America back to the Late Cretaceous. Science, 322(5903), 934-938.

Londoño, J., & Lorenzo, J. M. (2004). Geodynamics of continental plate collision during late tertiary foreland basin evolution in the Timor Sea: constraints from foreland sequences, elastic flexure and normal faulting. Tectonophysics, 392(1-4), 37-54.

Loucks, R. G., & Ruppel, S. C. (2007). Mississippian Barnett Shale: Lithofacies and depositional setting of a deep-water shale-gas succession in the Fort Worth Basin, Texas. AAPG Bulletin, 91(4), 579–601. https://doi.org/10.1306/11020606059

Lüning, S., Craig, J., Loydell, D. K., Århus, N., & Strogen, D. (2000). Lower Silurian 'hot shales' in North Africa and Arabia: Regional distribution and depositional model. Earth-Science Reviews, 49(1–4), 121–200.

Macellari, C. E. (2025). Present-day Foreland Development and its relation to Plate Tectonics in the Northern Andes. Journal of South American Earth Sciences, 105465. https://doi.org/10.1016/j.jsames.2025.105465

Mann, P., Escalona, A., & Castillo, M. V. (2006). Regional geologic and tectonic setting of the Maracaibo supergiant basin, western Venezuela. AAPG bulletin, 90(4), 445-477.

Marengo, H. (2015). Neogene micropaleontology and stratigraphy of Argentina: the Chaco-Paranense Basin and the Península de Valdés.

Marquillas, R. A., Del Papa, C., & Sabino, I. F. (2005). Sedimentary aspects and paleoenvironmental evolution of a rift basin: Salta Group (Cretaceous–Paleogene), northwestern Argentina. International Journal of Earth Sciences, 94, 94-113.

Marrett, R., Strecker, M.R., 2000. Response of intracontinental deformation in the central Andes to late Cenozoic reorganization of South American Plate motions. Tectonics 19, 452–467.

Marshak, S., Karlstrom, K., & Timmons, J. M. (2000). Inversion of Proterozoic extensional faults: An explanation for the pattern of Laramide and Ancestral Rockies intracratonic deformation, United States. Geology, 28(8), 735–738. https://doi.org/10.1130/0091-7613(2000)28<735: IOPEFA>2.0.CO;2

Martín-González, F., Freudenthal, M., Heredia, N., Martín-Suárez, E., & Rodríguez-Fernández, R. (2014). Palaeontological age and correlations of the Tertiary deposits of the NW Iberian Peninsula: the tectonic evolution of a broken foreland basin. Geological Journal, 49(1), 15-27.

Martinod, J., Husson, L., Roperch, P., Guillaume, B., & Espurt, N. (2010). Horizontal subduction zones, convergence velocity and the building of the Andes. Earth and Planetary Science Letters, 299(3-4), 299-309.

Mathalone, J.M.P., Montoya, M. 1995. Petroleum geology of the sub-Andean basins of Peru. In: Tankard, A., Suárez Soruco, R., Welsink, H.J. (eds.), Petroleum basins of South America, AAPG, Memoir 62: 423-444

Meeßen, C., Sippel, J., Scheck-Wenderoth, M., Heine, C., & Strecker, M. R. (2018). Crustal Structure of the Andean foreland in Northern Argentina: Results from data-integrative three-dimensional density modeling. Journal of Geophysical Research: Solid Earth, 123(2), 1875-1903.

Merewether, E. A., & Cobban, W. A. (1986). Biostratigraphic units and tectonism in the mid-Cretaceous foreland of Wyoming, Colorado, and adjoining areas.

Merewether, E. A., & Cobban, W. A. (1986). Biostratigraphic units and tectonism in the mid-Cretaceous foreland of Wyoming, Colorado, and adjoining areas.

Meyers, J. H., Suttner, L. J., Furer, L. C., May, M. T., & Soreghan, M. J. (1992). Intrabasinal tectonic control on fluvial sandstone bodies in the Cloverly Formation (early Cretaceous), west-central Wyoming, USA. Basin Research, 4(3-4), 315-335.

Miller, J. F., & Mitra, S. (2011). Deformation and secondary faulting associated with basement-involved compressional and extensional structures. AAPG bulletin, 95(4), 675-689.

Mingramm, A. & Russo, A. (1972). Sierras Subandinas y Chaco Salteño en A. Leanza (Dir. y Ed.): Geología Regional Argentina. 185-211. Academia Nacional de Ciencias, Córdoba.

Mingramm, A. (1965). Abandono del pozo estratigráfico FP-1 (Pirané, Formosa). Unpublished report for Yacimientos Petroliferos fiscales, YPF S.A.

Mingramm, A. (1966a). Abandono del pozo estratigráfico SE.EC.x-1 (El Caburé, Santiago del Estero). Unpublished report for Yacimientos Petroliferos fiscales, YPF S.A.

Mingramm, A. (1966b). Terminación del pozo estratigráfico SE.AB.x-1 (Arbol Blanco, Santiago del Estero). Unpublished report for Yacimientos Petroliferos fiscales, YPF S.A.

Mira, A., Veroslavsky, G., Rossello, E., Vives, L., & Rodríguez, L. (2015). Subsurface geological modeling of Corrientes province (NE Argentina) and its relationships with the Guaraní Aquifer system function. Journal of South American Earth Sciences, 62, 148-163.

Molnar, P., England, P., & Martinod, J. (1993). Mantle dynamics, uplift of the Tibetan Plateau, and the Indian monsoon. Reviews of Geophysics, 31(4), 357-396.

Mon, R. (1979). Esquéma estructural del Noroeste Argentino. Rev. Asoc. Geol. Arg, 35, 53-60.

Mon, R. and Salfity, J.A. (1995) Tectonic evolution of the Andes of northern Argentina, in Tankard, A. J., Suarez Soruco, R., Welsink, H.J., (eds) Petroleum basins of South America. Am. Assoc. Petrol. Geol. Memoir, 62, 269–83.

Montero-López, C., del Papa, C., Hongn, F., Strecker, M.R., Aramayo, A. (2018). Synsedimentary broken-foreland tectonics during the Paleogene in the Andes of NW Argentine: new evidence from regional to centimetre-scale deformation features. Basin Research, 30, 142-159.

Mora, A., Baby, P., Roddaz, M., Parra, M., Brusset, S., Hermoza, W., Espurt, N. (2010). Tectonic history of the Andes and sub-Andean zones: implications for the development of the Amazon

drainage basin. In: Hoorn, C., Wesselingh, F. (eds.), Amazonia, landscape and species evolution: a look into the past, 38-60. Blackwell Publishing, Chichester, UK.

Moreno, J.A. (1970). Estratigrafía y paleogeografía del Cretácico superior en la cuenca del noroeste argentino, con especial mención de los Subgrupos Balbuena y Santa Bárbara. Asociación Geológica Argentina, Revista 24: 9-44.

Moreno, J.A. (1973). Stratigraphy report of the well YPF.SE.LH.x-2 (Santiago del Estero, Argentina). YPF S.A. Unpublished report.

Mutti, M., Vallati, M., Tomás, S., Galli, C., Rumbelsperger, A. M. B., Maerz, S., & Coira, B. (2023). Constraining depositional evolution and reservoir compartmentalization in a mixed carbonate-siliciclastic lacustrine system: The Yacoraite formation, Salta Group, NW Argentina. Marine and Petroleum Geology, 149, 106049.

Oliver, J. (1986). Fluids expelled tectonically from orogenic belts: their role in hydrocarbon migration and other geologic phenomena. Geology, 14(2), 99-102.

Olsen, H., Briedis, N. A., & Renshaw, D. (2017). Sedimentological analysis and reservoir characterization of a multi-darcy, billion barrel oil field–The Upper Jurassic shallow marine sandstones of the Johan Sverdrup field, North Sea, Norway. Marine and Petroleum Geology, 84, 102-134.

Oncken, O., Hindle, D., Kley, J., Elger, K., Victor, P., & Schemmann, K. (2006). Deformation of the central Andean upper plate system—Facts, fiction, and constraints for plateau models. The Andes: Active Subduction Orogeny, 3-27.

Padula, E., & Mingramm, A. (1968). Estratigrafía, distribución y cuadro geotectónico-sedimentario del “Triásico” en el subsuelo de la llanura Chaco-Paranense. Tercera Jornada de Geología Argentina, Buenos Aires, 1, 191-231.

Padula, E., Rolleri, E., Mingramm, A., Criado Roque, P., Flores, M. & Baldis, B. (1967). Devonian of Argentina. International Symposium on the Devonian System. 2: 165-199. Calgary.

Peacock, D. C., & Banks, G. J. (2020). Basement highs: Definitions, characterisation and origins. Basin Research, 32(6), 1685-1710.

Pepper, A. S., & Corvi, P. J. (1995). Simple kinetic models of petroleum formation. Part I: Oil and gas generation from kerogen. Marine and Petroleum Geology, 12(3), 291–319.

Peri, V. G. (2012). Caracterización morfotectónica de las Lomadas de Otumpa (Gran Chaco, Santiago del Estero y Chaco): influencias en el control del drenaje (Doctoral dissertation, Universidad de Buenos Aires. Facultad de Ciencias Exactas y Naturales).

Peri, V. G., Barcelona, H., Pomposiello, M. C., & Favetto, A. (2015). Magnetotelluric characterization through the Ambargasta-Sumampa Range: The connection between the northern and southern trace of the Río de La Plata Craton–Pampean Terrane tectonic boundary. Journal of South American Earth Sciences, 59, 1-12.

Peri, V. G., Pomposiello, M. C., Favetto, A., Barcelona, H., & Rossello, E. A. (2013). Magnetotelluric evidence of the tectonic boundary between the Río de La Plata Craton and the Pampean terrane (Chaco-Pampean Plain, Argentina): The extension of the Transbrasiliano Lineament. Tectonophysics, 608, 685-699.

Perri, F., Barreda, V., & López-Ruiz, V. (2018). The Miocene Yacoraite Formation (Salta Group) in northwestern Argentina: Lithostratigraphy, age, and depositional environments. Journal of South American Earth Sciences, 88, 164-181.

Peters, K. E., Walters, C. C., & Moldowan, J. M. (2005). The biomarker guide: Volume 1, Biomarkers and isotopes in the environment and human history; Volume 2, Biomarkers and isotopes in petroleum systems and Earth history (2nd ed.). Cambridge University Press.

Pluspetrol S.A. (1990). Stratigraphy report of the well Pluspetrol.SE.Ch-x1001 (Santiago del Estero, Argentina). Pluspetrol S.A. Unpublished report.

Poelchau, H. S., Baker, D. R., Hantschel, T., Horsfield, B., & Wygrala, B. (1997). Basin simulation and the design of the conceptual basin model. Petroleum and basin evolution: Insights from petroleum geochemistry, geology and basin modeling, 3-70.

Poma, S., Rocher, S., & Sato, A. M. (2014). Geochronology and geochemistry of Permian-Triassic volcanic rocks in the Frontal Cordillera, Argentina: Implications for the Choiyoi magmatism. Journal of South American Earth Sciences, 55, 1–15.

Poma, S., Zappettini, E. O., Quenardelle, S., Santos, J. O., Koukharsky, M., Belousova, E., & McNaughton, N. (2014). Geochemistry, U-Pb SHRIMP zircon dating and Hf isotopes of the Gondwanan magmatism in NW Argentina: petrogenesis and geodynamic implications. Andean Geology, 41(2), 267-292.

Pons, M., Rodriguez Piceda, C., Sobolev, S. V., Scheck-Wenderoth, M., & Strecker, M. R. (2023). Localization of deformation in a non-collisional subduction orogen: The roles of dip geometry and plate strength on the evolution of the broken Andean foreland, Sierras Pampeanas, Argentina. Tectonics, 42(8), e2023TC007765. https://doi.org/10.1029/2023TC007765

Portner, D. E., Rodríguez, E. E., Beck, S., Zandt, G., Scire, A., Rocha, M. P., ... & Alvarado, P. (2020). Detailed structure of the subducted Nazca slab into the lower mantle derived from continent-scale teleseismic P wave tomography. Journal of Geophysical Research: Solid Earth, 125(5), e2019JB017884.

Price, R. A. (1973) Large-scale gravitational flow of supracrustal rocks, southern Canadian Rockies. In Gravity and tectonics, K.A. deJong, R. Scholten (Eds.), Wiley, New York, pp. 491-502

Quattrocchio, M., Durango de Cabrera, J., & Galli, C. (2003). Formación Anta (Mioceno Temprano/Medio), Subgrupo Metán (Grupo Orán), en el río Piedras, Pcia. de Salta: Datos palinológicos. Revista de la Asociación Geológica Argentina, 58(1), 117-127.

Ramos, V. A. (1988). Late Proterozoic-early Paleozoic of South America-a collisional history. Episodes Journal of International Geoscience, 11(3), 168-174.

Ramos, V. A. (2009). Anatomy and global context of the Andes: Main geologic features and the Andean orogenic cycle. Memoir of the Geological Society of America, 204, 31-65.

Ramos, V. A., & Folguera, A. (2009). Andean flat-slab subduction through time. Geological Society - Special Publications, 327(1), 31–54. https://doi.org/10.1144/SP327.3

Ramos, V. A., Alonso, R. N., & Strecker, M. (2006). Estructura y neotectónica de Las Lomas de Olmedo, zona de transición entre los Sistemas Subandino y de Santa Bárbara, provincia de Salta. Revista de la Asociación Geológica Argentina, 61(4), 579-588. Retrieved from https://revista.geologica.org.ar/raga/article/view/1357

Ramos, V. A., Cristallini, E. O., & Pérez, D. J. (2002). The Pampean flat-slab of the Central Andes. Journal of South American Earth Sciences, 15(1), 59–78. https://doi.org/10.1016/s0895-9811(02)00006-8

Ramos, V. A., Vujovich, G., Martino, R., & Otamendi, J. (2010). Pampia: a large cratonic block missing in the Rodinia supercontinent. Journal of Geodynamics, 50(3-4), 243-255.

Ramos, V.A. (1999). Rasgos estructurales del territorio argentino. Geología Argentina, 29, 15-75.

Ramos, V.A. (2010). The tectonic regime along the Andes: Present-day and Mesozoic regimes. Geological Journal, 45, 2-25.

Ramos, V.A., Aleman, A. (2000) Tectonic evolution of the Andes. In: Cordani, U.G., Milani, E.J., Thomaz Filho, A., Campos DA (eds.), Tectonic Evolution of South America. 31° International Geological Congress (Rio de Janeiro), 635-685.

Rapela, C.W., Pankhurst, R.J., Casquet, C., Fanning, C.M., Baldo, E.G., González-Casado, J.M., Galindo C., Dahlquist, J. (2007). The Río de la Plata craton and the assembly of SW Gondwana. Earth-Science Reviews, 83(1-2), 49-82.

Reinante, S., Olivieri, G., Salinas, A., Lovecchio, J. P., & Basile, Y. (2014). La cuenca Chacoparaná: estratigrafía y recursos de hidrocarburos. XIX Congreso Geológico Argentino. Córdoba, Argentina (pp. 895-912).

Reis, H. L., Suss, J. F., Fonseca, R. C., & Alkmim, F. F. (2017). Ediacaran forebulge grabens of the southern São Francisco basin, SE Brazil: Craton interior dynamics during West Gondwana assembly. Precambrian Research, 302, 150-170.

Repasch, M., Scheingross, J. S., Hovius, N., Lupker, M., Wittmann, H., Haghipour, N., Gröcke, D.R., Orfeo, O., Eglinton, T. I. & Sachse, D. (2021). Fluvial organic carbon cycling regulated by sediment transit time and mineral protection. Nature Geoscience, 14(11), 842-848.

Reyes, F. C., & Salfity, J. A. (1973). Consideraciones sobre la estratigrafía del Cretácico (Subgrupo Pirgua) del noroeste argentino. In V Congreso Geológico Argentino (Vol. 3, pp. 355-385). Buenos Aires, Argentina: Asociación Geológica Argentina, Actas III.

Reynolds, J. H., Galli, C. I., Hernández, R. M., Idleman, B. D., Kotila, J. M., Hilliard, R. V., & Naeser, C. W. (2000). Middle Miocene tectonic development of the transition zone, Salta Province, northwest Argentina: Magnetic stratigraphy from the Metan Subgroup, Sierra de Gonzalez. Geological Society of America Bulletin, 112(11), 1736-1751.

Riber, L., Dypvik, H., & Sørlie, R. (2015). Altered basement rocks on the Utsira High and its surroundings, Norwegian North Sea. Norwegian Journal of Geology, 95(1), 57-89.

Riel, N., Jaillard, E., Martelat, J. E., Guillot, S., & Braun, J. (2018). Permian-Triassic Tethyan realm reorganization: Implications for the outward Pangea margin. Journal of South American Earth Sciences, 81, 78-86.

Rocha-Campos, A. C., Basei, M. A. S., Nutman, A. P., Santos, J. O. S., & Passarelli, C. R. (2011). U–Pb zircon geochronology of ash fall tuffs in the Paraná Basin, Brazil: A new Permian chronostratigraphic framework for South America. Journal of South American Earth Sciences, 32(4), 360–371.

Rocha-Campos, A. C., Basei, M. A., Nutman, A. P., Kleiman, L. E., Varela, R., Llambias, E., ... & Da Rosa, O. D. C. (2011). 30 million years of Permian volcanism recorded in the Choiyoi igneous province (W Argentina) and their source for younger ash fall deposits in the Paraná Basin: SHRIMP U–Pb zircon geochronology evidence. Gondwana Research, 19(2), 509-523.

Rocher, S., Poma, S., & Sato, A. M. (2015). Geochemical and geochronological constraints on the Choiyoi magmatism in the Frontal Cordillera of Argentina. Journal of South American Earth Sciences, 63, 48–69.

Roddaz, M., Baby, P., Brusset, S., Hermoza, W., & Darrozes, J. M. (2005). Forebulge dynamics and environmental control in Western Amazonia: The case study of the Arch of Iquitos (Peru). Tectonophysics, 399(1-4), 87-108.

Rodgers, D. W., & Gunatilaka, A. (2003). Bajada formation by monsoonal erosion of a subaerial forebulge, Sultanate of Oman. Sedimentary Geology, 154(3-4), 127-146.

Rodgers, D. W., & Gunatilaka, A. (2003). Bajada formation by monsoonal erosion of a subaerial forebulge, Sultanate of Oman. Sedimentary Geology, 154(3-4), 127-146.

Rodríguez, E. E., Portner, D. E., Beck, S. L., Rocha, M. P., Bianchi, M. B., Assumpção, M., ... & Lynner, C. (2021). Mantle dynamics of the Andean Subduction Zone from continent-scale teleseismic S-wave tomography. Geophysical Journal International, 224(3), 1553-1571.

Rolleri, E.O. (1965). Stratigraphy report of the well YPF.F.MB-x1 (Mariano Boedo 1, Chaco, Argentina). YPF S.A. Unpublished report.

Rolleri, E.O. (1965). Stratigraphy report of the well YPF.F-P-1 (Formosa, Argentina). YPF S.A. Unpublished report.

Rolleri, E.O. (1966). Stratigraphy report of the well YPF.CHA.LBO-x1 (Chaco, Argentina). YPF S.A. Unpublished report.

Rolleri, E.O. (1967). Stratigraphy report of the well YPF.CHA.LB-x2 (Chaco, Argentina). YPF S.A. Unpublished report.

Rolleri, E.O. (1970). Stratigraphy report of the well YPF.CHA.ED-es-1 (El Desierto, Chaco, Argentina). YPF S.A. Unpublished report.

Rosa, M. L., Collaço, B., Assumpção, M., Sabbione, N., & Sánchez, G. (2016). Thin crust beneath the Chaco-Paraná Basin by surface-wave tomography. Journal of South American Earth Sciences, 66, 1-14.

Ruiz-Monroy, R. (2021). Organic geochemical characterization of the Yacoraite Formation (NW-Argentina)-paleoenvironment and petroleum potential (Doctoral dissertation, Universität Potsdam).

Russo, A., Ferello, R.E. & Chebli, G. (1979). Cuenca Chacopampena. In: Turner, J.C.M. (ed.), Geología Regional Argentina. 2 Simposio de Geología Regional Argentina. Academia Nacional de Ciencias (pp. 139-183).

Sabino, I. (2002). Geología del Subgrupo Pirgua (Cretácico) del noroeste argentino. Facultad de Ciencias Naturales, Universidad Nacional de Salta (Doctoral dissertation, Tesis doctoral, 258pp).

Salfity, J. A. & Marquillas, R. A. (1994). Tectonic and sedimentary evolution of the Cretaceous-Eocene Salta Group Basin, Argentina. In: Salfity, J.A. (ed.): Cretaceous Tectonics of the Andes, p. 266-315. Earth Evolution Sciences, Friedr. Vieweg & Sohn, Braunschweig/ Wiesbaden

Salfity, J. A. & Marquillas, R. A. (1999). La cuenca cretácico-terciaria del norte argentino. Geología Argentina: Buenos Aires, Instituto de Geología y Recursos Minerales, Anales, 29, 613-626. .

Sarmiento, L. F., & Rangel, A. (2004). Petroleum systems of the upper Magdalena Valley, Colombia. Marine and Petroleum Geology, 21(3), 373-391.

Sato, A. M., Llambías, E. J., Basei, M. A., & Castro, C. E. (2015). Three stages in the Late Paleozoic to Triassic magmatism of southwestern Gondwana, and the relationships with the volcanogenic events in coeval basins. Journal of South American Earth Sciences, 63, 48-69.

Schellart, W. P. (2008). Overriding plate shortening and extension above subduction zones: A parametric study to explain formation of the Andes Mountains. Geological Society of America Bulletin, 120(11-12), 1441-1454.

Schlagintweit, O. (1943). La posición estratigráfica del yacimiento de hierro de Zapla y la difusión del Horizonte Glacial de Zapla en la Argentina y Bolivia. Revista Minera13(4): 115-127. Buenos Aires.

Schwartz, R. K., & DeCelles, P. G. (1988). Cordilleran foreland basin evolution in response to interactive Cretaceous thrusting and foreland partitioning, southwestern Montana.

Shurr, G. W., & Rice, D. D. (1986). Paleotectonic controls on deposition of the Niobrara Formation, Eagle Sandstone, and equivalent rocks (Upper Cretaceous), Montana and South Dakota.

Simpson, C., Law, R. D., Gromet, L. P., Miro, R., & Northrup, C. J. (2003). Paleozoic deformation in the Sierras de Córdoba and Sierra de las Minas, eastern Sierras Pampeanas, Argentina. Journal of South American Earth Sciences, 15(7), 749-764.

Sinclair, H. D., Coakley, B. J., Allen, P. A., & Watts, A. B. (1991). Simulation of foreland basin stratigraphy using a diffusion model of mountain belt uplift and erosion: an example from the central Alps, Switzerland. Tectonics, 10(3), 599-620.

Snoke, J. A., & James, D. E. (1997). Lithospheric structure of the Chaco and Paraná basins of South America from surface-wave inversion. Journal of Geophysical Research: Solid Earth, 102(B2), 2939-2951.

Spalletti, L. A., Fanning, M., & Washington Rapela, C. (2008). Dating the Triassic continental rift in the southern Andes: the Potrerillos Formation, Cuyo basin, Argentina. Geologica Acta, 6(3), 0267-283.

Spickert, A., 2014, Petroleum system analysis: Middle Magdalena Valley Basin, Colombia, South America [M.S. thesis]: Seattle, University of Washington, 48 p

Starck, D. (2011). Cuenca Cretácica-Paleógena del noroeste argentino. In VIII Congreso de Exploración y Desarrollo de Hidrocarburos Simposio Cuencas Argentinas: Visión Actual, Instituto Argentino del Petróleo y el Gas (pp. 407-453).

Starck, D., & Vergani, G. (1996). Desarrollo tecto-sedimentario del Cenozoico en el sur de la Provincia de Salta-Argentina. In Congreso Geológico Argentino (Vol. 8, pp. 433-452).

Stauffer, K. W., & Croft, G. D. (1995). A modern look at the petroleum geology of the Maracaibo basin, Venezuela. Oil and Gas Journal, 93(23).

Strecker, M. & Alonso, R. & Bookhagen, Bodo & Carrapa, Barbara & Hilley, G.E. & Sobel, Edward & Trauth, Martin. (2007). Tectonics and Climate of the Southern Central Andes. Annu. Rev. Earth Planet. Sci. 35. 747-87.

Strecker, M. R., Alonso, R., Bookhagen, B., Carrapa, B., Coutand, I., Hain, M. P., Hilley, G.E., Mortimer, E., Schoenbohm, L., and Sobel. E.R. (2009). Does the topographic distribution of the central Andean Puna Plateau result from climatic or geodynamic processes?. Geology, 37(7), 643-646.

Strecker, M. R., Cerveny, P., Bloom, A. L., & Malizia, D. (1989). Late Cenozoic tectonism and landscape development in the foreland of the Andes: Northern Sierras Pampeanas (26–28 S), Argentina. Tectonics, 8(3), 517-534.

Strecker, M. R., Hilley, G. E., Bookhagen, B., & Sobel, E. R. (2011). Structural, geomorphic, and depositional characteristics of contiguous and broken foreland basins: examples from the eastern flanks of the central Andes in Bolivia and NW Argentina. Tectonics of sedimentary basins: Recent advances, 508-521.

Sweeney, J. J., & Burnham, A. K. (1990). Evaluation of a simple model of vitrinite reflectance based on chemical kinetics. AAPG bulletin, 74(10), 1559-1570.

Tegelaar, E. W., & Noble, R. A. (1994). Kinetics of hydrocarbon generation as a function of the molecular structure of kerogen as revealed by pyrolysis-gas chromatography. Organic Geochemistry, 22(3-5), 543-574.

Tissot, B. P., & Welte, D. H. (1984). Petroleum formation and occurrence (2nd ed.). Springer-Verlag.

Torres Acosta, V., A. Bande, E. R. Sobel, M. Parra, T. F. Schildgen, F. Stuart, and M. R. Strecker (2015), Cenozoic extension in the Kenya Rift from low-temperature thermochronology: Links

to diachronous spatiotemporal evolution of rifting in East Africa, Tectonics, 34, 2367–2386, doi:10.1002/2015TC003949.

Trice, R. (2014). Basement exploration, West of Shetlands: progress in opening a new play on the UKCS. London: The Geological Society of London.

Turner, J. C. M. (1960). Estratigrafía de la Sierra de Santa Victoria y adyacencias. Boletín de la Academia Nacional de Ciencias de Córdoba, 41(2), 163-196.

Turner, J. C. M., & Mon, R. (1979). Cordillera oriental. In Segundo simposio de geología regional argentina (Vol. 1, pp. 57-94). Academia Nacional de Ciencias de Córdoba.

Turner, J.C.M. (1958). Estratigrafía del cordón de Escaya y de la sierra de Rinconada (Jujuy). Revista de la Asociación Geológica Argentina, 13, 15-41.

Vallati, M., Tomás, S., Galli, C., Winterleitner, G., & Mutti, M. (2023). Depositional controls in an ancient, closed lake system: A high-resolution and multi-scalar case study from the Yacoraite Formation (Salta Basin, Argentina). Sedimentary Geology, 106456.

Vergel, M. D. M. (1993). Palinoestratigrafía de la secuencia neopaleozoica en la Cuenca Chacoparanense, Argentina. In 12º Internacional Congress on the Carboniferous-Permian (Buenos Aires, 1991) Compte Rendu (Vol. 1, pp. 201-212).

Verges, I. M. J. (1998). Estudi geologic del vessant sud del Pirineu oriental i central Evolucio cinematica en 3D.

Veroslavsky, G. (2004). Depósitos del Jurásico y Cretácico Temprano de la región meridional de Uruguay: el lineamiento Santa Lucía-Aiguá-Merín. Cuencas sedimentarias de Uruguay: geología, paleontología y recursos naturales: Mesozoico, 117-142.

Vilela, C.R. (1967). El petróleo en las cuencas de Orán y Metán, provincia de Salta. 2º Jornadas Geológicas Argentinas (Salta), Acta Geologica Lilloana 7, 425-438.

Viramonte, J.G., Kay, S.M., Becchio, R., Escayola, M., Novitski, I. (1999). Cretaceous rift related magmatism in central-western South America. Journal of South American Earth Sciences 12, 109–121.

Wagner, L. S., Jaramillo, J. S., Ramírez-Hoyos, L. F., Monsalve, G., Cardona, A., & Becker, T. W. (2017). Transient slab flattening beneath Colombia. Geophysical Research Letters, 44(13), 6616-6623.

Waschbusch, P. J., & Royden, L. H. (1992). Spatial and temporal evolution of foredeep basins: lateral strength variations and inelastic yielding in continental lithosphere. Basin Research, 4(3-4), 179-196.

Welte, D. H., Horsfield, B., & Baker, D. R. (Eds.). (2012). Petroleum and basin evolution: Insights from petroleum geochemistry, geology and basin modeling. Springer Science & Business Media.

White, T., Furlong, K., & Arthur, M. (2002). Forebulge migration in the Cretaceous Western Interior basin of the central United States. Basin Research, 14(1), 43-54.

Williams, T. A., Graham, S. A., & Constenius, K. N. (1998). Recognition of a Santonian submarine canyon, Great Valley Group, Sacramento basin, California: Implications for petroleum exploration and sequence stratigraphy of deep-marine strata. AAPG bulletin, 82(8), 1575-1595.

Winn Jr, R. D., & Steinmetz, J. C. (1998). Upper Paleozoic strata of the Chaco-Paranábasin, Argentina, and the great Gondwana glaciation. Journal of South American Earth Sciences, 11(2), 153-168.

Wygrala, B. P. (1989). Integrated study of an oil field in the southern Po Basin, Northern Italy: PhD thesis. University of Cologne, Germany.

Yalcin, M. N., & Welte, D. H. (1988). The thermal evolution of sedimentary basins and significance for hydrocarbon generation. Bull. Turk. Assoc. Petr. Geol, 1, 12-26.

Yalcin, M. N., Littke, R., & Sachsenhofer, R. F. (1997). Thermal history of sedimentary basins. In Petroleum and basin evolution: Insights from petroleum geochemistry, geology and basin modeling (pp. 71-167). Berlin, Heidelberg: Springer Berlin Heidelberg.

Yonkee, W. A., & Weil, A. B. (2015). Tectonic evolution of the Sevier and Laramide belts within the North American Cordillera orogenic system. Earth-Science Reviews, 150, 531-593.

Zaleha, M. J., Way, J. N., & Suttner, L. J. (2001). Effects of syndepositional faulting and folding on early Cretaceous rivers and alluvial architecture (Lakota and Cloverly Formations, Wyoming, USA). Journal of Sedimentary Research, 71(6), 880-894.

Zapata, S., Sobel, E. R., Del Papa, C., & Glodny, J. (2020). Upper plate controls on the formation of broken foreland basins in the Andean retroarc between 26 S and 28 S: From Cretaceous rifting to Paleogene and Miocene broken foreland basins. Geochemistry, Geophysics, Geosystems, 21(7), e2019GC008876.

Zappettini, E. O., & López-Gamundí, O. R. (1995). Geología y metalogénesis del orógeno andino central. In Anales (Vol. 23). Subsecretaría de Minería de la Nación, Dirección Nacional del Servicio Geológico.

Zhao, J. Z., Li, J., Wu, W. T., Cao, Q., Bai, Y. B., & Er, C. (2019). The petroleum system: a new classification scheme based on reservoir qualities. Petroleum science, 16, 229-251.

Ziegler, P. A., & Dèzes, P. (2007). Cenozoic uplift of Variscan Massifs in the Alpine foreland: Timing and controlling mechanisms. Global and Planetary change, 58(1-4), 237-269.